Journal of Engineering

ISSN 1726-4073

A Scientific Refereed Journal
Published by College of
Engineering University of
Baghdad

March

201 3

Number 3

Volume 19

ISSN 1726-4073

مجلة الهندسة

مجلة علمية محكمة تصدرها
كلية الهندسة ـ جامعة بغداد

أذار
2013

العدد 3
المجلد 19

ENGINEERING

College of Engineering Baghdad University Baghdad

List of Contents

English Section: Page

Behavior of Partially Saturated Cohesive Soil under Strip Footing

Mohammed Yousif Fattah
Prof. Dr. in Building and Construction Engineering Dept., University of Technoilogy,
Emial: myf_1968 @ Yahoo.com

Mahmood Diab Ahmed
Inst. Dr. in Civil Engineering Dept., College of Engineering, University of Baghdad, Iraq.
Email: mahmoud_baghdad @ Yahoo.com

Hadeel Ammar Mohammed
Assist. Inst. in Division of Engineering Affairs, University of Al-Mustansiriyah, Baghdad, Iraq.
Emial: eng.hadeel84 @ Yahoo.com

ABSTRACT

In this paper, a shallow foundation (strip footing), 1 m in width is assumed to be constructed on fully saturated and partially saturated Iraqi soils, and analyzed by finite element method. A procedure is proposed to define the H – modulus function from the soil water characteristic curve which is measured by the filter paper method. Fitting methods are applied through the program (SoilVision). Then, the soil water characteristic curve is converted to relation correlating the void ratio and matric suction. The slope of the latter relation can be used to define the H – modulus function.

The finite element programs SIGMA/W and SEEP/W are then used in the analysis. Eight nodded isoparametric quadrilateral elements are used for modeling both the soil skeleton and pore water pressure. A parametric study was carried out and different parameters were changed to study their effects on the behavior of partially saturated soil. These parameters include the degree of saturation of the soil (S) and depth of water table.

The study reveals that when the soil becomes partially saturated by dropping water table at different depths with different degrees of saturation, the bearing capacity of shallow foundation increases about (4 – 7) times higher than the bearing capacity of the same soil under saturated conditions. This result is attributed to matric suction value (i.e negative pore water pressure). The behavior of soil in partially saturated condition is like that of fully saturated condition but with smaller values of displacement. It is found that the settlement is reduced when the water table drops to a depth of 2 m (i.e. twice the foundation width) by about (92 %).

KEYWORDS: unsaturated soil, soil water characteristic curve, H-modulus function, matric suction.

تصرف الترب المتماسكة و المشبعة جزئيا بالماء أسفل الأساس الشريطي

محمد يوسف فتاح محمود ذياب أحمد هديل عمار محمد

الخلاصه

في هذا البحث، تم تحليل أساس سطحي (أساس شريطي بعرض ١ م) أنشئ على تربة عراقية مشبعة كليا مرة و مشبعة جزئيا مرة اخرى، بواسطة طريقة العناصر المحددة. حيث إن الطريقة افترضت إيجاد دالة (H – Modulus) من منحني خصائص الرطوبة للتربة الذي أوجد بواسطة طريقة ورقة الترشيح، ومن خلال البرنامج (Soil Vision) وبعد تعريف الخواص الأساسية للتربة مثل حدود أتربيك، توزيع حجم الحبيبات، الوزن النوعي، المسامية والكثافة الوزنية الرطبة والجافة. ومن خلال تحويل منحني خصائص الرطوبة للتربة الى منحني العلاقة بين نسبة الفجوات ومقدار الامتصاص للتربة، ومن ميل العلاقة الأخيره تم إيجاد دالة (H – Modulus).

أستخدم في التحليل برنامج العناصر المحدده (SIGMA/W) و(SEEP/W) حيث تم إستخدام عناصر رباعية بثماني عقد لتمثيل هيكل التربة و ضغط ماء المسام. وتم تغيير قيم المعاملات التالية [درجة التشبع (S)، عمق منسوب الماء ودراسة تأثيرها على سلوك التربة غير المشبعة.

لقد بينت الدراسة إن انخفاض منسوب المياه الجوفية إلى أعماق مختلفة وبدرجات تشبع مختلفة يزيد من قابلية التحمل للأساس السطحي بحوالي (□ – □) مرات عن قابلية التحمل لنفس التربة في حالة التشبع الكلي وهذه النتيجه تنسب الى ضغط الماء المسامي السالب المتولد من قابلية المص للتربة.

تم إستنتاج أن تصرف التربة غير المشبعة يشبه تصرف التربة المشبعة لكن بقيم أقل للهبوط الشاقولي حيث وجد إن الهبوط يقل عند انخفاض منسوب المياه أسفل الاساس الى عمق □م (مرتين من عرض الاساس) بمعدل (□□%).

الكلمات الرئيسية: تربة غير مشبعة، منحني خصائص التربة – الرطوبة ، دالة معامل H ، قابلية المص للتربة.

INTRODUCTION

The mechanical behavior of partially saturated soils is different from that of fully saturated soils. A common engineering problem which often involves partially saturated soils is that of a shallow foundation resting above the ground water table. In many cases, a capillary zone exists above the ground water table, where the soil is partially saturated and which can be very large depending on the soil type. Typical footing analyses ignore this zone and assume that the soil above the ground water table is dry. The bearing capacity is one of the key parameters required in the design of shallow foundations. Several approaches are available in the literature for determination of the bearing capacity of soils based on the saturated shear strength parameters. However, in many arid and semi-arid regions, shallow foundations are usually located above the ground water table where the soil is typically in a state of unsaturated condition. Nevertheless, the bearing capacity of soils is commonly determined assuming fully saturated conditions ignoring the influence of capillary stresses or the matric suction. Due to this reason, estimation of the bearing capacity of shallow foundations using the conventional approaches may not be reliable leading to uneconomical designs **(Vanapalli and Mohammed, 2007)**.

Limited research work has been performed so far on shallow foundations in which the negative pore-water pressures of the soil were explicitly accounted for. **Rahardjo and Fredlund (1992)** presented example demonstrated the role of matric suction in affecting the value of undrained shear strength (Cu) and consequently the bearing capacity of the soil. They showed that the initial bearing capacity for the strip and the square footing was 257 and 309 kPa, respectively. The initial bearing capacity was observed to increase by 27 % when the matric suction increased by an amount equals to the undrained shear. **Fredlund and Rahardjo (1993)** proposed an extension of bearing capacity formulations to account for the increase in bearing capacity due to soil suction. The increase in bearing capacity is considered as an additional cohesive component due to matric suction, which can be estimated as $\{(u_a - u_w) \tan\phi^b\}$. The angle ϕ^b, represents the increase in shear strength contribution due to matric suction. **Costa et al. (2003), and Mohamed and Vanapalli (2006)** showed that the bearing capacities of unsaturated soil are significantly influenced by the matric suction from their investigations on model footing tests or in situ plate load tests. **Costa et al. (2003)** used plate load test with diameter (0.8 m) and thickness (25 mm) on clayey sandy soil. **Mohamed and Vanapalli (2006)**, used model footings of different sizes (i.e., 100 mm x 100 mm and 150 mm x 150 mm) on sandy soil classified using USCS as poorly graded sand (SP) with internal friction angle of (35.3°) from direct shear test. The bearing capacity of a surface footing on saturated and unsaturated, compacted coarse-grained soil was measured using the University of Ottawa Bearing Capacity Equipment (UOBCE) that was specially designed and built for this research program at the University of Ottawa student work shop. It was shown that the matric suction values in the range of 2 to 6 kPa contributes to an increase in the bearing capacity of soil by 4 to 7 times in comparison to bearing capacity values under saturated condition.

In this paper, the finite element method is used to simulate the behavior of strip footing on unsaturated soil.

SOIL WATER CHARACTERISTIC CURVE

The soil water characteristic curve (SWCC) defines the relationship between the amount of water in the soil and soil suction. The amount of water can be a gravimetric water content, w, volumetric water content, θ, or degree of saturation, S. The SWCC is also called the water retention curve, (WTC) or the capillary pressure curve. The SWCC divides soil behavior into three distinct stages of desaturation as shown in **Fig. 1**. The stages of desturation are referred to as the "boundary effect stage" at low soil suction, the "transition stage" at intermediate soil suction, and the "residual stage" at the high soil suction that extend to 1,000,000 kPa **(Fredlund, 2006).**

There are two defining breaks along most SWCC and these are referred to as the “air entry value” of the soil and the “residual value” of the soil. These points are illustrated in **Fig. 1**, the air entry value is the point at

which the difference between the air and water pressure becomes sufficiently large such that water can be displaced by air from the largest pore space in the soil. The residual degree of saturation is the point at which a further increase in suction fails to displace a significant amount of water **(Brooks and Corey, 1964)**.

The general shape of the SWCC for various soils reflects the dominating influence of material properties including pore size distribution, gain size distribution, density, organic material content, clay content, and mineralogy on the pore water retention behavior **(Lu and Likos, 2004)**.

THE PROGRAM (SIGMA/W)

SIGMA/W is a finite element software product that can be used to perform stress and deformation analyses of earth structures. Its comprehensive formulation makes it possible to analyze both simple and highly complex problems. For example, one can perform a simple linear elastic deformation analysis or a highly sophisticated nonlinear elastic-plastic effective stress analysis. When coupled with SEEP/W, another GEO-SLOPE software product, it can also model the pore-water pressure generation and dissipation in a soil structure in response to external loads. SIGMA/W has applications in the analysis and design for geotechnical, civil, and mining engineering projects **(Krahn, 2004)**.

Constitutive Models

SIGMA/W includes eight different soil constitutive models. It may be difficult to decide which model to select for a particular application, but the model which is selected must be consistent with the soil conditions and the objective of the analysis. SIGMA/W is formulated for several elastic and elastic-plastic constitutive soil models. All models may be applied to two-dimensional plane strain and axisymmetric problems.

Two constitutive models are used to study the bearing capacity of the unsaturated soils:

1. Linear elastic model

he simplest SIGMA/W soil model is the linear elastic model for which stresses are directly proportional to the strains. The proportionally constants are Young's Modulus, (E), and Poisson's Ratio, (ν). The stress and strain are related by the eq. (1):

$$\begin{Bmatrix} \sigma_x \\ \sigma_y \\ \sigma_z \\ \tau_{xy} \end{Bmatrix} = \frac{E}{(1-\nu)(1-2\nu)} \begin{bmatrix} 1-\nu & \nu & \nu & 0 & \varepsilon_x \\ \nu & 1-\nu & \nu & 0 & \varepsilon_y \\ \nu & \nu & 1-\nu & 0 & \varepsilon_z \\ 0 & 0 & 0 & \frac{1-2\nu}{2} & \gamma_{xy} \end{bmatrix} \quad (1)$$

For two – dimensional plane strain analysis, (ε_z) is zero.

2. Elastic – plastic model

The elastic – plastic model in SIGMA/W describes an elastic perfectly – plastic relationship. A typical stress – strain curve for this model is shown in **Fig. 2** where stresses are directly proportional to strains until the yield point is reached. Beyond the yield point, the stress – strain curve is perfectly horizontal. The material properties required for this model are given in **Table 1**.

Coupled Consolidation

A fully coupled analysis requires that both the stress – deformation and seepage dissipation equations be solved simultaneously. SIGMA/W computes displacements and stresses while SEEP/W computes the changes in pore-water pressure with time. Running these two software products in a coupled manner makes it possible to do a consolidation analysis. When coupled, both SIGMA/W and SEEP/W contribute to forming a common global characteristic (stiffness) matrix. Three equations are created for each node in the finite element mesh. Two are equilibrium (displacement) equations formed by SIGMA/W and the third is a continuity (flow) equation formed by SEEP/W. Solving all the three equations simultaneously gives both displacement and pore-water pressure changes. When doing a coupled analysis, it is essential to recognize that all equilibrium (force and displacement) conditions are defined in SIGMA/W and all hydraulic (flow) conditions are specified in SEEP/W. In SIGMA/W, the usual force and displacement boundary conditions have to be specified together with soil properties. In SEEP/W, the head and flow boundary conditions have to be specified together with hydraulic

Conductivity and volumetric water content functions.

ADDITIONAL MATERIAL PROPERTIES FOR UNSATURATED COUPLED ANALYSIS

H-Modulus Function

H is the unsaturated modulus that relates the volumetric strain of the soil to a change in negative pore-water pressure or change in suction. The H modulus may be defined as a function of negative pore-water pressure. At saturation, H is related to the elastic constants E and ν by eq. (2):

$$H = \left(\frac{E}{1-2\nu}\right) \qquad (2)$$

Therefore, H must be set to *E/(1-2ν)* at zero pore-water pressure when defining an H-Modulus versus pore-water pressure function. As a soil dries and the pore-water pressure becomes highly negative, the soil becomes very stiff. This increase in stiffness can be represented by an increase in H.

Fig. 3 illustrates a potential increase in H as a function of the negative pore-water pressure. The H modulus cannot be specified less than E/(1-2ν) . If an H modulus function is defined with an H value less than E/(1-2ν), SIGMA/W will automatically set H to E/(1-2ν) during the analysis. Consequently, when an H modulus function is defined, the lowest H value should be E/(1-2ν) at the point where the pore-water pressure is zero.

For a coupled analysis involving unsaturated soils, two additional material properties H and R need to be defined. H is a modulus relating to the change of volumetric strain in the soil structure to a change in suction. R is another modulus relating the change in volumetric water content to suction; therefore, it is given by the inverse of the slope of the soil water characteristic curve.

In this section, a procedure to obtain the H modulus parameter from the slope of a void ratio (e) versus matric suction ($u_a - u_w$) curve is described. For a soil element, a change in its volume can be decomposed into two parts:

$$dV = dV_s + dV_v \qquad (3)$$

where dV_s = the change in volume of the soil particles, and
dV_v = the change in the volume of voids.

If the volume change of the soil particles, dV_s, is small and thus neglected, the volumetric strain can be approximated as follows eq. (4):

$$\varepsilon_v = \frac{dV}{V} \approx \frac{dV_v}{V} \qquad (4)$$

From the definition of void ratio, e, a change in void ratio, *de*, is given by eq. (5):

$$de = d\left(\frac{V_v}{V_s}\right) = \frac{dV_v}{V_s} = \frac{dV_v}{(1-n)V} = \frac{d\varepsilon_v}{(1-n)} \qquad (5)$$

where: n = the porosity of the soil.

The slope of a void ratio versus matrix suction curve can be written as eq.(6):

$$\frac{de}{d(u_a - u_w)} = \frac{d\varepsilon_v}{(1-n)d(u_a - u_w)} \qquad (6)$$

In an unsaturated soil element, when only a change in matric suction occurs, the incremental volumetric strain, $d\varepsilon_v$, can be written as:

$$d\varepsilon_v = d\varepsilon_x + d\varepsilon_y + d\varepsilon_z = \frac{3d(u_a - u_w)}{H} \qquad (7)$$

or: $$\frac{d\varepsilon_v}{d(u_a - u_w)} = \frac{3}{H} \qquad (8)$$

After substituting Eq. (8) into Eq. (6), it can be seen that the slope of a void ratio versus matric suction curve is: **(Wong, et al., 1998, and Krahn, 2004)**.

$$\text{Slope} = \frac{3}{(1-n)H} \qquad (9)$$

Definition of Hydraulic Conductivity

A conductivity function defines the relationship between pore water pressure and hydraulic conductivity. **Fig. 4** shows a typical conductivity function.

As soil desaturates and the water content decreases when the pore water pressure becomes negative; the ability of the soil to conduct water decreases as the water content decreases. The soil hydraulic conductivity consequently decreases as the pore water pressure becomes increasingly negative. A conductivity function is defined by specifying a series of discrete data points and fitting a weighted spline

curve to the data points in order to create a continuous function.

Conductivity functions can be defined in the program SEEP/W in any of the following ways:

- Specifying each data point in the function by typing the coordinates or by clicking on the function graph.
- Estimating the function from an existing volumetric water content function.
- Importing an existing conductivity function from the SEEP/W function database or from another SEEP/W problem and modify it.

EXPERIMENTAL WORK

In this study, the aim of experimental work is to define the soil water characteristic curve (SWCC) by measuring of the soil suction.
Soil samples were collected from a three sites within Baghdad city – Al-Rusafa region namely, Sahat Al – Wathiq from depth (3.5 m), in this study referred to as (Rusafa 1), Bab Al – Muadham from depth (9.5 m, and 3.5 m) referred to as (Rusafa 2, and Rusafa 3), respectively. The physical and mechanical properties of these soil were studied by conducting a series of tests in the laboratory, these include: specific gravity, Atterberg limits, unconfined compression test, grain size distribution by sieve analysis and hydrometer, and consolidation test. **Table 2** shows the index properties of the soil. For each sample, the total and matric suction were measured by the filter paper method (Whatman No. 42) at different degrees of saturation according to **ASTM-D-5298**. With the aid of SOILVISION program, the fitted curve for the SWCC was predicted by **using Fredlund and Xing (1994)** fitting curve as shown in **Fig. 5**.

The result for Rusafa 1, soil will be presented here and shall be used in numerical analysis.

BEARING CAPACITY PROBLEM

A shallow foundation (strip footing) with width equals to 1 m is constructed on saturated and unsaturated soils. The strip footing is constructed on soil with dimensions (20 m) in width and (10 m) in height, to take into account the effect of the stress distribution below the footing. The finite element mesh is illustrated in **Fig. 6** Due to symmetry, 260 elements are used for modeling half of the footing and the soil beneath it. Eight nodded quadrilateral isoparametric elements are used for modeling the soil skeleton. The right and left hand edges of the mesh are restricted to move horizontally while the bottom of the mesh is restricted in both horizontal and vertical directions. The top edge is free in both directions. In addition, the side boundaries are assumed to be impermeable (i.e. no flow is allowed through these sides), and the top and bottom edges are assumed to be permeable.

In this work, two constitutive models are used to characterize the stress – strain behavior of the soil. Linear elastic model is used for the soil existing above the water table, while elastic – plastic model with Mohr-Coulomb failure criterion is used for modeling the soil existing below the water table.

Material Properties

The soil beneath the footing has the properties shown in **Table 3**, which were calculated from laboratory tests carried out on undisturbed samples. The soil is classified as silty clay according to the ASTM classification.

The undrained shear strength (Cu) of the soil was measured by carrying out unconfined compression test through remolding the sample at different degrees of saturation (100%, 90%, 80%, and 70%). The results demonstrate that the unconfined compressive strength (q_u) increases with the decrease of saturation (S), and consequently increase of undrained shear strength (Cu). The results of unconfined compression test are shown in **Table 4**. The initial tangent modulus of elasticity (E) was evaluated as given in **Table 4**.

H – Modulus Function

There are sets of steps considered to find the H-modulus function. These steps are proposed in this work in order to characterize the behavior of unsaturated soils:

1. The relation between gravimetric water content and suction is converted to relations correlating the void ratio and the matric suction based on the relation:

$$e = \frac{w_w G_s}{S} \qquad (10)$$

where w_w = gravitation water content,

G_s = specific gravity, and
S = degree of saturation.

Then, the slope of the void ratio versus the matric suction, m is predicted:

$$m = \frac{\Delta e}{\Delta h_m} \qquad (11)$$

where: $\Delta e = (e_2 - e_1)$, and
$\Delta h_m = (h_{m1} - h_{m2})$

h_{m1}, h_{m2} are the initial and final matric suctions, respectively.
e_1, e_2 are the initial and final void ratios, respectively.
Hence, five to seven values of the slope are predicted from this curve as show in **Table 5**.
Fig. 7 shows the steps followed to find the slope of the void ratio versus the matric suction relation the soil.

2. After finding the slope of the void ratio versus the matric suction, it can be seen that the slope, m is equal to $\frac{3}{(1-n)h}$ **(Krahn, 2004)**:
Hence, the H-modulus function becomes:

$$H = \frac{3}{(1-n)m} \qquad (12)$$

where: n = porosity of soil,
m = the slope of the void ratio versus the matric suction.

In addition, the H must be set to E/ (1-2ν) at zero pore water pressure when defining it **(Krahn, 2004)**.

Fig.8 shows the relations between the H-modulus and the matric suction calculated for Rusafa 1 soil.

The relationship between the hydraulic conductivity and pore water pressure can be estimated from SEEP/W program as shows in **Fig. 9.**

RESULTS OF FINITE ELEMENT ANALYSIS AND DISCUSSION

At first, each type of soil was analyzed as fully saturated soil by the programs SIGMA/W and SEEP/W. The results as shown in **Fig. 10** and **Table 6** demonstrate that the failure mechanism is close to the general shear failure mode and the ultimate bearing capacity according to the criterion of the load corresponding to settlement equals to (10%) of the width of footing is in a good agreement with Trezaghi's bearing capacity equation for a surface strip footing:

$$q_u = Nc\ Cu \qquad (13)$$

where q_u = ultimate bearing capacity,
Cu = undrained shear strength, and
Nc = bearing capacity factor, which is equal to (5.7) when ø equals to zero.

Then, each type of soil was analyzed as partially saturated soil with different water table levels (2 m, 4 m, and 6 m) below the ground surface with the same degree of saturation. Later, each problem is re-analyzed with another degree of saturation. This means that for each case, the degree of saturation is changed from (90%) to (80%) and (70%) keeping the other parameters constant, and for each degree of saturation, the problem was re-analyzed with the same water table level.

In unsaturated soil (i.e. soil located above the water table), practically, the water content of this soil is varying with depth from the ground surface reaching to the water table level, and consequently the matric suction value is varied with depth above the water table level. In SIGMA/W program, it is difficult to measure the variation of matric suction with depth, therefore; in this work the matric suction is assumed constant with depth above the water table level.

Effect of Degree of Saturation and Water Table Level

Figs. 11 to 13 show the effect of dropping water table level on the behavior of unsaturated soil.
Fig.11 illustrates that the dropping of water table to depth of (2 m) leads to increasing the bearing capacity of the soil, and this increase continues when dropping the water table to 4 m, and 6 m depth. This can be attributed to increasing in matric suction value as a result of increasing of unsaturated zone and also increasing of overburden pressure.
The same trend is shown in **Figs. 12 and 13** for degree of saturation 80% and 70%, respectively.
But when comparing the three figures at same water table level with different degrees of

saturation, it can be noticed that when moving from degree of saturation 90% to 80% and 70%, the increase in bearing capacity becomes small due to small contribution of matric suction only.

The values of the ultimate bearing capacity which were obtained from these figures according to the criterion of a load corresponding to a settlement equal to (10 %) of the width of the footing are summarized in **Table 7**. From the table, it can be noticed that the ultimate bearing capacity of partially saturated soil is higher than that for fully saturated by about (4 to 7) times. This result is attributed to increasing in matric suction and overburden pressure as a result of dropping of water table. These results are consistent with the observation of **Mohammed and Vanapalli (2006)** who reported that the bearing capacity of coarse grained unsaturated soil to be (5 to 7) times higher than the bearing capacity of the same soil under saturated conditions.
From **Table 7**, it can also be noticed that at the same water table level, the increase in bearing capacity due to matric suction is only about (50 – 100) kPa.

Vertical Displacement

Fig. 14 shows the relation between the vertical surface displacement and distance from the center line of the model footing. The figure represents the soil in fully saturated and partially saturated conditions, and loaded to the same maximum value of footing stress.

Fig. 14 a illustrates that when the applied stress is equal to zero, the vertical displacement is zero along the distance from the center line, and this value is changed as the footing stress is increased. It can be noticed that with progress of applying stress, the vertical displacement starts to change, and heave at the footing end takes place.

It is also noticed that the vertical displacements near the center line of the footing are negative (downward movement), while at a distance far from the center line of the footing, they are positive (upward movement). The maximum value of vertical displacement occurs at the center line of the footing. The displacement increases with increase of the applied stress and reaches a value of (154 mm). This is due to concentration of stresses of the footing in this region. The small vertical displacement, observed under the far end away from the center line of the footing, is due to upward movement of the soil under the footing which reduces the downward movement.

In **Fig. 14 b**, the vertical displacement is traced when the soil is partially saturated and the water table is dropping to depth 2 m and the degree of saturation is 90 %. It is noticed that the distribution of vertical displacement is similar to that in condition of fully saturation state but with less values when compared at a certain value of loading. For example, when the value of stress reaches the maximum value (770 kPa), the maximum vertical displacement is (154 mm), and the maximum heave is (49 mm), when the soil is fully saturated, but the maximum vertical displacement is only (9.8 mm), and the maximum heave is (2.1 mm) when the soil is partially saturated. This is due to existing of negative pore water pressure which increases the shear strength of the soil and consequently reduces the settlement.

It is also, noticed in **Fig. 14** that the heave continues to the end of the problem mesh, another run was carried out in which the mesh was extended to a distance of 20 m, the heave was noticed to decrease gradually at about 15 m from the foundation center.
The percentage of reduction in settlement can be defined as:

Reduction in settlement (%) =

$$\frac{S_{sat} - S_{unsat}}{S_{sat}} \times 100\% \quad (13)$$

where S_{sat} = settlement for fully saturated soil, and
S_{unsat} = settlement for partially saturated soil.

It is found that the settlement decreases when the water table drops to depth 2 m (i.e. 2 B) by about (94 %). These results approximately agree with those of **Agarwal and Rana (1987)**, who reported that when the water table is at surface, the settlement is 95 % higher than when the water table is at depth (1.5 B).

Variation of Bearing Capacity with Matric Suction

Fig. 15 shows the variation of the bearing capacity with respect to matric suction for the model footing.

These relationships demonstrate that there is significant increase in the bearing capacity of the model footing due to the contribution of suction. The results also suggest that the bearing

Capacity approximately increases linearly with matric suction up to the air – entry value and there is a non – linear increase in the bearing capacity with respect to matric suction beyond the air – entry value.

From the SWCC **(Fig. 5)** fitting curve proposed by **Fredlund and Xing (1994)**, the air – entry values of the soil is 350 kPa. The trends of the results of the bearing capacity of unsaturated soil are similar to the shear strength behavior of unsaturated soils which were reported by **Vanapalli et al. (1996)** who found that there is a linear increase in shear strength up to the air – entry value.

Vanapalli et al. (1996), demonstrated a typical relationship between the shear strength and the SWCC in **Fig. 16**. There is a linear increase in shear strength up to the air – entry value. The rate of desaturation with respect to an increase in matric suction is greatest between the air – entry value and the suction corresponding to residual water content condition. There is a nonlinear increase in shear strength in this region. Beyond the residual suction condition, the shear strength of an unsaturated soil may increase, decrease, or remain relatively constant during further desaturation depending on the type of soil. In the clayey soil, the residual state may not be well defined that even at high value of suction; it could still be considerable water available to transmit suction along the soil particle or aggregate contents, which contributes towards increases in the shear strength. This phenomenon can occur for a large range of suction value for clay soil.

CONCLUSIONS

Based on the experimental results obtained from this research work and the analysis of the behavior of partially saturated soil beneath a strip footing by the finite element method, the following conclusions can be made:

1) From the soil water characteristic curve (SWCC) which was determined by experimental method (i.e. filter paper method) the matric suction value was found to increase with decrease of the degree of saturation, and the rate of increase is not equal to rate of decrease in degree of saturation. The values of matric suction also increase with decrease of the void ratio at the same degree of saturation.
2) The procedure of analysis of the bearing capacity of shallow foundation on partially saturated soil required a proposed procedure to define the H – modulus function (H is a modulus relating the change of volumetric strain in the soil structure to change in suction). The procedure is found to be successful.
3) The water table level and the degree of saturation have the great effect on the behavior of partially saturated soil. In this work, it is found that due to dropping of water table and contribution of matric suction (i.e. negative pore water pressure), the bearing capacity of partially saturated soil increases by about (4 – 7) times higher than the bearing capacity of the same soil under saturated conditions. But, at the same water table depth, the bearing capacity increases in a small value due to contribution of matric suction only.
4) There are two phenomena governing the behavior of footing represented by settlement (negative vertical displacement) and heave (positive vertical displacement). This behavior can be explained as follows; an increase of load on the foundation will increase the settlement and the failure surface will gradually extend outward from the foundation in heave behavior. The vertical displacement of fully saturated soil is greater than that of partially saturated soil.
5) The settlement reduces when the water table drops to a depth of 2 m (i.e. 2 B) by about (94 %).

REFERENCES

Agarwal, K. B. and Rana, M. K., (1987), "Effect of Ground Water on Settlement of Footings in Sand," Proceedings, Ninth European Conference on Soil Mechanics and Foundation Engineering, E. T. Hanrahann, T. L. L. Orr, and T. F. Widdis, Eds., Vol. 2, A. A.Balkema, Dublin, pp. 751–754.

ASTM-D-5298-03, "Standard Test Method for Measurement of Soil Potential (Suction) Using Filter Paper", Annual Book of ASTM Standards, Vol. 04.08, Soil and Rock, pp. 1 – 6.

Brooks, R.H., and Corey, A.T., (1964), "Hydraulic Properties of Porous Media", Colorado State University, Hydrology paper No.3, March.

Costa, Y.D., Cintra, J.C. and Zornberg, J.C., (2003), "Influnce of Matric Suction on the Results of Plate Load Tests Performed on a Lateritic Soild Deposit", Geotechnical Testing Journal, Vol. 26, No. 2, pp. 219-226.

Fredlund , D.G., and Rahardjo, H. (1993), "Soil Mechanics for Unsaturated Soils" John Wiley & Sone Inc. New York, United States of America.

Fredlund, D.G., Xing, A., (1994), "Equation for the Soil Water Characteristic Curve", Canadian Geotechnical Journal Vol. 31, No. 3, pp. 521 – 532.

Fredlund, D. G., (2006), "Unsaturated Soil Mechanics in Engineering Practice", Journal of Geotechnical and Geoenvironmental Engineering, ASCE, Vol. 132, No. 3, pp. 286 – 321.

Krahn, J., (2004), "Stress and Deformation Modeling With SIGMA/W", GEO-SLOPE International, Ltd.

Lu, N., and Likos, W. J., (2004), "Unsaturated Soil Mechanics", John Wiley & Sons, New York.

Mohamed, F. M. O. and Vanapalli, S. K., (2006), "Laboratory Investigations for the Measurement of the Bearing Capacity of an Unsaturated Coarse-Grained Soil", Proceedings of the 59th Canadian Geotechnical Conference, Vancouver 1-4 October, pp. 219-226.

Rahardjo, H. and Fredlund, D. G., (1992), "Mechanics of Soil with Matric Suction," Proceedings, International Conference in Geotechnical Engineering—Geotropika 92, Universiti Teknologi Malaysia, Johor Bahru, Malaysia.

Vanapalli, S. K., Fredlund, D. G., Pufahl, D.E., and Clifton, A.W., (1996), " Model for the Prediction of Shear Strength with Respect to Soil Suction" , Canadian Geotechnical Journal, Vol. 33, No. 3, pp. 379-392.

Vanapalli, S. K. and Mohamed, F. M. O., (2007), "Bearing Capacity of Model Footings in Unsaturated Soils", in Experimental Unsaturated Soil Mechanics, Springer Proceedings in Physics, Springer -Verlag Berlin Geidelberg, Vol. 112, pp. 483-493.

Wong, T.T., Ferdlund, D.G., and Krahn, J., (1998), "A Numerical Study of Coupled Consolidation in Unsaturated Soils", Canadian Geotechnical Journal, Vol. 35, pp. 926 – 937.

Table 1 Elastic – plastic material properties.

Property	Definition
Elastic Modulus, E	Initial linear – elastic stiffness of the soil
Poisson's Ratio, ν	Constant value
Cohesion, c	Cohesive strength of the soil
ϕ	Soil internal friction in degree
Dilation Angle, ψ	Soil dilation angle in degree ($0 \le \psi \le \phi$)
ϕ^b	a value used to make the cohesive strength a function of soil suction (negative pore – water pressure)

Table 2 Index properties of the soils for undisturbed sample.

Natural water content, W %	24.32
Dgree of saturation, S %	100
Liquid limit, L.L	34
Plastic limit, PL %	19
Plasticity index, PI %	15
Specific gravity, Gs	2.74
% clay	68.3

Table 3 Material properties for the soils beneath the footing.

Parameter	Value	Unit
Total unit weight, (γ_t)	20.21	kN/m^3
Dry unit weight, (γ_d)	16.25	kN/m^3
Angle of internal friction, (ø)	0	Degree
Poisson's ratio, (ν)* for saturated soil	0.45	—
Poisson's ratio, (ν)* for unsaturated soil	0.3	—
Hydraulic conductivity, (k_s)	2.55×10^{-10}	m/sec
Void ratio, (e)	0.666	—
Coefficient of volume change (m_v)	0.646	m^2/MN

Table 4 Results of unconfined compression test on remolded samples at different degrees of saturation.

S (%)	q_u (kPa)	Cu (kPa)	E (kPa)
100%	270	135	108000
90%	287	143.5	114800
80%	311	155.5	124400
70%	329	164.5	131600

Table 5 Values of the slopes predicted from the void ratio versus matric suction curve.

Slope	e_1	e_2	h_{m1}	h_{m2}
m_1	0.143	0.096	20000	40000
m_2	0.096	0.07	40000	60000
m_3	0.07	0.06	60000	80000
m_4	0.06	0.051	80000	100000

Table 6 Results of bearing capacity analysis of fully saturated soils for remolded sample.

Soil name	q_u according to Trezaghi's equation (kPa)	q_u by the finite element analysis (kPa)
Rusafa 1	770	760
Rusafa 2	584	580
Rusafa 3	371	380

Table 7 Results of ultimate bearing capacity (kPa) for unsaturated soil obtained from finite element analysis.

W.T depth	Degree of saturation	Bearing Capacity (kPa)
0 m	100 %	760
2 m	90 %	3200
	80 %	3250
	70 %	3300
4 m	90 %	4700
	80 %	4750
	70 %	4800
6 m	90 %	5400
	80 %	5500
	70 %	5600

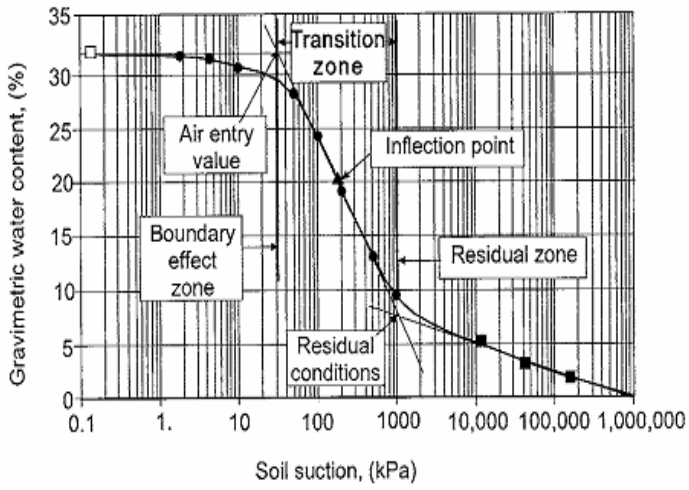

Fig. 1: Illustration of the in situ zones of desaturation defined by a soil – water characteristic curve (after Fredlund, 2006).

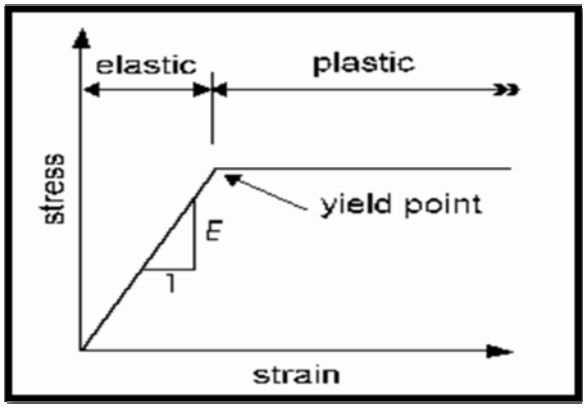

Fig.2 Elastic – perfectly plastic constitutive relationship (from Krahn, 2004).

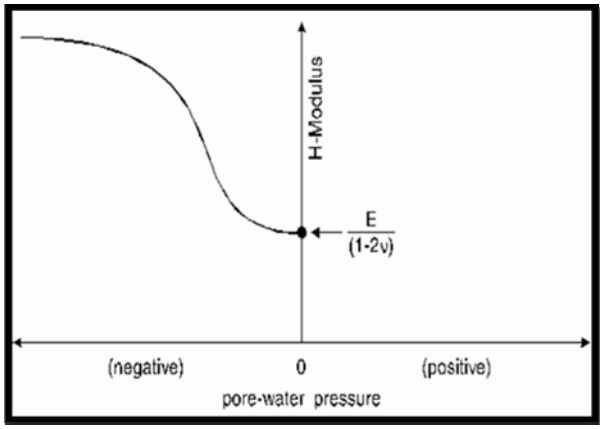

Fig.3 H-modulus as a function of pore-water pressure, (from Krahn, 2004).

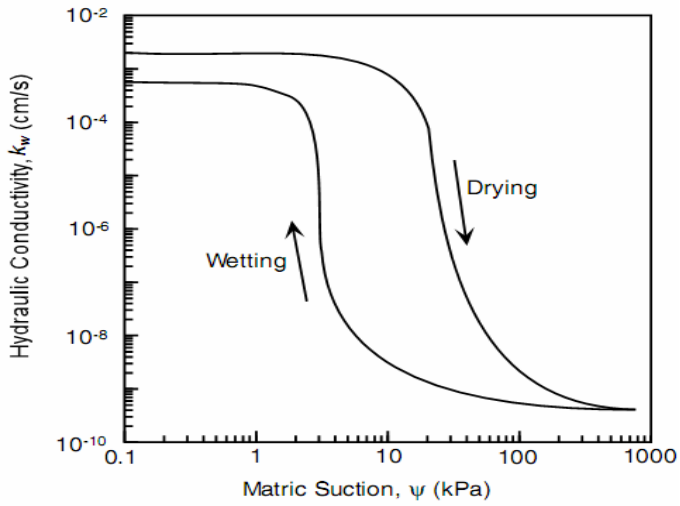

Fig. 4 Conductivity Function, (from Lu and Likos, 2004).

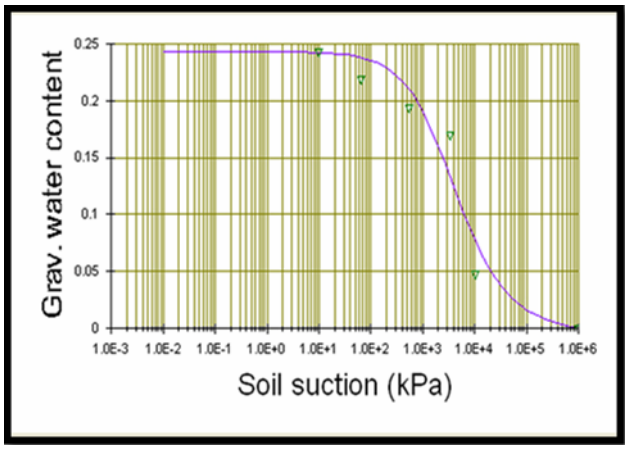

Fig. 5 Soil water characteristic fitting curve.

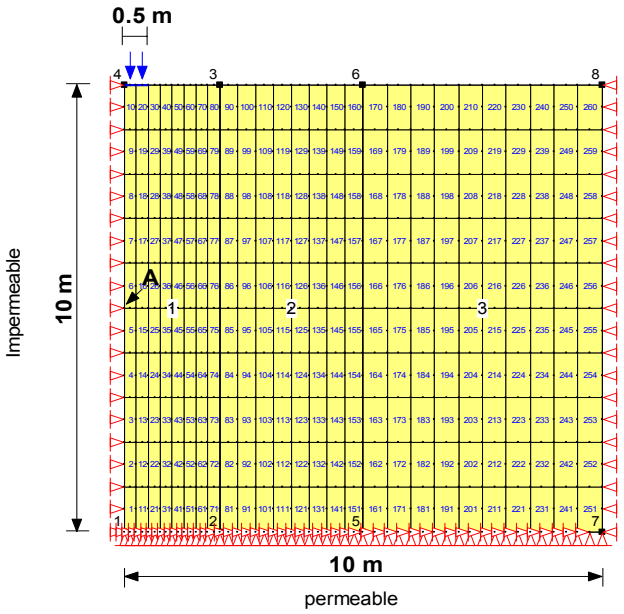

Fig.6 Typical finite element mesh of the soil beneath the footing.

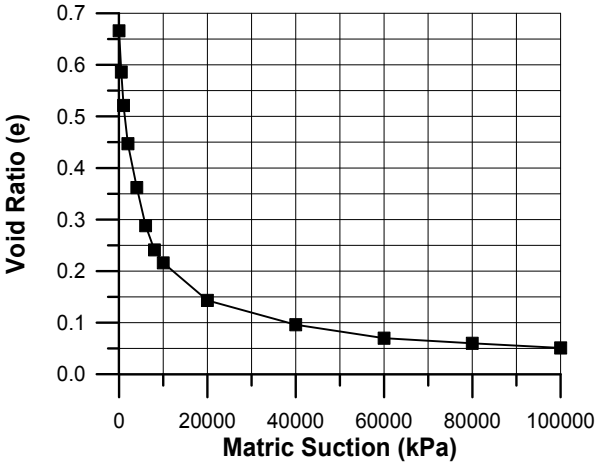

Fig. 7 Void ratio versus matric suction curve.

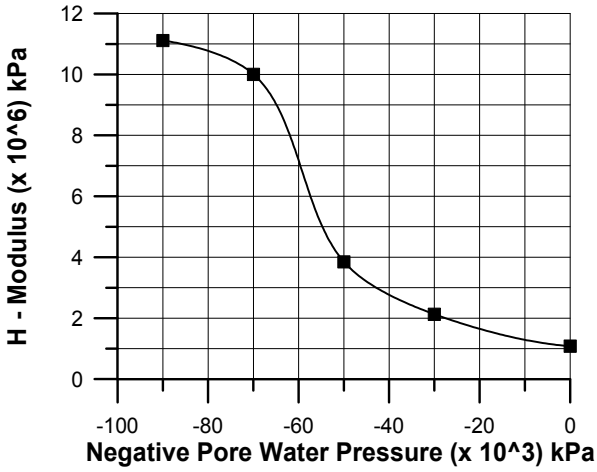

Fig. 8 H – Modulus function.

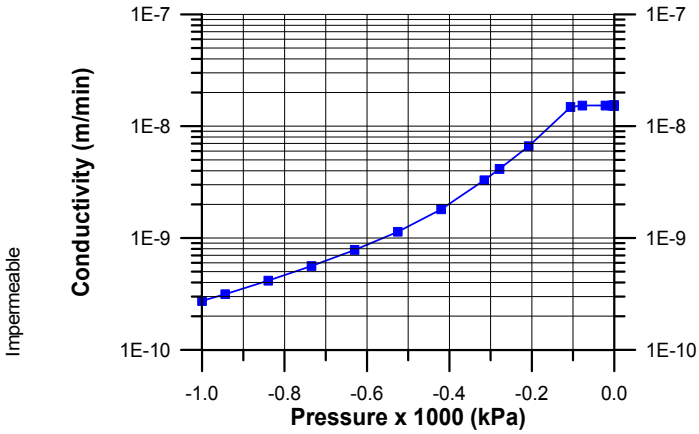

Fig. 9 Relation between the hydraulic conductivity and pore water pressure for partially saturated soils from Rusafa 1 as predicted from SEEP/W program.

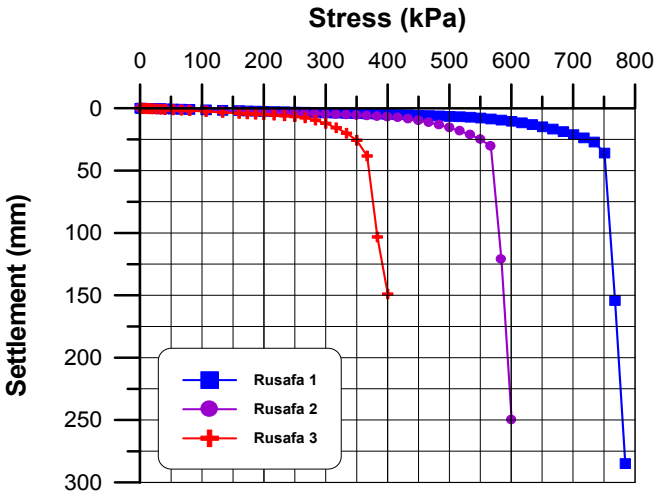

Fig. 10 Stress – settlement curve for a footing (1 m) wide over different types of fully saturated soil.

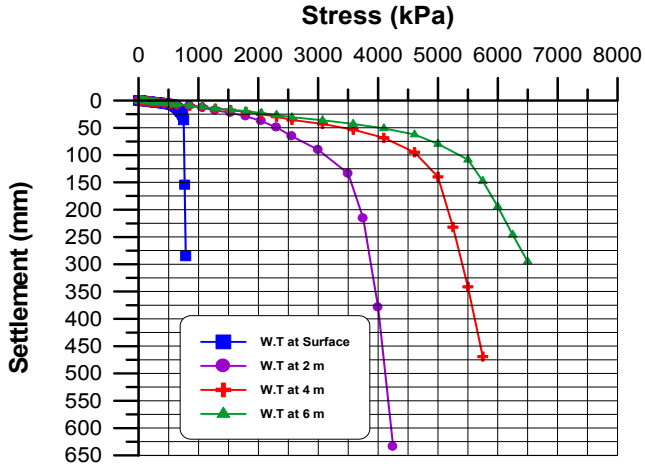

Fig.11 Stress – settlement curve for a footing (1 m) wide over Rusafa 1 soil with different conditions of water table depth at S = 90 %.

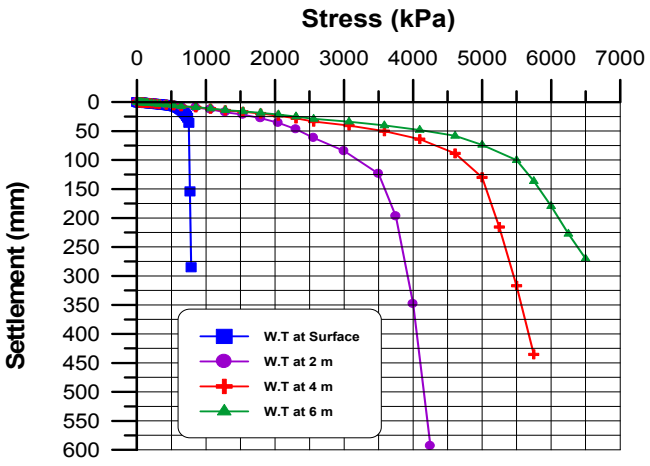

Fig 12 Stress – settlement curve for a footing (1 m) wide over Rusafa 1 soil with different conditions of water table depth at S = 80 %.

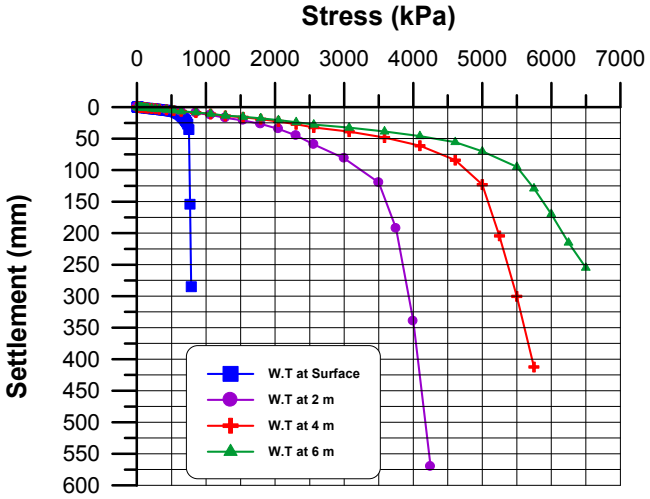

Fig.13 Stress – settlement curve for a footing (1 m) wide over Rusafa 1 soil with different conditions of water table depth at S = 70 %.

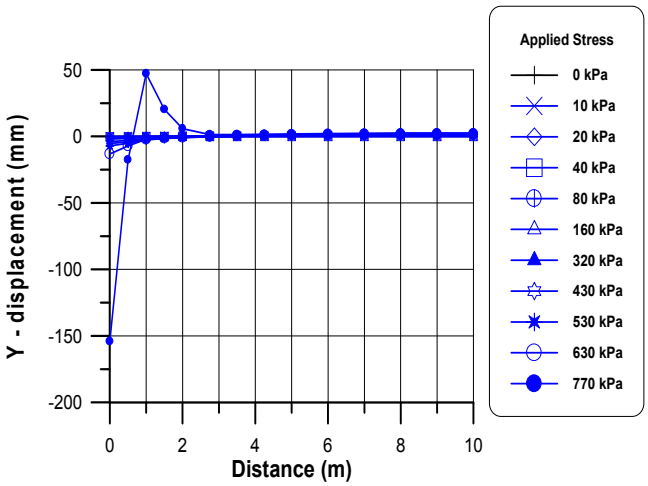

(a) Fully saturated soil.

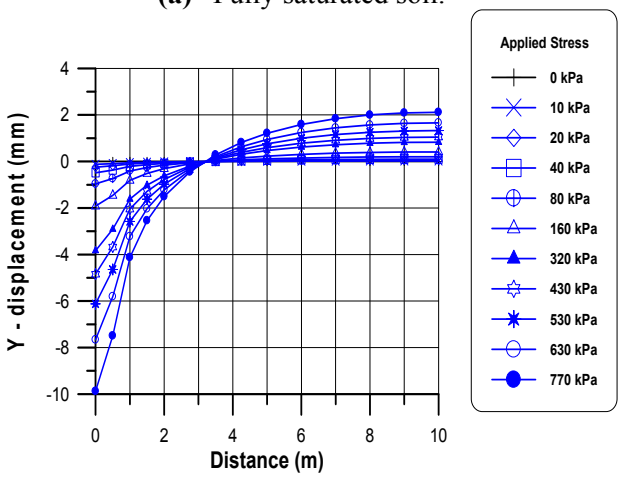

(a) Partially saturated soil, water table at depth 2 m (S = 90%).

Fig. 14 Variation of the vertical surface displacement along the distance from the center line of the footing of Rusafa soil.

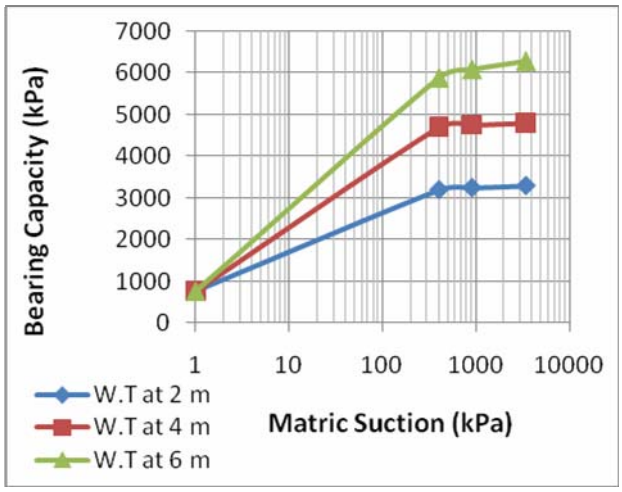

Fig. 15 Variation of the bearing capacity with respect to matric suction of Rusafa 1.

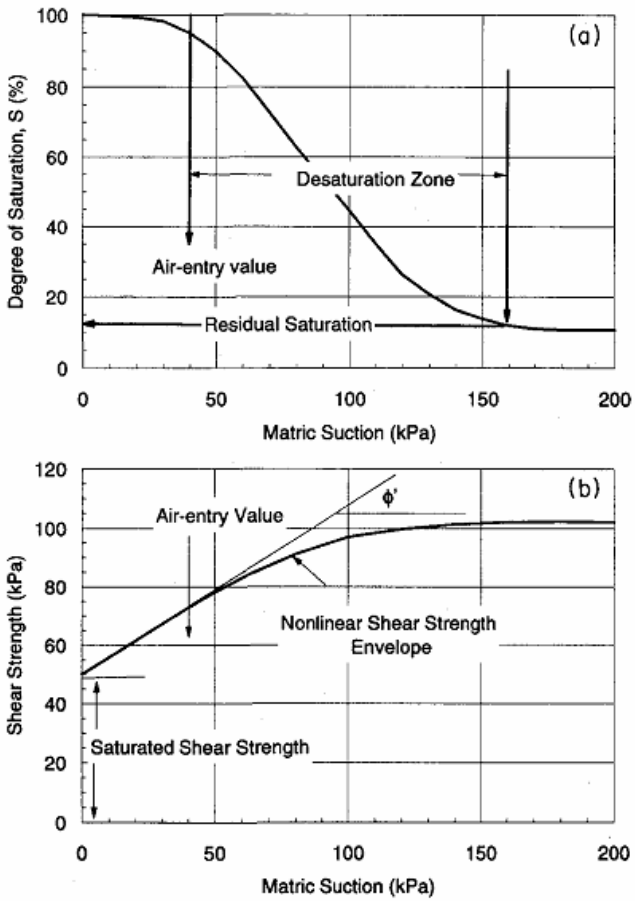

Fig. 16 Typical behavior of unsaturated soil.
(a) A typical soil water characteristic curve.
(b) Shear strength behavior of soil as it is related to the soil water characteristic curve, (from Vanapalli, et al., 1996).

Genetic Algorithm Optimization Model for Central Marches Restoration Flows with Different Water Quality Scenarios

Prof. Dr Rafa H. Al-Suhili and Zeren Jamal Ghafour

College of Engineering, University of Baghdad, Iraq.

ABSTRACT:

A Genetic Algorithm optimization model is used in this study to find the optimum flow values of the Tigris river branches near Ammara city, which their water is to be used for central marshes restoration after mixing in Maissan River. These tributaries are Al-Areed, Al-Bittera and Al-Majar Al-Kabeer Rivers. The aim of this model is to enhance the water quality in Maissan River, hence provide acceptable water quality for marsh restoration. The model is applied for different water quality change scenarios ,i.e. , 10%,20% increase in EC,TDS and BOD. The model output are the optimum flow values for the three rivers while, the input data are monthly flows(1994-2011),monthly water requirements and water quality parameters (EC, TDS, BOD, DO and pH).The objective function adopted in the optimization model is in a form the sum of difference in each of the 5 water quality parameters, resulting from the mixing equation of the waters of the rivers, from the accepted limits of these parameters , weighted by a penalty factor assigned for each water quality parameter according to its importance. The adopted acceptable limits are 1500,1000, 6,4 and 7, while the penalty factors are 1,0.8,0.8,0.8,and 0.2 for EC,TDS,BOD,DO,and pH respectively. The constraints adopted on the decision variables which the monthly flows of the three rivers are those that provide the monthly demands downstream each river, and not exceed a maximum monthly flow limits. The maximum flow limits adopted are for three flow cases, wet, average and dry years. For each flow case three scenarios for the monthly water quality parameters were adopted , the average values(scenario 1),the 10% increase in EC,TDS, and BOD (Scenario 2),and the 20% increase in these three water quality parameters (Scenario 3). Hence nine cases are adopted and for each an optimum monthly flows are found for each river. The genetic optimization model adopt a variable number of population of 100 to 1000 in a step of 100,0.8 and 0.2 cross over and mutation rates, and three iterations to reach the stable optimum solutions. The results indicates that the flow analysis shows a significant decrease in the flow values of the three rives after year 2000,hence, the flow values for the period of (1994-1999), are excluded and the only used values are those for (2000-2011). The estimated monthly demands exhibits low variation. The observed optimum monthly flow values decrease in general as the case flow changed from wet to normal and dry cases. The change in Scenarios from S1 to S2 and S3 , do not necessarily increase all the required optimum monthly flow values. The obtained minimum objective functions do not exhibits a certain trend with the change in the flow cases and/or the change in the scenarios.

KEY WORDS: Genetic Algorithm, Optimization, Water Quality Parameters, Electrical Conductivity, Total Dissolved Solids, BioChemical Oxygen Demand

نموذج الجينات الوراثية لايجاد الاطلاقات المطلوبة للجريان لانعاش الاهوار المركزية باستخدام عدة صيغ لنوعية المياه

الاستاذ الدكتور رافع هاشم السهيلي والباحثه زيرين جمال غفور
جامعه بغداد / كليه الهندسة / قسم المدني

لقد تم استخدام نموذج الجينات الوراثية في هذا البحث لحساب التصاريف المثلى لتفرعات نهر دجلة قرب مدينة العمارة حيث تستخدم مياهها لأعادة انعاش الاهوار المركزية وهذه التفرعات هي انهر العريض والبتيره والمجر الكبير بعد خلطها في مياه نهر ميسان. الهدف من هذا النموذج هو الحصول على افضل نوعية مياه لغرض الانعاش للاهوار المركزية.ولغرض الحصول على امثل التصاريف لهذه الانهر تم بناء برنامج حاسبة بلغة (MATLAB) حيث ان النتائج المستخرجة من البرنامج تمثل قيم التصاريف المثلى للانهر الثلاث وان المدخلات للبرنامج هي التصاريف للفترة من (1994-2011) و معدل الاستهلاك المائي الشهري ومعاملات نوعية المياه وهي (EC, TDS, BOD, DO and pH).

تهدف الدالة الهدفية (Objective Function) المستخدمة في نموذج البرمجة لتقليل المجموع الكلي لانحرافات معاملات نوعية المياه عن قيمها المسموح بها. الاولوية التي تم التعامل بها مع معاملات نوعية المياه تم تمثيلها باوزان معينة حسب اهمية كل معامل القيم للاوزان المستخدمة هي (1,0.8,0.8,0.8,0.2) لكل من (EC,TDS,BOD,DO,pH) على التوالي وذلك حسب اهمية كل معامل. اما معدل التزاوج و معدل المراوحة فهما (0.8, 0.2) على التوالي.

اما حجم المجتمع المطلوب فقد تم ايجاده بطريقة المحاولة والخطأ ابتداأ من (100) وحتى (1000) وبخطوة قدرها 100) حيث اعطت القيمة الأ خيرة حلا مستقرا وبعدد معاودات قدره (3).

استخدم النموذج ثلاث حالات لقيم معاملات نوعية المياه وثلاث حالات من الجريان (سنوات رطبة وطبيعية وجافة) لكل نهر. اما المحددات للتصاريف فقد كهنت قيم التصاريف الشهرية حسب نوع السنة المائية كحدود عليا وقيم المتطلبات الشهرية كقيم دنيا. تم تشغيل النموذج على الحالات التسعة ثلاث حالات للجريان كما ذكر سابقا رطبة و طبيعية وجافة ولكل حالة جريان ثلاث حالات لقيم نوعية المياه الحالة (S1) استخدمت فيها معدلات معايير نوعية المياه المقاسة والحالتين (S2) و(S3) باستخدام زيادة في قيم (EC,TDS, BOD) قدرها (10% و 20%) على التوالي. اضهرت النتائج لتحليل الجريان وجود انخفاض واضح بعد سنة (2000) عليه تم اعتماد التصاريف للفترة (2000-2011) فقط. كما وجد بان قيم المتطلبات الشهرية المحسوبة ذات تغاير قليل. اما قيم التصاريف الشهرية المثلى فقد وجد بانها تقل بشكل عام كلما تغيرت حالة الجريان من رطبة الى طبيعية و جافة. اما التغاير في قيم الجريان الامثل مع تغير حالة نوعية المياه من (S1) الى و (S2, S3) فقد وجد بانه ليس من الضروري وجود زيادة في قيمها. اما دالة الهدف الدنيا التي وجدت لكل الحالات التسعة اضهرت عدم وجود تدرج واضح في قيمها مع تغير حالة الجريان وحالة نوعية المياه.

INTRODUCTION:

The past activities in the Iraqi Marshes region had destroyed the environment and the nature of these marshes. These activities are either, establishing agriculture projects, holding ground roads , redistributing the rural settlement, and diverting water from those marshes by constructing dykes and canals. The central marsh is one of the largest marshes of the Mesopotamian. It consists of interconnected small marshes. The central marshes are bounded by Tigris river to the east and the Euphrates river to the south. The central marshes are roughly located between Nasiriyah, Maimona, Qalat Saleh and Al-Qurna Cities, and cover of about 3000 square Kilometers during flood season. This area reduced to 600 square Kilometers during normal season. The main sources of the water for the central marshes are the Tigris river tributaries within Ammara governorate. These tributaries are Al-Areed, Al-Bittera and Al-Majar Al-Kabeer rivers. Figure (1) and (2) shows the Mesopotamian marshes before and after the drying process respectively, (Al-Suhiaili and Hraizeو 2006).

Al-Badri and Artin (1972) had studied the salinity problem in Tigris and Euphrates rivers and Thurthar lake. They concluded that at future an expected increase in the salinity levels due to upstream increasing water use and disposal and due to the Turkish activites proposed a case which observed later. Buras (1972) had proposed an optimum management of water resources for Iraqi marshes for a better water quality.. Firas (1989) had pointed out the importance of environmental considerations in optimization models for Derbindikhan reservoir. Mussab(1998) had presented an optimization model for Saddam and Dokan reservoir and their effect on Tigris River water Quality.Hassan(2001) had pointed out the environmental effects of marshes drying process.

Nicholson et. al,(2002), and Clarck et. al,(2001) had conducted an environmental study of Iraqi marshes and pointed out the negative effect of the drying process. Iraq Foundation (2003) had studied the scientific bases for marshes restoration in Iraq. Richardson and Hussain (2005) had conducted an ecological study for the Iraqi marshes and pointed out the importance of water quality to the eco-system of these marshes. Farhan (2005) had reported the importance of water quality for marshes restoration.

The construction of Maissan River with dykes along its sides was the main action performed by the past regime for conducting a drying process for the central marshes.. The alignment of this river prevents water of the Tigris three tributaries Al-Areed, Al-Bittera and Al-Majar Al-Kabeer from entering the central marshes. The proposed restoration process is to remove or break these dykes to allow the water to enter the marshes. Therefore the control of this river water quality is important for this restoration process. The problem of the high salinity level of the dried soil of the marshes left after the drying process is an important issue; hence, the proper control of the salinity and other environmental parameters will improve the water quality in Maissan river and will have an important role on the quality of the water used for the restoration process.

Since at the upstream side of each of the three rivers Al- Areed, Al-Bittera and Al-Majar Al-Kabeer there exists a regulator , which can control the released flow. An optimization model could be adopted to find these optimum releases to get the best water quality in Maissan river, and then the best water quality of the water entering the marshes for restoration. In this research , a proposed optimization model was used for this purpose. This model is a

modified one of that proposed optimization model used by Al-Suhaili and Hraze (2006). The modifications made herein from this model are the use of additional flow and water quality measured data of these rivers (2006-2011), in addition to the original set used in the former model (1994-2005). This modification impose changes in the constraints used for the optimization process. Moreover the proposed solution of the new model is the use of Genetic Algorithm instead of the general search method. Furthermore the estimation of monthly demands along the mentioned three rivers was also extended to the new period added. Moreover the model analysis was extended for three scenarios (S1: using obtained average monthly water quality parameters as Electrical Conductivity EC, Total Dissolved Solids TDS,Biochemical oxygen Demand BOD, Dissolved Oxygen DO, and pH.), and Scenarios S2 and S3 with 10% and 20% increase in EC,TDS,and BOD, respectively. The adopted acceptable limits are 1500,1000, 6,4 and 7, while the penalty factors are 1,0.8,0.8,0.8,and 0.2 for EC,TDS,BOD,DO,and pH respectively

The Proposed Optimization Model:

The proposed optimization model is to minimize the water quality function represented by the following function:

$$Min(f) = \sum\sum_{k=1}^{nk}\left[\frac{\sum_{k=1}^{3}\overline{Q}_{i,j}C_{i,j,k}}{\sum_{i=1}^{3}\overline{Q}} - C_k\right] * P_k \quad (1)$$

Where:

$$\overline{Q}_{i,j} = Q_{i,j} - D_{i,j} \geq 0, otherwise Qi, j = 0, \quad (2)$$

Subject to the following constraints:

$$D_{i,j} \leq Q_{i,j} \leq Q_{i,j\max}$$

During wet years

And

$$D_{i,j} \leq Q_{i,j} \leq Q_{i,j\min}$$

During dry years

And

$$D_{i,j} \leq Q_{i,j} \leq Q_{i,jave.}$$

During normal years

Where:

C_k = Acceptable limit of water quality parameter k.

p_k = Relative penalty weight for the k quality parameter.

For the upper limit acceptable concentration of the water quality parameter p_k will be positive and:

$$P_k = \begin{bmatrix} greaterthan0, lessorequal1 \\ o \end{bmatrix}_{C^*_{k,j}<0}^{C^*_{k,j}\geq 0}$$

For the lower limit acceptable water quality parameter p_k will be negative,and:

$$P_k = \begin{bmatrix} greaterthan0, lessorequal1 \\ 0 \end{bmatrix}_{C^*_{k,j}>0}^{C^*_{k,j}\leq 0}$$

$$C^*_k = \frac{\sum_{i=1}^{m} Q_{i,j}C_{i,j}}{\sum_{i=1}^{m} Q_i C_i} - C_k \quad (3)$$

J= 1, 2, 3 ….12, represent the month starting from October and ending at September, respectively, as the water year of Tigris river.

K= Subscript for water quality parameters type k

i=1, 2, and 3, which represent the rivers, Al-Areed, Al-Bittera, and Al-Majar Al Kabeer rivers respectively.

Qi, j: are the optimum water release from the river i, at the month j.

Di, j: are the demand along the river i, at month j for the area located between the upstream of regulator to the location where the river i, enters Maissan river.

Qi, j min: are the minimum flow from river i at month j(Dry Year).

Qi, j max: are the maximum flow from river i at month j(Wet Year).

Qi, j ave: are the average flow from river i at month j(Normal Year).

Ci, j, k: Is the average values of the river i, at month j of the k water quality parameter.

The objective function was adopted by assuming complete mixing of water at Maissan river. The above formulated optimization model requires the monthly flow values of the three rivers, the average EC, TDS, BOD, DO and pH and the monthly demands for each area downstream each river. These are estimated from the observed flows and water quality parameters for the three rivers for (1994-2011).

PREPERATION OF THE DATA REQUIRED FOR THE PTIMIZATION MODEL:

Flow Data Analysis:

The data collected were the monthly flow data in $m^3/\sec$ for a record of (18) year long (1994-2011) for the three rivers. Examination of those data indicates a remarkable decrease in the available water for Al-Areed, Al-Bittera and Al-Majar Al-Kabeer rivers as shown in figure (3). Hence, the flow data for the first six years were excluded and the analysis were performed on the flow of the most resent years (2000-2011), for the three rivers.

If we, consider the flow data as normally distributed with mean value μ and standard deviation σ, so the data can be divide into three categories for each river.

I. Normal year: represents the average of flow values that fall within the interval $(\mu+\sigma/2, \mu-\sigma/2)$.

II. Dry year: represents the average of flow values below the value $(\mu-\sigma/2)$.

III. Wet year: represents the average of flow values above the value $(\mu+\sigma/2)$.

Table (1) shows the average flow values available in the selected three rivers in $m^3/\sec$,for wet,normal and dry years.

Demand Analysis:

The demand data were collected from different authorities that had conducted demand calculations during the most recent years (2000-2011). These data were collected from the demand sheets recorded

by the general management of water resources, and the office of environmental of Maissan governorate (unpublished records). Table (2) shows the estimated demand values for the three rivers.

WATER QUALITY DATA USED IN THE OPTIMIZATION MODEL:

The available records of the water quality data for Al-Areed, Al-Bittera and Al-Majar Al-Kabeer rivers are inadequate for the purpose of the proposed optimization model. Hence, a water quality-testing program was conducted in some selected points to get the required additional data. The criteria of the selection adopted for those points is for each river two points were selected at the upstream side (downstream of the regulator existing on the river), while the other point is at the downstream side of the river, just before its outfall to Maissan river. The water quality parameters gathered are TDS, EC, pH, DO, BOD water temperature and air temperature. Tables (3), (4) and (5) show the measured and estimated average monthly values of (EC, TDS, BOD, DO and pH) for Al-Areed, Al-Bittera and AL-Majar Al-Kabeer rivers respectively.

APPLICATION OF THE OPTIMIZATION MODEL:

In this study, a MATLAB program was used to find the optimum flow values for Al-Areed, Al-Bittera and Al-Majar Al-Kabeer rivers using genetic algorithm optimization .The optimum flow values and the objective function are obtained for the three scenarios and the three flow cases wet , normal and dry years. Tables(3,4, and 5) show the water quality parameters for scenario S1,while tables (6,7, and 8) show these values for scenario S2. For scenario S3 these values are shown in tables(9,10, and 11). Hence the total cases analyzed are 9 cases S1(Wet, Normal, and Dry),S2 (Wet, Normal, and Dry), and S3 (Wet,Normal, and Dry).

RESULTS AND DISCUSSION:

For the optimization process a MATLAB code is written. The adopted cross over and mutation rates are 0.8 and 0.2 respectively. The number of population is found by trial and error procedure until obtaining a stable optimum solution. It is increased from 100 to 1000 in a step of 100, at 1000 a stable solution is found .

Table(12) shows the optimum monthly flow values for the three rivers for Scenarios S1 for the three flow cases. Figures (4,5, and 6) show these values with the adopted average water quality parameters and the estimated flows and demands. It is shown that in general as the flow case changes from wet to normal and dry year the optimum flow decreases.

Table(13) shows the optimum monthly flow values for the three rivers for Scenarios S2 for the three rivers with the three flow cases. Figures (7,8, and 9) show these values with the adopted 10% increase in water quality parameters (EC,TDS, and BOD)and the estimated flows and demands. It is shown that in general as the flow case changes from wet to normal and dry year the optimum flow decreases.

Table(14) shows the optimum monthly flow values for the three rivers for Scenarios S2 for the three flow cases. Figures (10,11, and 12) show these values with the adopted 20% increase in water quality parameters (EC,TDS, and BOD) and the estimated flows and demands. It is shown that in general as the flow case changes from wet to normal and dry year the optimum flow decreases.

Table(15) shows the obtained minimum objective function for the 9 cases adopted in the analysis. It is shown that the values do not exhibit a certain trend with the changes of flow case or the change in the scenario.

Figure(13) shows the comparison between the obtained optimum flow values for each of the three rivers, for Scenario S1, for wet, normal and dry years . It is found that the dry case flow gives the minimum flow

values, while the maximum values are obtained for the wet year flow cases, the normal flow case are in between the wet and dry values ,however some few values exceed the corresponding values for the wet case flow.
Figures(14 and 15) show the comparison between the obtained optimum flow values for each of the three rivers, for Scenarios S2, and S3 for wet, normal and dry years . Similar observation can be deduced as those for Figure (13).
Figure(16) shows the comparison between the obtained optimum flow values for each of the three rivers, for a wet year and the different scenarios. It is observed that for scenario S3 the optimum flow are almost the highest, however for few monthly optimum flow it becomes lower than that for S2 and/or S1 flow values.
Figures(17 and 18) show the comparison between the obtained optimum flow values for each of the three rivers, for a normal and a dry year respectively and each for the different three scenarios. Similar observations can be deduced as those observed from Figure(16).

CONCLUSIONS:

1. The analysis of the (12) years for the period (1994-2005), of historical monthly stream flow for the three rivers indicates significant changes occurred through the period of record which means that the series is not homogeneous. Hence, the values for the flow for the period(1994-1999) are excluded from the analysis and those used are for the period of (2000-2011).

2. The demand analysis indicates low variation with little increase in summer months.

3. The Genetic algorithm optimization model that use a 0.8 and 0.2 cross over and a mutation rates, required a minimum population of 1000 to obtain a stable optimum solution.

4. In general as the flow case changes from wet to normal and dry year , the optimum flow values required decreases, however for few months sometimes the optimum flow for normal year exceeds the corresponding value for the wet year. This conclusion is true for all of the three scenarios analyzed.

5. The comparison between the optimum monthly flow values for different scenarios for a given case flow , indicates in general the highest flow are for S3,however it is not always the case since so many values exhibits high flow values for S2 and/or S1.

6. The minimum observed objective function obtained for the 9 cases analyzed exhibits no certain trends with the change in case flow or with the change in the water quality scenario.

REFERENCES:

Al-Badri, M. and Artin, Y., "Study of salinity of Tigris and Euphrates rivers and Thurthar Lake with Environmental consideration", 1972.

Al-Suhaili, R.H, and Hraze, S. J.. "Optimum Releases for the Central Marshes restoration", submitted for publication to Journal of Engineering, College of Engineering, Univ. of Baghdad, 2006.

Buras, N., "Scientific allocation of water resources", American Elsevier publishing company, New York, 1972.

Richardson, C.J. and Hussain, N. A. Hussain, "An ecological assessment of the marshes of Iraq", 2005.

Farhan, A., "The role of hydrology in marsh restoration in southern Iraq", Montréal/Canada, 2005.

Firas, T.N., "optimum operation of Derbendi-Khan with environmental considerations", M.Sc. Thesis, university of Baghdad, 1989.

Hassan, "The Mesopotamian marshlands report united nations environmental program", 2001. Available online at: http//earthobservatory.nasa.gov/newsroom /newimages/meso2.pdf.

Hussain NA., "Ahwar of Iraq: An environmental approach", Marine Science Center / Basra University, 2001.

Mussab, M.R., "Optimum operation for Saddam and Dokan and their effect on Tigris River", M.Sc. Thesis, University of Baghdad, 1998.

Nicholson, Emma and Clarck, "The Iraqi marshlands: a human and environmental study", 2002.

Clarck, P. and Magee, S., Amar International Charitable Foundation, "The Iraqi marshlands environmental study", 2001.

Tewei Dai and John W.Labadi, "Integration of Water quantity/quality in river basin", Colorado University Department of Civil Engineering,1997.

The Iraq Foundation, "Building and scientific basis for restoration of the Mesopotamian marshlands", 2003.

United Nation Environmental Program (UNEP), "The Mesopotamian marshlands: demise of an ecosystem", 2001.

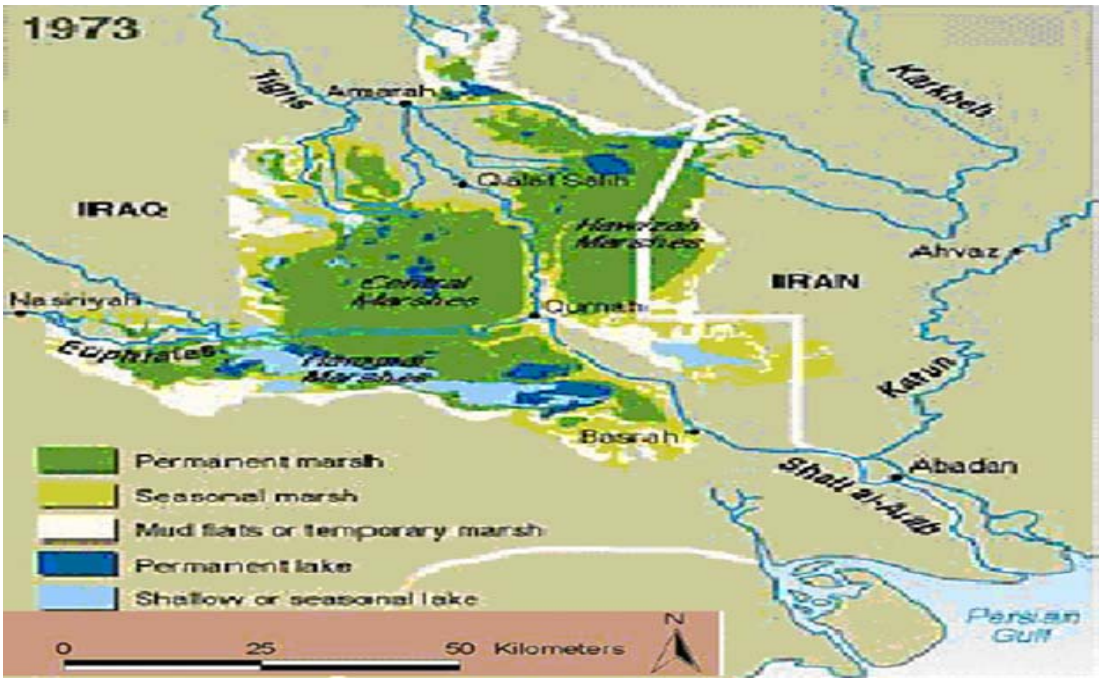

Figure (1) The Mesopotamian Marshes before Drying (UNEP, 2001).

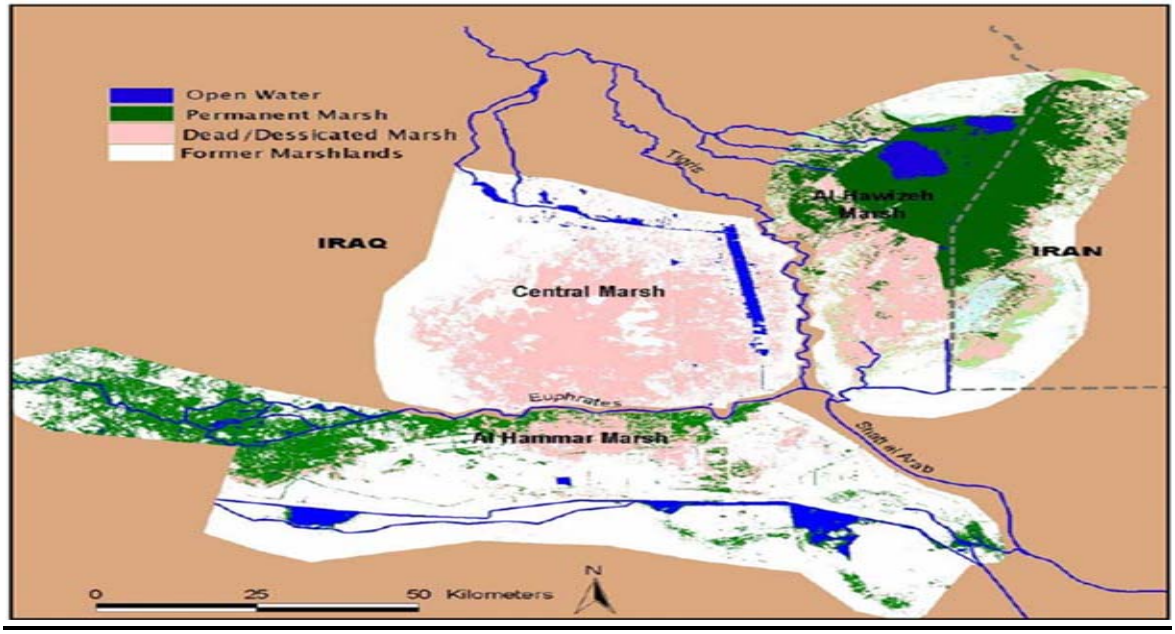

Figure (2) The Mesopotamian Marshes after Drying (UNEP, 2001).

Table (1) Average monthly Flow Values in m^3/sec Available in the Selected Three rivers.(2000-2011)

Month	Oct	Nov	Dec	Jan	Feb	Mar	Apr	May	Jun	Jul	Aug	Sep
Al-Areed river												
Wet	18	16	21	14	16	19	35	25	28	24	25	16
norm	11	11	14	11	11	12	16	12	12	13	14	12
Dry	7	6	10	7	6	8	11	7	9	9	8	9
Al-Bittera river												
Wet	28	44	45	41	45	59	130	58	32	33	41	33
norm	15	22	22	16	23	22	33	26	20	26	31	25
Dry	10	12	14	10	12	9	11	10	9	10	11	12
Al-Majar Al-Kabeer river												
Wet	28	32	34	32	28	31	32	31	30	28	27	24
norm	24	23	28	28	27	25	28	24	25	20	22	19
Dry	16	16	22	19	17	18	20	14	18	12	19	13

Table (2) Estimated Monthly Demand Values in m^3/sec Upstream of Maissan river.

month river	Oct	Nov	Dec	Jan	Feb	Mar	Apr	May	Jun	Jul	Aug	Sep
Al-Areed	6	5	7	5	5	6	8	5	7	7	7	7
Al-Bittera	8	9	11	9	9	8	10	8	9	8	8	8
Al-Majar Al-Kabeer	10	10	9	9	9	10	10	10	10	10	10	9

Table (3) Average values of (EC, TDS, BOD, DO and pH) for Al-Areed river (downstream)(2000-2011) Scenario S1.

month par.	Oct	Nov	Dec	Jan	Feb	Mar	Apr	May	Jun	Jul	Aug	*Sep*
EC	1650	1498	1498	1487	1456	1466	1489	1350	1440	1895	1560	*1950*
TDS	910	1115	1002	1046	1067	1115	1076	1185	1096	1022	1089	*886*
BOD	6.5	5.3	5.2	4.9	4.8	4.7	4.6	4.1	3.9	5.0	4.2	*5.8*
DO	6	5.0	5.2	5.8	5.0	5.8	5.4	4.8	5.2	5.3	6.1	*6*
pH	*8*	*7.8*	*7.9*	*7.7*	*7.8*	*7.9*	*7.8*	*8*	*7.8*	*7.6*	*7.8*	*8*

Table (4) Average values of (EC, TDS, BOD, DO and pH) for Al-Bittera river (downstream) (2000-2011) Scenario S1..

month par.	Oct	Nov	Dec	Jan	Feb	Mar	Apr	May	Jun	Jul	Aug	*Sep*
EC	1500	1808	1780	1757	1780	1830	1710	1750	1870	1920	2200	*1600*
TDS	1020	1140	1143	1140	1150	1145	1140	1150	1200	1200	1250	*990*
BOD	5	3.9	3.9	4	3.6	4	3.9	4	4.5	3.8	3.7	*5*
DO	5.7	6.5	6	5.8	6	6.5	6.5	5.3	5.1	5.4	5.5	*5.4*
pH	*8*	*8.1*	*8.1*	*8.2*	*8.1*	*8.1*	*8.1*	*7.9*	*8.3*	*8.1*	*8.1*	*6*

Table (5) Average values of (EC, TDS, BOD, DO and pH) for Al-Majar Al-Kabeer river (downstream).(2000-2011) Scenario S1.

month par.	Oct	Nov	Dec	Jan	Feb	Mar	Apr	May	Jun	Jul	Aug	*Sep*
EC	1560	1470	1550	1570	1350	1780	1700	1450	1600	1500	1500	*1800*
TDS	980	800	1020	950	1010	800	850	800	850	690	1000	*800*
BOD	5.2	5.9	6	6.2	6.1	6	6.2	6.3	5.9	6.7	5.2	*6.1*
DO	6	6	6.8	6.3	6	6.2	5.5	5.7	5.8	5.1	5.1	*5.7*
pH	*8.1*	*8.2*	*8.2*	*8.2*	*8.2*	*8.2*	*8.2*	*7.8*	*8.1*	*8.1*	*8.1*	*8*

Table (6) Proposed values of (EC, TDS, BOD, DO and pH) for Al-Areed river (downstream) for Senario (2)

month par.	Oct	Nov	Dec	Jan	Feb	Mar	Apr	May	Jun	Jul	Aug	Sep
EC	1815	1647.8	1637.9	1635.7	1601.6	1612.6	1637.9	1485	1584	2084.5	1716	2145
TDS	1001	1226.5	1102.2	1150.6	1173.7	1226.5	1183.6	1303.5	1205.6	1124.2	1197.9	974.6
BOD	7.15	5.83	5.72	5.39	5.28	5.17	5.06	4.51	4.29	5.5	4.62	6.38
DO	6	5.0	5.2	5.8	5.0	5.8	5.4	4.8	5.2	5.3	6.1	6
pH	8	7.8	7.9	7.7	7.8	7.9	7.8	8	7.8	7.6	7.8	8

Table (7) Proposed values of (EC, TDS, BOD, DO and pH) for Al-Bittera river (downstream) for Senario (2)

month par.	Oct	Nov	Dec	Jan	Feb	Mar	Apr	May	Jun	Jul	Aug	*Sep*
EC	1650	1988.8	1958	1932.7	1958	2013	1881	1925	2057	2112	2420	1760
TDS	1122	1254	1257.3	1254	1265	1259.5	1254	1265	1320	1320	1375	1089
BOD	5.5	4.29	4.29	4.4	3.96	4.4	4.29	4.4	4.95	4.18	4.07	5.5
DO	5.7	6.5	6	5.8	6	6.5	6.5	5.3	5.1	5.4	5.5	*5.4*
pH	*8*	*8.1*	*8.1*	*8.2*	*8.1*	*8.1*	*8.1*	*7.9*	*8.3*	*8.1*	*8.1*	*6*

Table (8) Average values of (EC, TDS, BOD, DO and pH) for Al-Majar Al-Kabeer river (downstream) Senario (2)

month par.	Oct	Nov	Dec	Jan	Feb	Mar	Apr	May	Jun	Jul	Aug	*Sep*
EC	1716	1617	1705	1727	1485	1958	1870	1595	1760	1650	1650	1980
TDS	1078	880	1122	1045	1111	880	935	880	935	759	1100	880
BOD	5.72	6.49	6.6	6.82	6.71	6.6	6.82	6.93	6.49	7.37	5.72	6.71
DO	6	6	6.8	6.3	6	6.2	5.5	5.7	5.8	5.1	5.1	*5.7*
pH	*8.1*	*8.2*	*8.2*	*8.2*	*8.2*	*8.2*	*8.2*	*7.8*	*8.1*	*8.1*	*8.1*	*8*

Table (9) Proposed values of (EC, TDS, BOD, DO and pH) for Al-Areed river (downstream) for Senario (3)

month par.	Oct	Nov	Dec	Jan	Feb	Mar	Apr	May	Jun	Jul	Aug	*Sep*
EC	1980	1797.6	1786.8	1784.4	1747.2	1759.2	1786.8	1620	1728	2274	1872	2340
TDS	1092	1338	1202.4	1255.2	1280.4	1338	1291.2	1422	1315.2	1226.4	1306.8	1063.2
BOD	7.8	6.36	6.24	5.88	5.76	5.64	5.52	4.92	4.68	6	5.04	6.96
DO	6	5.0	5.2	5.8	5.0	5.8	5.4	4.8	5.2	5.3	6.1	*6*
pH	*8*	*7.8*	*7.9*	*7.7*	*7.8*	*7.9*	*7.8*	*8*	*7.8*	*7.6*	*7.8*	*8*

Table (10) Average values of (EC, TDS, BOD, DO and pH) for Al-Bittera river (downstream) For Senario (3)

month par.	Oct	Nov	Dec	Jan	Feb	Mar	Apr	May	Jun	Jul	Aug	*Sep*
EC	1800	2169.6	2136	2108.4	2136	2196	2052	2100	2244	2304	2640	1920
TDS	1224	1368	1371.6	1368	1380	1374	1368	1380	1440	1440	1500	1188
BOD	6	4.68	4.68	4.8	4.32	4.8	4.68	4.8	5.4	4.56	4.44	6
DO	5.7	6.5	6	5.8	6	6.5	6.5	5.3	5.1	5.4	5.5	*5.4*
pH	*8*	*8.1*	*8.1*	*8.2*	*8.1*	*8.1*	*8.1*	*7.9*	*8.3*	*8.1*	*8.1*	*6*

Table (11) Average values of (EC, TDS, BOD, DO and pH) for Al-Majar Al-Kabeer river (downstream) Scenario (3)

month par.	Oct	Nov	Dec	Jan	Feb	Mar	Apr	May	Jun	Jul	Aug	*Sep*
EC	1872	1764	1860	1884	1620	2136	2040	1740	1920	1800	1800	2160
TDS	1176	960	1224	1140	1212	960	1020	960	1020	828	1200	960
BOD	6.24	7.08	7.2	7.44	7.32	7.2	7.44	7.56	7.08	8.04	6.24	7.32
DO	6	6	6.8	6.3	6	6.2	5.5	5.7	5.8	5.1	5.1	*5.7*
pH	*8.1*	*8.2*	*8.2*	*8.2*	*8.2*	*8.2*	*8.2*	*7.8*	*8.1*	*8.1*	*8.1*	*8*

Table (12) Optimum Flow Values for (wet, normal and dry years) for Al-Areed, Al-Bittera and Al-Majar Al-Kabeer rivers (Scenario 1).

Month	Oct	Nov	Dec	Jan	Feb	Mar	Apr	May	Jun	Jul	Aug	Sep
Wet years												
Areed	9.4	10.6	20.8	8.5	12.5	6,5	21.1	23.3	23.2	9.5	23.5	12
Bittera	12.8	18.3	16.5	19.5	18.2	16.9	30.6	43.53	24	11.2	31	14.5
Majar	14	30	30	29	16.5	25.9	22.4	30.2	29.2	18.9	21.8	19.6
Normal years												
Areed	7	9.3	13.6	7.8	6.3	10.8	15.3	10.2	7.3	7.7	10.4	9
Bittera	11.2	15.3	12.1	10.3	17.6	20.5	28.6	18.1	10.7	14	14.8	12.3
Majar	20	20	26	26	20	20	20	21	23	17	22	18
Dry years												
Areed	6.1	5.7	8.8	5	5.8	7.8	9.1	6.1	8.9	8.9	7.2	7.8
Bittera	9.6	9.2	12.5	9.7	11.5	8.7	10.7	8.4	9	8.8	9.9	9.2
Majar	15.6	14	16.9	12	15.7	14.4	16.8	12.5	15.1	10.9	11.7	12.6

Table (13) Optimum Flow Values for (wet, normal and dry years) for Al-Areed, Al-Bittera and Al-Majar Al-Kabeer rivers (Scenario 2).

Month	Oct	Nov	Dec	Jan	Feb	Mar	Apr	May	Jun	Jul	Aug	Sep
Wet years												
Areed	6	12.5	18.6	11.2	11.9	8.8	30.9	9.4	25.1	24	16.8	10.8
Bittera	16.3	41.4	40	14.8	36	15.5	102.8	17.5	24.5	21.1	32.8	32.1
Majar	26.6	31.5	25.1	21.3	21	25.2	26.1	14.8	29.4	19	17.9	32.1
Normal years												
Areed	7.2	8.7	9	6.9	8.2	7.7	15.7	8.3	11.8	10	10.6	7.8
Bittera	11.7	13.5	14.6	12.9	12.7	15	31.2	22.5	15.4	10.1	9	19
Majar	17.8	22.6	17.4	21.3	17.5	15.3	20.8	22.5	12.5	14.9	21.8	16.1
Dry years												
Areed	6.1	5.8	8.8	6.6	5.9	7.1	10.7	5.8	8.2	7.5	8	7
Bittera	8.6	9.6	13.9	9.8	9.2	8	10.8	9.8	9	8	9.5	9.6
Majar	12.9	12.6	18.6	14.4	10.6	11.8	19.5	11.2	10.9	11.8	13.8	11.7

Table (14) Optimum Flow Values for (wet, normal and dry years) for Al-Areed, Al-Bittera and Al-Majar Al-Kabeer rivers (Scenario 3).

Month	Oct	Nov	Dec	Jan	Feb	Mar	Apr	May	Jun	Jul	Aug	Sep
Wet years												
Areed	17.2	14.6	20.7	13.6	15.7	10	28.2	16.5	27.9	16.9	23.9	13.4
Bittera	21	22	29	18.7	32.6	19.3	82.3	23.3	15.6	12.4	32.8	10.4
Majar	27.9	21.2	19.5	31.5	13.6	30.6	32	17.5	19.7	27	26.5	12.9
Normal years												
Areed	10.3	10.3	9.7	5.9	7.3	8.8	12.1	7.9	11.3	12.2	13	11.7
Bittera	8.2	18.5	16.5	15	12.8	16.7	21.8	14.9	11.9	20.2	16.4	14.5
Majar	23.1	16.8	16	18.7	14.5	19	27.3	17.6	21.2	17.5	14	18.2
Dry years												
Areed	7	5.5	9.6	5.8	5	8	10.5	5.6	8.4	8.8	7.8	7.6
Bittera	9.2	11.4	13.7	9.4	11.2	8.7	10.9	8.9	9	9.3	9.5	9.3
Majar	16	15	12.2	11	14.3	10.6	15.5	11	13	12.9	12.8	12.4

Table (15) Minimum Obtained Objective Function Values for all of the Scenarios and Flow Cases.

Scenario	Wet	Normal	Dry
S1	74.96	77.30	76.19
S2	79.57	78.20	79.82
S3	85.87	76.86	76.88

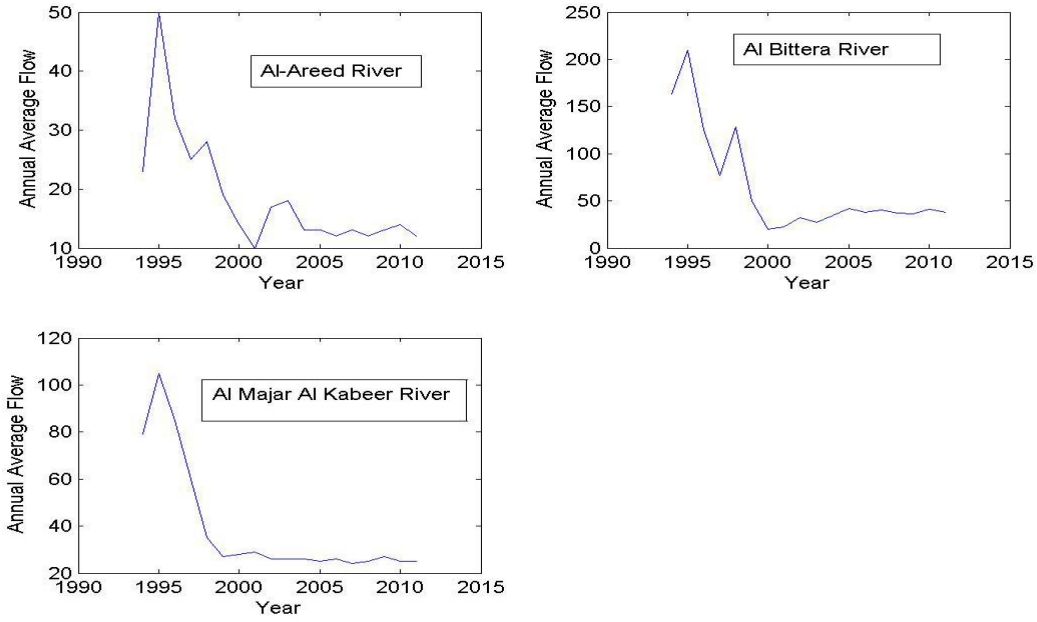

Fig(3) Average Annual Flow for the Three Rivers, Al Areed, Al Bittera ,and Al Majar Al kabeer (1994-2011).

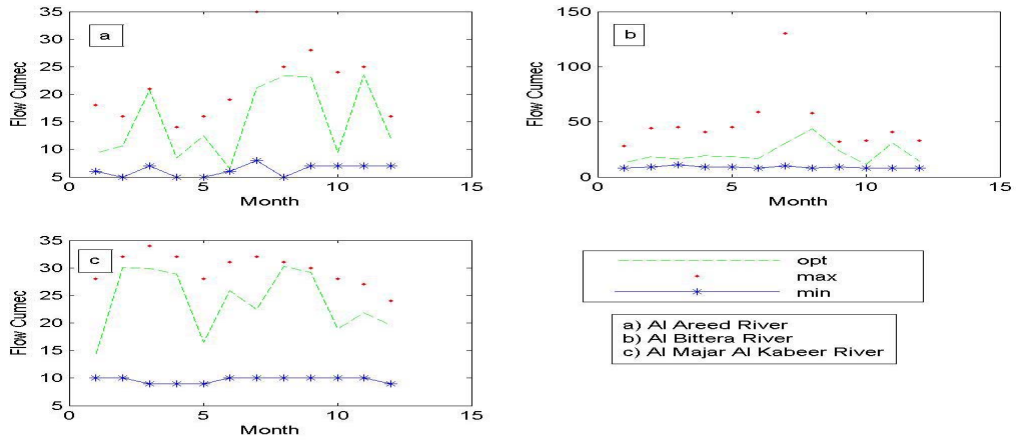

Fig(4) Optimum Monthly Flow Values for Scenario (S1), Average Water Quality, for a Wet year.

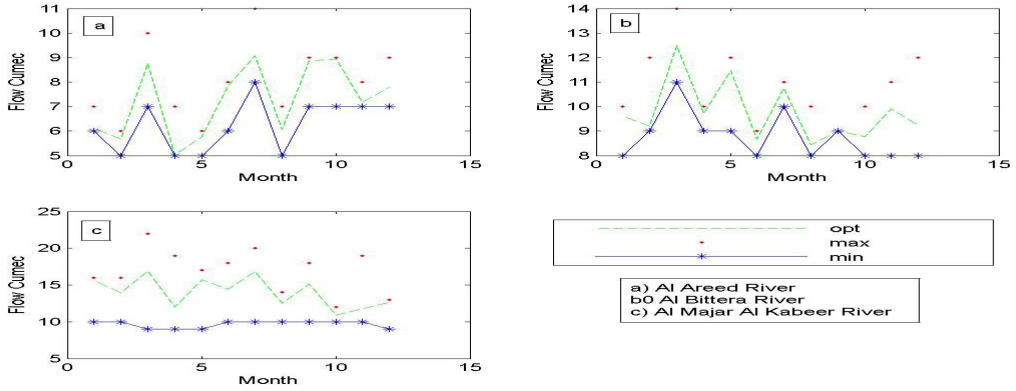

Fig(5) Optimum Monthly Flow Values for Scenario (S1), Average Water Quality, for a Normal Year.

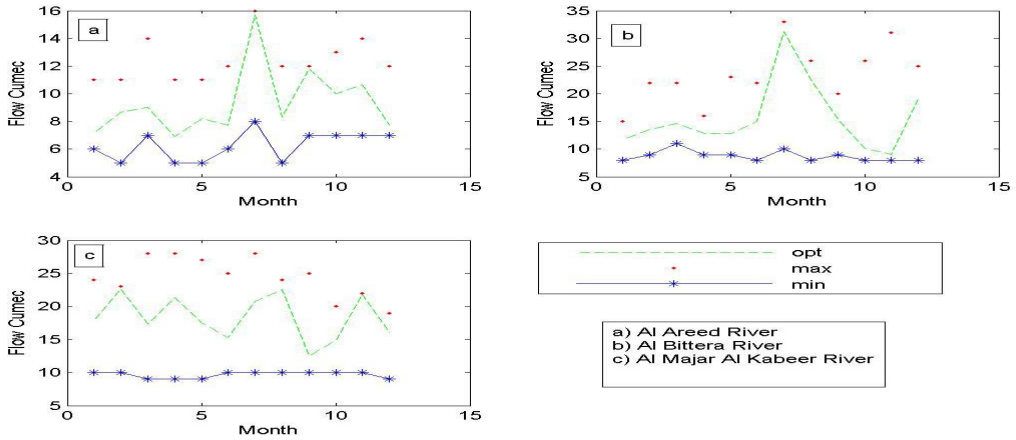

Fig(6) Optimum Monthly Flow Values for Scenario (S1), Average Water Quality, for a Dry Year.

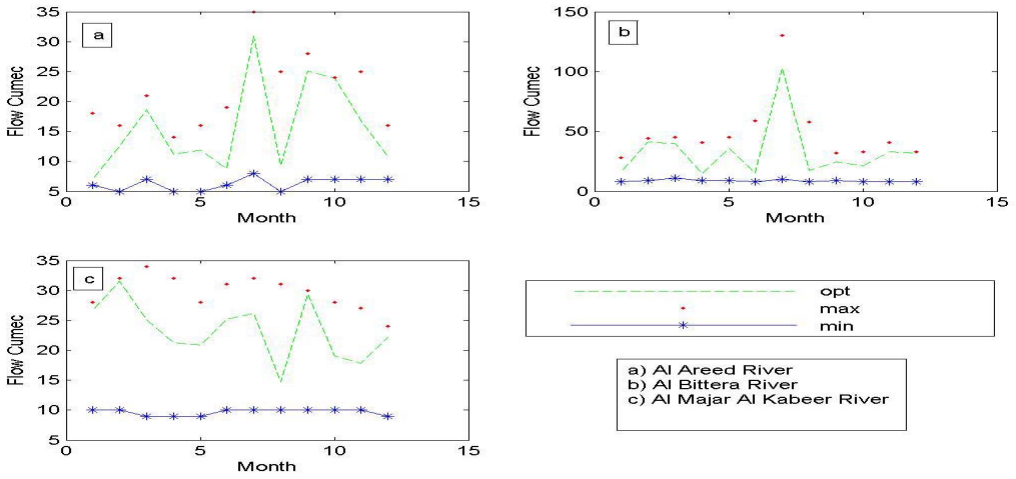

Fig(7) Optimum Monthly Flow Values for Scenario (S2), 10% Increase in EC,TDS,and BOD Values, for a Wet Year.

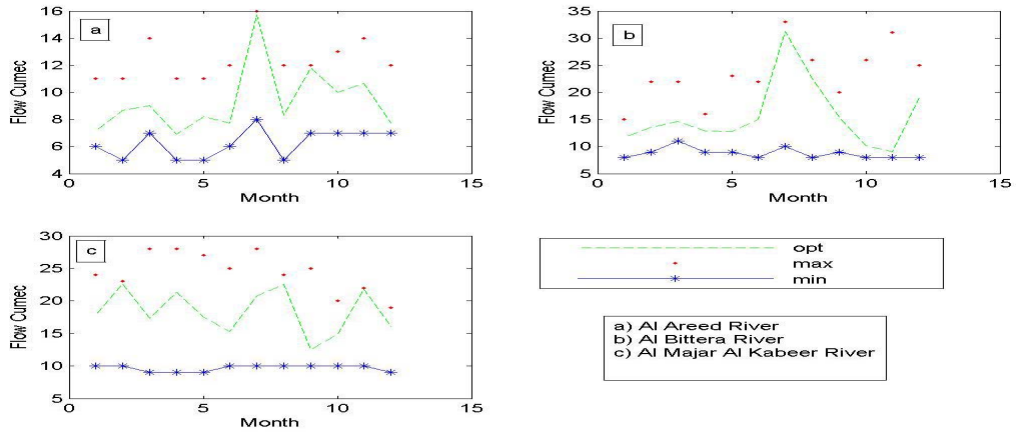

Fig(8) Optimum Monthly Flow Values for Scenario (S2), 10% Increase in EC,TDS,and BOD Values, for a Normal Year.

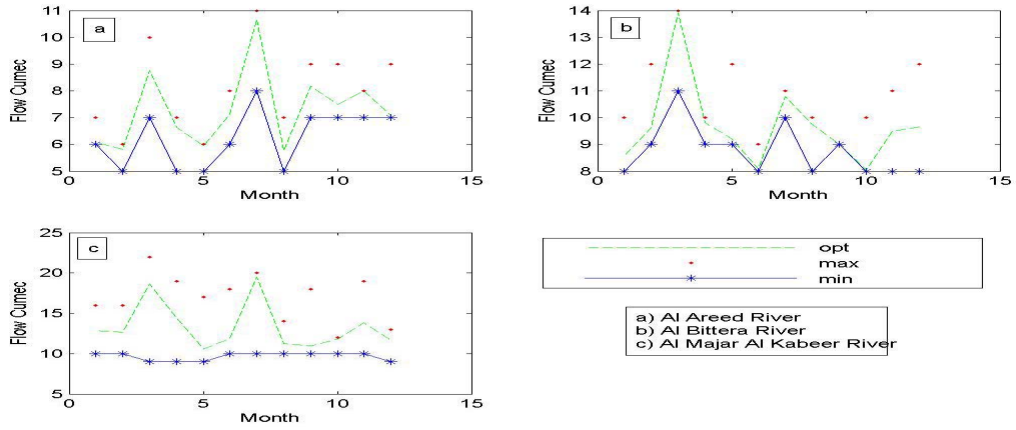

Fig(9) Optimum Monthly Flow Values for Scenario (S2), 10% Increase in EC,TDS,and BOD Values, for a Dry Year.

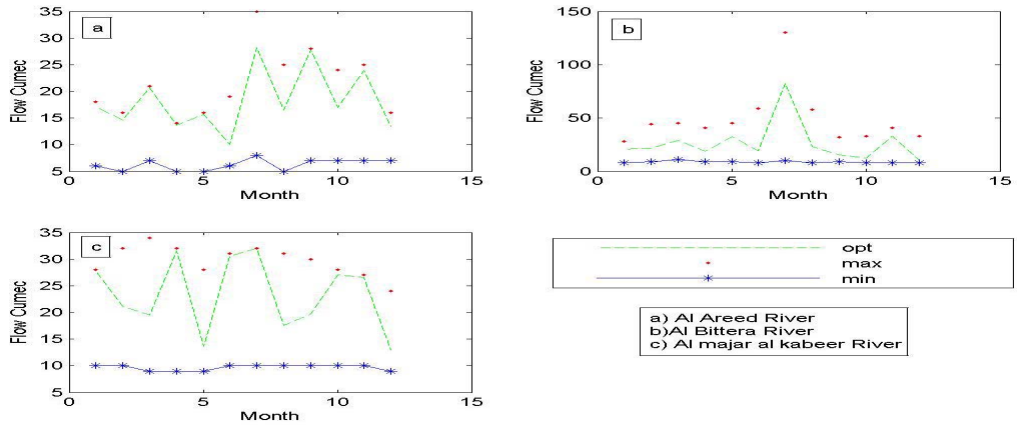

Fig(10) Optimum Monthly Flow Values for Scenario (S3), 20% Increase in EC,TDS,and BOD Values, for a Wet Year.

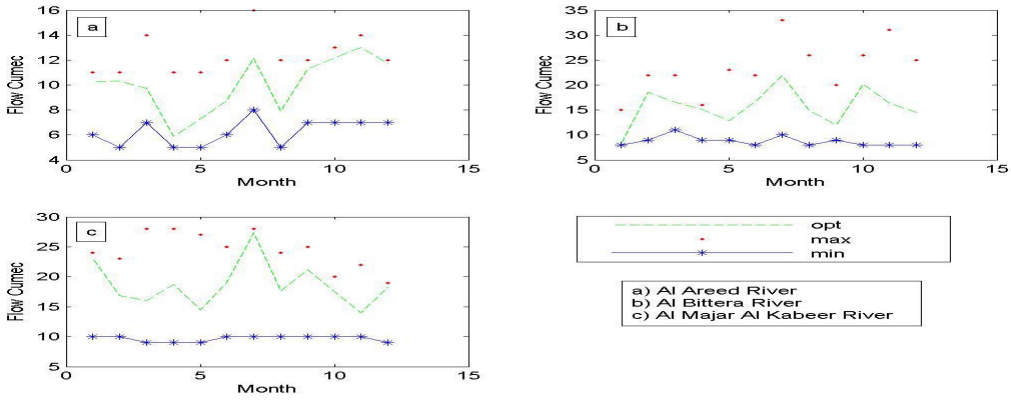

Fig(11) Optimum Monthly Flow Values for Scenario (S3), 20% Increase in EC,TDS,and BOD Values, for a Normal Year.

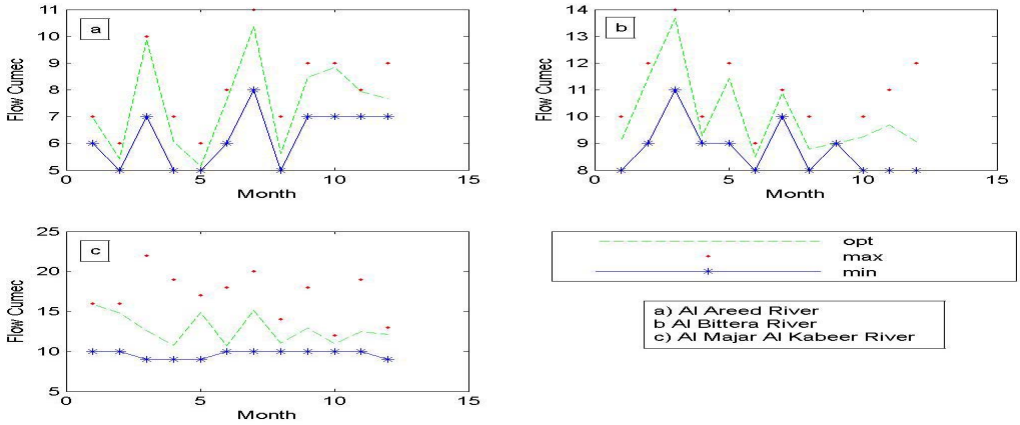

Fig(12) Optimum Monthly Flow Values for Scenario (S3), 20% Increase in EC,TDS,and BOD Values, for a Dry Year.

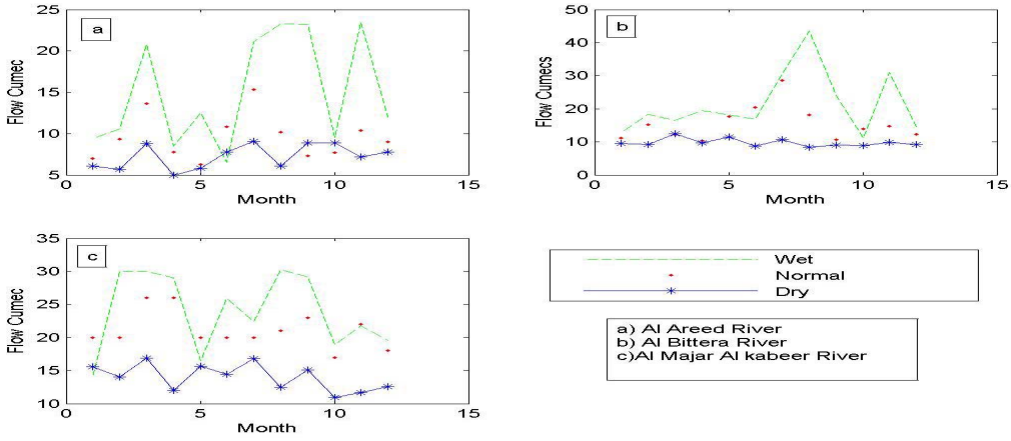

Fig(13) Optimum Flow for the Three Rivers for Wet , Normal and Dry Years, for Scenario S1.

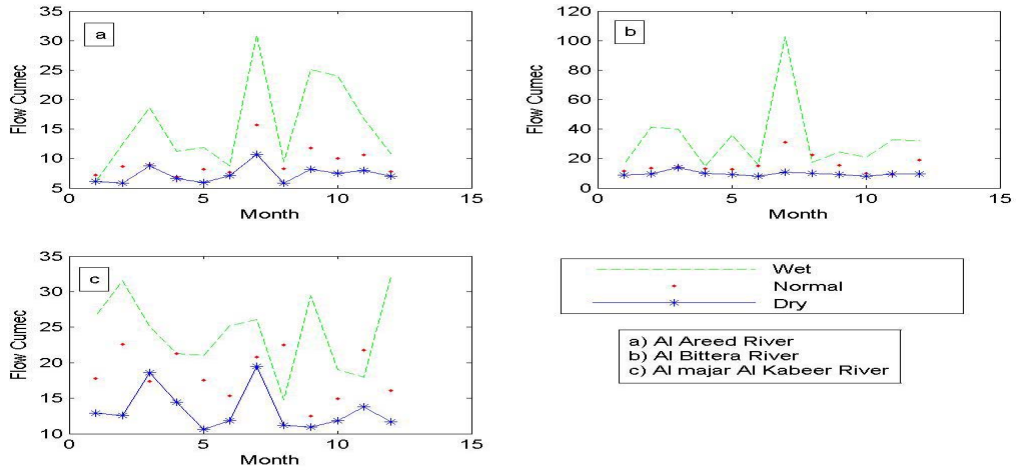

Fig(14) Optimum Flow for the Three Rivers for Wet , Normal and Dry Years,for Scenario S2.

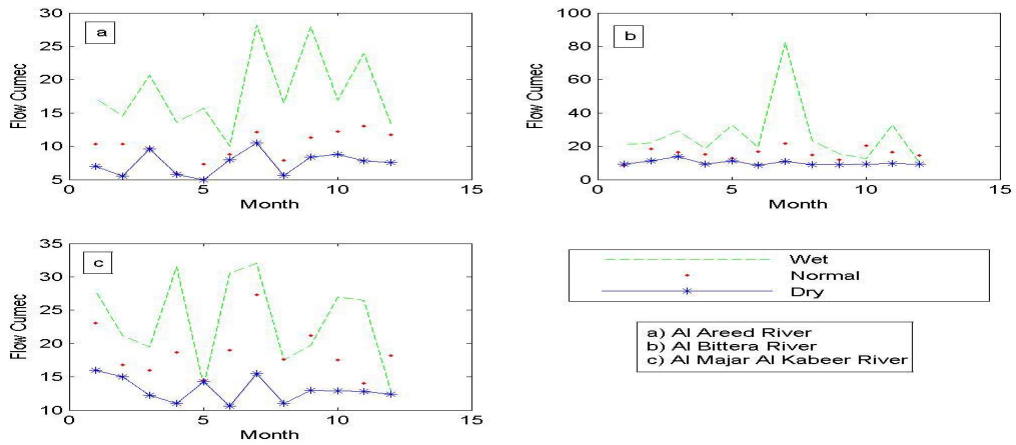

Fig(15) Optimum Flow for the Three Rivers for Wet , Normal and Dry Years, for Scenario S3.

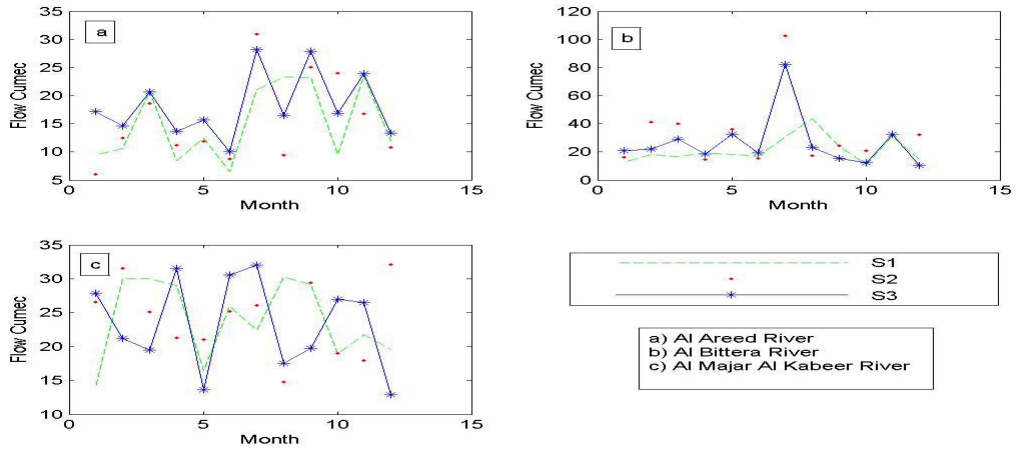

Fig.(16) Optimum Flow for the Three Rivers for all Scenarios for Wet Year Flow.

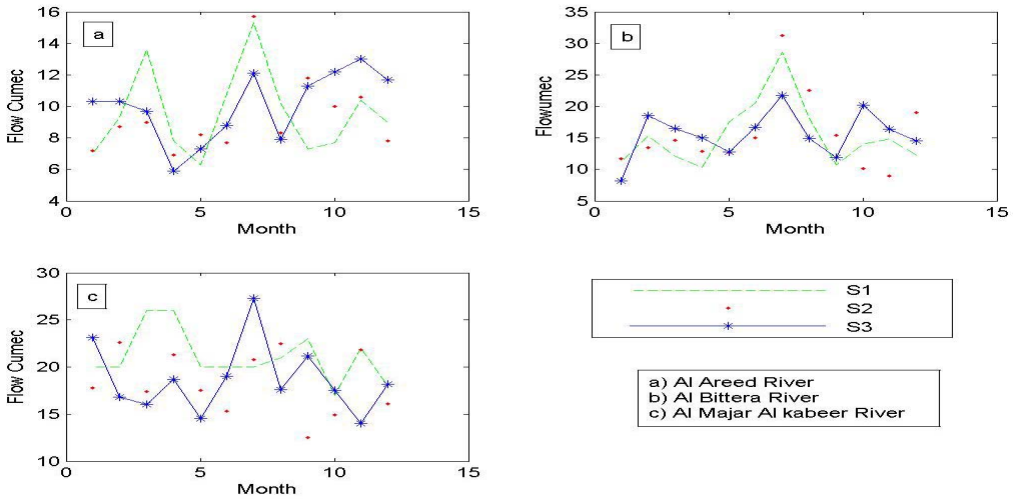

Fig.(17) Optimum Flow for the Three Rivers for all Scenarios for Normal Year Flow.

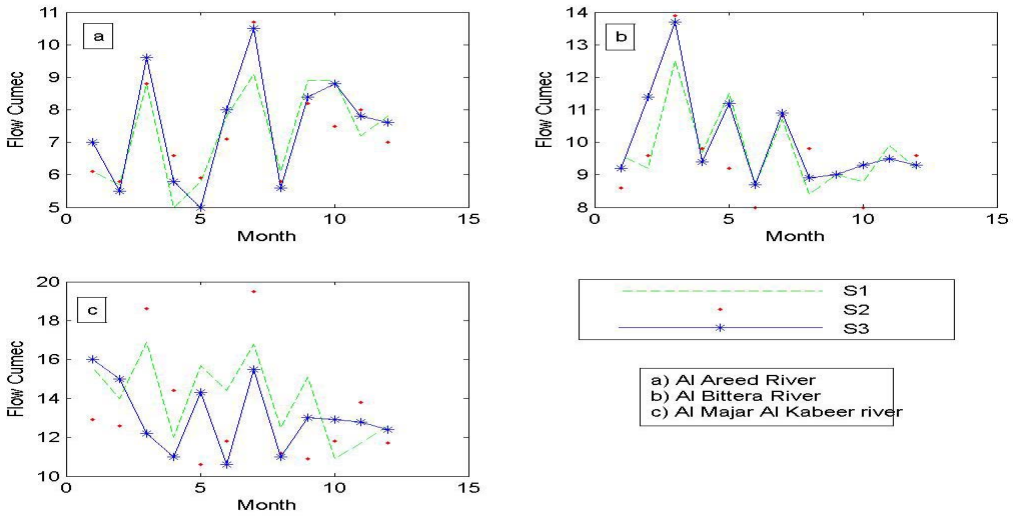

Fig.(18) Optimum Flow for the Three Rivers for all Scenarios for Dry Year Flow.

Design and Implementation of a Generalized N-Digit Binary-To-Decimal Converter on an FPGA Seven-Segment Display Using Verilog Hdl

Asst. Lec. Asma Taha Saadoon
University of Baghdad/ Engineering College
Computer Engineering Department
asma_1683@yahoo.com

ABSTRACT
It is often needed to have circuits that can display the decimal representation of a binary number and specifically in this paper on a 7-segment display. In this paper a circuit that can display the decimal equivalent of an n-bit binary number is designed and it's behavior is described using Verilog Hardware Descriptive Language (HDL). This HDL program is then used to configure an FPGA to implement the designed circuit.

KEYWORDS: binary to decimal converter, FPGA, Verilog HDL, seven segment display, Cyclone II de1 board.

تصميم وتنفيذ محول من التمثيل الرقمي الثنائي الى التمثيل الرقمي العشري المكون من سلسلة رقمية طولها (N) على شاشة العرض ذات السبع قطع لحيز البوابات المرتبة بهيئة صفوف القابلة للبرمجة (FPGA) باستخدام لغة وصف الأجهزة فيرلوغ (verilog)

م.م. أسماء طه سعدون
جامعة بغداد/ كلية الهندسة
قسم هندسة الحاسبات

الخلاصة
غالبا ما تكون الحاجة الى دوائر تعرض العدد ممثل بالنظام العشري المكافئ الى ذلك العدد ممثل بالنظام الثنائي خصوصا في هذا البحث على شاشة العرض ذات السبع قطع. في هذا البحث تم تصميم دائرة لعرض التمثيل العشري لعدد ممثل بالنظام الثنائي طوله (n) وسلوك هذه الدائرة موصوف باستخدام لغة فيرلوغ (verilog) . واستخدم هذا الوصف بلغة فيرلوغ لتنفيذ الدائرة على ال FPGA.

الكلمات الرئيسية: محول من النظام العشري الى النظام الثنائي، حيز البوابات المرتبة بهيئة صفوف القابلة للبرمجة PGAF، لغة وصف الأجهزة فيرلوغ (verilog)، شاشة العرض ذات السبع قطع، لوحةCyclone II de1.

1. INTRODUCTION

In many electronic applications outputs are in binary form especially circuits designed using Hardware Descriptive Languages. Most of these applications require displaying the decimal equivalent of their outputs on for example a seven segment display. The design of a system that can be an interface between those outputs and a seven segment display is necessary, which is the aim of this work.

1.1 Related Work

Altera is a corporation that supplies programmable semiconductors, it provides a software tool called Quartus II to reconfigure these programmable devices. [Altera laboratory exercise, 2006] gives a basic idea of how to display the decimal equivalent of a 4-bit binary number on a seven segment display, its details are given in appendix A at the end of this paper. In addition [Wan-Fu H., 2011] has implemented a digital clock being displayed on a seven segment display, it differs with this paper in the objective but has some relevance about being both displayed on a seven segment display.

1.2 The Aim Of This Work

The aim of this work is to design a system that can display the decimal equivalent of any n-bit binary number on a seven segment display. This system is designed using Verilog HDL and then is implemented on an FPGA. In this work the idea in [Altera laboratory exercise, 2006] is developed to convert an n-bit binary number to its decimal equivalent. The complete system of this converter is explained in block form shown in **Fig. 1** and then each block is designed. Each block is explained by a truth table and a program code written in verilog HDL that describes its operation. The complete system is then written in verilog HDL and then downloaded on the programmable device (the FPGA) to implement it.

This paper is organized as follows, section 2 shows the block diagram of the system, and then each block in **Fig. 1** is explained in detail with its

code written in verilog HDL. In section 3 the systems behavior is shown including its code in Verilog HDL. In section 4 hardware implementation and results are given. The paper is concluded in section 5.

2. THE PROPOSED SYSTEM BLOCK DIAGRAM

The complete design is shown in block form in **Fig. 1**. The block diagram is composed mainly of three circuits :

1. A circuit that compares between two numbers and produces an output accordingly, this circuit is called in this paper **the compare circuit**. It can be seen in **Fig. 1** that there is compare(1), compare(2),….,compare(N) this will be explained in the next sections.
2. A circuit that converts it's input to a value that is always between (0-9), and hence controls the seven segment display, this circuit is called in this paper **the convert circuit**. Since N-digits are assumed (N- seven segment displays) so there will be N-convert circuits.
3. The third circuit takes the output of the convert circuit and converts it to another code that will give the right display of the decimal digit on the seven segment display, this circuit is called in this paper the **seg7_display circuit**.

A general idea for the block diagram in **Fig. 1** is that the n-bit binary input (**in the bottom left**) enters the compare1 circuit. The compare1 circuit gives an output that together with the n-bit binary input enter the convert1 circuit. The output of the convert1 circuit then enters the seg7_display1 circuit. Now the latter controls the first seven segment display (HEX0) to give the required digit. The output of the compare1 circuit enters the compare2 circuit and gives an output that together with the input to the compare2 circuit enter the

convert2 circuit. The output of the convert2 circuit enter the seg7_display2 circuit and controls the second seven segment display (HEX1). This operation will be repeated for all digits until the full decimal number is obtained. In the next sections the operation of each circuit is explained in detail.

2.1 The Compare Circuit

The compare circuit has 1 input and 1 output as shown in **Fig. 1**. It checks whether its input is between [0,9]* if not then it checks if it's between [10,19] if not then it checks if it's between [20,29] and so on, and gives a unique output for each case. **Table 1** shows the truth table of this circuit where its input has n bits and its output has (n-3) bits. For example If a 5-bit input is applied to the compare circuit (as in **Table 1**) then the output has 2 bits. As n increases the number of output bits also increases, for example if n = 6 then the decimal output is between [0,63]. In this case the compare circuits output has three bits to show the seven different cases ([0-9], [10-19], [20-29],….., [60-63]). The verilog HDL code describing the compare circuit is shown in **Program code(1)**.

2.2 The Convert Circuit

The convert circuit has two inputs and one output, one of the inputs is the n-bit binary number and the other is the output of the compare circuit. **Table 2** shows the truth table for this circuit also for a 5-bit input as in the compare circuit. **Program code(2)** shows the code describing the convert circuits behavior written in verilog HDL language. The convert circuit converts the input to a value that is always between 0 and 9, that will be displayed on the seven segment via the **seg7_display** circuit.

In **Table 2** if the n-bit input (x) is 00000, 01010, 10100, or 11110 the output (Y) for all of these inputs is 00000, the decimal value of this output (y) is 0 which equals the first digit D_0 (first seven segment display). The second digit D_1 for the same mentioned inputs also from **Table 2** equals the decimal value of the second input (z) that is the output of the compare circuit, so in order to display D_1 then z is applied to another compare circuit (compare2) and its output will be applied to another convert circuit (convert2) that will display D_1 on the seven segment display (HEX1) via the second seg7_display circuit (seg7_display2). The input z can be thought of as a control variable, let **init** = 10 (decimal), it can be seen from **Table 2** that if z=00 then y = x-0*init, else if z =01 then y = x-init*1, else if z = 10 then y = x-init*2 , else if z = 11 then y = x-init*3, this is designed using verilog language by a while loop and making z the control variable as shown in Program code(2).

2.3 Seg7_display

The seg7_display has one n-bit input and a one 7-bit output. The input to this circuit is the output of the convert circuit which when applied to the seg7_display circuit will be decoded to another code. The seg7_display is designed in verilog HDL by [Ciletti. M. D., 2005] and the same design is used in this paper. The seven segment display shown in **Fig. 1** (HEXi, where i = 0, 1, 2, …,N-1) has 7 light-emitting diodes which illuminate when a low voltage is applied to them. So by illuminating the right diodes the required decimal value is displayed. In **Program code(3)** the code in verilog HDL is given [Ciletti. M. D., 2005].

* **The [ ] means a closed interval.**

Table 1 The compare circuit truth table

n-bit input (5-bit) $b_4\ b_3\ b_2\ b_1\ b_0$	(n-3) output (2-bit) $C_1\ C_0$	Decimal equivalent $D_1\ D_0$
00000	00	00
00001	00	01
00010	00	02
00011	00	03
00100	00	04
.	.	.
01001	**00**	**09**
01010	01	10
01011	01	11
.	.	.
01111	01	15
.	.	.
.	.	.
10011	**01**	**19**
10100	10	20
.	.	.
.	.	.
11101	**10**	**29**
11110	11	30
11111	11	31

```
module compare (b,c);
parameter no_bit = n;
parameter comt_sig = (n-3);
parameter comp = 9;
parameter add = 10;
input [no_bit-1:0] b;
output [comt_sig -1:0] c;
reg [ comt_sig -1:0] c;
integer count;
always @ (b) begin
count = 0;
while ( b > (comp + count*add)) begin
count = count +1;
end
c = count;
end
endmodule
```

Program code(1) The compare circuit code in Verilog HDL

```
module convert (x,z,y);
parameter  no_bit1 = n;
parameter  comt1_sig = (n-3);
parameter  init = 10;
input [no_bit1 -1:0] x;
input [comt1_sig -1:0]z;
output [no_bit1-1:0] y;
reg [no_bit1-1:0] y;
integer q;
always @ (x , z) begin
q = 0;
while (q < (2**comt1_sig)) begin  // **
means to the power
if (z == q) begin
y <= x - q*init;
end
q = q + 1;
end
end
endmodule
```

Program code(2) The convert circuit code in Verilog HDL

Table (2) The convert circuit truth table

n-bit input (5-bit) $x_4\ x_3\ x_2\ x_1\ x_0$	(n-3) input (2-bit) $z_1\ z_0$	n-bit output $y_4\ y_3\ y_2 y_1\ y_0$	Decimal equivalent $D_1\ D_0$
00000	**00**	**00000**	**00**
00001	00	00001	01
00010	00	00010	02
00011	00	00011	03
00100	00	00100	04
00101	00	00101	05
.	.	.	.
01001	**00**	**01001**	**09**
01010	**01**	**00000**	**10**
01011	01	00001	11
.	.	.	.
01111	01	00101	15
.	.	.	.
10011	**01**	**01001**	**19**
10100	**10**	**00000**	**20**
.	.	.	.
11101	**10**	**01001**	**29**
11110	**11**	**00000**	**30**
11111	11	00001	31

```
module seg7_display (m,n);
input [n-1:0] m;
output [6:0] n;
reg [6:0] n;
parameter blank = 7'b 1111111;
parameter zero = 7'b 1000000;
parameter one = 7'b 1111001;
parameter two = 7'b 0100100;
parameter three = 7'b 0110000;
parameter four = 7'b 0011001;
parameter five = 7'b 0010010;
parameter six = 7'b 0000010;
parameter seven = 7'b 1111000;
parameter eight = 7'b 0000000;
parameter nine = 7'b 0010000;
always @ (m) begin
case (m)
0: n <= zero;
1: n <= one;
2: n <= two;
3: n <= three;
4: n <= four;
5: n <= five;
6: n <= six;
7: n <= seven;
8: n <= eight;
9: n <= nine;
default: n <= blank;
endcase
end
endmodule
```

Program code(3) The seg7_display circuit code in Verilog HDL.

3. THE PROPOSED SYSTEM HDL DESIGN

The complete design in verilog HDL for the block diagram of **Fig. 1** is shown in **Program code(4)**. This code shows four 7-segment displays (HEX0, HEX1, HEX2, HEX3), one for each decimal digit (it can easily be generalized to N digits).

To understand the binary-to-decimal converter circuit, take n=5. Observe **Fig.1**, **Table 1** and **Table 2** it can be seen that:

1. If a binary input with n= 5, is applied to compare1, output **(c)** is as in **Table 1**.
2. Now this same binary input is applied together with **(c)** to the convert1 circuit, which gives **(y)** as in **Table 2**. Output y is always between (0-9) so if for example:
   The binary input is 15 (01111), the first digit is 5 and the second is 1. In this case c =01, which means that the binary input is between [10-19]. At the same time y = binary input – 10, y = 15-10=5. Y is applied to the seg7_display1 that gives an output of (0010010) to the first 7-segment display (HEX0). This bit pattern illuminates LED0, LED2, LED3, LED5, and LED6 of the (HEX0) 7-segment display which in return displays a 5.
3. Now to display the second digit on the second seven segment display HEX1, observe the output (z) in **Table 1** it can be seen that it corresponds to the second digit. So (z) is applied to compare2 and an output z' is obtained. z together with z' is applied to convert2 and gives an output y'. y' is applied to the seg7_display2 which gives the binary bit pattern that illuminates the correct LEDs that shows the decimal value (in this example it shows a **1**).
4. The same is repeated as is shown in the block diagram of **Fig. 1** to display all digits on all displays.

4. HARDWARE IMPLEMENTATION AND RESULTS

The convert_b_to_d (**program code(4)**) is written in verilog HDL using Quartus II software tool version 7.2 [Altera software installation manual, 2011]. **Program code(4)** is downloaded on an FPGA (Cyclone II EP2C20F484C7) [Cyclone II, User Guide], and the flow summary of the compilation report is shown in **Table 3 and Table 4** (this flow summary is if the number of input binary bits is 10, which is the maximum number for this FPGA kit). Table 3 and 4 show that only 206 logic elements (1%) are used, which means that a very small part of the FPGA kit is reconfigured to implement this system.

In **Fig. 2** the cyclone II EP2C20F484C7 starter development board is shown with the seven segment display and the toggle switches (SW) [Cyclone II, Reference manual]. In the figure the toggle switches (SW (SW_0, SW_1, ….SW_9)) represent the binary input and the seven segment display represent their decimal equivalent. When the toggle switches position is down (up)* then the input is logic **"0" ("1")**.

* Down (up) is the bottom (top) of the page.

```
module convert_b_to_d (sw,
hex0,hex1,hex2,hex3);
parameter bit_input = n;
parameter comp_out = n-3;
input [bit_input -1:0] sw;
output [6:0] Hex0, Hex1, Hex2, Hex3;
// array of wires ( 4 is the number of
digits) in general N.
wire [bit_input-1:0] kwire [4:0];
wire [comp_out-1:0] owire [3:0];
wire [bit_input-1:0] kowire [3:0];
  wire [6:0] hex [3:0];
// module loop using generate
genvar i;
generate for ( i = 0; i <4; i = i+1 )
  begin: inst
assign kwire[0]=sw;
compare compare_i (kwire[i], kowire[i] );
convert convert_i (kwire[i],
kowire[i],owire[i]);
seg7_display seg7_display_i
(owire[i],hex[i]);
assign kwire[i+1]=kowire[i];
    end
assign hex0=hex[0];
assign hex1=hex[1];
assign hex2=hex[2];
assign hex3=hex[3];
  endgenerate
endmodule
```

Program code(4) The convert_b_to_d system code in Verilog HDL

Table (3) The compilation flow

Compilation Flow Status	Successful
Quartus II Version	7.2 Build 151 09/26/2007 SJ
Revision Name	convert_b_to_d
Top-level Entity Name	convert_b_to_d
Family	Cyclone II
Device	EP2C20F484C7
Timing Models	Final
Met timing requirements	Yes
Total logic elements	206 / 18,752 (1 %)
Total combinational functions	206 / 18,752 (1 %)
Dedicated logic registers	0 / 18,752 (0 %)
Total registers	0
Total pins	38 / 315 (12 %)
Total virtual pins	0
Total memory bits	0 / 239,616 (0 %)
Embedded Multiplier 9-bit elements	0 / 52 (0 %)
Total PLLs	0 / 4 (0 %)

Table (4) The Analysis and synthesis

Analysis & Synthesis Status	Successful
Quartus II Version	7.2 Build 151 09/26/2007 SJ
Revision Name	convert_b_to_d
Top-level Entity Name	convert_b_to_d
Family	Cyclone II
Total logic elements	206
Total combinational functions	206
Dedicated logic registers	0
Total registers	0
Total pins	38
Total virtual pins	0
Total memory bits	0
Embedded Multiplier 9-bit elements	0
Total PLLs	0

5. CONCLUSION

In this paper a binary-to-decimal converter is designed and implemented on an FPGA. This design can be used for any number of input binary bits, which can be made directly by changing only the number of input bits in the code and increasing the number of digits that will display the decimal number. Table 3, and 4 show that a small part of the FPGA is reconfigured to implement this system, and since this system is used mainly as an interface between any electronic circuit implemented on an FPGA and a seven segment display then the small size is a good feature.

REFERENCES

Altera corporation, Laboratory Exercise 2" Numbers and Displays" 2006, ftp://ftp.altera.com/up/pub/Laboratory_Exercises/DE1/Digital_Logic/Verilog/lab2_Verilog.pdf.

Altera Software Installation and Licensing Manual, 101 Innovation Drive, San Jose, CA 95134, November 2011 Altera Corporation.

Ciletti. M. D. , "Advanced Digital Design with the Verilog HDL", Prentice-Hall of India, New Delhi, 2005.

Cyclone II FPGA Starter Development Board, Reference manual, Altera San Jose, CA 95134, October 2006.

Cyclone II FPGA Starter Development Kit, User Guide, Altera San Jose, CA 95134, October 2006.

Wan-Fu H., "The design of a 6-digit digital clock with a four-digit seven-segment display module", IEEE Electrical and Control Engineering, International conference Page(s): 2656 – 2659, 2011.

LIST OF ABBREVIATIONS:

FPGA: Field Programmable Gate Array.
HDL: Hardware Descriptive Language.
LED: Light Emitting Diode.

APPENDIX A

You are to design a circuit that converts a four-bit binary number $V = v3v2v1v0$ into its two-digit decimal equivalent $D = d1d0$. **Table A1** shows the required output values. A partial design of this circuit is given in **Fig. A1**. It includes a comparator that checks when the value of V is greater than 9, and uses the output of this comparator in the control of the 7-segment displays. You are to complete the design of this circuit by creating a Verilog module which includes the comparator, multiplexers, and circuit A (do not include circuit B or the 7-segment decoder at this point). Your Verilog module should have the four-bit input V , the four-bit output M and the output z.

Table A1 Binary-to-decimal conversion values

Binary value	Decimal Digit
0000	0 0
0001	0 1
0010	0 2
. . .	. . .
1001	0 9
1010	1 0
1011	1 1
1100	1 2
1101	1 3
1110	1 4
1111	1 5

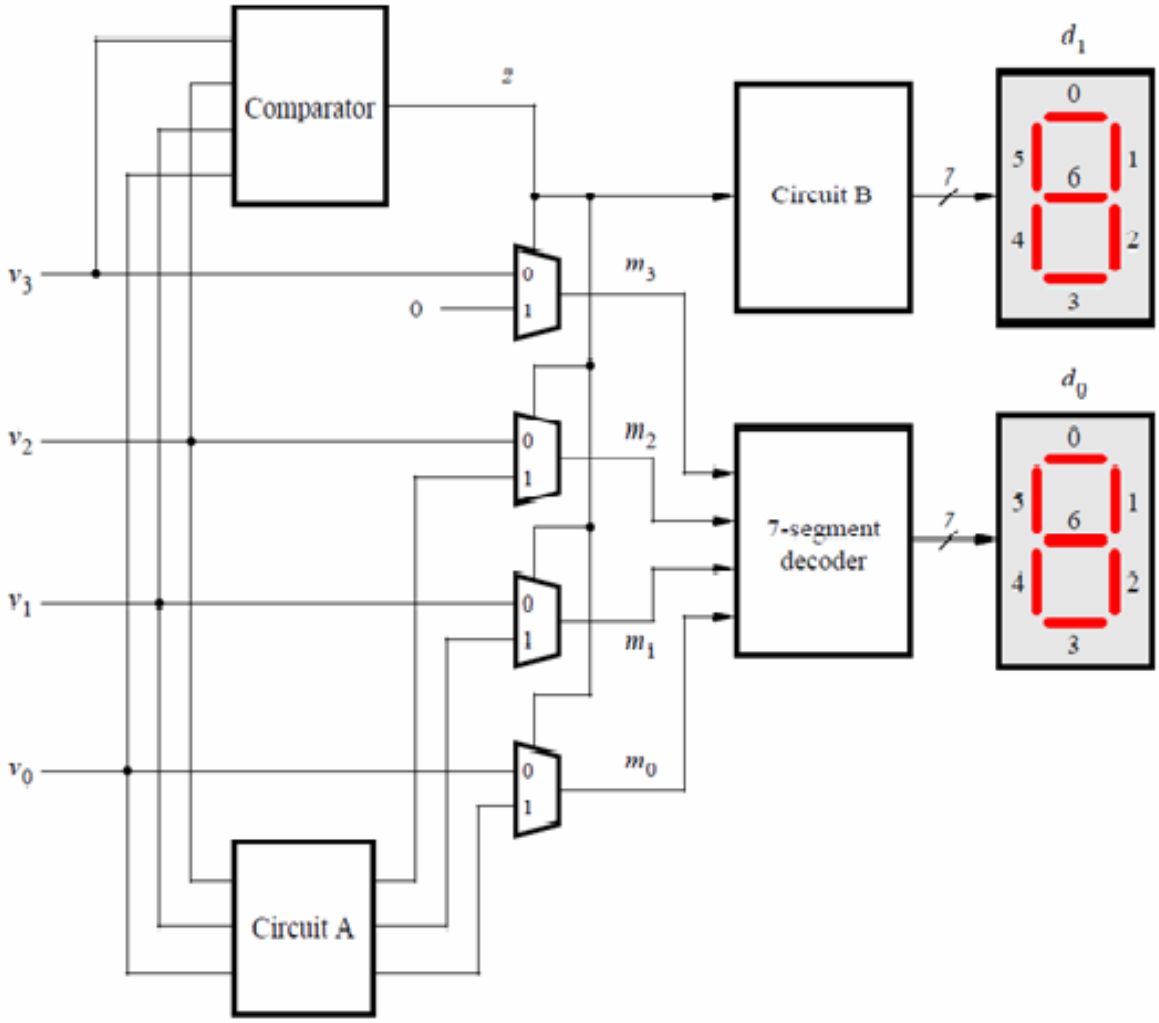

Fig. A1 Partial design of the binary-to-decimal conversion circuit.

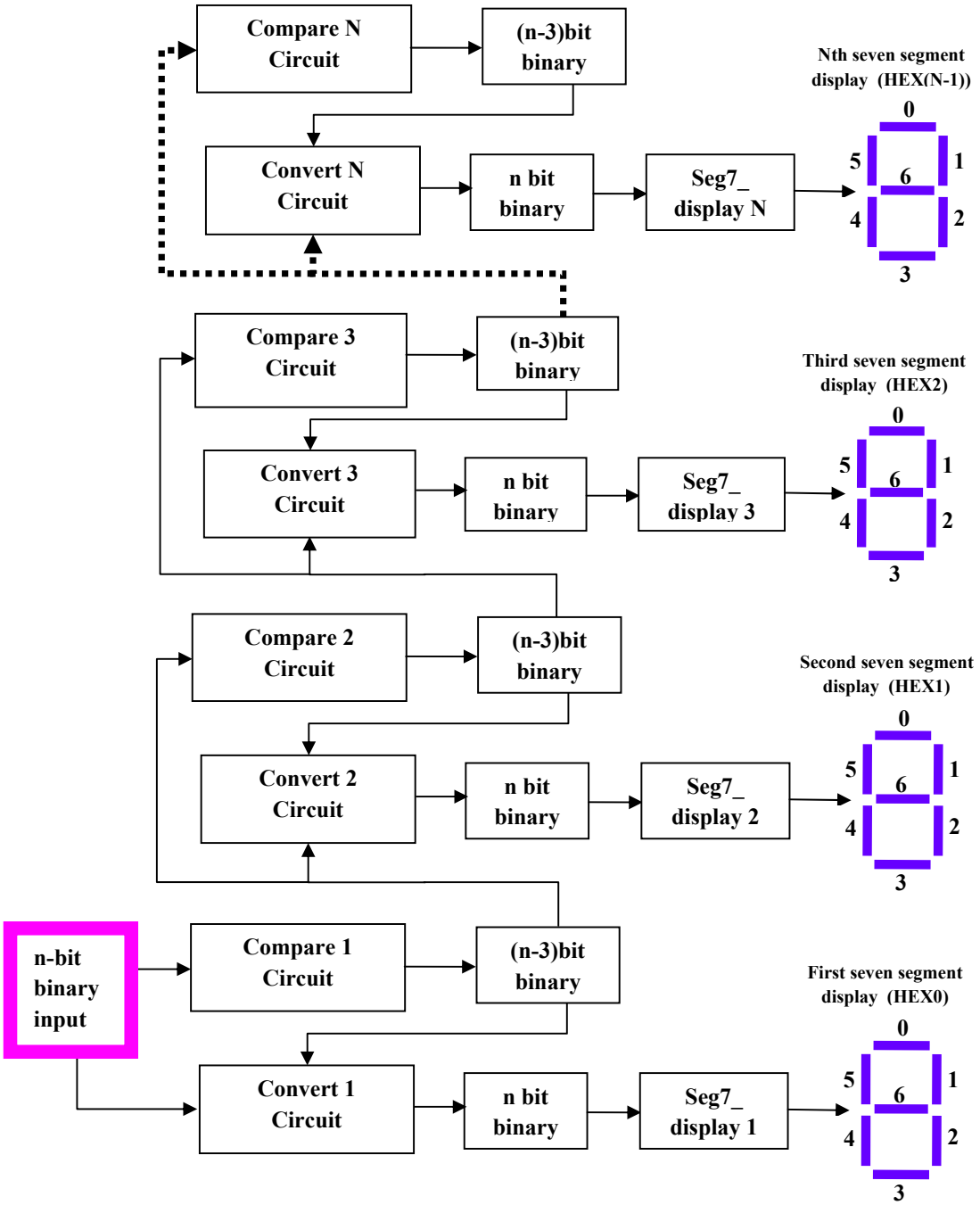

Fig. 1 The binary-to-decimal converter block diagram

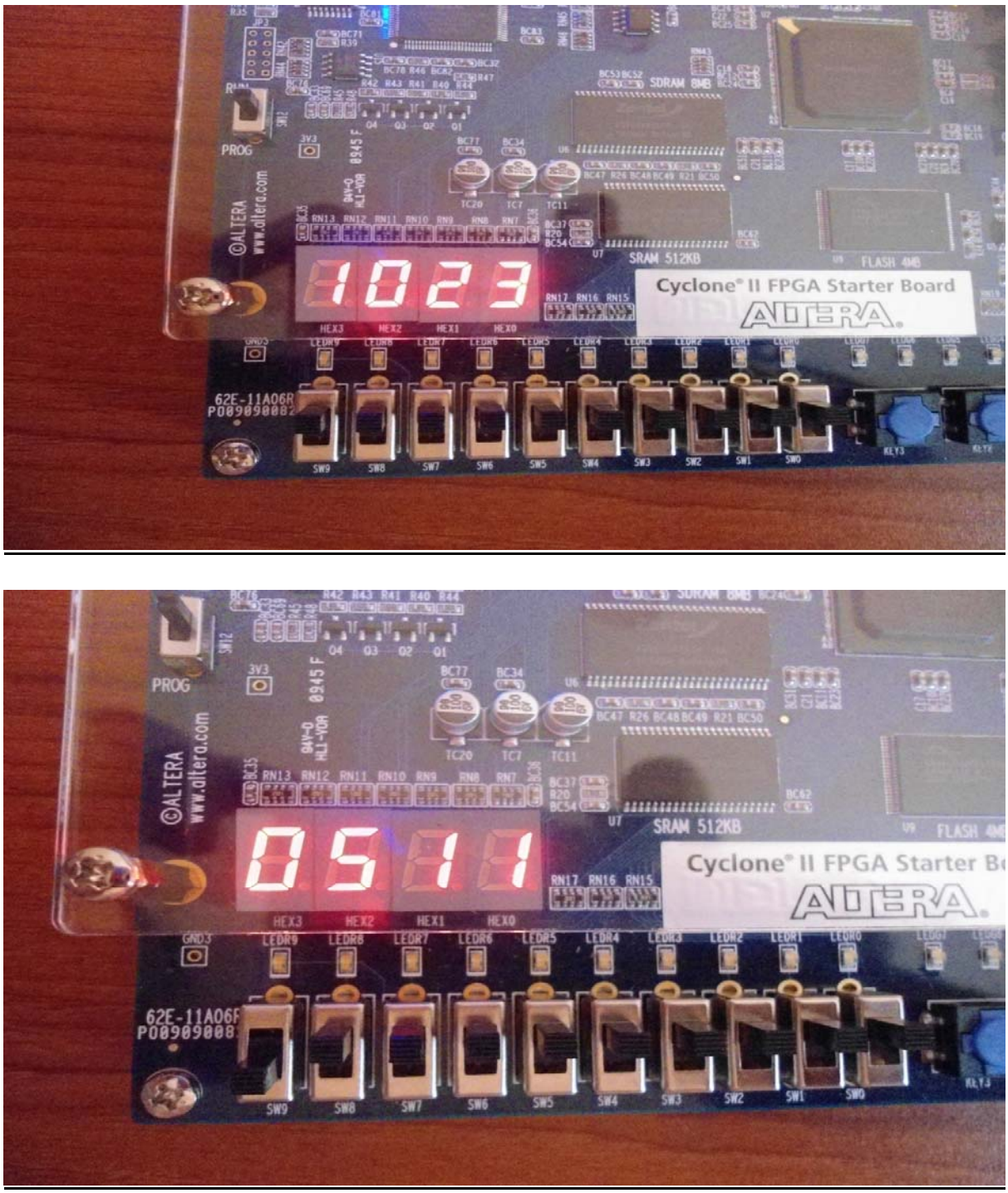

Fig. 2 Cyclone II EP2C20F484C7 FPGA
seven segment display

Numerical Study Of Heat Transfer In Cooling Passages Of Turbine Blade

Dr. Ahmed F. Khudheyer
Mech. Eng. Dept.
Al- Nahrain University
Baghdad, Iraq
ahyaja@yahoo.com

Hussein T. Dhaiban
Mech. Eng. Dept.
Al- Nahrain University
Baghdad, Iraq
huso0ony@yahoo.com

ABSTRACT

As the temperature of combustion gases is higher than the melting temperature of the turbine materials, cooling of turbine parts in a gas turbine engine is necessary for safe operation. Cooling methods investigated in this computational study included cooling flow losses. Film-cooling is one typically used cooling method whereby coolant is supplied through holes passage, in present study the holes placed along the camber line of the blade.

The subject of this paper is to evaluate the heat transfer that occur on the holes of blade through different blowing coolant rates. The cases of this study were performed in a low speed wind tunnel with two tip gap at small and large (0.03 and 0.09cm) and multiple coolant flow rates through the film-cooling holes. The blowing ratios was studied whereby coolant was injected from holes placed along the tip of a large scale blade model with Reynolds number (2.1×10^5) of the engine was matched. Results showed that baseline Nusselt numbers on the holes were reduced along the holes passage, and heat transfer coefficient is high values at iterance region. Overall, the cooling by holes appears to be a feasible method for prolonging blade life.

KEYWORDS: heat and mass transfer, gas turbine cooling

الخلاصة:

درجة حرارة غازاتِ الاحتراق تكون عالية بالمقارنة مع درجةِ حرارة ذَوَبان معادن التوربين، تَبريد أجزاء التوربين في محرّك التوربين الغازي ضروريُة لعمله في ظروف أمنة. نظريات التبريد تحققت في الدراسة النظرية بحيث تضمنت خسائر جريان التبريد. التبريد الغشائي (film-cooling) هو احد طرق التبريد النموذجية حيث أن مائع التبريد يجهز من خلال الثقوب، في الدراسة الحالية تقع الثقوب على طول خط المنتصف (camber) لريشة التوربين.

هدف هذا البحث هو حساب انتقال الحرارة الذي يحدث داخل ثقوب الريشة من خلال نسب تبريد متغيرة. حالات الدراسة أنجزت على جريان بطيء في النفق الهوائي مع فجوتان للقمة صغيرة وكبيرة (0.03 و 0.09 سم) مع اختلاف نسب مائع التبريد من خلال ثقوب التبريد الغشائي (film-cooling). تم دارسة Blowing Ratios من خلال جريان مائع التبريد الذي يحقن من الثقوب التي تقع على طول القمة مع مقياس كبير لنموذج الريشة مع رقم رينولد ($2.1 * 10^5$) للمحرك الذي يكون محسوب. النتائج توضح أرقام نسلت في الثقوب تقل على طول الثقوب، ومعامل انتقال الحرارة يكون ذو قيمة عالية عند منطقة الدخول. عموماً، التبريد بواسطة الفتحات تَبْدو طريقة ملائمة لإطالة عمر الريشة.

INTRODUCTION

Gas turbine engines are widely used to power aircraft because they are light and compact and have a high power to-weight ratio. One way to increase power and efficiency of gas turbines is

by increasing turbine-operating temperatures. The motivation behind this is that higher temperature gases yield higher energy potential. However, the components along the hot gas path experience high thermal loading, which can cause distress. The HPT (High Pressure Turbine) first stage blade is one component that is extremely vulnerable to the hot gas**.**

The two main objectives of blade design engineers are (1) to reduce the leakage flow either by reducing the tip gap or by implementing a more effective tip leakage sealing mechanism and (2) to cool the blade tips with the least possible usage of cooling fluid, Bunker, (2002).

The degree of cooling which may be achieved is dependent upon a number of factors, chief among which are (a) the temperature difference between the main gas stream and the inlet cooling air and (b) the 'conductance ratio', this being defined as the ratio of the heat input to the blade per unit temperature difference between gas stream and blade to the heat passed to the cooling air per unit temperature difference between blade and cooling air, Nasir et al. (2003).

Clearly to achieve a high degree of cooling the lowest possible value of conductance ratio is required in conjunction with the largest possible temperature difference between gas stream and cooling air. The heat input to the blade per unit temperature difference between gas stream and blade is the product of the average gas-to-blade heat transfer coefficient and the external surface area, and this in turn is dependent upon the blade shape, gas flow incidence, gas flow Reynolds number, gas Prandtl number, and to a lesser extent upon the ratio of gas temperature to blade temperature, and also gas stream Mach number, Jonas (2002).

The cooling air is forced through a porous blade wall. This method is by far the most economical in cooling air, because not only it remove heat from the wall more uniformly, but the effusion layer of air insulates the outer surface from the hot gas stream and so reduces the rate of heat transfer to the blade, Cohen (1987)**.**

Gas turbine blades usually have a gap between the blade tip and the stationary casing or the shroud surface known as tip gap. This clearance gap is necessary to allow for the blade's mechanical and thermal growth. The leakage flow (flow through the tip gap) results in a reduction in the blade force, the work done and therefore the efficiency. Fig. (1) shows the gap between the blade and shroud**,** Allen and Kofskey (1955).

Allen and Kofskey (1955) performed some visualization tests to see what these secondary flows looked like. Additionally, they also studied the effect of ejecting flow from the turbine tips on the shape of the secondary flows. At the time of these tests, engine temperatures were not so high as to require cooling of the turbine blades for operation but they noted that, "turbine blade cooling may become an engine requisite. The turbine rotor blade cooling method of passing cooling air through hollow blades and discharging it at the blade tip may be one of the most feasible methods of changing the secondary-flow pattern".

Yang et al. (2004) predicted film cooling effectiveness and heat transfer coefficient for three types of film-hole arrangements: 1) the holes located on the mid-camber line of the tips, 2) the holes located upstream of the tip leakage flow and high heat transfer region, 3) combined arrangements of camber and upstream holes. They found that upstream film hole arrangements provided better film cooling performance than camber arrangements.

Acharya et al. (2003) indicated that film cooling injection lowered the local pressure ratio and altered the nature of the leakage vortex. High film-adiabatic effectiveness and low heat transfer coefficients were predicted along the coolant trajectory with the lateral spreading of the coolant jets being quite small for all cases. With an increased tip gap the coolant was able to provide better downstream effectiveness through increased mixing. For the smallest tip gap, the coolant was shown to impinge directly on the surface of the shroud leading to high film effectiveness at the impingement point. As the gap size increased, their predictions indicated that

the coolant jets were unable to penetrate to the shroud.

Nasir et al. (2003) found that a single squealer on the suction side performed the test. The performance of different recessed tip geometries were investigated and compared with plane tip performance. A transient liquid crystal technique was employed to measure detailed heat transfer coefficient distributions. Coolant injection from holes located on the blade tip, near the tip along the pressure side and combination cases were also investigated. Experiments were performed for plane tip and squealer tip for different coolant to mainstream blowing ratios of 1.0, 2.0, and 3.0. A transient infrared (IR) thermography technique was used to simultaneously measure heat transfer coefficient and film cooling effectiveness. He shows the tip injection reduced heat transfer coefficient on the blade tip and an increase in blowing ratio caused a decrease in heat transfer coefficient for both plane and squealer tip blade.

Christophel et al. (2004) evaluated the adiabatic effectiveness levels that occur on the blade tip through blowing coolant from holes placed near the tip of a blade along the pressure side. Also present were dirt purge holes on the blade tip, which is part of a commonly used blade design to expel any large particles present in the coolant stream. Experiments were conducted in a linear cascade with a scaled-up turbine blade, from these tests indicated that the performance of cooling holes placed along the pressure side tip was better for a small tip gap than for a large tip gap. Disregarding the area cooled by the dirt purge holes, for a small tip gap the cooling holes provided relatively good coverage. For all of the cases considered, the cooling pattern was quite streaky in nature, indicating very little spreading of the jets. As the blowing ratio was increased for the small tip gap, there was an increase in the local effectiveness levels resulting in higher maxima and minima of effectiveness along the middle of the blade.

Hohlfeld et al. (2003) investigated in this computational study included cooling flow losses and microcircuit channels. This study evaluated the benefit of external film-cooling flow exhausted from strategically placed microcircuits. Along the blade tip, predictions showed mid-chord cooling was independent of the blowing from microcircuit exits. The formation of a pressure side vortex was found to develop for most microcircuit film-cooling cases. Significant leading edge cooling was obtained from coolant exiting from dirt purge holes with a small tip gap while little cooling was seen with a large tip gap.

Couch (2003) studied examinations of a novel cooling technique called a microcircuit, which combines internal convection and pressure side injection on a turbine blade tip. Holes on the tip called dirt purge holes expel dirt from the blade, so other holes are not clogged. Wind tunnel tests were used to observe how effectively dirt purge and microcircuit designs cool the tip. Tip gap size and blowing ratio are varied for different tip cooling configurations. Results show that the dirt purge holes provide significant film cooling on the leading edge with a small tip gap. Coolant injected from these holes impacts the shroud and floods the tip gap reducing tip leakage flow. Also, results suggest that blowing from the microcircuit diminishes the tip leakage vortex.

The objectives of the work presented in this paper are to present the benefits of heat transfer of a holes using coolant exhausted from holes to tip at different blowing ratio.

NUMERICAL ANALYSIS

The basic equations that describe the flow and heat are conservation of mass, momentum and energy equations. These equations describe two-dimensional, turbulent and incompressible flow takes which the following forms: (Arnal, M.P,1982):

The assumptions that used for the instantaneous equation are:-

1- Steady, two-dimensional, incompressible flow, single phase flow, shock free, inviscous, no slip, irrotational.
2- The fluid is Newtonian.
3- Cylindrical coordinate for flow in cooling passages.

(i) *Conservation of Mass*

$$\frac{\partial}{\partial z}(\rho u) + \frac{1}{r}\frac{\partial}{\partial r}(\rho r v) = 0 \qquad (1)$$

(ii) *Momentum Equations*

u-momentum (z-direction)

$$\frac{1}{r}\left[\frac{\partial}{\partial z}(\rho ruu)+\frac{\partial}{\partial r}(\rho ruv)\right]=-\frac{\partial p}{\partial z}+\frac{1}{r}\left[\frac{\partial}{\partial z}\left(r\mu_{eff}\frac{\partial u}{\partial z}\right)+\frac{\partial}{\partial r}\left(r\mu_{eff}\frac{\partial u}{\partial r}\right)\right]+S_u \quad (2)$$

v-momentum (r-direction)

$$\frac{1}{r}\left[\frac{\partial}{\partial z}(\rho ruv)+\frac{\partial}{\partial r}(\rho rvv)\right]=-\frac{\partial p}{\partial r}+\frac{1}{r}\left[\frac{\partial}{\partial z}\left(r\mu_{eff}\frac{\partial v}{\partial z}\right)+\frac{\partial}{\partial r}\left(r\mu_{eff}\frac{\partial v}{\partial r}\right)-\Gamma^v\frac{v}{r^2}\right]+S_v \quad (3)$$

(iii) *Energy Equation*

$$\frac{1}{r}\left[\frac{\partial}{\partial z}(\rho ruT)+\frac{\partial}{\partial r}(\rho rvT)\right]=\frac{1}{r}\left[\frac{\partial}{\partial z}\left(r\Gamma_{eff}\frac{\partial T}{\partial z}\right)+\frac{\partial}{\partial r}\left(r\Gamma_{eff}\frac{\partial T}{\partial r}\right)\right] \quad (4)$$

The turbulence model utilized in this analysis is the two equation k-Epsilon model. This model is utilized for its proven accuracy in turbine blade analysis and for its applicability to confined fluid flow. (k- ε) Turbulence Model is one of the most widely used turbulence models is the two-equation model of kinetic energy (k) and its dissipation rate (**ε**). The turbulence according to Launder and Spalding (1972) is assumed to be characterized by its kinetic energy and dissipation rate (**ε**), where

(i) *Turbulence Energy, k*

$$\frac{1}{r}\left[\frac{\partial}{\partial z}(\rho ruk)+\frac{\partial}{\partial r}(\rho rvk)\right]=\frac{1}{r}\left[\frac{\partial}{\partial z}\left(r\Gamma^k\frac{\partial k}{\partial z}\right)+\frac{\partial}{\partial r}\left(r\Gamma^k\frac{\partial k}{\partial r}\right)+G-\rho\varepsilon\right] \quad (5)$$

(ii) *Energy Dissipation Rate, ε*

$$\frac{1}{r}\left[\frac{\partial}{\partial z}(\rho ru\varepsilon)+\frac{\partial}{\partial r}(\rho rv\varepsilon)\right]=\frac{1}{r}\left[\frac{\partial}{\partial z}\left(r\Gamma^\varepsilon\frac{\partial \varepsilon}{\partial z}\right)+\frac{\partial}{\partial r}\left(r\Gamma^\varepsilon\frac{\partial \varepsilon}{\partial r}\right)\right]+c_1\frac{\varepsilon}{k}G-c_2\rho\frac{\varepsilon^2}{k} \quad (6)$$

where

$$G=\mu_t\left\{2\left[\left(\frac{\partial u}{\partial z}\right)^2+\left(\frac{\partial v}{\partial r}\right)^2+\left(\frac{v}{r}\right)^2\right]+\left(\frac{\partial u}{\partial z}+\frac{\partial v}{\partial r}\right)^2\right\}+S_G \quad (7)$$

given by (Ideriah, F. J. K.,1975)

$$S_G=-\frac{2}{3}\mu_t\left[\frac{\partial u}{\partial z}+\frac{\partial v}{\partial r}\right]^2-\frac{2}{3}\rho k\left[\frac{\partial u}{\partial z}+\frac{\partial v}{\partial r}\right] \quad (8)$$

The values of the empirical constant used here are given in Table (1). (Launder and Spalding,1974) **[11]**.

The governing equations (1),(2),(3),(4),(5) and (6) can be write in one general form as shown below:

$$\frac{\partial(\rho u\phi)}{\partial z}+\frac{1}{r}\frac{\partial(\rho rv\phi)}{\partial r}=\frac{\partial}{\partial z}\left(\Gamma^\phi\frac{\partial \phi}{\partial z}\right)+\frac{1}{r}\frac{\partial}{\partial r}\left(r\Gamma^\phi\frac{\partial \phi}{\partial r}\right)+S_\phi \quad (10)$$

where :-

(ø) is any dependent variable.

(Γ^ϕ) is any exchange coefficient of ø.

($S_ø$) is the source term of ø.

The transform equation (10) from physical domain to computational domain, and that lead to obtained the transformation of the governing equations as follows:-

$$\frac{\partial}{\partial\zeta}(\rho\phi G_1)+\frac{\partial}{\partial\eta}(\rho\phi G_2)=\frac{\partial}{\partial\zeta}\left(\Gamma^\phi Ja\frac{\partial\phi}{\partial\zeta}\right)+\frac{\partial}{\partial\eta}\left(\Gamma^\phi Jc\frac{\partial\phi}{\partial\eta}\right)+S_{total} \quad (11)$$

where:-

G_1 and G_2 are the contravariant velocities or the mass flow rates in the ζ and η direction respectively. Also (a, b and c) are the transformation coefficient to computational domain and S_{total} is the total source terms.

The governing equations are integrated over each control volume (C.V.) with each its neighbor nodes. This discretization of the steady, 2-D governing equations is done by using finite volume method with collocated grid arrangement by using the upwind differencing scheme. Also discretization the terms of source term to give the solving the governing equations.

After solving the momentum equation, the velocity field obtained does not guarantee the conservation of mass unless the pressure field is correct, therefore, the velocity component (u, v), (G_1,G_2), pressure must be corrected according to the continuity equation, (Karki and Patankar, 1989)[13].

In the present work, the (SIMPLE) algorithm (**S**emi-**I**mplicit **M**ethod for **P**ressure

$$\text{Also, } \mu_t = \rho c_\mu k^2 / \varepsilon \qquad (9)$$

Linked **E**quation) is used to couple the pressure and velocity as in (Veresteeg & Malalasekera, 1995). This method is done by solving the momentum equations using the guessed pressure field to obtain the velocity then, the velocity field that obtained satisfies the momentum equations, then the velocity and pressure are corrected because the velocity field violates the conservation of mass.

GEOMETRY OF FLOW AND BOUNDARY CONDITIONS

A Three-dimensional blade profile was created for these low speed. The scaling and design of blade profile and duct are discussed in Hohlfeld (2003)**.** Table (2) lists the run conditions and input to the numerical simulations. The boundary condition on a blade surface assumes zero relative velocity between the blade surface and the shroud. All walls were adiabatic for adiabatic effectiveness cases. The main inlet was specified as a constant velocity inlet at **11.3** m/s. The inlet temperature in the duct (T_g) is 750 □C (taken from al-Dorah power station), the temperature that is used in cooling (T_c) take at 27 □C and the pressure that used at atmosphere condition. The cooling holes locations is shown in Tables (3). The coordinate system was adjusted so that no coordinates are negative**.**

COMPUTATIONAL METHOLOGY

Computational fluid dynamics (CFD) simulation is performed to analyze the heat transfer in holes. A commercially available CFD code, Fluent 6.3.26 (2009) was used to perform all simulations. Fluent is a pressure based flow solver that can be used with structured or unstructured grids. An unstructured grid was used for the study presented in this paper. Solutions were obtained by numerically solving the Navier-Stokes and energy equation through a control volume technique. All geometric construction and meshing were performed with GAMBIT 2.4.6.

To ensure a high quality mesh, the flow passage was divided into multiple volumes, which allowed for more control during meshing. The tip gap region was of primary concern and was composed entirely of tetrahedral cells. Inlet conditions to the model were set as a uniform inlet velocity at approximately one chord upstream of the blade. Fig. (2) shows the mesh of the test rig. An inlet mass flow boundary condition was imposed for the coolant at the plenum entrance for the cooling holes. The mesh contained approximately 20 grid points across the hole exit. Mainstream flow angles were set to those of the experiments as well as the scaled values for the engine while the turbulence intensity and mixing length were set to 4.3% and 0.3 m, respectively.

To allow for reasonable computational times, all computations were performed using the RNG k-ε turbulence model with non-equilibrium wall functions whereby the near wall region was resolved to y^+ values ranging between 30 and 60. Mesh insensitivity was confirmed through several grid adaption based on viscous wall values, velocity gradients, and temperature gradients. Typical mesh sizes were composed of 4.8 million cells with 40% of the cells in and around the tip gap region. Typical computations required 2000 iterations for convergence.

HEAT TRANSFER CALCULATION

In the present study, the numerically measured mass flow rates and air exit temperatures for all cooling passages where used to calculate the total heat transfer is:

$$Q = \square\ Cp\ (T_e - T_{in}) \qquad (12)$$

where T_{in} is the cold temperature, T_e is the exit temperature from hole passage.

After that comparison is made between total heat transfer and heat transfer by convection in holes to find local heat transfer coefficient, which will be used to calculate local Nusselt number for different walls of the holes passages.

$$Nu_x = \frac{h_x d}{k} \quad (13)$$

where h_x is the local heat transfer coefficient, d is the diameter of pipe.

Next the average heat transfer coefficient for the cold side is found by averaging the heat transfer coefficients predicted by Dittus-Boelter correlation for each hole:

$$Nu = 0.023 (Re_{pipe})^n (Pr)^s \quad (14)$$

where n=0.8, s= 0.4 (heating flow)

The summery of present study is presented in Table (4)

RESULS AND DISCUSSION

Results are shown for cases with a baseline flat tip and coolant injection at a small and large tip gap (0.03 and 0.09 cm) respectively. Blowing ratio is the ratio between velocity at mainstream condition to velocity at cooling condition at constant density (BR= U_∞/U_c). In present study, the blowing ratios of 0.5%, 1%, 1.5% and 2% are studied.

Fig. (3) shows the pressure distribution around the blade at midspan for small tip gap in suction and pressure side with the pressure non-dimensionalized by the inlet pressure conditions and given in C_p parameters. Also this results comparison with experimental and computational data for Christophel et al (2004). When the air approaching the leading edge of a blade is first slowed down, it then speeds up again as it passes over or beneath the blade. As the velocity changes, so does the dynamic pressure and static pressure according to Bernoulli's principle. Air near the stagnation point has slowed down, and thus the static pressure in this region is higher than the inlet static pressure to main duct. Air that is passing above and below the blade, and thus has speeded up to a value higher than the main inlet path velocity, will produce static pressures that are lower than inlet static pressure. At a point near maximum thickness, maximum velocity and minimum static pressure will occur. Also this figure shows a good agreement with the experimental and computational data for Christophel et al..

Fig. (4) indicates the wall temperature distribution of the air flow through the holes passages and relation with the dimensionless distance of span (z/s). This figure shows hole 10 is at high temperature because the small distance between the suction and pressure side and high temperature at this region, also shows the hole 1 is high wall temperature because the effect of mainstream flow is high at leading edge region. Additionally, this figure shows the low temperature at hole 3 and hole 4 because maximum distance between suction and pressure and the high temperature at the surface does not affect largely on these holes. From Fig. (4), the wall temperature has minimum values (temperature of air) at zero dimensional horizontal z (at entrance region), and maximum values at the end of dimensional distance because of the mixing between cooled and high temperature, also shows stability in temperatures at mid of holes from (z/s=0.2 to z/s=0.8).

Fig. (5) shows the laterally averaged adiabatic effectiveness for small tip gap of the air flow through the holes passages and shows the relation between effectiveness and dimensionless distance of span (z/s). The effectiveness at zero dimensional is high value because the start of cooling happens, but at end of dimensionless distance (z/s) has low effectiveness because of mixing the cooled flow with hot mainstream. Additionally, this figure shows hole 10 has low effectiveness and hole 4 has high effectiveness.

Fig. (6) indicates the local heat transfer coefficient (h) in holes passages with small tip gap, and the relation between (h) and dimensionless distance of span (z/s). This figure shows the local heat transfer coefficient is stable at large range of dimension from (0.2 to 0.8), and decreases at the end of dimensionless distance (z/s), because the large temperature difference between the flow and wall. Additionally heat transfer coefficient at zero dimensionless (z/s) is very large because of low temperature difference between the surface and main temperature of the flow pipe.

Fig. (7) indicates the local Nusselt number distribution at the holes passages and relation with the dimensionless distance of span (z/s). This figure shows high value of Nusselt number in the region before (z/s=0.2) because of high value of local heat transfer coefficient and low value of temperature difference between the

pipe surface and flow inside it, it also shows stable values for the range of (0.2<z/s<0.8) and decrease at the end of dimensionless. Also, hole 1 and hole 10 have minimum Nusselt number and hole 4 has maximum Nusselt number. Also **Fig. (8)** shows the dimensionless Nusselt number relates with dimensionless distance of span (z/s) at small tip gap, when the dimensionless Nusselt is calculated by dividing local Nusselt number to average Nusselt number from Dittus-Boelter correlation. Results show the dimensionless Nusselt number has the same behavior of Fig. (6).

Fig. (9) indicates the average Nusselt number in all holes related with dimensionless distance of span. Twenty points from each segment are chosen and the average point in all hole is found, the equation representing Nusselt number using polynomial with ten degrees of curve fitting which is applied by Tecplot software computer program for drawings. This figure shows high value of Nusselt number at enterance region of dimensionless and low value at the end of diamensionless and shows the Nusselt is nearly stable at mid for the range of (0.2<z/s<0.8) at fully developed region.

*All figures take at small tip gap with blowing ratio at (1%), but in large tip gap is not different large in small tip gap only at exit of holes or at end of dimensionless when high temperature at this region because high leakage flow enter that mean high hot mainstream is entered to this region of mixing***.**

Fig. (10) indicates the relation between dimensionless Nusselt number with the dimensionless distance of span (z/s) at different blowing ratios of small tip gap at hole 1. **Hole 1** is the hot hole between all holes of blade. This figure shows low dimensionless Nusselt number at low blowing ratio and this value increases with increasing the blowing ratio, but that is limited, dimensionless Nusselt number of blowing ratio at 2% is lowest value of dimensionless Nusselt number of blowing ratio of 1.5%. When talk about small tip gap the coolant flow that exit from hole 1 at different blowing ratio is impact at shroud and mixed with the leakage flow and this mixing is not affected of high blowing ratio at 2% because when the velocity of hole passage increases, it impacts the shroud and some of the flow will be dissipated, therefore any increasing in coolant flow is dissipated also.

Fig. (11) indicates the relation between dimensionless Nusselt number with the dimensionless distance of span (z/s) at different blowing ratios of small tip gap at hole 4. **Hole 4** is the cold hole between all holes of blade. This figure shows that the Nusselt number is decreased along the hole which is verified with the temperature distribution behaviors, and shows low dimensionless Nusselt number at low blowing ratio at 0.5% and this value increases with increasing the blowing ratio to 1%, but that is limited also, dimensionless Nusselt number of high blowing ratios at 1.5% and 2% are lowest values of dimensionless Nusselt number of low blowing ratios at 0.5% and 1%, because the coolant flow impacts the shroud and makes the flow inside pipe slow, and notes the coolant flow is poor mixed with the leakage flow, therefore that makes the high blowing ratio decrease.

CONCLUSION

From the results, it can be concluded that the heat transfer can reach the max value at the hole of the number 4 (at maximum distance of blade) and min value at the hole of numbers 1 (when flow was impact at the blade at leading edge) and 10 (at minimum distance at trailing edge) [the number of holes shows in Fig.(2-b)]. Heat transfer coefficient is high values at entrance regions. Results showed that baseline Nusselt numbers on the holes were reduced along the holes. The cooling of blade increases as the amount of blowing ratio increases but that is limited because the flow will be dissipated**.** Finally, the pressure coefficient distribution is same in engine when compared with experimental data of Christophel et al. (2004).

Nomenclature

Symbol	*Description*	Dimension
A	Coefficient of the discretized equation, area	m^2
B_x	Axial chord of the blade	m
C	Chord of the blade	m
G_1,G_2	Contravariant velocity in ξ,η, respectively	m/s
J	Jacobian of coordinates transformation	
P	Pressure	pa
Re_{pipe}	Reynolds Number (Re=ρUD/μ)	
Nu	Nusselt number (hd/k)	
S	Span length	m
$S_{\square}$	Source term of □	
T	Temperature	K
u ,v	Velocity component in r, z respectively	m/s
U_∞	Velocity at mainstream conditions	m/s
U_c	Velocity at cooling condition	m/s
BR	Blowing ratio(U_∞/ U_c)	
P	Static pressure	N/m^2
T_g	Temperature of hot gases	□ C
T_c	Temperature of cooling air	□ C
T_{in}	Temperature at inlet condition	□ C
u, v	Velocity component in x ,y coordinate direction respectively	m/s
r,z	Cylindrical coordinate	
	Subscript	
ξ ,η	Partial derivative in the computational plane	
aw	Adiabatic wall	
	Superscript	
c	Coolant conditions	
∞	Mainstream conditions	
	Greek Letters	
□	Dependent variable	
η	Adiabatic effectiveness , $\eta = (T_{in}-T_{aw})/(T_{in}-T_c)$	
C_p	$(p - p_{in})/(0.5\,\rho\, U_{in}^2)$	
ρ	Density	kg/
ε	Rate of dissipation of kinetic energy	m^2
μ	Dynamic viscosity	N.n

	Abbreviation
C.F.D	Computational Fluid Dynamics
SIMPLE	Semi-Implicit Method for Pressure Linked Equation

REFRENCES

Acharya, S., Yonk, H., Prakash, C. and Bunker, R., "Numerical Study of Flow and Heat Transfer on a Blade tip with Different Leakage Reduction Strategies", ASME paper No. GT-2003-38617, 2003.

Allen, H. W. and. Kofskey, M.G, "Visualization Study of Secondary Flows in Turbine Rotor Tip Regions", NACA Technical Note 3519, 1955.

Arnal, M.P., "A General computer program for two-dimensional, turbulent, re-circulating flows", Report No.Fm-83-2, 1983.

Bunker, R. S., "Cooling Design Analysis", AIAA Journal of Propulsion and Power, 2002.

Christophel, J. R., Couch, E., Thole, K. A. and Cunha, F. J., "Measured Adiabatic Effectiveness and Heat Transfer for Blowing from the Tip of a Turbine Blade", ASME paper No. GT2004-53250, 2004.

Cohen H., Rogers G.F.C., and Saravanamutto H.I.H., "Gas turbine theory", 3rd edition, Longman scientific and technical, 1987.

Couch, E., "Measurement of Cooling Effectiveness along the Tip of a Turbine Blade", Master's Thesis, Virginia Polytechnic Institute and State University, Blacksburg, VA, 2003.

Fluent Inc., Fluent User's Guide, Version 6.3.26, 2009.

Hohlfeld, E. M., "Film Cooling Predictions Alone the Tip and Platform of a Turbine Blade",

Master's Thesis, Virginia Polytechnic Institute and State University, Blacksburg, VA, 2003.

Ideriah, F. J. K., "Review of equation solved in TEACH", private communication, 1975

Jonas, B., "Internal cooling of gas turbine blades", PhD, Chalmers university of Technology Goterborg, Sweden, 2002.

Karki, K., and Patankar, S., "Pressure Based Calculation Procedure for Viscous Flows at All Speeds in Arbitrary Configurations", ALAa Journal, Vol. 27, PP. 1167-1174, 1989.

Launder, B.E. and Spalding, D.B.," Mathematical models of turbulence", Academic press, London, 1972.

Nasir H. S., Ekkad, V., Divad M. K., Bunker, R. S. and Prakash C., "Effect of Tip Gap and Squealer Geometry on Measured Heat Transfer Over a HPT Rotor Blade Tip", J. of Turbomachinery, 125, pp. 221-228, 2003.

Verestage, H. K., and Malalasekera, W., "An Introduction to Computational Fluid Dynamic-The Finite volume Method", Longman Group Ltd, 1995.

Yang, H., Chen, H-C and Han, J-C, "Numerical Prediction of Film Cooling and Heat Transfer With Different Hole Arrangements on the plane and Squealer Tip of a Gas Turbine Blade", ASME Paper No. GT2004-53199, 2004.

Table (1) Values of constants in the (k-ε) model.

C_μ	C_D	C_1	C_2	σ_k	σ_ε
0.09	**1.0**	**1.44**	**1.92**	**1.0**	**1.3**

Table (2) Special design of geometry and flow condition of the blade from Hohlfeld (2003).

Parameter	Value
Scaling Factor	12X
Axial Chord, B_x	35 cm
True Chord, C	53 cm
Pitch, P	43 cm
Span, S	55.2 cm
Re	2.1E+05
Inlet Angle, θ	16.5°
Blade Angle, □	50□
Small tip gap, h	0.03 cm
Large tip gap, H	0.09 c m

Table (3) Holes locations.

Holes	X(cm)	Y(cm)	Diameter(cm)
1	3.43	40.5	0.7
2	6.86	40.43	0.7
3	10.3	39.5	0.7
4	13.7	37.68	0.6
5	17.15	34.91	0.6
6	20.3	31.48	0.6
7	23.2	27.15	0.6
8	26.02	21.857	0.6
9	28.45	16.802	0.6
10	30.88	10.66	0.6

Table (4) Summery of present study

Governing equations	Continuity, Navair-Stokes, Energy, Turbulent Kinetic Energy and dissipation rate
Coordinates	Non-Orthogonal body fitted coordinate system
Assumptions	Perfect gas, steady, incompressible, single phase, shock free, turbulent
Grid generation	Algebraic equations
Transformation from physical to computational domain	Jacopian
General form of discretization	Finite volume
Grid arrangement	Collocated
Convective Schemes	Upwind
Pressure-velocity coupling	SIMLPE algorithm
Matrix solution method	TDME
Boundary condition	**1.** No-slip condition was applied to the shroud and all blade surfaces. **2.** All walls were adiabatic for adiabatic effectiveness cases, and for heat transfer coefficient cases only the tip or tip and shelf were changed to have constant heat flux conditions. **3.** The main inlet was specified as a constant velocity inlet at **11.3** m/s .

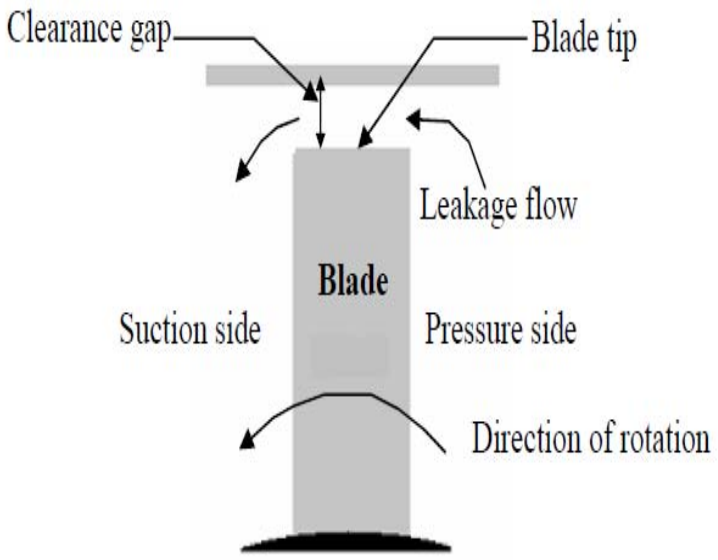

Fig. (1) Conceptual view of the leakage flow through the clearance gap.

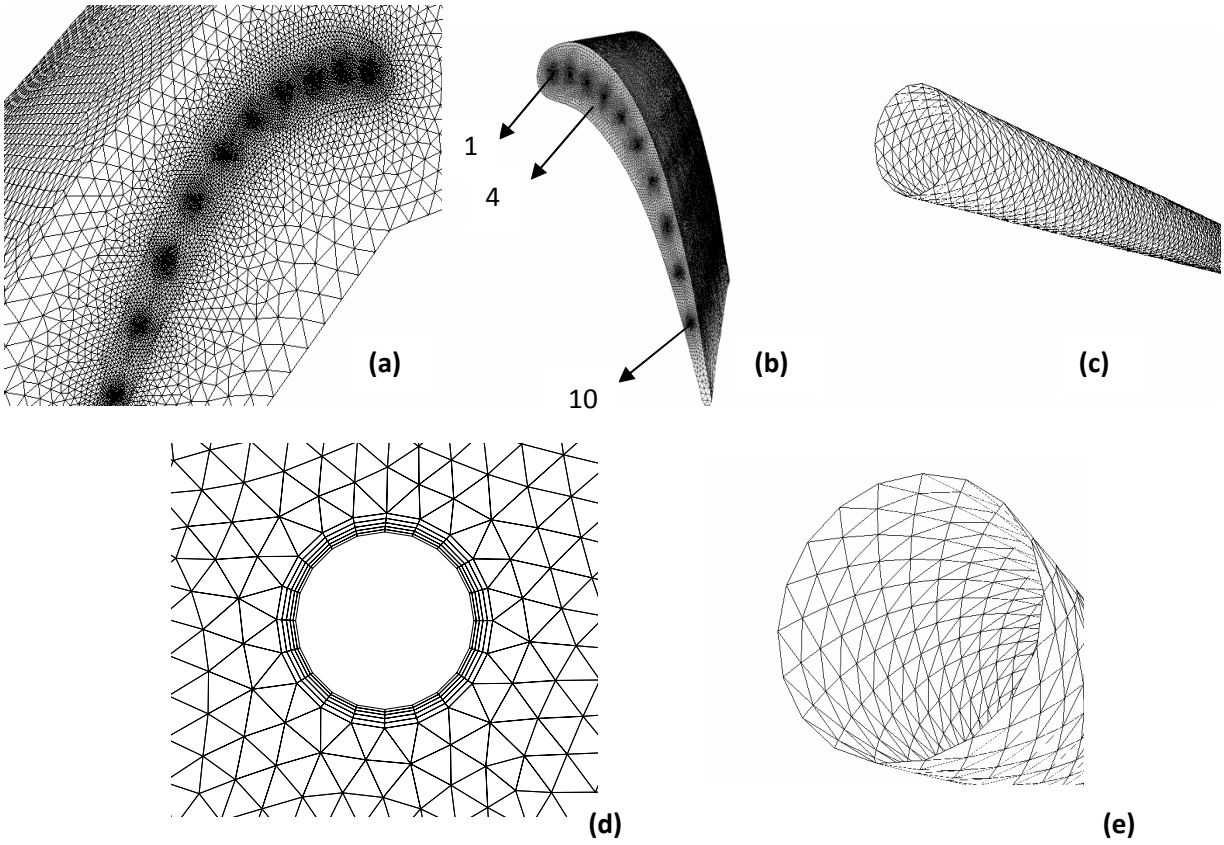

Fig. (2) Shows the mesh at (a) duct, (b) blade, (c) holes, (d) boundary layer around the holes and (e) point at holes edge.

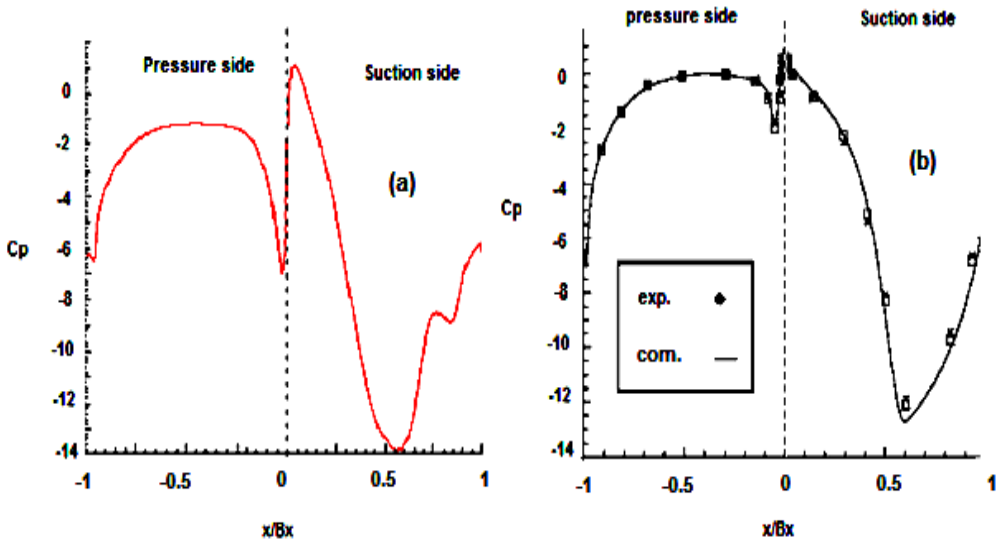

Fig. (3) Predicted static pressure distributions at suction and pressure side for (a) computational of present study, (b) experimental and computational from Christophel et al (2004).

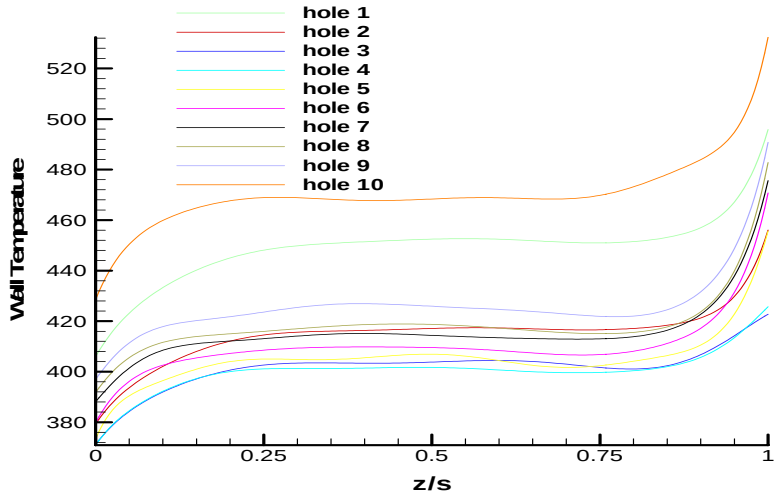

Fig. (4) The wall temperature distribution through the length of holes in small tip gap.

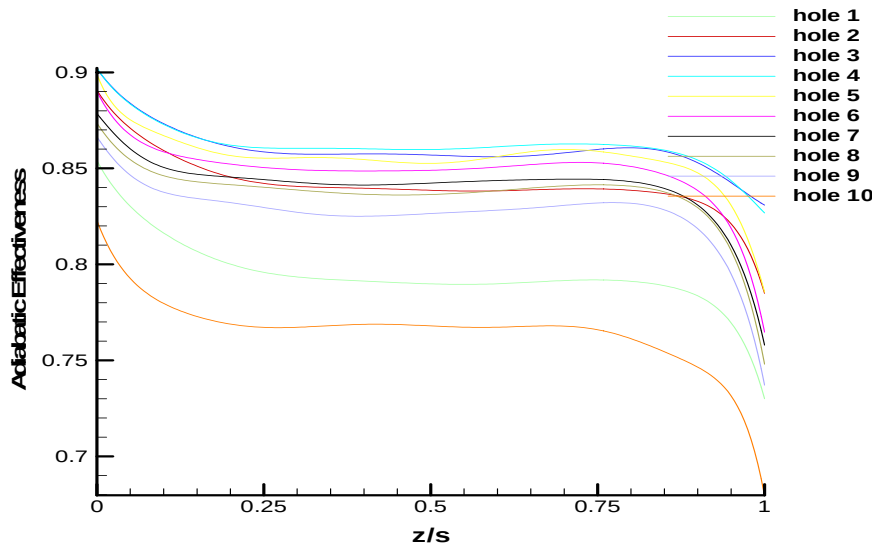

Fig. (5) Laterally averaged adiabatic effectiveness alone the holes at small tip gap.

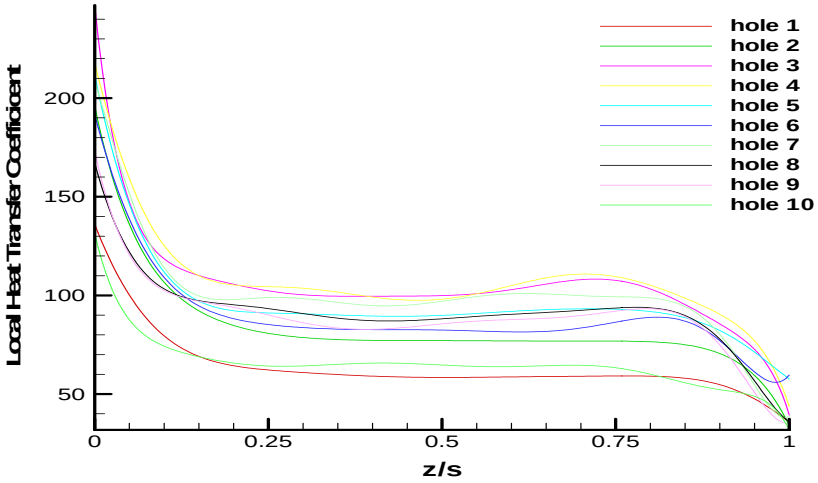

Fig. (6) Local heat transfer coefficient alone the holes at small tip gap.

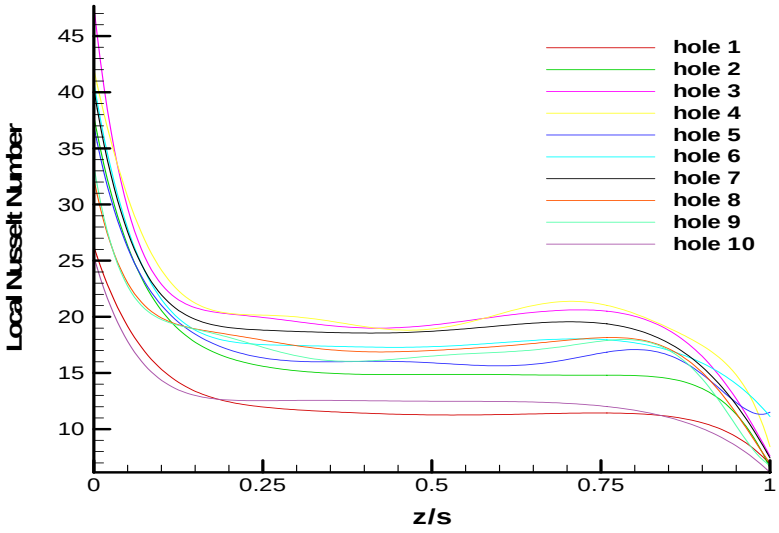

Fig. (7) Local Nusselt Number alone the holes at small tip gap.

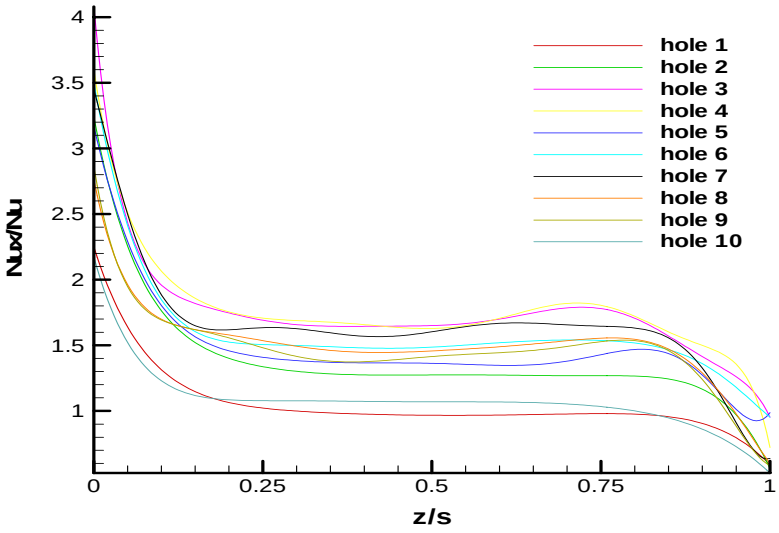

Fig. (8) The Relation between dimensionless Nusselt number and distance of span at different holes of blade.

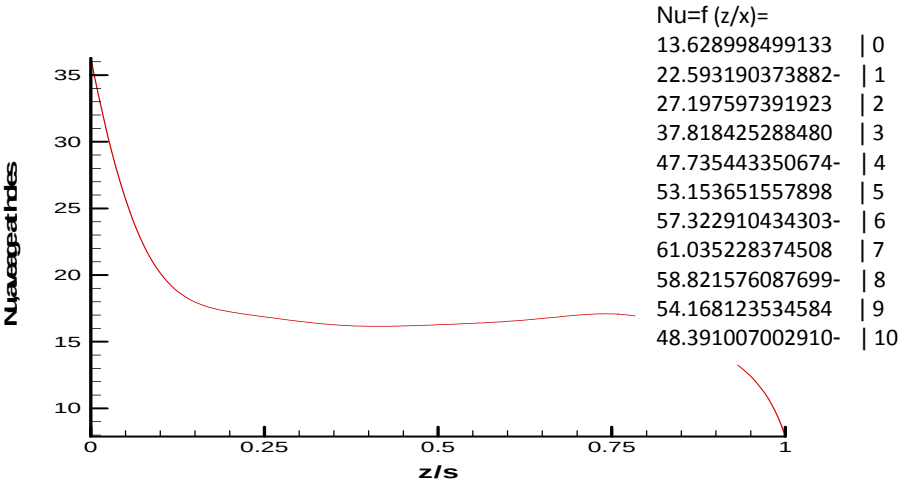

Fig. (9) Nusselt number average in all holes for small tip gap with blowing ratio (1%).

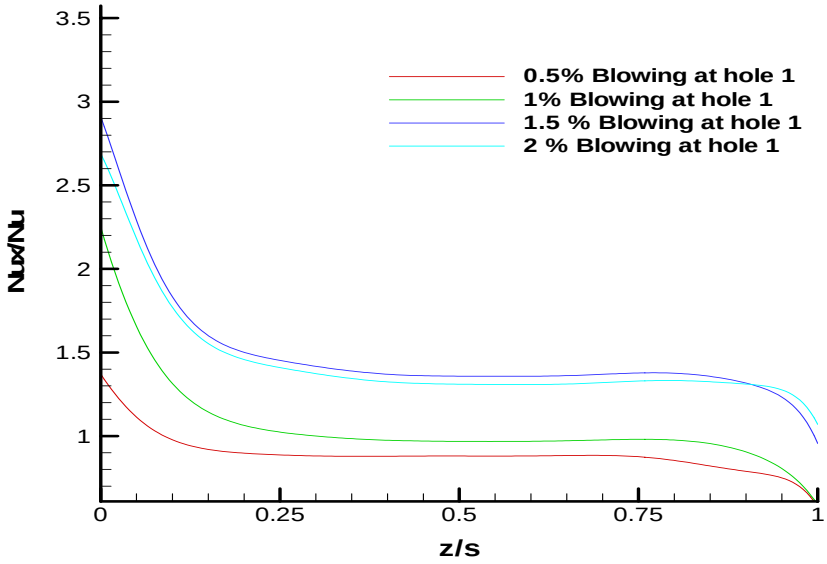

Fig. (10) The Relation between dimensionless Nusselt number and distance of span at different blowing ratio of hole 1.

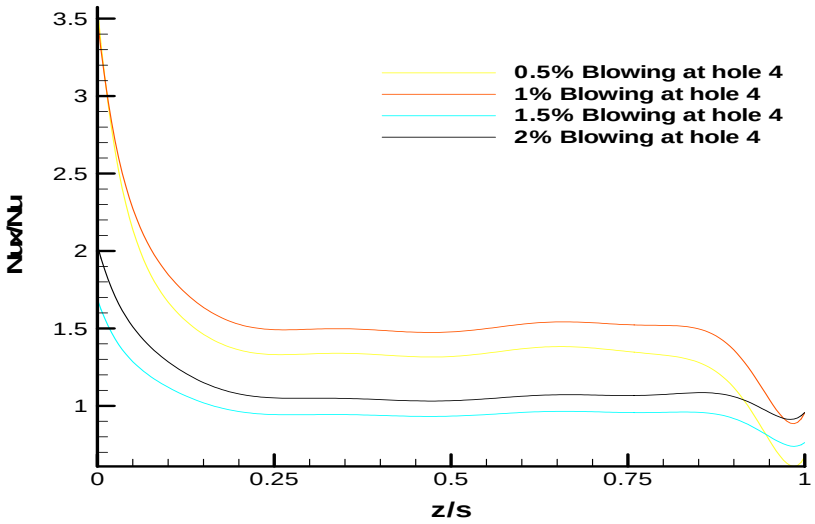

Fig. (11) The Relation between dimensionless nusselt number and distance of span at different blowing ratio of hole 4.

Simulation of Longitudinal Stability Of Helicopter In Forward Flight

Asst. Lect. Kareem Jawad Kadhim and Asst. Lect. Abid Noor Jameel shahid
Univ. of Baghdad, College of Eng., Mech. Dept.
Kareemjawad@yahoo.com : Abidnoor@yahoo.com

ABSTRACT

The present work describes the development of code for trim and longitudinal stability analysis of a helicopter in forward flight. In general, particular use of these codes can be made for parametric investigation of the effects of the external and internal systems integrated to UH-60 helicopters.

A forward flight longitudinal dynamic stability code is also developed in the work to solve the longitudinal part of the whole coupled matrix of equations of motion of a helicopter in forward flight. The coupling is eliminated by linearization. The trim analysis results are used as inputs to the dynamic stability code. The forward flight stability code is applied to UH-60 helicopter.

Keywords: Helicopter, UH-60, forward flight, hover, longitudinal, trim, dynamic stability

محاكاة الاستقرارية الطولية للهليكوبتر في الطيران الامامي

م.م كريم جواد كاظم وم.م عبد نور جميل شهيد

الخلاصة:

يوضح البحث الحالي تطوير برنامج لتحليل الاستقرارية الطولية للمروحية في الطيران الامامي. بشكل عام، الاستعمال العملي لهذه البرامج يمكن استعمالها في حساب العوامل المؤثرة على الانظمة الخارجية والداخلية للطائرة المروحية من نوع UH-60. تم بناء البرنامج الخاص بالاستقرارية الديناميكية الطولية للطيران الامامي لحل الجزء الطولي للمصفوفة الكاملة لمعادلات الحركة للطائرة المروحية. تم الغاء الارتباط باستخدام الطريقة الخطية. ان نتائج الاستقرارية الساكنة استخدمت كمدخلا الى برنامج الاستقرارية الحركية. تم تطبيق برنامج الاستقرارية للطيران الامامي على الطائرة UH-60.

الكلمات الرئيسية : هليكوبتر ،uh-60 ، الطيران الامامي ، حوامة ، الطولية، ألية الترم ، الاستقرارية الديناميكية

INTRODUCTION

A helicopter is an aircraft that uses rotating wings to provide lift, control, and forward, backward and sideward propulsion. Because of the rotating parts, it has much more capability of maneuvering, while having restrictions on high speeds and high altitudes. Unlike aircraft, the helicopter has the possibilities of vertical landing and takeoff, low speed flight, hover and safe autorotation. For these reasons, helicopters are used in low-altitude; small range combat and search-and-rescue purposes as well as pleasure travels. Although there are some commercial computational fluid dynamics (CFD) programs which may readily be used for helicopter aerodynamic analyses, there are not many off-the-shelf programs for analyzing trim and dynamic stability characteristics of rotorcraft.

Many of these codes interface with each other. One really much needed and extensively used feature that can be benefited from such codes during an aerodynamic analysis phase is the ability to link to some routines through which the trim parameters such as the main rotor tip path plane (TPP) angle, collective angle, longitudinal and lateral cyclic angles, etc. can be acquired and

placed very conveniently in hundreds of input files read in by the aerodynamic analysis codes, such as **VSAERO** and **USAERO**. Trim of a helicopter is the situation in which all the forces, inertial and gravitational, as well as the overall moment vectors are in balance in the three

mutually perpendicular axes. Stability is the tendency of a trimmed aircraft to return to the trim condition after a disturbance is applied. Static stability analyzes the initial tendency, while the dynamic stability considers the subsequent motion in time. The aircraft is said to be stable if it returns to equilibrium, and unstable if diverges. The case in which the aircraft has no change in motion is called neutral stability. The motion can be oscillatory or non-oscillatory. Although a full model should be used if a comprehensive helicopter dynamic stability analysis is to be performed, it is possible to look at a partial analysis using engineering judgments. Longitudinal and lateral dynamic stability can be differentiated. Also, since the transition from hover to a low-speed forward flight (e.g. 30 knots) is continuous, the hover and forward flight cases can be analyzed separately. The objective of linked together and used for helicopter trim and dynamic stability analyses. The mathematical development behind all these codes includes many simplifications and assumptions, which are explained in this work.

FORCES AND MOMENTS ACTING ON A HELICOPTER IN FLIGHT

The helicopters come in many sizes and shapes, but most share the same major components. The main rotor is the main airfoil surface that produces lift. The main rotor is the main control mechanism. A helicopter can have a single main rotor, two rotors can be mounted coaxially or they can be in tandem configuration. The main rotor provides the speed and maneuvering controls, as well as the lift needed for the helicopter to fly. The tail rotor is required from the torque effect produced by spinning the main rotor. The rotors are driven through a transmission system by one or two engines, generally being gas turbine engines. The horizontal stabilator serves as a wing which produces lift and helps stabilizing the helicopter in forward direction. The vertical stabilizer generally has a wing-like geometry which produces side force and helps stabilizing the helicopter in lateral directions. The forces and moments acting on a helicopter in trim position are shown. In the figure (1), the vertical stabilizer side force is given as Y_V, in ideal case it is not directed straight to the side and has an angle, but for simplicity purposes it is shown as directed to (-)Y-axis. It is assumed that the tail rotor has no incidence and its thrust vector is given as T_T. The drag forces on all of the components of the helicopter are shown as one vector *D,* which is directed to (–) X-direction for simplicity purposes again. The lift and pitching moment vectors *L* and *M* , stand for the lift and pitching moment produced by the fuselage and the horizontal stabilizer, as well as the wings if exist. Gross weight is shown as *W.* The torque vector produced by the main rotor which is rotating counter-clockwise is shown in order to state the anti-torque effect of the tail rotor.

HELICOPTER ROTOR SYSTEM

There are four primary types of rotor systems: articulated, teetering, semi-rigid and hingeless. The articulated rotor system first appeared on the autogyros of the 1920s and is the oldest and most widely used type of rotor system. The rotor blades in this type of system can move in three ways as it turns around the rotor hub and each blade can move independently of the others. They can move up and down (flapping), back and forth in the horizontal plane, and can change in the pitch angle (the tilt of the blade) as shown in figure (2). In the semi-rigid rotor system, the blades are attached rigidly to the hub but the hub itself can tilt in any direction about the top of the mast. This system generally appears on helicopters with two rotor blades figure (3). The teetering rotor system resembles a seesaw, when one blade is pushed down, the opposite one rises. The hingeless rotor system functions much as the articulated system does, but uses elastomeric bearings and composite flexures to allow for flapping and lead-lag movements of the blades in place of conventional hinges figure (4). Its advantages are improved control response with less lag and substantial improvements in vibration control. It does not have the risk of ground-resonance associated with the articulated type, but it is considerably more expensive. The use of hinges was first suggested by Renard in 1904 as a means of relieving the large bending stresses at the blade root and of eliminating the rolling moment which arises in forward flight, but the first successful practical application was due to Cierva in the early 1920s. The most important of these hinges is the flapping hinge which allows the blade to flap. A blade which is free to flap experiences large Coriolis moments in the plane of rotation and a further hinge – called the drag or lag hinge – is provided to relieve these moments. Lastly, the blade can be feathered about a third axis, parallel to the blade span, to enable the blade pitch angle to be changed. The hinges are shown in Figure (2), where an articulated rotor is demonstrated. The blades of two-bladed rotors

are usually mounted as a single unit on a 'seesaw' or 'teetering' hinge. No lag hinges are fitted. Figure (3) demonstrates a teetering rotor. The semi-rigid rotor resembles the teetering rotor, but now the hub itself also moves about the top of the mast. The hub is strictly attached to the blades.

Hingeless rotors does not have regular flapping and lagging hinges and have blades which are connected to the shaft in cantilever fashion but which have flexible elements near to the root, allowing the flapping and lagging freedoms. A hingeless rotor is shown in Figure (4). The collective changes the pitch angle of the rotor blades causing the helicopter to climb and descend. Through the swash plate, the cyclic controls the pitch angle distribution over the main rotor disc and by this way the disc is tilted sideways or backwards in order to turn, go backwards or change the speed of the helicopter. The anti-torque pedals control the helicopters tail rotor and are used to point the nose of the helicopter in the desired direction. The function of the throttle is to regulate the engine r.p.m.

HELICOPTER ROTOR ERODYNAMICS

There are two basic theoretical approaches to understand the generation of thrust from a rotor system: momentum theory and blade element theory. The momentum theory makes certain additional assumptions, which limit the accuracy:

• The flow both upstream and downstream of the disk is uniform, occurs at constant energy and is contained within a stream tube.

• No rotation is imparted on the fluid by the action of the rotor.

The blade element theory overcomes some of the restrictions inherent in the momentum theory. It considers the local aerodynamic forces on the blade at radial and azimuthally sections, and integrates the forces to find the overall thrust and drag on the rotor. The lift at the blade tips decreases to zero over a finite radial distance, rather than extending all the way out to the edge of the disk. Thus, there will be a reduction in the thrust, or increase in the induced power of the rotor. Forward flight is a more complex situation compared to the hover. Because of the forward velocity, the relative speed of the blade sections differ around the azimuth, and therefore, an imbalance of aerodynamic forces occur along the main rotor disc. The advancing blade has a velocity relative to the air higher than the rotational velocity, while the retreating blade has a lower velocity relative to the air. This lateral asymmetry has a major influence on the rotor and its analysis in forward flight. The dynamic stall phenomenon is another effect coming with the forward flight situation. As blade incidence increases beyond the static stall point, flow reversals are observed in the upper surface boundary layer, but for a time these are not transmitted to the outside potential flow region. Consequently, the lift force goes on increasing with incidence. Eventually, flow separation develops at the leading edge (it may be behind a recompression shock close to the leading edge), creating a transverse vortex which begins to travel downstream. The proximity of the ground to the hovering rotor disk constrains the rotor wake and reduces the induced velocity at the rotor, which means a reduction in the power required for a given thrust; this behavior is called ground effect. The effect exists at low speed forward flight also. Equivalently, ground proximity increases the rotor thrust at a given power.

TRIM AND STABILITY

When all of the forces and moments (i.e. the aerodynamic, inertial and gravitational) about three mutually perpendicular axes are equal, the aircraft is in a state of equilibrium. That equilibrium state is called trim. When propulsive force is greater than drag the aircraft will accelerate; when lift is greater than the weight the aircraft will climb. Each of the blades has two primary degrees of freedom: flapping and lagging, which take place about either mechanical or virtual hinges near the blade root. A third degree of freedom allows cyclic pitch or feathering of the blade. Despite the fact that helicopter blades are relatively flexible, the basic physics of the blade dynamics can be explained by assuming them as rigid. In hovering flight the air loads do not vary with azimuth, and so the blades flap up and lag back with respect to the hub and reach a steady equilibrium position under a simple balance of aerodynamic and centrifugal forces. However, in forward flight the fluctuating air loads cause continuous flapping motion and give rise to aerodynamic, inertial, and Coriolis forces on the blades that result in a dynamic response. The flapping hinge allows the effects of the cyclically varying air loads to reach equilibrium with air loads produced by the blade flapping motion. The flapping motion is highly damped by the aerodynamic forces. The helicopter system can be reduced to 6 DOF like a fixed wing aircraft, three for translation and three for rotation. A statically unstable motion is also dynamically

unstable but a statically stable motion may be either stable or unstable dynamically.

The following general simplifications are implemented in order to make the problem easier:
– The helicopter structure is considered to be absolutely rigid;
– Longitudinal and lateral motions are uncoupled so they can be treated independently;
– No time lags are considered;
– One DOF coming from the throttle is eliminated and the rotor speed is set as constant;
– The blades are assumed as uniform and the lag bending, elastic twist, and axial deflections are disregarded, except the flapping motion;
– The blades do not bend or twist elastically;
– The blades have homogeneous mass distribution;
– Harmonics higher than 2nd order of flapping and cyclic angles are neglected;
– Empirical downwash, side wash, L&D of empennage are used;
– The codes are applicable only to helicopters with single main rotor and a tail rotor;
– Climb angle and sideslip angle are set as zero.

On the basis of these simplifications, the system describing the helicopter motion can be reduced to six equations. These equations are the total forces and moments on each of the coordinate axis:

$$\sum X = 0 \Leftrightarrow X_M + X_T + X_H + X_V + X_F = W.Sin\Theta$$
$$\sum Y = 0 \Leftrightarrow Y_M + Y_T + Y_V + Y_F = -W.Sin\Phi$$
$$\sum Z = 0 \Leftrightarrow Z_M + Z_T + Z_H + Z_V + Z_F = -W.Cos\Phi$$
$$\sum L = 0 \Leftrightarrow L_M + Y_M h_M + Z_M y_M + Y_T h_T + Y_V h_V + Y_F h_F + L_F = 0$$
$$\sum M = 0 \Leftrightarrow \begin{pmatrix} M_M - X_M h_M + Z_M l_M + M_T - X_T h_T + Z_T l_T - X_H h_H \\ + Z_H l_H - X_V h_V + M_F + Z_F l_F - X_F h_F \end{pmatrix} = 0$$
$$\sum N = 0 \Leftrightarrow N_M - Y_M l_M - Y_T l_T - Y_V l_V + N_F - Y_F l_F = 0$$

The forces and moments with the moment arms are demonstrated in Figure (5). The details on the calculations of the forces expressed in the appendix (A).

TRIM CODE

The motion of helicopter in trim is governed by 6 equations, three for total forces acting on the aircraft and three for total moments on each coordinate of the body frame. One can separate the longitudinal and lateral equations and solve the related parameters without much degradation on the accuracy. Therefore, the code solves only for three equations, which are the total forces on the longitudinal and vertical axis and the total moments on the lateral axis.

The code is composed of two models, called CF and XZM. The first model supplies approximate trim parameters which are used as inputs to the second models. The second model, uses those input parameters in order to linearize the non-linear equations of motion and gives the exact parameters. The flow chart of the code is give in Fig (7).

The code is applicable to flight velocities higher than 30 Knots. This is because the angle of attack over the empennage diverges to unstable values. The first model is based on calculating the following two parameters α_{TPP} and T_M, and modifying the other trim variables according to those parameters.

$$\alpha_{TPP} = \tan^{-1}\frac{D_F + H_M + H_T}{W - L_F}$$
$$T_M = \sqrt{(W - L_F)^2 + (D_F + H_M + H_T)^2}$$

here L_F and D_F corresponding to the lift and drag over the fuselage for the empennage on case. The fuselage lift, drag and pitching moment parameters are calculated from experimental data published in previous works of the helicopter. The second model XZM calculates the total forces and moments in x, z and lateral moment directions.

DYNAMIC STABILITY CODE

Longitudinal stability of the helicopter in forward flight is analyzed in two modes: short period mode and phugoid mode. Those frequently oscillatory motions are observed just after a disturbance -like a vertical gust or a longitudinal cyclic step input- occurs. The short period response is based mainly on pitching motion and generally damps quickly. The energy is converted to kinetic energy while descending and the velocity increases; increased velocity increases the thrust and the helicopter is forced to climb; then as the climbing occurs, the velocity is decreased again. The responses of the helicopter after a disturbance are shown in Figure (8).

The dynamic stability code calculates the required stability derivative, the characteristic equation and the roots, and determines about the stability of the helicopter after a step disturbance given by longitudinal cyclic, the collective or due to a vertical gust. The calculation of the stability derivatives are given in appendix A.

TRIMING RESULTS

The helicopter type of UH-60 has input parameters as shown in table (1). The trim results are obtained at velocity 115 Knots and tabled in table (2). The code gives accurate results for the

main rotor parameters as compared with actual results and also for tail rotor thrust and torque.

STABILITY RESULTS OF UH-60 HELICOPTER

It is more logical to find out the static stability characteristics before the dynamic stability is analyzed. Partial derivative of pitching moment of the helicopter with respect to the vertical velocity is a good indicator of the static stability: If the sign of the derivative is positive, then the helicopter is statically stable, and vice versa. In Figure (8), it is clear that the helicopter is statically unstable up to about 130 knots, and becomes stable after that speed. For the dynamic stability, it can be concluded that the helicopter is unstable up 130 knots. Nothing can be said for the speeds higher than 130. The coefficients of the characteristic equation and the Routh's Discriminant values for all forward flight cases are shown in Figure (9). It is seen that until about 110 knots the helicopter shows tendency to go completely divergent in longitudinal aspect. After that speed until about 150 knots, there should be no unstable oscillations, according to the Routh's test. This means that either there are no oscillations, whether divergent or convergent, or the system is stable, whether oscillatory or not. After 150 knots, the helicopter goes divergent again. Looking to the coefficients, the criterion says that if one of the coefficients is negative, than pure divergence or unstable oscillations occur. This is just the case for UH-60 helicopter, since for all forward flight cases there is only one coefficient which is negative, it is C for speeds below 110 knots and D for speeds after 110 knots. Therefore, it can be concluded that for all forward velocity range the helicopter is purely divergent, even though it is statically stable at speeds higher than 130 knots.

The Phugoid motion characteristics change with changing speed (See Figure (10). The period values are very reasonable up to a point where the period goes to very high values. After that speed the attitude changes from divergent to convergent and the period tends to decrease. 110 knots is very likely to be the maximum range speed. The relation which can be occurring between the maximum range speed and the speed which changes the dynamic stability attitude of the helicopter is a good point of discussion. The divergency / convergency characteristics of phugoid motion are pretty obvious in Figure (11). The time-to-double values change sign at the speed the roots change sign. It is obvious that the motion changes attitude from divergent to convergent at about 110 knots. The non-oscillatory roots are also describing some of the dynamic stability characteristics. There is a change in mode from convergent to divergent at the same critical speed, 110 knots, as it is seen at Figure (12). Those roots belong to the short period mode. It can be concluded that, while the phugoid mode shows divergent characteristics up to that critical speed, the short period mode is convergent, and vice versa. This is an interesting result. The change in the X forces per unit change in the forward velocity is called the 'Drag Damping', since the dominant effect comes from the drag forces. The graph below shows that the effect of the drag forces increases as the forward flight increases. The same conclusion can be made for the vertical damping and the pitch damping. Those are the greatest parameters which affect the longitudinal stability of the

CONCLUSIONS

This work describes the development of codes for trim and longitudinal stability analysis of a helicopter in forward flight. The trim analysis results are obtained for a clean UH-60 configuration. One of the trim codes is based on momentum theory. These codes include many simplifying assumptions such as empirical uniform wake model. Nevertheless, application of these codes to some example helicopters indicated reasonably good agreement with the other available data, particularly for the main rotor performance. The results indicated that, improvements are needed in calculation of the torque, and thereby the parameters related to the tail rotor.

Table (1): UH-60 helicopter input parameters.

Description	Algebraic Symbol	Value	Unit
Moment of inertia about y axis	I_{yy}	40000	slug.ft^2
Weight of the helicopter	GW	20000	lb
MAIN ROTOR			
Radius	R_M	30	ft
Chord	c_M	2	ft
Number of Blades	b	4	
Revolution Speed	Ω	21.667	rad/sec
Lift curve slope (NACA 0012)	a	5.73	per radian
Zero Lift Angle of Attack	$\alpha_{L=0}$	0	
Blade twist angle	θ_1	-10	degrees
Height of the rotor above C.G.	h_M	7.5	ft
Long. Distance to C.G.	l_M	-0.4839	ft
Hinge offset ratio	e	0.05	
Blade cut-out ratio	$\frac{x_o}{R}$	0.15	
Flapping inertia of one blade	I_b	2900	slug.ft^2
Polar moment of inertia	J_M	11600	slug.ft^2
Shaft incidence	i_M	0	degrees
TAIL ROTOR			
Radius	R_T	6.5	ft
Chord	c_T	1	ft
Number of Blades	b_T	4	
Revolution Speed	Ω_T	100	rad/sec
Lift curve slope	a_T	6	per radian
Blade twist angle	$\theta_{1,T}$	-5	degrees
Height of the rotor above C.G.	h_T	6	ft
Long. Distance to C.G.	l_T	37	ft
Shaft incidence	i_T	0	degrees
Delta3 angle	δ_3	-30	degrees
Flapping inertia of one blade	$I_{b,T}$	6.25	slug.ft^2
HORIZONTAL STABILIZER			
Span	b_H	9	ft
Area (incl. area inside tail boom)	A_H	18	ft^2
Zero Lift Angle of Attack	$\alpha_{L=0,H}$	0	rad
Moment arm (measured from its rotational axis)	l_H	33	ft
Height above C.G	h_H	-1.5	ft
Incidence	i_H	-3	degrees
VERTICAL STABILIZER			
Span	b_V	7.7	ft
Area (incl. area inside tail boom)	A_V	33	ft^2
Rudder deflection	$\delta_{r,V}$	10	degrees
Moment arm	l_V	35	ft
Height above C.G	h_V	3	ft
FUSELAGE	f_o $\frac{\partial f}{\partial(\alpha_F^2)}$	17.9 0.023	ft^2 ft^2/deg^2
Wetted area	S_{W_F}	680	ft^2
Moment arm	l_F	-0.5	ft
Lift - Empennage on	$\left(L_F/q\right)_{\alpha_F=0}$ $\frac{\partial\left(L_F/q\right)}{\partial\alpha_F}$	-5 111.8987	ft^2 ft^2/rad
Pitch Moment $M_F = q\left\{\left(M_F/q\right)_{\alpha_F=0} + \frac{\partial\left(M_F/q\right)}{\partial\alpha_F}\alpha_F\right\}$	$\left(M_F/q\right)_{\alpha_F=0}$ $\frac{\partial\left(M_F/q\right)}{\partial\alpha_F}$	-160 1789	ft^3 ft^3/rad
Drag divergence Mach #	M_{dd}	0.725	

Table (2): Trim results compared with experimental results of ref (1).

Parameter	theory	experiment	unit
v_1	7.89	7.91	-
a_{1sm}	-0.9	-1.0886	deg
T_m	20544.29	20586	lbf
H_m	-287.58	-145	lbf
Q_m	33512.22	34573	lbf.ft
b_{1sT}	-0.17	-.3094	deg
Q_m	905.45	934.4	lbf.
T_t	629.7	661	lbf
H_t	-19.55	40	lbf
Q_t	120.73	127	lbf.ft
α_f	2.94	3.675	deg
L_f	-480.66	556	lbf
D_f	871.86	867	lbf
M_f	-11248.68	-11722	lbf.ft
Θ	-0.61	-0.9454	deg
α_v	-7.92	8.0743	deg
L_v	-267.46	-273	lbf
D_v	14.30	15	lbf
L_h	287.93	287	lbf
D_h	51.48	58	lbf

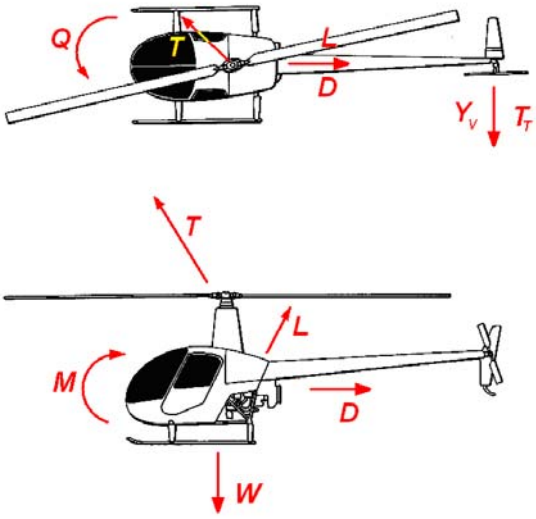

Figure (1): Forces and moments acting on a helicopter.

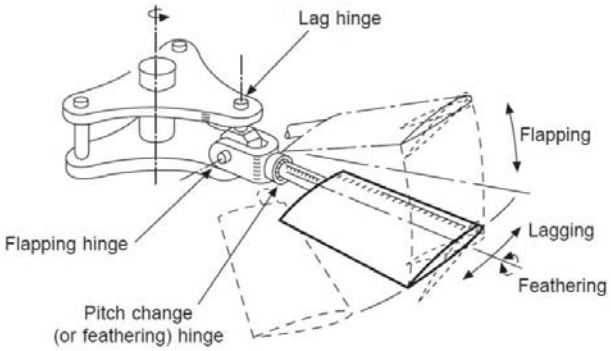

Figure (2): Hinges on an articulated rotor.

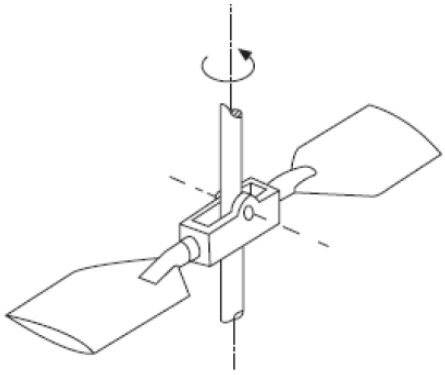

Figure (3): Teetering rotor.

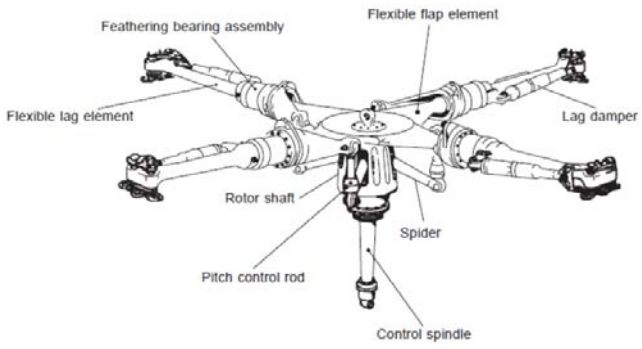

Figure (4): Hingeless rotor.

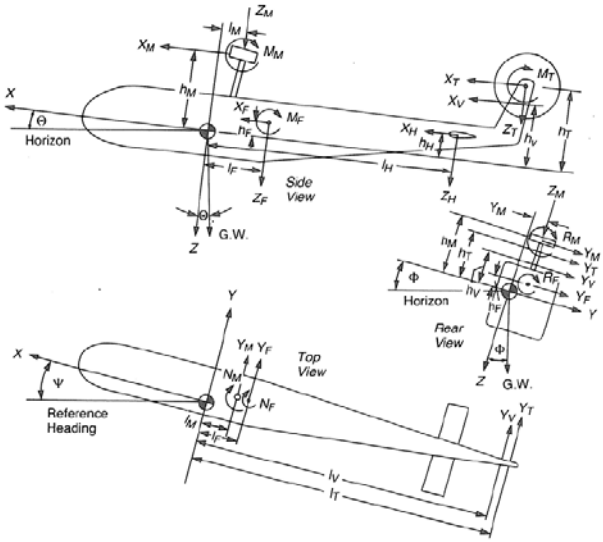

Figure (5): Forces and moments acting on a helicopter [3].

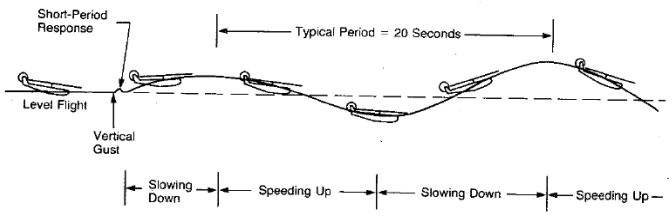

Figure (6): The Phugoid and Short Period Modes.

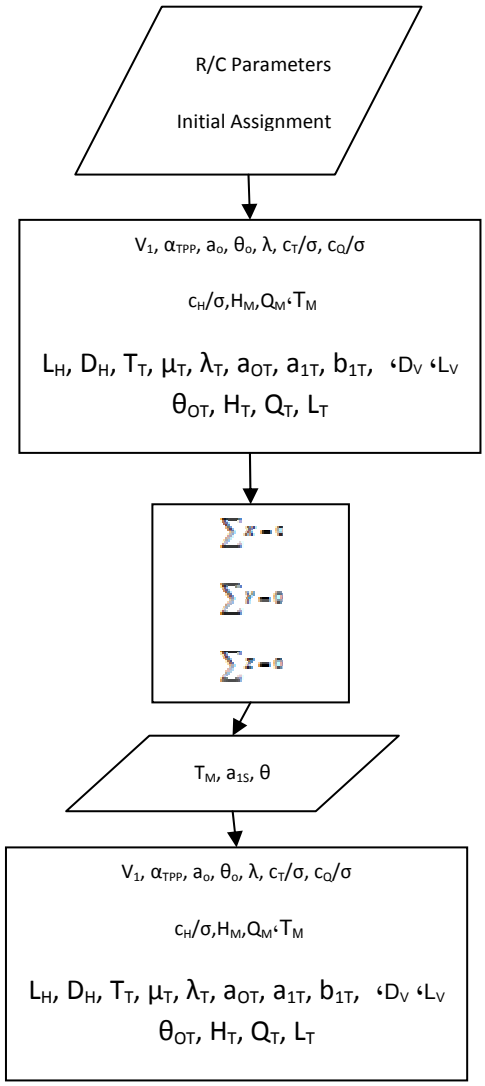

Figure(7): Trim program Flowchart.

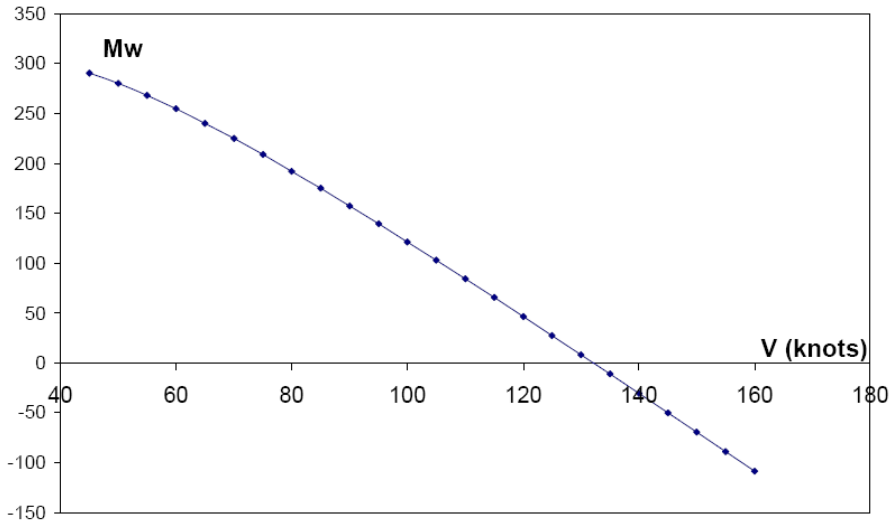

Figure (8): Derivative of pitching moment with respect to the vertical velocity.

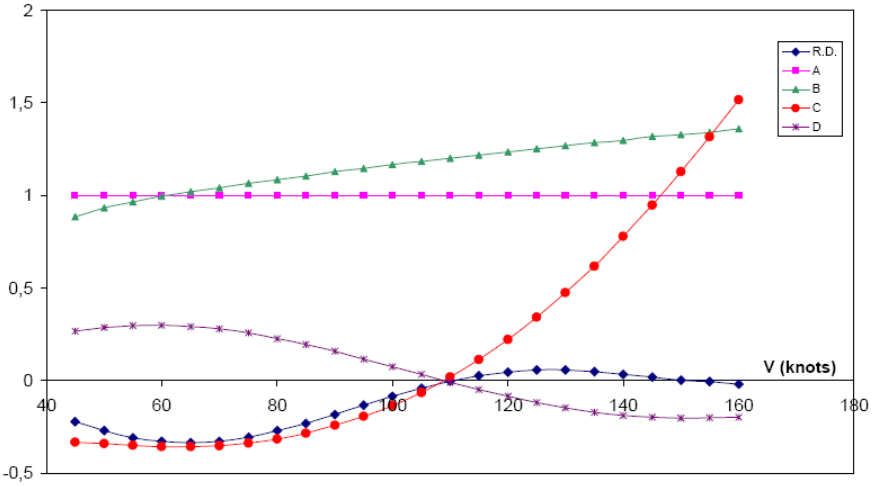

Figure (9): Routh's discriminant and the coefficients of characteristic equation.

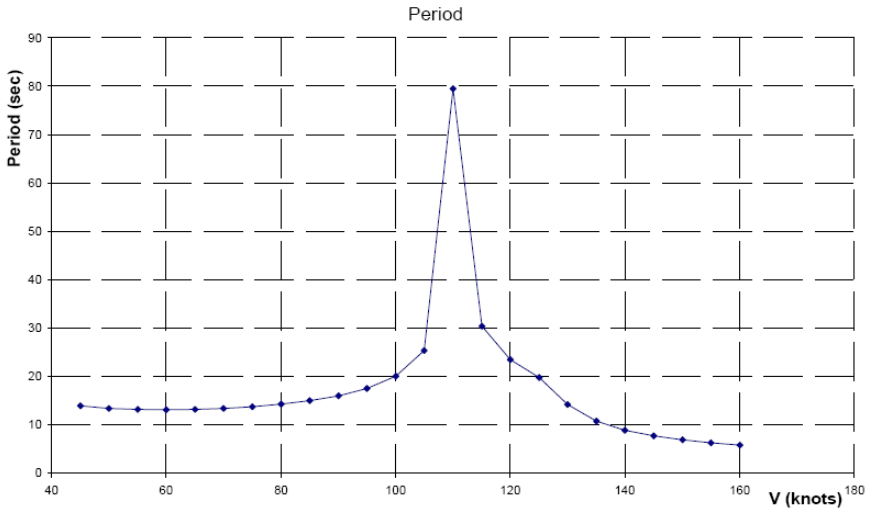

Figure (10): Period values belonging to the phugoid mode.

Figure (11): Time-to-Double values belonging to the phugoid mode.

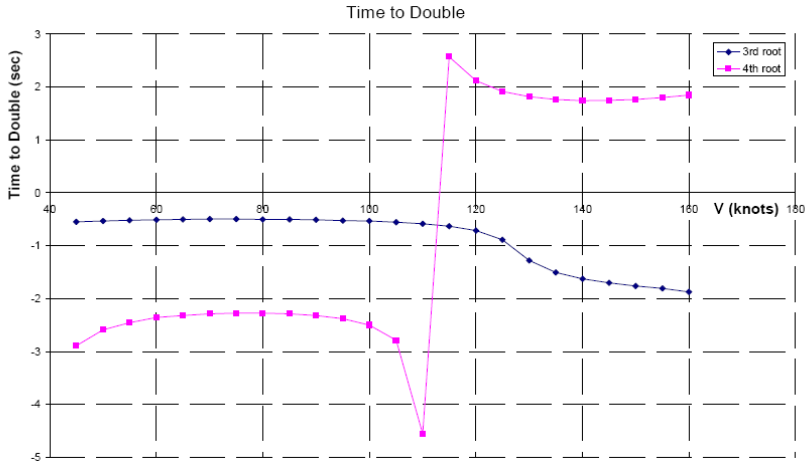

Figure (12): Time-to-double values belonging to the non-oscillatory roots.

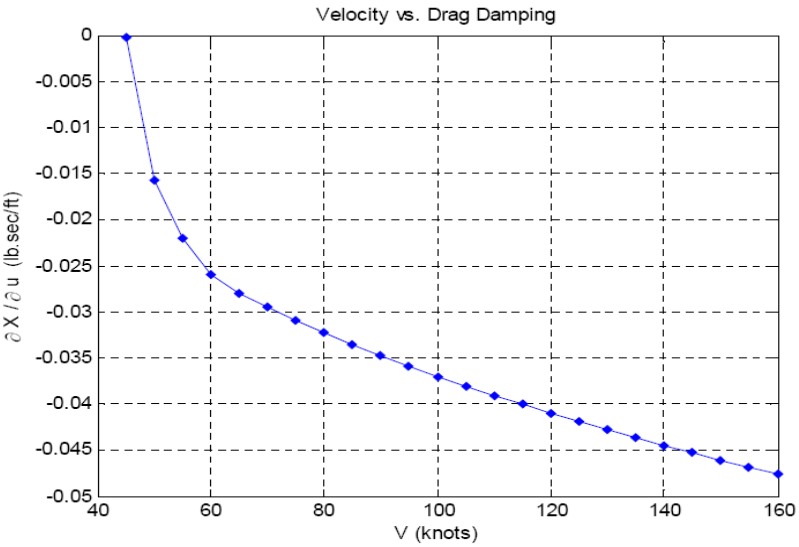

Figure (13): Drag Damping.

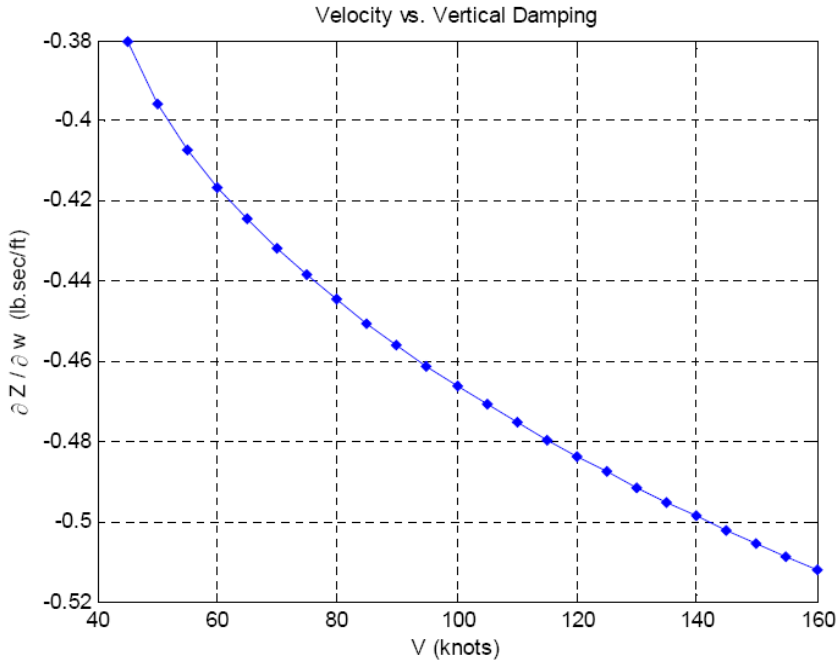

Figure (14): Vertical Damping.

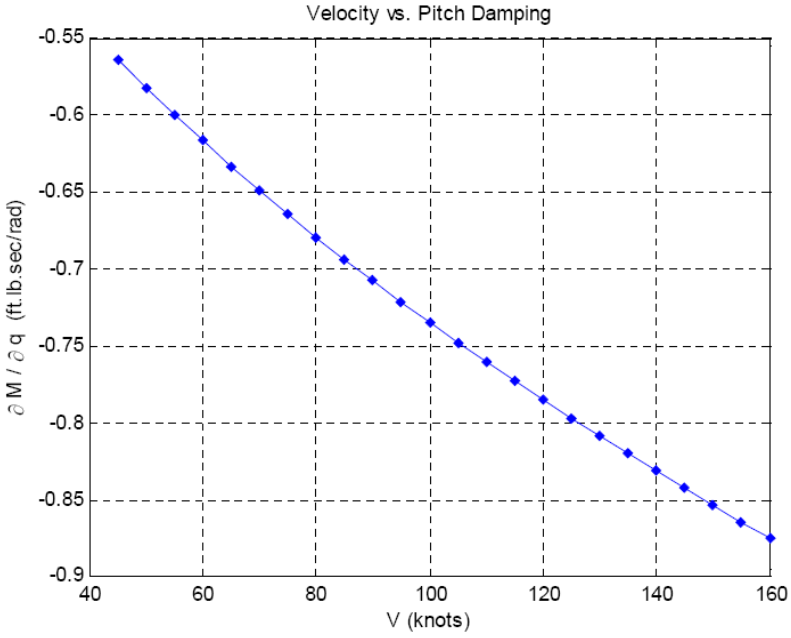

Figure (15): Pitch Damping.

REFERENCES

1.Seddon, J., Basic Helicopter Aerodynamics, AIAA Education Series, 1990.
2.Padfield,G. D., Helicopter Flight Dynamics: The Theory and Application of Flying Qualities and Simulation Modeling, 1995
3. Prouty, R.W., Helicopter Performance, Stability, and Control, Krieger Publishing Company, 1995.
4.Cooke,A.K.,Fitzpatrick, E.W.H., Helicopter Test and Evaluation, AIAA Education Series, 2002.
5.Leishman, J.G., Principles of Helicopter Aerodynamics, Cambridge University Press, 2000.
6. Sevinc C., Development of Forward Flight Trim and Longitudinal Dynamic Stability Codes, Master Thesis, Middle East Technical University, 2009.
7. U.S. Army Helicopter Design Datcom, Volume I – Airfoils, Boeing Doc. No. D210-11097-1, 1976.
8. Hoerner, Fluid Dynamic Drag, Published by Author, 1965.
9. MATLAB Getting Started Guide.
10. MATLAB help files helicopter.

NOMENCLATURE

Symbol Definitions

A	Area , m^2
A 1	1st harmonic lateral cyclic angle
AR	Aspect ratio (-)
B	Tip loss factor
B 1	1^{st} harmonic longitudinal cyclic Angle, deg
D	Fuselage drag, N
D.L.	Disc loading, N
H	H-force, N
HP	Power, hp
I	Inertia, m^4
L	Lift , N
M	Mach number / Pitch moment, N.m
Q	Torque, N.m
R	Radius, m
T	Thrust, N
U	Local velocity component, m/s
V	Forward velocity, m/s
X	Force on X-direction, N
Y	Force on Y-direction, N
Z	Force on Z-direction, N

A	Lift curve slope / Speed of sound, m/s
a 0	Coning angle, deg
a1	Longitudinal flapping w.r.t. the plane of no-feathering
as1	1^{st} harmonic longitudinal flapping angle, deg
b1	Lateral flapping w.r.t. the plane of no-feathering
bs1	1^{st} harmonic lateral flapping angle
c	Chord, m
e	Efficiency factor
f	Flat plate drag area, m^2
g	Gravitational acceleration, m/s^2
h	Height w.r.t. cg, m
I	Incidence, deg
L	Moment arm, m
m	Mass, kg
Q	Dynamic pressure / Pitch rate, Pa, rad/s
υ1	Induced velocity, m/s
υL	Local induced velocity, m/s
x	Displacement in X-direction, m
z	Displacement in Z-direction, m

GREEK LETTER

α Local angle of attack
α_S Shaft angle of attack
α_{TPP} Tip path plane angle of attack
β Angle of sideslip
δ_3 Delta-three angle
ε Downwash angle
γ Lock number / Climb angle
σ Solidity
θ_0 Collective angle
θ_1 Twist angle
λ Inflow ratio wrt the shaft plane
λ' Inflow ratio wrt TPP
μ Advance ratio
ρ Air density
θ Pitch angle
θ_O Collective angle
θ_1 Twist angle
ψ Azimuth angle
υ Local induced velocity
Θ Pitch angle of fuselage
Ω Revolution speed

APPENDIX A

The parameters with bars overhead are the output parameters supplied by a trim analysis

MAIN ROTOR STABILITY DERIVATIVES

$$\frac{\partial \mu}{\partial \dot{x}} = \frac{1}{\Omega R}$$

$$\frac{\partial \lambda'}{\partial \dot{x}} = \frac{1}{\Omega R}\left[\bar{\alpha}_{TPP} - \frac{\sigma}{2\mu}\left(\frac{\partial C_T/\sigma}{\partial \mu} - \frac{C_T/\sigma}{\mu}\right)\right]$$

$$\frac{\partial \lambda'}{\partial \dot{z}} = \frac{1}{\Omega R\left(1 + \frac{\partial C_T/\sigma}{\partial \lambda'}\frac{\sigma}{2\mu}\right)}$$

$$\frac{\partial C_H/\sigma}{\partial a_{1S}} = \frac{\bar{C}_T}{\sigma} + \frac{a}{8}\lambda'$$

$$\frac{\partial a_{1S}}{\partial q} = -\frac{16}{\gamma\Omega\left(1 - e/R\right)^2\left(1 - \mu^2/2\right)} - \frac{12\, e/R}{\gamma\Omega\left(1 - e/R\right)^3\left(1 - \mu^4/4\right)}$$

$$\frac{\partial a_{1S}}{\partial B_1} = -\frac{\left(1 + \frac{3\mu^2}{2}\right)}{\left(1 - \frac{\mu^2}{2}\right)}$$

$$\frac{\partial M}{\partial a_{1S}} = \frac{3}{4}\frac{e}{R}A_b\rho(\Omega R)^2\frac{a}{\gamma}$$

$$\left(\frac{\partial X}{\partial \dot{x}}\right)_M = -A_b\rho(\Omega R)^2\left\{\begin{array}{l}\left[\frac{\partial C_H/\sigma}{\partial \mu} + \frac{\partial C_H/\sigma}{\partial a_{1S}}\frac{\partial a_{1S}}{\partial \mu} + (\bar{a}_{1S} + i_M)\frac{\partial C_T/\sigma}{\partial \mu}\right]\frac{\partial \mu}{\partial \dot{x}} \\ + \left[\frac{\partial C_H/\sigma}{\partial \lambda'} + \frac{\partial C_H/\sigma}{\partial a_{1S}}\frac{\partial a_{1S}}{\partial \lambda'} + (\bar{a}_{1S} + i_M)\frac{\partial C_T/\sigma}{\partial \lambda'}\right]\frac{\partial \lambda'}{\partial \dot{x}}\end{array}\right\}$$

$$\left(\frac{\partial X}{\partial \dot{z}}\right)_M = -A_b\rho(\Omega R)^2\left[\frac{\partial C_H/\sigma}{\partial \lambda'} + \frac{\overline{C}_T}{\sigma}\frac{\partial a_{1S}}{\partial \lambda'} + (\overline{a}_{1S} + i_M)\frac{\partial C_T/\sigma}{\partial \lambda'}\right]\frac{\partial \lambda'}{\partial \dot{z}}$$

$$\left(\frac{\partial X}{\partial q}\right)_M = -A_b\rho(\Omega R)^2\frac{\partial C_H/\sigma}{\partial a_{1S}}\frac{\partial a_{1S}}{\partial q} - \left(\frac{\partial X}{\partial \dot{x}}\right)_M h_M$$

$$\left(\frac{\partial X}{\partial \theta_o}\right)_M = -A_b\rho(\Omega R)^2\left[\frac{\partial C_H/\sigma}{\partial \theta_o} + \frac{\partial C_H/\sigma}{\partial a_{1S}}\frac{\partial a_{1S}}{\partial \theta_o} + (\overline{a}_{1S} + i_M)\frac{\partial C_T/\sigma}{\partial \theta_o}\right]$$

$$\left(\frac{\partial X}{\partial B_1}\right)_M = -A_b\rho(\Omega R)^2\frac{\partial C_H/\sigma}{\partial a_{1S}}\frac{\partial a_{1S}}{\partial B_1}$$

$$\left(\frac{\partial Z}{\partial \dot{x}}\right)_M = -A_b\rho(\Omega R)^2\left[\frac{\partial C_T/\sigma}{\partial \mu}\frac{\partial \mu}{\partial \dot{x}} + \frac{\partial C_T/\sigma}{\partial \lambda'}\frac{\partial \lambda'}{\partial \dot{x}}\right]$$

$$\left(\frac{\partial Z}{\partial \dot{z}}\right)_M = -A_b\rho(\Omega R)^2\frac{\partial C_T/\sigma}{\partial \lambda'}\frac{\partial \lambda'}{\partial \dot{z}}$$

$$\left(\frac{\partial Z}{\partial \theta_o}\right)_M = -A_b\rho(\Omega R)^2\frac{\partial C_T/\sigma}{\partial \theta_o}$$

$$\left(\frac{\partial Z}{\partial B_1}\right)_M = -A_b\rho(\Omega R)^2\frac{\partial C_T/\sigma}{\partial \lambda'}\frac{\partial \lambda'}{\partial a_{1S}}\frac{\partial a_{1S}}{\partial B_1}$$

$$\left(\frac{\partial M}{\partial \dot{x}}\right)_M = \left(\frac{dM}{da_{1S}}\right)_M\left[\frac{\partial a_{1S}}{\partial \mu}\frac{\partial \mu}{\partial \dot{x}} + \frac{\partial a_{1S}}{\partial \lambda'}\frac{\partial \lambda'}{\partial \dot{x}}\right] - \left(\frac{\partial X}{\partial \dot{x}}\right)_M h_M + \left(\frac{\partial Z}{\partial \dot{x}}\right)_M l_M$$

$$\left(\frac{\partial M}{\partial \dot{z}}\right)_M = \left(\frac{dM}{da_{1S}}\right)_M\frac{\partial a_{1S}}{\partial \lambda'}\frac{\partial \lambda'}{\partial \dot{z}} - \left(\frac{\partial X}{\partial \dot{z}}\right)_M h_M + \left(\frac{\partial Z}{\partial \dot{z}}\right)_M l_M$$

$$\left(\frac{\partial M}{\partial q}\right)_M = \left(\frac{dM}{da_{1S}}\right)_M\frac{\partial a_{1S}}{\partial q} - \left(\frac{\partial X}{\partial q}\right)_M h_M$$

$$\left(\frac{\partial M}{\partial \theta_o}\right)_M = \left(\frac{dM}{da_{1S}}\right)_M\frac{\partial a_{1S}}{\partial \theta_o} - \left(\frac{\partial X}{\partial \theta_o}\right)_M h_M + \left(\frac{\partial Z}{\partial \theta_o}\right)_M l_M$$

$$\left(\frac{\partial M}{\partial B_1}\right)_M = \left(\frac{dM}{da_{1S}}\right)_M\frac{\partial a_{1S}}{\partial B_1} - \left(\frac{\partial X}{\partial B_1}\right)_M h_M$$

HORIZONTAL STABILIZER STABILITY DERIVATIVES

$$\frac{\partial \gamma_c}{\partial \dot{z}} = -\frac{1}{V}$$

$$\frac{\partial \varepsilon_{M_H}}{\partial \dot{x}} = \frac{\upsilon_H}{\upsilon_1}\frac{1}{4qA_M}\left[-\left(\frac{\partial Z}{\partial \dot{x}}\right)_M + \frac{2\overline{Z}_M}{V}\right]$$

$$\frac{\partial \varepsilon_{M_H}}{\partial \dot{z}} = -\frac{\upsilon_H}{\upsilon_1}\frac{1}{4qA_M}\left(\frac{\partial Z}{\partial \dot{z}}\right)_M$$

$$\frac{\partial \varepsilon_{F_H}}{\partial \dot{z}} = \frac{d\varepsilon_{F_H}}{d\alpha_F}\left[\frac{1}{4qA_M}\left(\frac{\partial Z}{\partial \dot{z}}\right)_M - \frac{\partial \gamma_c}{\partial \dot{z}}\right]$$

$$\frac{\partial \alpha_H}{\partial \dot{x}} = -\frac{\partial \varepsilon_{M_H}}{\partial \dot{x}}$$

$$\frac{\partial \alpha_H}{\partial \dot{z}} = -\left[\frac{\partial \varepsilon_{M_H}}{\partial \dot{z}} + \frac{\partial \varepsilon_{F_H}}{\partial \dot{z}} + \frac{\partial \gamma_c}{\partial \dot{z}}\right]$$

$$\frac{\partial \alpha_H}{\partial \ddot{z}} = -\left[\frac{\partial \varepsilon_{M_H}}{\partial \dot{z}}\right]\frac{l_H}{V}$$

$$\left(\frac{\partial X}{\partial \dot{x}}\right)_H = \left\{\frac{2}{V}X_H + \frac{q_H}{q}qA_H a_H \begin{Bmatrix}\left(\overline{\alpha}_H - \alpha_{L=0_H}\right)\left[1 - \dfrac{2a_H\left(1+\delta_{i_H}\right)}{\pi A.R._H}\right] \\ +\left(\overline{\alpha}_H - i_H\right)\end{Bmatrix}\right\}\frac{\partial \alpha_H}{\partial \dot{x}}$$

$$\left(\frac{\partial X}{\partial \dot{z}}\right)_H = \frac{q_H}{q}qA_H a_H\left\{\left(\overline{\alpha}_H - \alpha_{L=0_H}\right)\left[1 - \frac{2a_H\left(1+\delta_{i_H}\right)}{\pi A.R._H}\right] + \left(\overline{\alpha}_H - i_H\right)\right\}\frac{\partial \alpha_H}{\partial \dot{z}}$$

$$\left(\frac{\partial X}{\partial \ddot{z}}\right)_H = \left(\frac{\partial X}{\partial \dot{z}}\right)_H \frac{\dfrac{\partial \alpha_H}{\partial \ddot{z}}}{\dfrac{\partial \alpha_H}{\partial \dot{z}}}$$

$$\left(\frac{\partial Z}{\partial \dot{x}}\right)_H = \left\{\begin{matrix}\dfrac{2}{V}\overline{Z}_H \\ +\dfrac{q_H}{q}qA_H a_H \begin{Bmatrix}1 + \dfrac{a_H\left(1+\delta_{i_H}\right)}{\pi A.R._H}\begin{bmatrix}2\left(\overline{\alpha}_H - \alpha_{L=0_H}\right)\left(\overline{\alpha}_H - i_H\right) \\ +\left(\overline{\alpha}_H - \alpha_{L=0_H}\right)^2\end{bmatrix} \\ +c_{D_{o,H}}\end{Bmatrix}\end{matrix}\right\}\frac{\partial \alpha_H}{\partial \dot{x}}$$

$$\left(\frac{\partial Z}{\partial \dot{z}}\right)_H = -\frac{q_H}{q}qA_H a_H\left\{1 + \frac{a_H\left(1+\delta_{i_H}\right)}{\pi A.R._H}\begin{bmatrix}2\left(\overline{\alpha}_H - \alpha_{L=0_H}\right)\left(\overline{\alpha}_H - i_H\right) \\ +\left(\overline{\alpha}_H - \alpha_{L=0_H}\right)^2\end{bmatrix} + c_{D_{o,H}}\right\}\frac{\partial \alpha_H}{\partial \dot{z}}$$

$$\left(\frac{\partial Z}{\partial \ddot{z}}\right)_H = \left(\frac{\partial Z}{\partial \dot{z}}\right)_H \frac{\frac{\partial \alpha_H}{\partial \ddot{z}}}{\frac{\partial \alpha_H}{\partial \dot{z}}}$$

$$\left(\frac{\partial Z}{\partial q}\right)_H = \left(\frac{\partial Z}{\partial \dot{z}}\right)_H l_H$$

$$\left(\frac{\partial M}{\partial \dot{x}}\right)_H = -\left(\frac{\partial X}{\partial \dot{x}}\right)_H h_H + \left(\frac{\partial Z}{\partial \dot{x}}\right)_H l_H$$

$$\left(\frac{\partial M}{\partial \dot{z}}\right)_H = -\left(\frac{\partial X}{\partial \dot{z}}\right)_H h_H + \left(\frac{\partial Z}{\partial \dot{z}}\right)_H l_H$$

$$\left(\frac{\partial M}{\partial \ddot{z}}\right)_H = -\left(\frac{\partial X}{\partial \ddot{z}}\right)_H h_H + \left(\frac{\partial Z}{\partial \ddot{z}}\right)_H l_H$$

$$\left(\frac{\partial M}{\partial q}\right)_H = \left(\frac{\partial Z}{\partial q}\right)_H l_H$$

VERTICAL STABILIZER STABILITY DERIVATIVES

$$\left(\frac{\partial X}{\partial \dot{x}}\right)_V = \frac{2}{V}\left[\overline{X}_V + 2\Delta\overline{D}_{V_{\text{int}}}\right]$$

Where V_{int} ΔD is the additional drag coming from the interference effect between the vertical stabilizer and the tail rotor:

$$\Delta\overline{D}_{V_{\text{int}}} = \frac{8}{\pi q}\left|\frac{T_T}{2R_T}\frac{Y_V}{b_V}\right|K_{\text{int}}$$

FUSELAGE STABILITY DERIVATIVES

$$\frac{\partial \gamma_c}{\partial \dot{z}} = -\frac{1}{V}$$

$$\frac{\partial \varepsilon_{M_F}}{\partial \dot{x}} = \frac{\upsilon_F}{\upsilon_1}\frac{1}{4qA_M}\left[-\left(\frac{\partial Z}{\partial \dot{x}}\right)_M + \frac{2\overline{Z}_M}{V}\right]$$

$$\frac{\partial \varepsilon_{M_F}}{\partial \dot{z}} = -\frac{\upsilon_F}{\upsilon_1}\frac{1}{4qA_M}\left(\frac{\partial Z}{\partial \dot{z}}\right)_M$$

$$\frac{\partial \alpha_F}{\partial \dot{x}} = -\frac{\partial \varepsilon_{M_F}}{\partial \dot{x}}$$

$$\frac{\partial \alpha_F}{\partial \dot{z}} = -\left[\frac{\partial \varepsilon_{M_F}}{\partial \dot{z}} + \frac{\partial \gamma_c}{\partial \dot{z}}\right]$$

$$\left(\frac{\partial X}{\partial \dot{x}}\right)_F = \frac{2}{V}\overline{X}_F$$

$$\left(\frac{\partial X}{\partial \dot{z}}\right)_F = \left(\overline{L}_F - q\frac{\partial f}{\partial \alpha_F}\right)\frac{\partial \alpha_F}{\partial \dot{z}}$$

$$\left(\frac{\partial Z}{\partial \dot{x}}\right)_F = \frac{2}{V}\overline{Z}_F$$

$$\left(\frac{\partial Z}{\partial \dot{z}}\right)_F = -\left(\overline{D}_F + q\frac{\partial L/q}{\partial \alpha_F}\right)\frac{\partial \alpha_F}{\partial \dot{z}}$$

$$\left(\frac{\partial M}{\partial \dot{x}}\right)_F = \frac{2}{V}\overline{M}_F + q\frac{\partial M/q}{\partial \alpha_F}\frac{\partial \alpha_F}{\partial \dot{x}}$$

$$\left(\frac{\partial M}{\partial \dot{z}}\right)_F = q\frac{\partial M/q}{\partial \alpha_F}\frac{\partial \alpha_F}{\partial \dot{z}}$$

TOTAL STABILITY DERIVATIVES

The total derivatives are found by adding the corresponding terms of main rotor, tail rotor, empennage and the fuselage:

$$\frac{\partial X_i}{\partial x_i} = \left(\frac{\partial X_i}{\partial x_i}\right)_M + \left(\frac{\partial X_i}{\partial x_i}\right)_T + \left(\frac{\partial X_i}{\partial x_i}\right)_{HS} + \left(\frac{\partial X_i}{\partial x_i}\right)_{VS} + \left(\frac{\partial X_i}{\partial x_i}\right)_F$$

Where $Xi = X\ Z\ M$

TRIM EQUATIONS

Harmonic pitch angles are found using the first harmonic flapping angles

$$A_1 = b_{1s} - \frac{\left[a_0\left(\frac{4}{3}\mu + \frac{16}{45\pi}\mu^4\right) + \frac{\upsilon_1}{\Omega R}\left(1 + \frac{\mu^4}{24}\right)\right]}{\left(1 + \frac{\mu^2}{2} - \frac{\mu^4}{24}\right)}$$

$$B_1 = -a_{1s} + \frac{\mu\left[\left(\frac{8}{3} + \frac{32}{45}\frac{\mu^3}{\pi}\right)\theta_0 + \left(2 + \frac{\mu^4}{12}\right)\theta_1 + \left(2 - \frac{\mu^2}{2}\right)\lambda'\right]}{\left(1 + \frac{3}{2}\mu^2 - \frac{5\mu^4}{24}\right)}$$

The total thrust force is calculated by multiplying the lift by the number of blades.

$$T_M = \frac{bR}{2\pi}\left\{\int_0^{\pi}\int_{x_0}^{B}\frac{\Delta L}{\Delta r}d\frac{r}{R}.d\psi + \int_{\pi-\mu\sin\psi}^{2\pi}\int^{B}\frac{\Delta L}{\Delta r}d\frac{r}{R}.d\psi - \int_{\pi}^{2\pi-\mu\sin\psi}\int_{x_0}\frac{\Delta L}{\Delta r}d\frac{r}{R}.d\psi\right\}$$

Where L lift force on each bald and B is the loses factor station, this is for eliminate the root and tip losses. The reverse flow region defined by μsinψ.

The local angle of attack is defined as ;

$$\alpha = \theta + \tan^{-1}\left(\frac{U_P}{U_T}\right)$$

Introducing the pitch angle

$$\theta = \theta_0 + \frac{r}{R}\theta_1 - A_1\cos\psi - B_1\sin\psi$$

The tangential velocity component is

$$\overline{U}_T = \frac{r}{R} + \mu \sin\psi$$

The vertical velocity component is

$$U_P = V\alpha_S - \upsilon_L - r\dot{\beta} - V\beta\cos\psi$$

The flapping angle is

$$\beta = a_0 - a_{1S}\cos\psi - b_{1S}\sin\psi$$
$$\dot{\beta} = \left(a_{1S}\sin\psi - b_{1S}\cos\psi\right)\Omega$$

So that the collective angle becomes

$$\theta_0 = \frac{\left(\begin{array}{l}\left(\frac{4}{a}\left(1+\frac{3}{2}\mu^2-\frac{5}{24}\mu^4\right)C_T/\sigma - \left(1-\frac{3}{2}\mu^2+\frac{\mu^4}{6}-\frac{9}{16}\mu^6-\frac{3}{192}\mu^8\right)\frac{\theta_1}{2}\right) \\ -\left(1+\frac{13}{24}\mu^4+\frac{\mu^6}{48}\right)\lambda'\end{array}\right)}{\left(\frac{2}{3}-\frac{2}{3}\mu^2-\frac{8}{9\pi}\mu^3+\frac{25}{36}\mu^4-\frac{92}{45\pi}\mu^5-\frac{5}{24}\mu^6+\frac{\mu^7}{135\pi}\right)}$$

TOTAL FORCES AND MOMENTS

The forces and moments can be calculated by the following formulas;

$$X_M = -\overline{H}_{a_{1S}=0_M} - \overline{T}_M a_{1S} - T_M i_M$$
$$X_T = -\overline{H}_T$$
$$X_H = \overline{L}_H\left(\alpha_H - \varepsilon_{F_H}\right) - \overline{L}_H a_H\left(\begin{array}{l}\alpha_H + i_H \\ -\alpha_{L=0_H} - \varepsilon_{F_H}\end{array}\right)\frac{\left(1+\delta_{i_H}\right)}{\pi A R_H} - q\frac{q_H}{q}A_H C_{D_{0,H}}$$
$$X_V = -\overline{D}_V - \overline{L}_V\left(\eta_{M_V} + \eta_{T_V}\right)$$
$$X_F = -\overline{D}_F + \overline{L}_F\alpha_F$$

$$Z_M = -T_M$$
$$Z_T = \overline{b}_{1S_T}\overline{T}_T$$
$$Z_H = -q\frac{q_H}{q}A_H a_H\left(\alpha_H + i_H - \alpha_{L=0_H} - \varepsilon_{F_H}\right) - \overline{D}_H\left(\alpha_H - \varepsilon_{F_H}\right)$$
$$Z_V = -\left(\overline{D}_V + \overline{L}_V\left(\eta_{M_V} + \eta_{F_V}\right)\right)\left(\Theta - \frac{\upsilon_V}{\upsilon_1}\frac{T_M}{4qA_M} - \varepsilon_{F_V}\right)$$

$$Z_F = -q\left(\left(L_F/q\right)_{\alpha_F=0} + \frac{\partial\left(L_F/q\right)}{\partial\alpha_F}\alpha_F\right) - \overline{D}_F\alpha_F$$

$$M_M = \frac{\partial M}{\partial a_{1S}}a_{1S}$$

$$M_T = -\overline{Q}_T$$

$$M_F = q\left(\left(M_F/q\right)_{\alpha_F=0} + \frac{\partial\left(M_F/q\right)}{\partial\alpha_F}\alpha_F\right)$$

The total force and moments are;

$$\sum X = X_M + X_T + X_H + X_V + X_F - W\Theta = 0$$

$$\sum Z = Z_M + Z_T + Z_H + Z_V + Z_F + W = 0$$

$$\sum M = \begin{pmatrix} M_M + M_T + M_F - X_M h_M + Z_M l_M - X_T h_T \\ + Z_T l_T - X_H h_H + Z_H l_H - X_V h_V + Z_F l_F - X_F h_F \end{pmatrix} = 0$$

Effect of Hydrated Lime on the Properties of Roller Compacted Concrete

Prof. Saad I. Sarsam Dr. Abeer A. Salih Suha Ghazi Abdullah

Civil Engineering department, College of Engineering, University of Baghdad

Email:saadisasarsam3@hotmail.com

ABSTRACT

Roller compacted concrete (RCC) is a concrete of no slump, no reinforcement, no finishing, and compacted using vibratory roller. When compared with conventional concrete, it contains less water content when compared to traditional concrete. The RCC technique achieves significant time and cost savings during the construction of concrete. This study demonstrates the preparation of RCC slab of (38 ×38× 10) cm samples by using roller compactor which is manufactured in local markets. The Hydrated lime additive is used to study the mechanical and physical properties of that RCC slab samples. This investigation is divided into two main stages: The First stage consists of hammer compaction method with two gradation of aggregate, dense and gap graded aggregate, using five percentages of cement content (10, 12, 14, 16, and 18) as a percentage of the total aggregate content. This stage is carried out for selecting the maximum dry density, optimum moisture content, and optimum cement content which is utilized in RCC slab samples construction, a total of 49 cylinder samples sized (10 cm diameter and 11.6 cm high) are prepared.

The Second stage is classified into two sub stages; the first one consists of constructing RCC slab samples using roller compaction, 12% cement as a percentage of total aggregate weight has been used according to the data obtained from first stage, this group presents reference mixes without additives. While the second sub stage presents RCC mix with hydrated lime additive and with the same gradation of mixes compact by hammer compaction method, hydrated lime was implemented as (5, 10, 12, and 15) percentage as a partial replacement of cement content. Both of physical and mechanical properties of RCC are studied using cores, sawed cubes, and sawed beams obtained from RCC slab samples. The properties studied were porosity, absorption, and compressive strength, splitting tensile strength and flexural strength by using third point loading method. The results show that hydrated lime improved the overall properties of RCC as compared to reference mix. Mixes with 5% lime give the optimum values for most of strength properties. Dense graded mixes with hydrated lime show superior properties as compared to gap graded mixes.

Keywords: Additives, compressive strength, dense and gap gradations, hydrated lime, porosity, roller compacted concrete, RCC slabs.

الخلاصة

الخرسانه المرصوصه بالحدل هي خرسانه عديمة الهطول لاتحتاج الى حديد تسليح او عمليات انهاء وترص بأستخدام الحادلات الهزازه، عند مقارنتها بالخرسانه التقليديه فإنها تتميز بأن محتوى الماء قليل للحصول على خرسانه عديمة الهطول. هذا النوع من الخرسانه يقلل من فترة انجاز العمل وكلفة التنفيذ (معهد الخرسانة الاميركي، لجنة 211-3ر 1997). تعرض هذه الدراسه تنفيذ بلاطات من الخرسانه المرصوصه بالحدل بأبعاد (38×38×10) سم باستخدام جهاز حدل صنع محليا وباستخدام مضاف النوره المطفأه لغرض دراسة الخواص الفيزيائيه و الميكانيكيه لنماذج البلاطات هذه.يتضمن الجزء العملي مرحلتين أساسيتين هما:-

المرحله الأولى تتضمن تصميم الخلطات باستخدام طريقه الرص بالمطرقة وباستخدام تدرجين من الركام هما العالي الكثافه والتدرج المنقطع التسلسل وباستعمال خمس نسب سمنت هي (10، 12، 14، 16و 18) كنسبه مئويه من الوزن الكلي للركام .هذه المرحله نفذت لاختيار الكثافه الجافه القصوى، محتوى الماء الامثل و محتوى السمنت الامثل والتي تستخدم في تنفيذ بلاطات الخرسانه المرصوصه بالحدل، حيث تم عمل 49 نموذج بأبعاد (10سم قطرا و11،6 سم ارتفاعا) بأستخدام هذه الطريقه.

المرحله الثانيه: قسمت هذه المرحله الى مجموعتين ثانويتين هما: المجموعه الأولى تشمل إنشاء بلاطات من الخرسانة المرصوصة بالحدل وترص بأستعمال الحادله لتشابه ظروف الموقع، في هذه المرحله تم اختيار نسبة السمنت المثاليه 12 كنسبه مئويه من الوزن الكلي للركام والتي تم الحصول عليها من المرحله الاولى ولنوعي التدرج السابقين لغرض دراسة سلوك وخواص الخرسانه المرصوصه بالحدل بدون إضافات تحت تأثير نسبة السمنت هذه.

اما المجموعه الثانيه فتمثل تصميم خلطات الخرسانه المرصرصه بالحدل وبوجود مضاف النوره المطفأه كجزء مستبدل من وزن السمنت وبالاعتماد على نسبة سمنت 12٪ فقط ولنفس تدرجات الركام السابقه المستعملة في طريقة الرص بالمطرقه، تم استخدام المضاف كجزء من وزن السمنت وبنسب (5٪، 10٪، 12٪، 15٪). تم دراسة الخواص الفيزيائيه و الميكانيكية للخرسانة المرصوصة بالحدل باستعمال عينات من اللباب والمكعبات والاعتاب استخرجت من بلاطات الخرسانه المرصوصه بالحدل، و الخواص التي تم دراستها شملت المسامية، الامتصاص، مقاومة الانضغاط ، ومقاومة شد الانفلاق، ومقاومة الانثناء باستخدام ثلاث نقاط للتحميل.
بينت النتائج إن مادة النوره المطفأة تحسن من خواص الخرسانه المرصوصه بالحدل، كما تبين إن افضل نتائج يمكن الحصول عليها عند نسبة نوره 5٪ من وزن السمنت. إن الخلطات ذات تدرج عالي الكثافه والحاويه على مضاف النوره تعطي نتائج جيده مقارنة بالخلطات ذات النواقص في التدرج.

INTRODUCTION

Roller Compacted Concrete (RCC) takes its name from the construction method used in concrete placement; RCC is being used in many parts of the world such as Canada, U.S.A., and France, Vorobieff and Whitaker (2003).

ACI committee 211-3R-(1996) define RCC as "concrete compacted by roller compaction; concrete that in it's unhardened state that is transported, placed, and compacted using earth and rock fill construction equipment". The use of RCC as a material to construct pavement was stated in 1970 in Canada, it was originally used by the logging industry to provide an all-weather platform for unloading logging trucks and storing and sorting logs, Piggott (1999). Most of the investigations in Iraq have studied the behavior and properties of RCC usually used in dams, but no wide investigation has been carried out on using this new concrete in pavements design and construction. RCC has been used in Iraq in mid-eighties below the foundations of the medical drug factory near Mosul and also in the AL-Adaim Dam, Ahmed (2001). Another reported use was in the construction of extra lane for Mosul- Duhok highway during 1988, Sarsam (1988).In comparing RCC with conventional slump concrete, less water is needed to achieve a no slump concrete; therefore, less cement is required to produce an equivalent water to cement ratio. Less water in the mixture leads to less shrinkage and no bleeding water, and less cement is one means of reducing thermal induced cracking, Hansen (1996). Roller compacted concrete for pavement (RCCP) mixes compared with conventional concrete contain larger sized fine aggregate to ensure a uniform concrete mix with less surface voids.

The use of the additives such as pozzolana, lime, slags…..etc. as a partial replacement of cement had improved the properties of RCC; Rodrigues (2002) showed that the pozzolanic materials type serves some purposes as a partial replacement for cement to reduce heat generation; to increase the compressive strength at later ages; to improve the durability; to reduce the cost and; as a mineral addition to the mixture to provide fines to improve workability. The development of RCC causes a major shift in United state American, Japan and other countries; mainly for the construction of water control structures (dams) and pavements, while the same term is used to describe both types of concrete, the design and construction processes are different as shown in **Table (1),** Gupta (2004).

MATERIALS CHARACTERISTICS

1. Cement

Ordinary Portland cement (Type I) named Tasluja cement. The chemical compositions and physical properties of cement are presented in **Tables (2)** and **(3)**. The test results have shown that the cement conforms to the provisions of Iraqi specification No.5 (1984). Chemical compositions and physical properties are tested at The National Center Construction Laboratories, while the main compounds are calculated by using Bogue equations.

2. Coarse Aggregate

Crushed aggregate with 1″ (25.4mm) maximum size is used and obtained from Nibaai region, the properties of coarse aggregate is determined according ASTM C127-(2001) except SO_3 content, which was tested at The National Center Construction Laboratories. Test results are shown in **Table (4)**.

3. Fine Aggregate

Natural fine aggregate with 4.75mm maximum size is obtained from Al-Ukhaider region, the properties of fine aggregate is determined according to ASTM C128-(2001) except SO_3content, which was tested at the National Center Construction Laboratories and given in **Table(4)**.

4. Hydrated Lime

Hydrated lime is a derivative of burnt lime. It is produced by reacting burnt lime with water in a continuous hydrator, during this process, large amounts of heat are given off.

This material is available in local markets with low cost and is manufactured at Ad factory in Iran. Hydrated lime is light and fluffy and used as an additive (filler) and also as partial replacement of cement in this work. Chemical composition was tested at the laboratories of General Directorate of Geological Survey and Mining and given in **Table (5)**.

5. Preparation of Dense and Gap Gradations

The gradation of aggregate is defined as the frequency of a distribution of the particle size of a particular aggregate**,** Rached and et al (2009).

The gradation determine the paste requirement for a workable concrete since the amount of void requires needs to be filled by the same amount of cement paste in a concrete mixture. Dense graded aggregate is desirable for making concrete, as the space between larger particles is effectively filled by smaller particles to produce a well-packed structure. Gap graded aggregate is defined as a gradation at which one or more intermediate fractions are omitted.

The coarse and fine aggregates were sieved to different separate fraction sizes (seven sieves in this work) and combined to satisfy the requirements of gradation, dense gradation with 1″ (25mm) maximum size of aggregate represents the average requirement of Iraqi Standard Specification for Roads and Bridges SCRB (2004), while the gap gradation with also 1″ (25mm) maximum size aggregate represents the average requirements of British Standards B.S. (1961). The overall grain size distribution used is illustrated in **Table (6)**.

PREPARATION OF RCC SLAB SAMPLES

1. Preparation the Roller Compactor and Mould:

The roller compactor manufactured in local workshop was used throughout this investigation. It consists of a roller with (16cm) diameter and (33cm) length and its self-weight was 36 kg, while the steel mould used in this investigation was manufactured also at local workshop. It consists of four sides made from steel angle section, and base plate which has (1cm) thickness. The internal dimensions of the mould are (38× 38 ×10) cm. The roller compactor and mould are shown in **Figure (1)**.

2. Mix Proportioning Techniques of RCC

Mixture proportioning techniques of using modified soil compaction, optimum moisture content and maximum dry density, was implemented, such procedure correlates well with the work by Sarsam (2002). In this method, the overall combined gradation of aggregate which is suitable for base layers of the pavement is implemented. A number of concrete mixtures varying in cement and water content are prepared by using modified compaction as per ASTM D1557-(2002). The dry density-water content curve is plotted for each percentage of cement as shown in **Figure (2),** then the optimum water and cement content which give the maximum dry density is adopted as an initial design mix. Five different percentage of cement content were used in this work, (10, 12, 14, 16, 18) by weight of air dried aggregate for each gradation type (dense and gap). Different percentage of moisture content with a range of (4 –11%) of air dried aggregate weight with 1% increment were added; These percentages of moisture content are applicable for each percentage of cement content to determine the dry density-moisture content relationships. The samples were compacted using the modified hammer and steel cylinder mold of size 10cm diameter and 11.6cm high for determining maximum dry density. The mixture is placed by filling the cylinder mold in three layers and compacting each layer with 56 blows of a modified proctor hammer (4.5kg falling from 45cm high), when compaction is finished, the extension collar is removed and the surface of concrete was leveled with the mold. The wet density was calculated using eq. (1), and then the dry density was obtained using eq. (2), ASTM C-1557 (2008).

$$\gamma_{wet} = \frac{W_m}{V} \qquad (1)$$

Where:

γ_{wet}= the wet density (gm/cm³),
W_m = the wet weighting of material (gm),
V = the volume of the cylinder mold (cm³)

$$\gamma_d = \frac{\gamma wet}{1+w} \qquad (2)$$

Where:

γ_d = the dry density (gm/cm³),
ω = the moisture content (%).

After determinations of the dry density for each percentage of moisture content and the five

Percentages of cement content, it can be noticed from **figures (2)** that the maximum dry density is at cement contents of 12% and 18% of total dry aggregate weight for dense and gap graded respectively. For mix proportion of RCC slab samples with and without additive, it was felt that cement content of 12% of total dry aggregate weight for two gradations is suitable and economical for design. **Table (7)** gives the proportions of mixes used.

3. Determination of the Effect of Hydrated Lime on RCC Mixes

Hydrated lime as a partial replacement of cement content was used to study the effect of this additive on the properties of RCC slab samples, four percentages of lime were used depending on trial mortar mixes. the compressive strength of these mortar mixes contains hydrated lime and compressive strength of cement paste without hydrated lime at 7 and 28 days were compared, **Table (8)** gives the percentages of hydrated lime used with RCC mixes.

4. Construction of RCC Slab Samples

The mixture was placed in the mold of size (38× 38 × 10) cm and subjected to initial compaction on a vibrating table for 3 cycles of 30 seconds time interval. Then, the mold was placed in front of the roller compactor machine as shown in **Figure (3)** and subjected to three stages of rolling as described below, based on the work done by Sarsam (2002). Each rolling stage was conducted by applying 10 passes of the roller for each rolling direction. This number of passes was felt to be suitable to achieve the good rolling with lowest labor power.

The first stage represents the primary compaction which was performed by applying 10 passes of the machine with weight only 1.1 kg/cm width (36 kg of roller compactor weight) for each direction.

The second stage represents the breakdown compaction by applying 10 passes using a load of 3.2kg/cm width (by using 69kg standard loads plus roller compactor weight) for each direction; this stage can represent the compaction applied by steel and pneumatic type roller in the field.

The third stage represents the final compaction which is demonstrated by application of 10 passes of the roller compactor under 5.3kg/cm width load (by using 138kg standard loads plus roller compactor weight) for each direction. This stage represents the finishing compaction in the field.

5. Curing

After finishing the rolling,, the rolled compacted samples were covered tightly with polythene sheet and kept for 24 hours at room temperature of 32±3˚c for initial setting, then, the samples are withdrawn from the moulds and immersed in a water bath for 27 days for curing at 32±3˚c.

DETERMINATION OF PHYSICAL AND ENGINEERING PROPERTIES RCC SLAB SAMPLES

Sawed beams, cores and sawed cubes were obtained from RCC slabs by using the procedure of ASTM C42/C42M-(2003). The specimens were subjected to physical properties determination as explained below.

1. Porosity Test

Porosity represents the volume of permeable pores (voids). This test was carried out using cores (6.2cm diameter and 10cm high) according to ASTM C642-(1997) and eq. (3). The average porosity of three samples was recorded.

$$V = \frac{C - A}{C - D} \times 100 \qquad (3)$$

Where:

V = Volume of permeable pore space (voids) or (porosity), %

A = mass of oven-dried sample in air, gm.

C = mass of surface-dry sample in air after immersion and boiling, gm.

D = apparent mass of sample in water after immersion and boiling, gm.

2. Water Absorption Test

According to ASTM C642-(1997), the water absorption test is carried out using cores (6.2cm diameter and 10cm high), and the average water absorption of three samples was recorded by using eq. (4).

$$\text{Absorption after immersion}, \% = \frac{B-A}{A} \times 100 \qquad (4)$$

Where:

A = mass of oven-dried sample in air, gm.

B = mass of surface-dry sample in air after immersion, gm.

3. Compressive Strength

sawed cube samples of size (10 × 10 × 10) cm were used for determining the compressive strength at 28 days age according to B.S.1881 part 116 (1983). The compressive strength is determined by using eq. (5).

$$f_c = \frac{P}{A} \quad (5)$$

Where:
fc = compressive strength, psi (MPa),
P = maximum applied load indicated by the testing machine, lb.f (N), and
A = area exposed for load, in² (mm²).

4. Splitting Tensile Strength

The splitting tensile strength was carried out on core specimens according to ASTM C496-(2002). Cores has dimensions of (2.5″ (6.2cm) diameter and 4″ (10cm) high) were used in this test. Eq. (6) was used to determine the splitting tensile strength:

$$T = \frac{2\,P}{\pi\,d\,L} \quad (6)$$

Where:
T = splitting tensile strength, psi (MPa),
P = maximum applied load indicated by the testing machine, lbf (N),
L = length, in. (mm), and
d = diameter, in. (mm).

5. Flexural Strength

Sawed beams of sizes (38 × 10 × 8) cm obtained from each slab sample are tested using third- point loading of simple beam according to ASTM C78-(2003), eq.(7) was used to determine the flexural strength property.

$$R = \frac{P\,L}{b\,d^2} \quad (7)$$

Where:
R = modulus of rupture, psi, or MPa,
P = maximum applied load indicated by the testing machine, lbf, or N,
L = span length, in., or mm,
b = average width of specimen, at the fracture, in., or mm, and
d = average depth of specimen, at the fracture, in., or mm.

DISCUSSIONS ON TEST RESULTS

1. Porosity of RCC Samples:

The change of porosity of RCC with hydrated lime is shown in **Figure (4)**. It can be noticed that the presence of this material does not has a constant trend, this leads to decrease porosity at some ratios of lime/cement and increase it in other ratios, it can be seen in the same figure that all percentages of lime give porosity better than reference mix with 12% cement content because these materials work as fillers and partially replaces cement. Lime has high surface area that leads to decrease in voids in the mixes and reduce the porosity, but this effect is changeable and had reliance on the percentage of additive. The lowest value of porosity is achieved in mixes at 5% lime for dense and gap graded and decreases by about 13.85 % and 23.7% respectively than reference mixes with 12% cement content. The porosity of mixes with dense graded aggregate is less by 8.4% than porosity of mixes with gap graded aggregate at 5% hydrated lime

2. Absorption of RCC Samples:

Results of the effect of mixing hydrated lime on absorption of RCC with two gradations of aggregate are presented in **Figure (5)**. These results have shown that the absorption trend was the same as for porosity. For dense graded mixes, the lowest value of absorption was in the mix with 5% lime and decreases about 6.7% from reference mix (mix with 12% cement content), after that the absorption increases with increasing lime/cement ratio. The rate of increase at 10% lime mix reaches to 2.5% than reference mix, then decreases again until reaching second lower value of absorption at 12% lime, and then increases with further increase of lime. In gap graded mixes, the absorption trends are as in dense mixes but all lime/cement ratios lead to absorption less than reference mix. The rate of decrease reaches to 24.3% at 5% lime mix and 19.8% at 12% lime mix as compared to reference mix. Dense mixes show higher absorption (4.1% and 2.1%) than gap mixes at 5% and 12% hydrated lime respectively.

3. Compressive Strength of RCC Samples:

The effect of hydrated lime on compressive strength of dense and gap RCC

mixes is presented in **Figure (6)**. It can be seen that the effect of lime is changeable on

compressive strength. The compressive strength increases with increasing lime/cement ratio until reaches an optimum value at 5% lime. This increase may be attributed to that the lime at this ratio of replacing worked as a filler material and fill the voids in the mixture so that it leads to increase the compressive strength, then decreases with further increasing lime content. Hydrated lime has low specific gravity (2.3) than cement (3.15) and that causes reduction in compressive strength, after that it increases again and has the second optimum value at 12% lime, that may be attributed to that the lime $Ca(OH)_2$, when mixed with cement, reacts with carbon dioxide CO_2 from atmosphere, and results calcium carbonate $CaCO_3$ which is sediments in voids in the mixture, then increases the compressive strength. Compressive strength decreases with further increasing of lime more than 12%. From the same figure, it can be seen that the gradation of aggregate does not have a constant effect on RCC mixes with hydrated lime. At 5% lime, gap mixes show high compressive strength with slightly higher value than dense mixes. This variation reaches to 1.4% at 5% lime, but after this ratio of lime, Dense mixes shows higher compressive strength (44% and 22%) than gap mixes at 10% and 12% lime respectively. After 12% lime, gap mixes give again higher compressive strength by 5% as compared to dense mixes at 15% lime.

4. Splitting Tensile Strength of RCC Samples:

Figure (7) shows that the splitting tensile strength of RCC mixes increases as lime/cement ratio increases for both gradation of aggregate until reaches an optimum value at 5% lime, then decreases. The rate of increase at 5% lime is 150% for both dense and gap mixes. The decrease in splitting tensile strength continues until reaches the lowest tensile strength at 10% lime, then increases again and reaches to second high value of splitting tensile strength at 12% lime, then decreases again with further increasing of lime content.

Dense mixes give higher splitting tensile strength than gap mixes at lime/cement ratio of approximately 7.5%, up to this ratio; gap mixes give higher splitting tensile strength than dense mixes. It can be seen that dense mixes at 5% lime show higher tensile strength (8.76%) than gap mixes, but at 12% lime, gap mixes have higher splitting tensile strength (7.78%) than dense mixes. It was noticed that the splitting tensile strength for RCC mixes with 5% lime is 20% and 18% of compressive strength, and it is 46.4% and 74.7% of flexural strength for dense mixes and gap mixes respectively, such results are in agreement with Sarsam (2002).

5. Flexural Strength of RCC Samples:

Figure (8) show the flexural strength of RCC mixes containing different percentages of hydrated lime. It can be noticed that flexural strength for dense mixes has similar trends as compressive strength and there are two optimum value of flexural strength at 5% and 12% lime. This may be attributed to the same reasons explained in compressive strength item. The rate of increase in flexure strength as compared to reference mix is 96.3% for mixes at 5% and 12% lime.

As seen from the same figure, gap mixes show that the flexural strength increases with increasing lime/cement ratios until reaches an optimum value at 5% lime then decreases with increasing lime/cement ratios, the rate of increase in the mix with 5% lime as compared to reference mix (at 12% cement content) reaches to 86.36%.

Mixes with dense graded aggregate give higher flexural strength than mixes with gap graded aggregate and for all percentages of lime. The variation is 62% at mixes with 5% lime, the flexural strength for RCC mixes contain 5% hydrated lime is 36.4% and 22.2% of compressive strength for dense mixes and gap mixes respectively, such results are in agreement with Sarsam (2002) work.

CONCLUSION

1. The lowest porosity and absorption for dense and gap RCC mixes with hydrated lime can be obtained at 5% lime. The porosity of these mixes decreases about 13.85% and 23.7% as compared to reference mix for dense and gap mixes respectively. While absorption decreases about 6.7% for dense RCC mixes and 24% for gap RCC mixes.
2. The optimum compressive strength for mixes with lime can be obtained at 5% lime. The rate of increase in compressive strength is 109% for dense mixes and 115.8% for gap mixes.
3. For RCC mixes with lime, the occurred flexural strength for dense specimens is at 5% lime and the rate of increase is 96.3% by using third-point loading method, while for gap specimens tested by this method, the optimum flexural strength is

also at 5% lime and higher about 86.36% than reference mix.

4. The use of hydrated lime causes increase in splitting tensile strength of RCC mixes. Dense and gap specimens show increase in tensile strength and the rate of increase as compared to reference mixes is 150% for dense and gap specimens at 5% lime.

REFERENCES

ACI Committee 211-3R-97, (1997), "Guide for Selecting Proportions for No-Slump Concrete", ACI Manual of Concrete Practice**,** pp. (14-21).

Ahmed H.K, (2001), "Factors Influencing the Properties of Roller Compacted Concrete", Ph.D. Thesis, Department of Building and Construction, University of Technology.

ASTM C42/42M (2003), "Standard Test Method for Obtaining and Testing Drilled Cores and Sawed Beams of Concrete", Annual Book of ASTM Standards, Vol. (04.02), West Conshohocken, PA., Issued October.

ASTM C78 (2002), "Standard Test Method for Flexural Strength of Concrete (Using Simple Beam with Third-Point Loading) ", Annual Book of ASTM Standards, Vol. (04.02), West Conshohocken, PA., Issued October.

ASTM C127 (2001), "Standard Test Method for Density, Relative Density (Specific Gravity), and Absorption of Coarse Aggregate ", Annual Book of ASTM Standards, Vol. (04.02), West Conshohocken, PA., Issued October.

ASTM C128 (2001), "Standard Test Method for Density, Relative Density (Specific Gravity), and Absorption of Fine Aggregate ", Annual Book of ASTM Standards, Vol. (04.02), West Conshohocken, PA., Issued October.

ASTM C496 (1996), "Standard Test Method for Splitting Tensile Strength of Cylindrical Concrete Specimens", Annual Book of ASTM Standards, Vol. (04.02), West Conshohocken, PA., Issued October.

ASTM C642 (1997), "Standard Test Method for Density, Absorption, and Voids in Hardened Concrete ", Annual Book of ASTM Standards, West Conshohocken, PA., Issued October.

ASTM D1557 (2002), "Standard Test Methods for Laboratory Compaction Characteristics of Soil Using Modified Effort", Annual Book of ASTM Standards, Vol. (04.08), West Conshohocken, PA., United States.

British Standard B.S. 594, (1961), "Rolled Asphalt-Hot Process", British Standard Institution, London. Cited in **Sarsam (1988)**.

British Standard B.S. 1881, (1983), "Method for Determination of Compressive strength of Concrete Cubes"**,** part 116.

Gupta, B.L., and Gupta, A., (2004), "Concrete Technology", 3rd Edition, Delhi, 27th, February, 2004.

Hansen K.D., (1996), "Roller Compacted Concrete: A Civil Engineering Innovation", Concrete International, March, (1996), pp. (49-53).

Iraqi Standard Specification, No.5, (1984), "The Portland Cement".

Rached, M., Moya, M.D. and Fowler, D.W., (2009), "Utilizing Aggregates Characteristics to Minimize Cement Content in Portland Cement Concrete", 2nd, June, 2009.

Rodrigues, A.F., (2002), "RCC-Materials Availability- Properties and Practices in Different Regions", Proceedings of the 2002 International Conference on Roller Compacted Concrete, Jordan University of Science and Technology, pp. (42-67).

Sarsam, S.I., (1988), "Construction of Additional Slow Lane for Mosul-Duhok Highway Using RCCP", Technical report; Ashour Constructing Company-Ministry of Housing and Construction.

Sarsam S.I., (2002), "Evaluation of Roller Compacted Concrete pavement Properties" Engineering and Development, Scientific Journal of Almustansiria University, Vol. (6), No. (1), March, 2002, pp. (59-74).

Piggott, R.W., (1999), "Roller Compacted Concrete Pavement-A study of Long Term Performance", Portland Cement Association.

SORB, (2004) "Standard specification for roads and bridges" Ministry of Housing and construction, 2004, Iraq.

Vorbieff, G., and Whitaker, C., (2003), "State of the Art of RCC Pavements in Australia", CIA Conference, July, 2003, pp. (1-9). www.concreteroads.net/rcc/RCCpaperJuly

Table (1): The primary distinction between two types of RCC (dams and pavements), Gupta(2004).

Characteristics	Dams	Pavement
Binder content (Kg/m³) (cement)	60 - 250	__
Water/cement ratio	0.40 – 0.80	0.30 – 0.40
Maximum aggregate diameter (mm)	75	20
28 day compressive strength (MPa)	15	45
Vebe time (sec)	10 - 25	30 - 60

Table (2): Chemical compositions and main compounds of the cement used through this work.

Oxide	% by weight	Limit of Iraqi specification No.5/ 1984
CaO	60.78	----------
SiO_2	20.54	----------
Al_2O_3	5.88	----------
Fe_2O_3	3.28	----------
MgO	1.93	< 5.0
SO_3	1.87	< 2.80
Loss on ignition	3.47	≤ 4.0
Insoluble residue	0.15	< 1.5
Lime saturated Factor	0.85	≥ 0.66 ≤ 1.02
Main compounds (Bogue's equations)		
C_3S	41.74	----------
C_2S	27.65	----------
C_3A	10.04	----------
C_4AF	9.97	----------

Table (3): Physical properties of cement.

Physical properties	Test result	Limit of Iraqi specification No.5/1984
Specific surface area, Blain's method, m²/kg	341	≥ 230
Soundness, Autoclave's Method, %	0.03	< 0.8
Setting time, Vicat's method Initial setting hr:min Final setting hr:min	 2:35 4:45	 ≥ 45 min ≤ 10 hours
Compressive strength 3 days N/mm² 7 days N/mm²	 18.8 23.3	 ≥ 15 ≥ 23

Table (4): Properties of coarse and fine aggregate.

Type of aggregate	Bulk Specific Gravity	Density(kg/m³)	Absorption %	SO_3 %
Crushed coarse aggregate	2.56	1600	1	0.06
Fine aggregate	2.45	1780	3.13	0.45

Table (5): Chemical components of hydrated lime

Oxide	SiO_2	Fe_2O_3	Al_2O_3	CaO	MgO	L.O.I
Percent	0.74	0.19	0.5	64.23	1.17	29.94

Table (6): Grain size distributed used for RCC mixes

Sieve size (mm)	% Passing by weight	
	Dense graded (SCRB, 2004)	Gap graded(BS,1961)
25.4	100.0	100.0
19.2	98.0	95.0
12.5	85.0	80.0
9.5	76.5	75.0
4.75	62.5	70.0
0.6	26.5	17.0
0.075	7.0	7.0

Table (7): Maximum dry density and moisture content for dense and gap RCC mixes

% cement	Maximum dry density (gm/cm³)		Moisture content %	
	Dense graded	Gap graded	Dense graded	Gap graded
12	2.395	2.347	6.0	7

Table (8): Compressive strength of mixes containing hydrated lime

Additives	Percentages %	Compressive strength (MPa)	
		7 days	**28 days**
Cement paste	0	15.7	18.65
Hydrated lime	5	19.39	29.67
	10	23.6	32.12
	12	25.45	27.2
	15	19.39	23.03

Figure (1) Roller compactor and mould

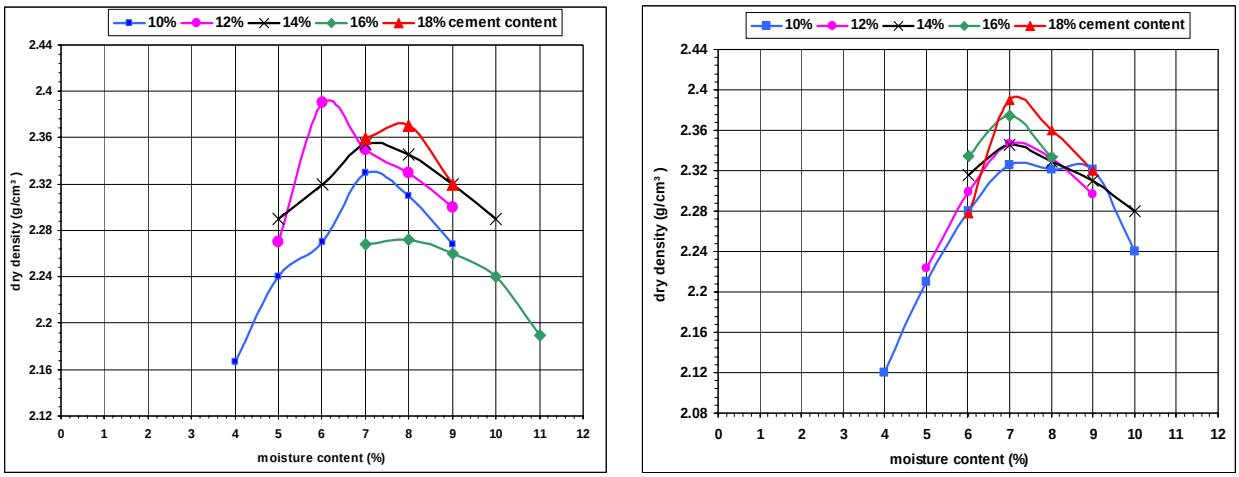

a. dense graded b. gap graded

Figure (2) Dry density-moisture content relationship of dense and gap graded mixes

Figure (3) Construction of RCC slab samples

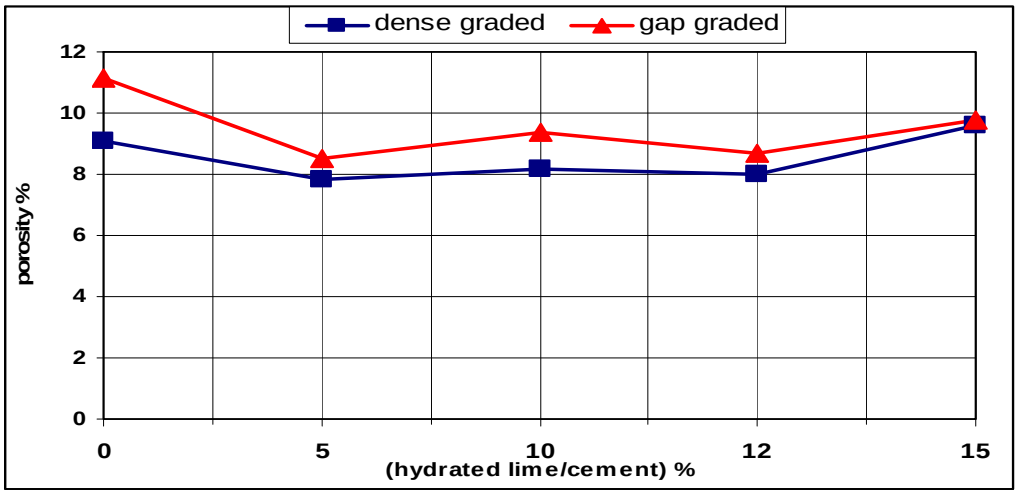

Figure (4) Variation in porosity with lime/cement ratio of dense and gap RCC mixes.

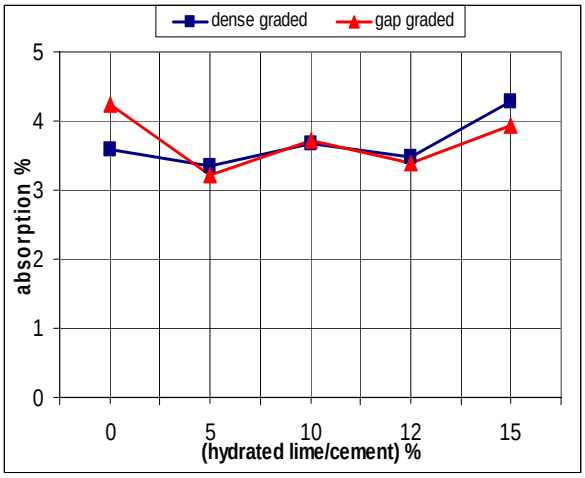

Figure (5) Variation in absorption with Lime/cement ratio of dense and gap RCC mixes.

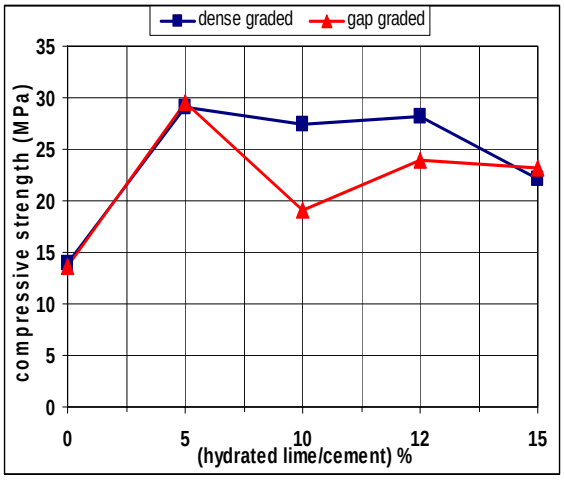

Figure (6) Variation in compressive strength with Lime/cement ratio of dense and gap RCC mixes.

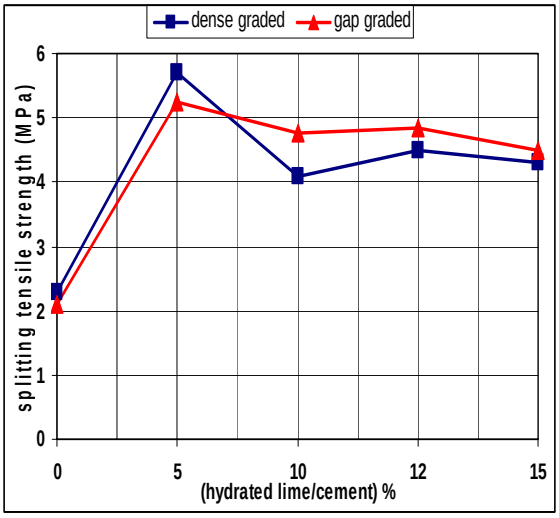

Figure (7) Variation in splitting tensile strength With lime/cement ratio of dense and gap RCC mixes.

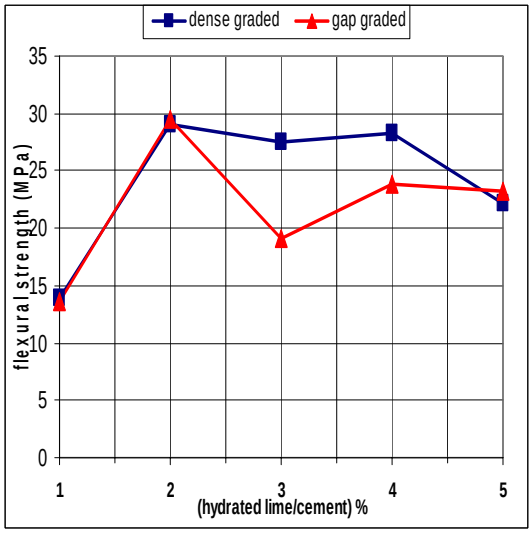

Figure (8) Variation in flexural strength with Lime/cement ratio of dense and gap RCC mixes.

Behaviour of Fire Exposed Reinforced Concrete Rigid Beams with Restrained Ends

Mohammed Mohammed Kadhum
Assist. Prof. Dr.
E-mail : Moh_Alkafaji@yahoo.com

Nada Mahdi Fawzi Alwaan
Assist. Prof. Dr.
E-mail :naljalawi@yahoo.com

ABSRACT

This paper is devoted to investigate the effect of burning by fire flame on the behavior and load carrying capacity of rectangular reinforced concrete rigid beams. Reduced scale beam models (which are believed to resemble as much as possible field conditions) were suggested.

Five end restrained beam specimens were cast and tested. The specimens were subjected to fire flame temperatures ranging from (25-750) ºC at age of 60 days, two temperature levels of 400ºC and 750ºC were chosen with exposure duration of 1.5 hour. The cast rectangular reinforced concrete beam (2250×375×375 mm) (length× width× height respectively) were subjected to fire.

Results indicate remarkable reduction in the ultrasonic pulse velocity and rebound number of the rigid beams after cooled in water were (2-5 %) more than rigid beam specimens cooled in air.

Load-deflection curves indicate deleterious response to the fire exposure. Also, it was noticed that the maximum crack width increases with increasing fire temperature.

Keywords: Rigid Beams; Fire Flame; Fire Endurance; Crack Pattern; Moment Capacity

سلوك الاعتلب الخرسانية الجاسئة والمقيدة النهايات تحت تأثير لهب النار المباشر

د. محمد منصور كاظم
استاذ مساعد
جامعة بابل / كلية الهندسة / قسم الهندسة المدنية

د. ندى مهدي فوزي علوان
استاذ مساعد
جامعة بغداد / كلية الهندسة / قسم الهندسة المدنية

الكلمات الرئيسية: الأعتاب الجاسئة، لهب النار، مقاومة الحريق، نمط الشق، تحمل العزوم

الخلاصة

ان الغرض من هذا البحث هو التحري عن سلوك وسعة التحمل القصوى للأعتاب الخرسانية المسلحة الجاسئة والمقيدة النهايات والمعرضة الى لهب النار المباشر. ان تعرض الأعتاب الى لهب النار المباشر يسبب تغيرات في سلوكها الانشائي. في هذه الدراسة تم استخدام نماذج اعتاب مصغرة يعتقد بأنها توفر ظروفآ مشابهة للظروف الطبيعية الموقعية.

تضمن الجزء العملي تهيئة وفحص خمسة أنموذجا لأعتاب خرسانية مسلحة ومقيدة النهاية. عرضت النماذج الخرسانية المستعملة إلى لهب النار في مستويات حرارة تتراوح ما بين (25-750) درجة مئوية ثم بردت بواسطة الهواء أو الماء وجرى حرق و فحص نماذج العتبات في عمر (60) يوم ولفترة تعرض ساعة ونصف. ان ابعاد نماذج الاعتاب الخرسانية المسلحة ثابتة وهو (375×375×2250ملم).

لقد أشرت النتائج انخفاض ملحوظ في فحص الامواج فوق الصوتية و مقدار الارتداد بعد التعرض إلى لهب النار، للنماذج الخرسانية المبردة بالماء حيث كانت (2-5)% اكثر من النماذج المبردة بالهواء.

اما منحنيات الحمل_الانحراف فقد كانت الاستجابة سلبية مع درجة التعرض للنار. كذلك يمكن ملاحظة ان عرض الشق الاقصى يزداد بزيادة درجة الحرارة للنار.

INTRODUCTION

One of the problems confronting buildings is the exposure to elevated temperatures, hence, should be provided with sufficient structural fire resistance to withstand the effect of fire, or at least give occupants time to escape before strength and, or stability failure occurs.

In structural design of buildings, in addition to the normal gravity and lateral loads, it is, in many cases necessary to design the structure to safely resist exposure to fire. However, it is usually necessary to guard against structural collapse for a given period of fire exposure **Shettey, 1988**.

RESEARCH SIGNIFICAT

There are indeed little research about temperature gradient and exposure time of concrete in direct contact with fire flames.

In order to simulate this problem to practical site conditions, reduced scale rigid beam models were cast and they were as close as possible to practical circumstances. This research is seeked to cover the limited area of research about this problem. This will guide and facilitate the suggestion of rehabilitation of such members exposed to fires under loading of different degrees.

The current research proposes a reinforced concrete rigid beams model which resembles the simulation of the state of stress which the reinforced concrete rigid beams are subjected to during fire in laboratory. Simulation of real fires in laboratory using a set of methane burners which subjecting the rigid beams specimens to real fire flame.

In the present work, there is an attempt to investigate the effect of exposure of concrete to fire flame on shrinkage cracking of reinforced concrete beams and some mechanical properties of concrete.

LITERATURE REVIEW

The Effect of Fire on Reinforced Concrete Structure

In the 1986, **Khan and Royles** studied the behavior of reinforced concrete beams after subjecting them to elevated temperatures. They investigated the load-deflection relationship, cracks pattern and steel to concrete bond. Prismatic concrete beams (960× 140× 66 or 107mm) were used. 8-mm plain bars and 16mm toolbars were used to reinforce them. The specimens were heated to temperature ranges from 20-800ºC at a slow rate of heating (2ºC/min) for one hour exposure duration. They found that the effect of temperature is insignificant at temperatures ranging from 100 to 200ºC, but the strength decreases significantly between 350 to 500ºC compared with normal ambient condition, the flexural strength characteristics weakened by 50% of the original strength.

The behavior of composite beams composed of rolled steel and concreted between flanges during a fire by conducting a fire resistance test with different cross sections and load ratios, was studied by numerical analysis **Kodaira, and et al., 2004**. The results they obtained are as follows:

1. In steel-concrete composite beams which were simply supported and to which positive bending moment was applied, deformations were downward in the early period of fire, and then the deformation rate decreased once but increased again as heating was continued, leading to the limit of fire resistance.
2. The fire resistance of steel-concrete composite beams increased when the applied bending moment ratio decreased. The fire resistance time was affected by the size of the cross-section, whether steel-concrete composite beams were connected to the reinforced concrete floor or not, as well as by the applied bending moment ratio.

A case study of cracking in a concrete building subjected to fire, with particular emphasis on the depths to which cracks penetrate the concrete was made by **Georgali and Tsakiridis, 2005**. It was found that the penetration depth is related to the temperature of the fire, and that generally the cracks extended quite deep into the concrete member. Major damage was confined to the surface near to the fire origin, but the nature of cracking and discoloration of the concrete pointed to the concrete around the reinforcement reaching 700°C. Cracks which extended more than 30mm into the depth of the structure were attributed to a short heating/cooling cycle due to the fire being extinguished.

Residual bearing capabilities of five-exposed reinforced concrete beams were investigated by **Hsu and Lin, 2006**. The analysis method includes combining thermal and structural analyses for

assessing the residual bearing capabilities, flexural and shear capacities of reinforced concrete beams after fire exposure. The thermal analysis uses the finite difference method to model the temperature distribution of a reinforced concrete beam maintained at high temperature. The structural analysis, using the lumped method, is utilized to calculate the residual bearing capabilities, flexure and shear capacities of reinforced concrete beams after fire exposure. This novel scheme for predicting residual bearing capabilities of fire-exposed reinforced concrete beams is very promising in that is eliminates the extensive testing otherwise required when determining fire ratings for structural assemblies.

In recent years a number of notable fires have occurred during construction of concrete-framed buildings, when formwork and false work has caught fire, see Figure (1). Fortunately, even after a sever fire, reinforced concrete structures are generally capable of being repaired rather than demolished **Ingham and Tarada, 2007**.

After a fire, an appraisal is normally required as soon as the building can be safely entered and generally before the removal of debris. To ensure safety, temporary false work may be required to secure individual members and stabilize the structure as a whole.

Dong and Prasad, Accepted for publication in 2008 conducted a furnace test on three full- scale two-story, two-bay composite steel frames to understand the performance of structural frames under fire loading. The three tests differed from each other in the number of heated compartments by the furnace and in the relative location of the heated compartments. For each test, the burners were operated so as to replicate the temperature prescribed by ISO 834 standard and the loads were applied using vertical loads at the top of each column by hydraulic jacks in addition to block loads placed on each composite beam. In the first test, the burners in compartment "I" was in operation, while in the second test the burners in compartment "I" and "II" were in operation, Figure (2). In the third test, the burners in compartments "I" and "III" were in operation.

In all tests, the beams to column connections as well as the columns were protected. None of the columns in any of the three tests showed signs of local buckling. Observations on local buckling of steel beams, cracking of concrete slabs and failure of the beam-to-column connections are presented.

The results showed that the deformation process and time to failure of a structure are highly dependent on the number of compartments that are heated and the relative location of the compartments that are subjected to fire loading.

EXPERIMENTAL WORK

Materials and Mixes

Introduction

The properties of materials used in any structure are of considerable importance (Neville, 1995, and ACI Committee 211, 1997). The properties of materials used in the current study are presented in this chapter. Standard tests according to the American Society for Testing and Materials (ASTM) and Iraqi specifications IQS were conducted to determine the properties of materials.

Materials

Tasluga-Bazian Ordinary Portland Cement (O.P.C) (ASTM Type I). This cement complied with the Iraqi specification (IQS, No.5:1984). Well-graded natural sand from Al-Akhaidher region through sieve size (9.5mm) to separate the aggregate particles of diameter greater than 9.5mm. The gravel was sieved at sieve size of (20 mm). The sand and gravel were then washed and cleaned with water several times, then it were spread out and left to dry in air, after which it were ready for use. Galvanized welded wire meshes were used throughout the test program. Deformed steel bars of diameters (Ø8 mm) and (Ø10 mm) were used as reinforcement.

Mix Design and Proportions

The concrete mix was designed according to American mix design method (ACI 211.1-91) specification. The proportions of the concrete mix are summarized in Table (1).

Reinforced Concrete Rigid Beam Specimens

The experimental work was carried out to decide upon the temperature range and duration of burning. It was decided to limit the maximum exposure to fire flame to about 400ºC and 750ºC, with duration of exposure to fire flame of 1.5 hours which cover the range of situation in the majority of elevated temperature test.

After greasing the moulds of the rigid beams specimens, reinforcement bars were held carefully in their position inside these moulds. In order to get a

Cover, small pieces of steel were placed at sides of the rigid beams reinforcement. Figure 2 shows the details of the reinforcement of rigid beam specimens.

Figure a, b and c in Figure 4 show the formwork was strike after 7 days from casting and the beams were covered with wetted hessian and polythene sheets during 7 days. The hessian sheets were wetted two times a day during the curing.

Burning of Reinforced Concrete Rigid Beams

The reinforced concrete rigid beams were burnt with direct fire flame from a net work of methane burners inside the frame. The fire flame hits the lower face of these beams. The dimensions of this burner net are (2250×2250) (length × width respectively) as shown in Figure (5). The bars of flame were intended to simulate the heating condition in an actual fire. When the target was reached, the temperature was continuously measured by digital thermometers, one of them was positioned in the bottom surface of the beam in contact with the flame, while the other was positioned at the unexposed upper surface of the beam, and by thermocouple that was inserted in the center of each beam to measure the temperature at the mid-depth (187.5 mm from the exposed or unexposed surface).

Reinforced Concrete Rigid Beams and Testing Procedure

The rigid beam specimens were tested using a load cell of maximum capacity of (150 Tons) at the age of 60 days. The load was applied using steel beam that divided the load to two equal point loads. The load was applied in small increments and the readings were taken every 3.0 kN load until failure occurrs. For each increment, the load was kept constant until the required measurements were recorded.

The mid-span deflection of the beam specimens exposed to fire are resulting from loading to 25% of ultimate load before burning, loading 25% and applied fire flame, thereon, cooled by water or air then residual ultimate loading after burning was applied until failure. While, for beam specimens without burning the mid-span deflection is resulting from applied load only. Testing continued until the reinforced concrete beam shows a drop in load capacity with increasing deformation. For the column specimens which were subjected to fire flame under loading as shown in Figure (6).

Figure 7 shows a schematic diagram for loading arrangement. The specified (target) fire temperature was reached by mounting the fire subjecting burners by a sliding arm to control the fire distance to the surface of the beam specimens, and also by monitoring the fire intensity through controlling the methane gas pressure in the burners. The temperature was measured by the digital thermometer and infrared rays thermometer continuously till reaching the specified (target) fire temperature. Then, the sliding arm and gas pressure were kept at this position along the period of burning (1.5 hour). The deflection of the rigid beams exposed to fire are resulting from loading to 25% of ultimate load before burning, loading 25% and applied fire flame, and loading after burning until failure. While, for rigid beams without burning the deflection is resulting from applied load only.

For the beam specimens which were subjected to burning by fire flame under loading, the real problem which faced this process was exposing the dial gauge of deflection measurement to elevated temperatures without spoiling it. A protection system is especially made for this purpose. This equipment consists of a thin steel cover around the dial gauge. This steel cover is surrounded by a copper pipe of 7.5mm with a spiral fashion. The surface of the spiral pipe coated with a layer of glass fibre of 10mm, which is covered by a thin aluminum sheet. To protect the moving rod of the dial gauge, it was elongated by a porcelain rod. This porcelain rod is covered with a steel tube to be fitted with the moving rod as shown in Figure 8. The performance of this equipment depends on the principle of thermal exchange. Water flows in the copper pipe with a suitable discharge that keeps the temperature of dial gauge low during exposing to fire.

RESULTS AND DISCUSSION

Non-Destructive Test Results

The ultrasonic pulse velocity (U.P.V) and surface hardness of reinforced concrete rigid beams was assessed by the "Schmidt rebound hammer" test

results are presented in Table (2). Figures (9 and 10) show the effect of exposure to fire flame on ultrasonic pulse velocity and rebound number respectively for the rigid beams before and after exposure to burning. It can be seen from the figure below that the reductions in the ultrasonic pulse velocity after exposure to fire flame were as follows:

At 400ºC, the reduction in (U.P.V) was (28 and 33 %) when rigid beams were cooled by air and water respectively. Whereas, at 750ºC the reduction was (52 and 54 %) when beams were cooled by air and water respectively.

The effect of burning by fire flame on rebound number is shown in Figure below, it can be seen that subjecting the reinforced concrete rigid beams surface to fire causes to decrease the rebound number significantly as follows:

At 400ºC, the reduction in rebound number was (22 and 27 %) for beams which were cooled in air and water respectively. Whereas, at 750ºC the reduction was (42 and 45%) for beams cooled in air and water respectively.

Effect of Burning on Load Versus Deflection Results

The load versus mid-span deflection relationship of reinforced concrete rigid beam specimens which were loaded and exposed to fire flame at the same time was measured during this process are summarized in Table(3) and presented in Figure (11). Each beam specimen was loaded to 25% of the ultimate load before burning for a period of 25 minute; then exposed to fire flame temperatures of (400°C, and 750°C) thereon, cooled by water or air and finally the residual ultimate load was applied until failure.

Deflection of these rigid beam specimens, which occurred immediately when they were loaded and subjected to fire flame, this deflection is called immediate deflection or instantaneous deflection. Deflection measurement was taken continually during the test and the rate of increase in deflection was controlled to provide warning of impending collapse of the beam specimens.

From this Figure, it can be seen that the increase in the fire temperature has a significant effect on deflection of beam specimens cooled. In addition, it can be noted that the increase in the fire temperature decreases the load carrying capacity and increases deflection in beam specimens. This can be attributed to the fact that heating causes a reduction in beam stiffness, which is essentially due to the reduction in the modulus of elasticity of concrete and the reduction in the effective section due to cracking. These Figures reveal that the load-deflection relation of the beam specimens is almost linearly proportional for temperature exposure (400°C and 750°C).

Also, it can be indicated from the results in this Figure that the ultimate load capacity of the rigid beams is adversely influenced by the fire flame exposure and this deleterious effect decreases the ultimate load capacity by about 15-37%. Also the maximum deflection at ultimate load increases by about 30% which shows clearly reduced stiffness behavior.

It is obvious from the results that the values of residual first crack load decrease when the beams are exposed to fire flame except (RB2) which increase by (4.2%) over original first crack load. This increase can be attributed to the general stiffening of the cement gel or the increase in surface forces between gel particles due to the removal of absorbed water. Figure 12 reveals the effect of fire flame on the residual first crack load for the rigid beam specimens.

Verification of Building Codes Provisions

Several existing equations are available to predict the bending moment capacity of reinforced concrete beams. These equations are selected and used in this study for comparison with the results of the experimental work. These equations are outlined in the Table (4).

Where:

M_n = Nominal moment, kN.m

$$f_{cu} = 0.85 f'_c \qquad \text{eq. (1)}$$

The ultimate moment Mu (for design) is

$$M_u = \emptyset M_n \text{ and } \emptyset = 0.9 \qquad \text{eq. (2)}$$

The test results were utilized to verify the recommendations and design simplifications of the various Building Codes pertaining to bending moment capacity (Mu) design. Table (5) presents the comparison between the experimental results with (ACI and B.S) Codes. The relationship between fire temperature with residual moment capacity and ultimate moment capacity are

Illustrated in Figures (13) and (14). To utilize these equations after exposure to fire flame temperatures the relative between the values (Mu test/Mu calculated) were calculated for the rigid beam specimens.

At fire temperature (400°C), for the rigid beam specimens cooled by air, the ACI and B.S Building codes close results to predict bending moment capacity, while ACI Code gave overestimated values whereas, the B.S Code gave well predicted results of beam moment capacity cooled by water.

At fire temperature (750°C), for the beam specimens cooled by air and water, the ACI and B.S Building codes became unable to predict bending moment capacity.

From the results, it is clear that the predicted ultimate bending moment capacity obtained from (ACI and B.S) Codes provisions is greater than that obtained in the experimental work after exposure o fir flame. This can be attributed to the precracking which happens upon burning.

Fire Endurance of the Tested Rigid Beams

The aim of design for fire safety should be to limit damage due to fire. The unexposed surface of each tested beam was observed throughout (1.5 hours) fire test.

Figure (15) shows the temperature-time curves for the exposed, mid-depth and unexposed surface for the reinforced concrete beams. At the beginning, the beams are at room temperature, measured to be 25°C. The experimental results clearly indicated that the temperature near the surface to fire is higher and decreases towards the top unexposed surface. It can be seen from this Figure, that the behavior of all beams tested is similar.

Fire endurance periods are determined usually by physical tests conducted according to the provisions of (ASTM E119-01) [14]. Under this standard, the fire endurance of a member or assembly is determined by the time required to reach any of the following three end points:

1- The passage or propagation of flame to the unexposed surface of the test assembly;

2- A temperature rise of 163oC at a single point or 121oC as an average on the unexposed surface of the test assembly; and

3- Failure to carry the applied design load or structural collapse.

Based on the results of this work, it was noticed that the test results agreed with [14]. While, these beam specimens were subjected to fire flame temperatures of (400 and 750 oC) for (90 minutes), the fire endurance of all the beam specimens investigated was reached when the inability to carry the applied design load, then these beams were considered failed according to [14].

Crack Pattern and Mode of Failure

In the present study, the development of cracks and the time at which they appeared and propagated in the reinforced concrete rigid beam specimens were detected throughout testing to assess the behavior of the beam specimens exposed to fire flame and the control beam specimens. The cracks were marked with a blue marking pen, and then photographs were taken to the crack pattern. When the load was increased, the cracks initiated from the bottom concrete surface, propagation and can be detected at early loading stages. Flexural cracks appear initially in the constant moment region. Further, flexural cracks were formed progressively and widened as the loading increased. Scabbing occurred prior to the rigid beam failure due to the crushing of the concrete. The rigid beam specimens are failed with the typical flexural failure mode (yielding of steel followed by crushing of concrete),

The beam burnt at 400oC, the flexural cracks were wide speared along the beam outside the pure bending moment region. However inclined cracks are formed due to the presence of increasing shear stresses as the load and temperature increase. For rigid beams burnt at 750oC, additional vertical cracks appeared on the beam surface, followed by formation of diagonal cracks, the failure began outside the mid span of beam. Figure (16) shows photographs for crack patterns for the rigid beams before and after exposure to fire flame.

Fire Testing Observations For Rigid Beam Specimens

During the tests, special attention was drawn to visual observations. The followings are some of the observations that were recorded

1. uring the experimental test, the beam was monitored continuously for development of surface cracks. It was observed that the surface cracks formed earlier than expected, at approximately 23 and 12 minutes during burning to temperature 400oC and 750oC

respectively. These cracks eventually led to spalling of concrete cover, when the specimens were loaded after burning.

2. fter the beams were subjected to fire flame, two types of cracks developed, the first was thermal cracks appearing randomly in a honeycomb fashion all over the surface. They originated from top or bottoms edges and terminated near the mid-depth of the rigid beam. The crack width was about (1.5mm). The patterns of fine cracks were consistent with the release of moisture being greater in the outer layers than in the interior resulting in differential shrinkage. The second cracks were flexural tensile cracking due to loading developed in the mid-span region.
3. hese cracks were observed in rigid beam specimens during burning at about (15-24 minutes) of burning.

4. Generally, runoff water from all surfaces of beam specimens in the first few minutes was noticed. This phenomenon was observed at about 10-15 minutes and continued for approximately 9minutes for all burning temperatures 400 and 750°C. This can be attributed to the increase in vapor pressure inside the saturated voids which causes water to escape out from the cracks on the surface generated by fire exposure.

5. As loading increased, the cracks widened and extended to join and form a triangular-shaped cracks of (125-150 mm) length and (35-45mm) width as shown in Figure 14.

COCLUSIONS

Based on the limited number of observations made in this research the following conclusions can be drawn:

1. The ultrasonic pulse velocity tested showed a response to the effect of fire flame, the reduction in (U.P.V) was (28 and 33) % and (52 and 54) % for beams cooled in air and water at 400°C and 750°C respectively. It appears that this non-destructive test gives good predicted values for the residual strength.

2. The reduction in rebound number was (22 and 27) % and (42 and 45) % for beams cooled in air and water at 400°C and 750°C respectively. The decrease in the rebound number with increasing in fire temperature can be attributed to the fact that fire causes damage to the surface of concrete rigid beams rather than to concrete in the core of the member.

3. It was found that the ultimate load capacity of rigid beam specimens decreases significantly when subjected to burning by fire flame.

4. In this study, it is noticed that the load-deflection relation of rigid beam specimens exposed to fire flame temperature around 750°C are more leveled indicating softer load-deflection behavior than that of the control beams. This can be attributed to the early cracks and lower modulus of elasticity.
5. The ACI and B.S Codes predict ultimate moment capacity after exposure to 750°C fire flame temperature conservatively.
6. The experimental results clearly indicate that the crack width in reinforced concrete beams that are subjected to fire flame are higher than the beams that are not burned at identical loads.

REFERENCES

ACI 318-08, 2008, "Building Code Requirements for Reinforced Concrete", American Concrete Institute, Detroit.

ACI Committee 211, 1997, "Standard Practice for Selecting Proportions for Normal, Heavyweight, and Mass Concrete (ACI 211.1-91)", American Concrete Institute, Michigan, U.S.A.

ASTM, Test Method E119-01, 2001,"Standard Methods of Fire test of Building Construction and Materials", American Society for Testing and Materials, West Conshohocken, PA.

BS-8110 part 2, 1997, "Design Curves of Concrete Strength with Temperature".

Dong, Y. and Prasad, K., 2008, "Thermal and Structural Response of a Two-Story, Two-Bay Composite Steel Frame under Fire Loading", Proceedings of the Combustion Institute, 8pp.

Georgali, B., Tsakiridis, P.E., 2005, "Microstructure of Fire- Damaged Concrete", Case study, Cement and Concrete Composite, pp225-259.

Hsu, H.J, and Lin,C.S, 2006, "Residual Bearing Capabilities of Fire-Exposed Reinforced Concrete Beams", International Journal of Applied Science and Engineering, Chaoyang University of Technology, ISSN 1727-239.

Ingham, J., and Tarada, F., 2007, "Turning up the Heat-Full Service Fire Safety Engineering for Concrete Structures", Durable Concrete, October, pp.27-30.

Iraqi Organization of Standards, IOS 45: 1984; for Aggregate.

Iraqi Organization of Standards, IOS 5: 1984; for Portland Cement.

Khan, M. R., and Royles, R., 1986, "Post – Heat Exposure Behavior of Reinforced Concrete Beams", Magazine of Concrete Research, Vol.38, No.135, June, pp.59-66.

Kodaira, A., Fujinaka, H., Ohashi, H. and Nishimura, T., 2004, "Fire Resistance of Composite Beams Composed of Rolled Steel Profile Concreted between Flanges", Fire Science and Technology 23(3), 192-208.

Neville, A. M., 1995, "Properties of Concrete", Longman Group, Ltd., 4th and Final Edition, 1995, pp.388.

Shettey, M. S., 1988, "Concrete Technology Theory and Practice", Third Edition, PP.361.

Figure (1): The concrete frame of a ten-storey building that was fire-damaged during construction, [Georgali and Tsakiridis, 2005].

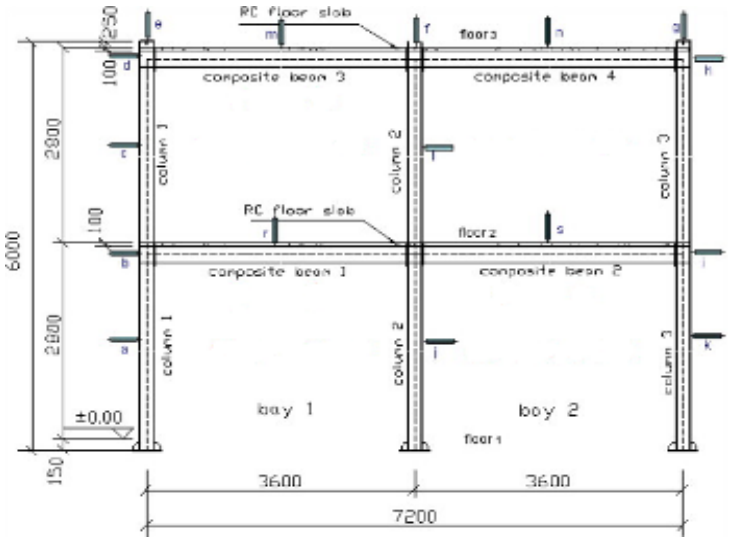

Figure (2): Elevation of the tested two-story two-bay portal frame [Hsu and Lin, 2006].

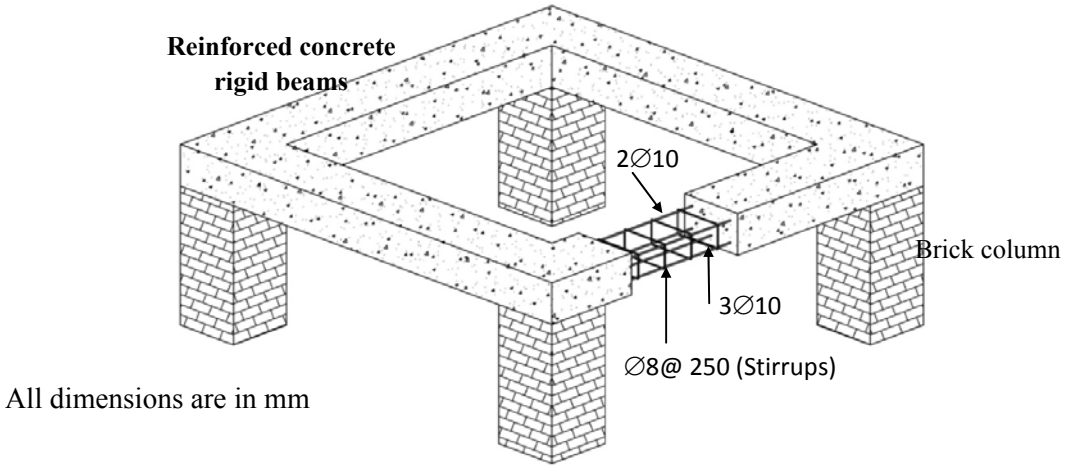

Figure (3): Details of the reinforced concrete rigid beams.

Figure (4): (A) The wood formwork of the rigid beams; (B) The rigid beams after lifting of the wood formwork; (C) Curing of Rigid beam with the wetted hessian and polythene sheets.

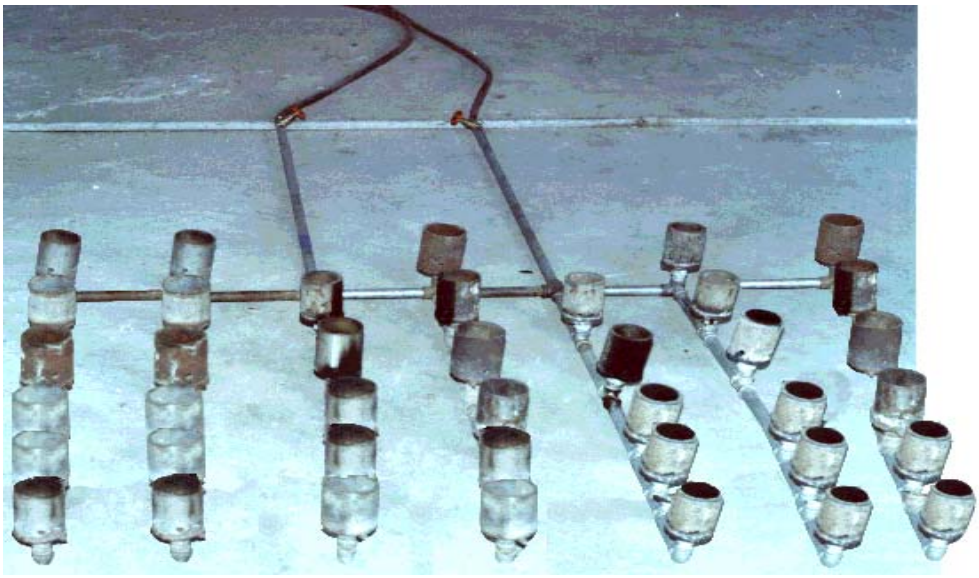

Figure (5): The work of net methane burners.

Figure (6): Testing of rigid beam specimens under 25% of ultimate load with exposure to fire flame.

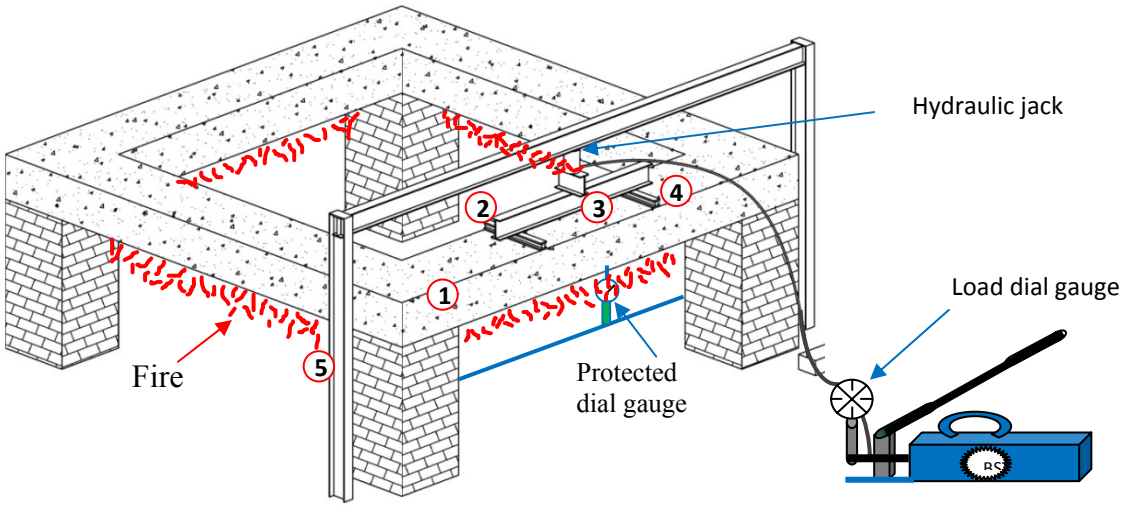

(1) Test specimen
(2) Loading arm
(3) Main bed
(4) Bearing seats
(5) Frame

Figure (7): Schematic diagram showing the testing of beam specimens under 25% of ultimate load with exposure to fire flame.

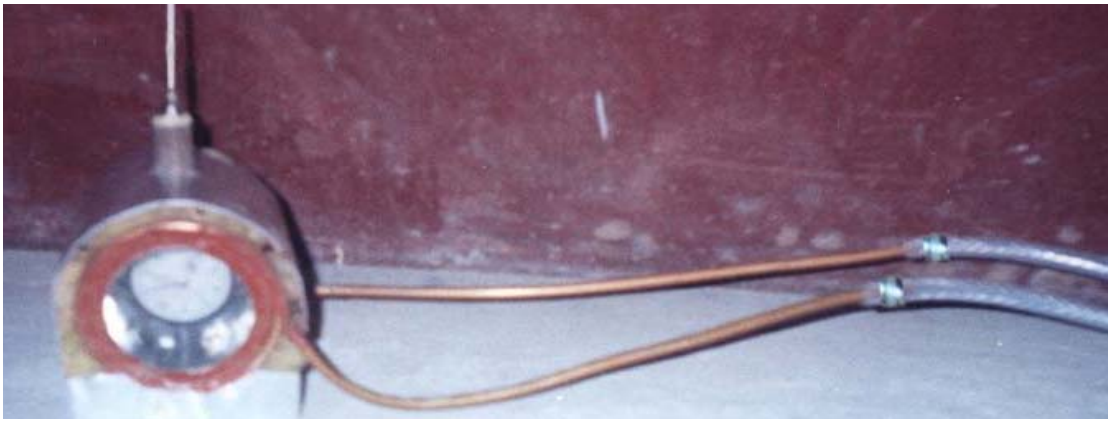

Figure (8): Protection system of the dial gauge of deflection measurement.

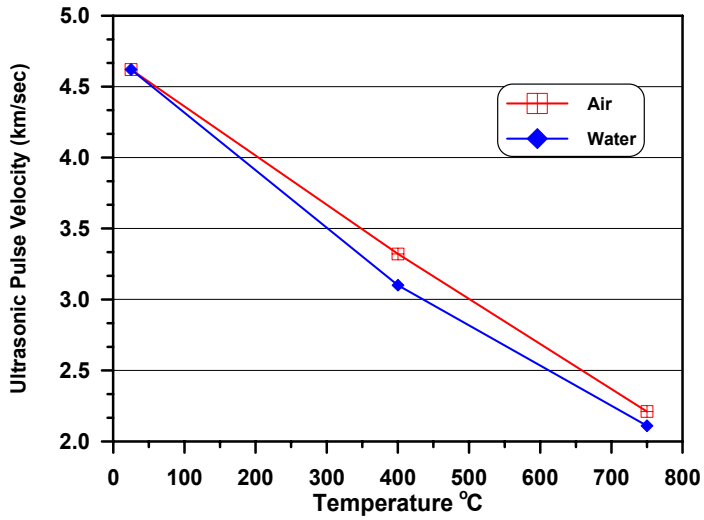

Figure (9): The effect of fire flame on the ultrasonic pulse velocity for 1.5 hour period exposure to fire flame.

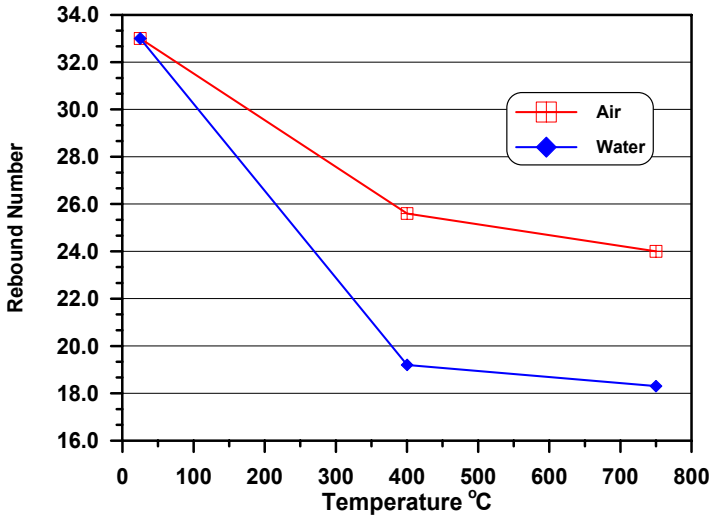

Figure (10): The effect of fire flame on the rebound number for 1.5 hour period exposure to fire flame.

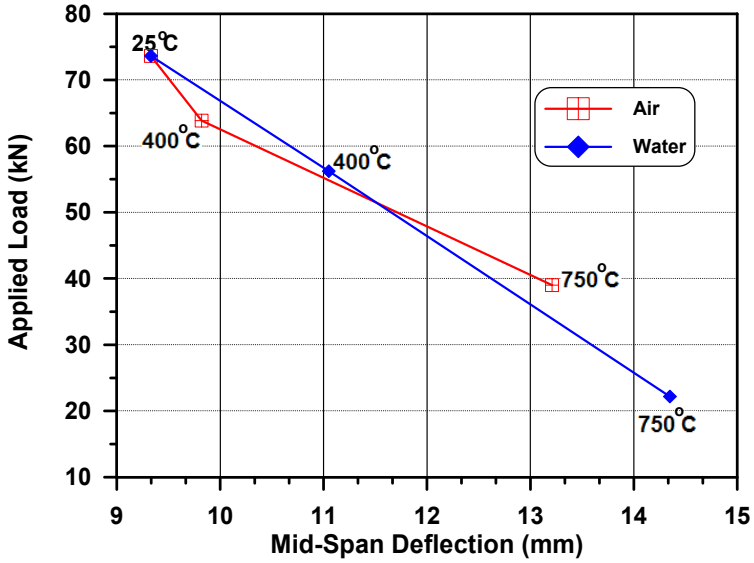

Figure (11): Load versus mid-span deflection curve of reinforced concrete rigid beam specimens.

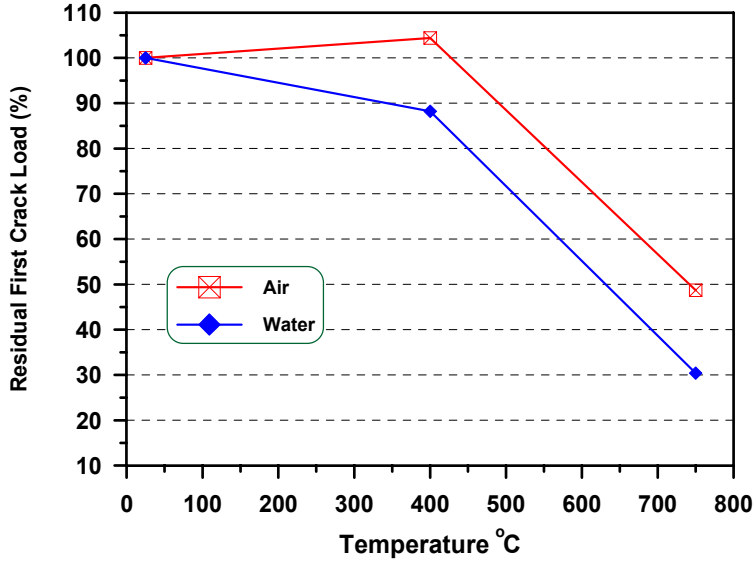

Figure (12): Effect of fire flame on the residual first crack load for the rigid beam specimens.

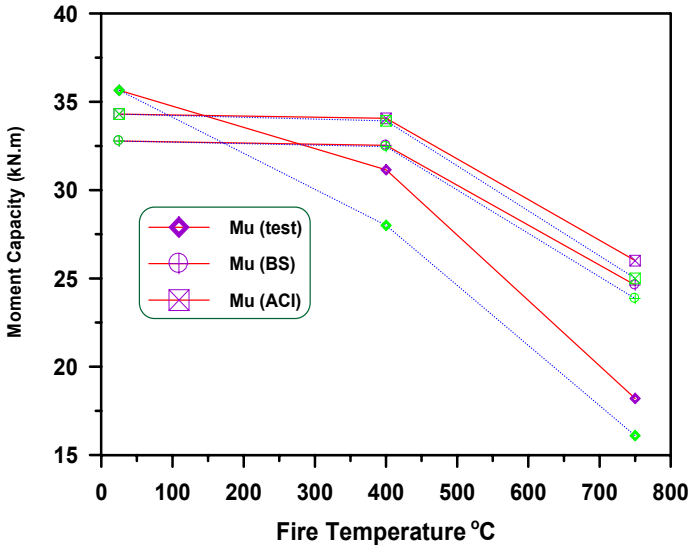

Figure (13): Effect of fire temperature on the moment capacity of beam specimens.

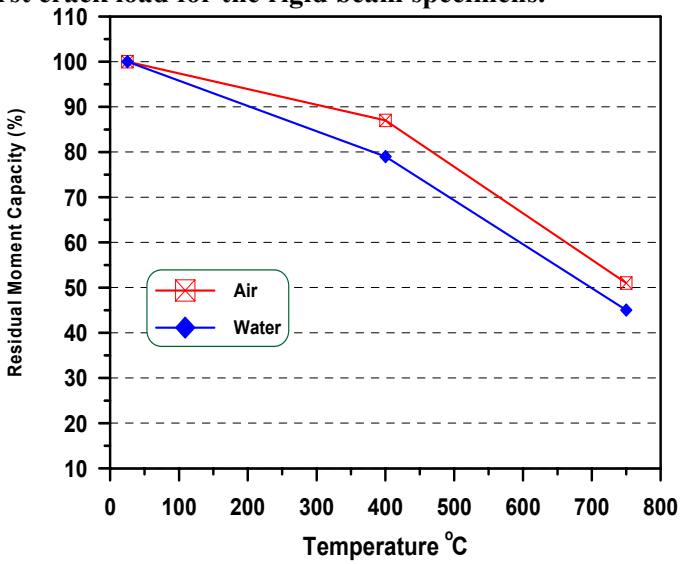

Figure (14): Effect of fire temperature on the residual moment capacity of rigid beam specimens.

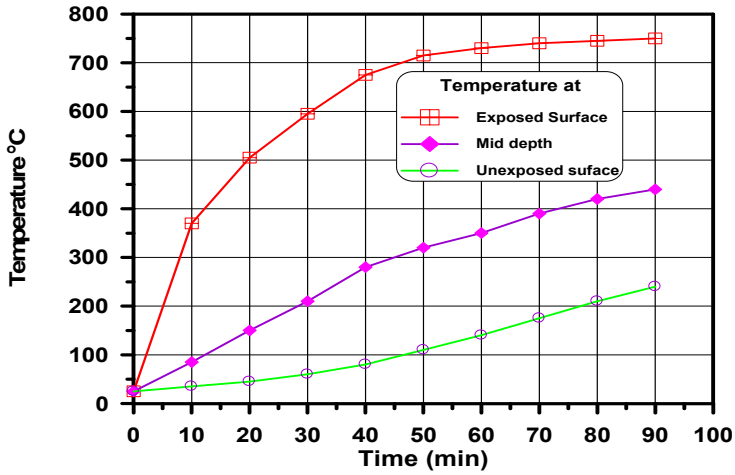

Figure (15): Effect of fire temperature on the residual moment capacity of rigid beam specimens.

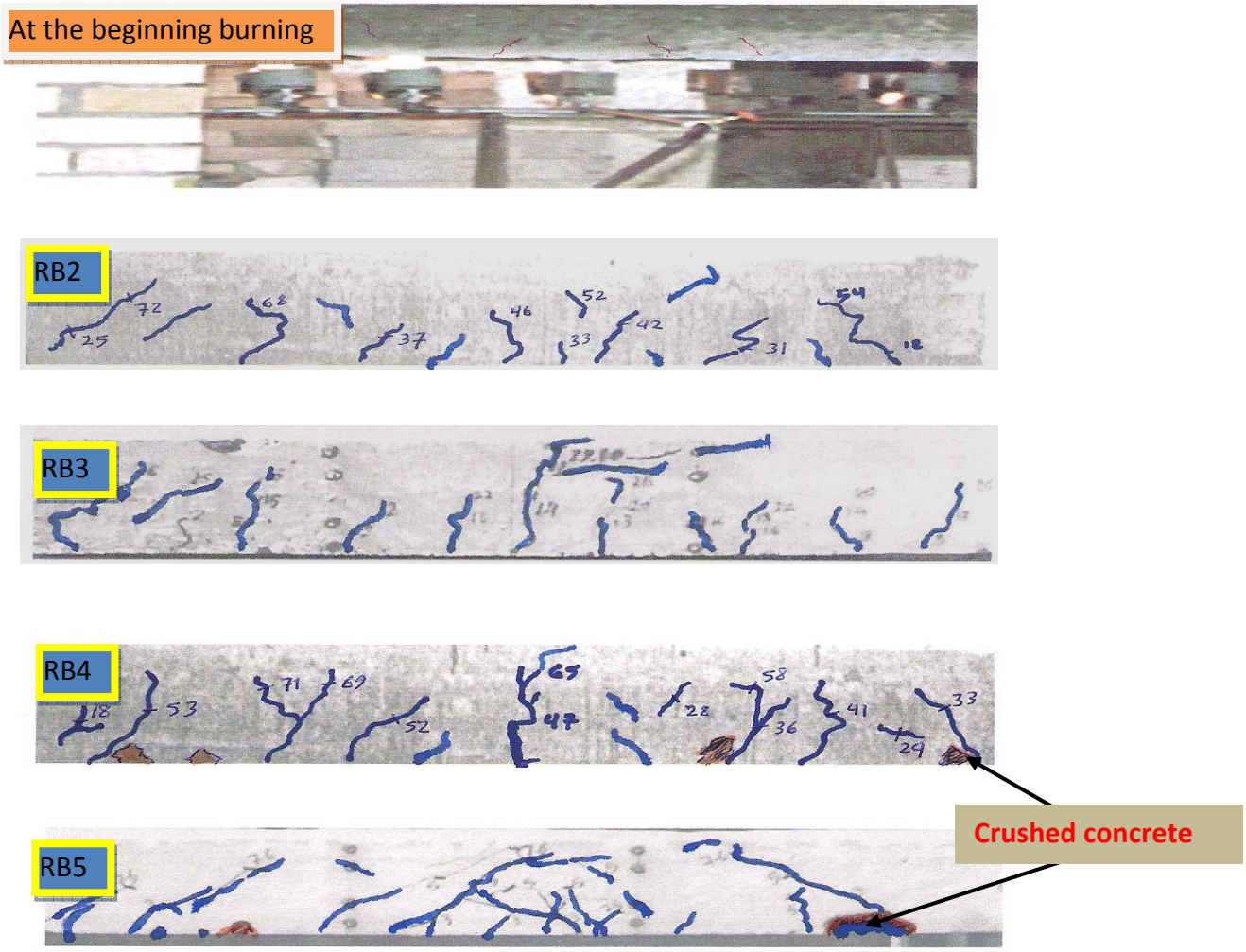

Figure (16): Typical crack pattern of rigid beam specimens before and after burning and subjected to loading.

Table (1): Mix proportions.

	Mix Proportion kg/m^3				
W/c ratio	Water	Cement	Sand	Gravel	Slump (mm)
0.45	195	435	525	1215	60

Table (2): The test results of ultrasonic pulse velocity and rebound number of reinforced concrete rigid beams before and after exposure to fire flame.

Type of Test	Temperature ºC			(Va/Vb) Ratio		Type of Cooling
	25 A	400 B	750 C	B/A	C/A	
UPV (Km/Sec)	4.62	3.32	2.21	0.72	0.48	Air
		3.32	2.11	0.67	0.46	Water
Rebound Number	32	26.0	20.6	0.78	0.58	Air
		24.7	18.3	0.73	0.55	Water

Va and Vb Values of test results after and before exposure to fire flame respectively.

Table (3): Test results of the first crack load, ultimate load and deflection for control rigid beam and rigid beams exposed to burning.

Specimen Identification	First Crack Load (kN)	Percentage Residual First Crack Load %	Ultimate Load (kN)	Max Center Deflection (mm)	Type of Cooling
RB1-25ºC	26.3	100	73.74	9.33	---
RB2-400ºC	27.4	104.2	63.85	9.82	Air
RB3-400ºC	23.2	88.2	56.22	11.05	Water
RB4-750ºC	12.8	48.7	39.00	13.21	Air
RB5-750ºC	8.0	30.4	22.18	14.35	Water

Table (4): Summary of formulas for predicting moment beam capacity.

Method	Equation	EQ. NO.
ACI-318M-08 Code	$M_n = \emptyset \rho b d^2 f_y \left(1 - 0.59\rho \frac{f_y}{f_c'}\right)$	1
B.S 8110-97 Code	$M_u = 0.87 f_y A_s \left(d - \frac{f_y A_s}{1.34 f_{cu} b}\right)$	2

Table (5): Comparison of the moment capacity test results with that obtained from (ACI and B.S) Codes for beam .

Specimen Identification	Cylinder Compressive Strength (MPa)	Steel Yield Stress (GPa)	Ultimate Load (kN)	Percentage Residual Moment Capacity	M_u (kN.m)			$\frac{M_u(Test)}{M_u(BS)}$	$\frac{M_u(Test)}{M_u(ACI)}$
					Test	BS	ACI		
RB1	24.0	530	142.6	100	35.65	32.78	34.30	1.09	1.04
RB2	19.7	530	124.4	0.87	31.15	32.53	34.06	0.96	0.91
RB3	18.5	530	112.0	0.79	28.00	32.46	33.92	0.86	0.83
RB4	12.4	408	72.8	0.51	18.20	24.62	26.00	0.74	0.70
RB5	6.6	408	64.2	0.45	16.10	23.56	25.00	0.68	0.64

Theoretical and Experimental Investigation of Fluidic Oscillator

Dr.Ali Abdul AL-Muhsin AL-Asady
Asst. prof. Dept of Mech. Eng
Baghdad University
Email: dralicit@yahoo.com

Bahaa Aldeen M. Razouqi
Dept of Mech. Eng
Baghdad university

ABSTRACT

A symmetric feedback fluidic oscillator design is proposed. Theoretical and experimental studies have been conducted to evaluate the relation between the fluidic feedback oscillator frequency and temperature of the air which is the working substance. Two methods of calculations were used, lumped and distributed parameter system. Then the results obtained experimentally. It was found that the results of the lumped parameter system are closer to experimental results than the distributed parameter system and also give the nonlinearity by (0.915%) between the lumped and experimental results show linear relationship between air temperature and oscillator frequency with a coefficient of determination (0.9977) And also found that the oscillator readings have a margin of error very small amount (0.0011 Hz / C^o) as well as a percentage (hysteresis) of about (1.663%) when measuring the temperature and to overcome the hysteresis we suggest the use of fins to get rid of (residual heat), the rig sensitivity was ($3.66*10^{-3}$ s/C^o) finally, the rig resolution was (0.002 s).

KEYWORDS: fluidics, oscillator, coanda effect, wall attachment

الخلاصة

تم اقتراح تصميم مذبذب موائعي متناظر في هذا البحث، وقد تم اجراء الدراسات العملية والنظرية لايجاد العلاقة بين تردد المذبذب ودرجة حرارة الهواء الذي يعتبر وسيط العمل وبالتالي استخدام المذبذب كمتحسس لدرجة الحرارة. طريقتان لحساب تردد المذبذب تم استخدامهما، الاولي تعتمد نظام المعايير (lumped) والثانية تعتمد نظام المعايير (distributed)، وبعدها تم ايجاد النتائج عمليا. لقد وجد بان طريقة (lumped) تكون نتائجها اكثر واقعية وكذلك اعطت نسبة (nonlinearity) بمقدار (0.915%) بين النتائج العملية والنظرية، وكذلك ووجد بان العلاقة تكون خطية بين تفير درجة الحرارة و تغير مقدار تردد المذبذب وبمعامل تحديد (0.9977).

ومن النتائج العملية وجد بان الجهاز له نسبة خطأ بمقدار (0.0011 Hz/C^o) بالاضافة الى نسبة (hysteresis) بمقدار (1.663%) ولتقليل هذه النسبة تم اقتراح استخدام زعانف (fins) لتبديد الحرارة (residual heat)، وكذلك ووجد ان حساسية الجهاز (sensitivity) تكون بمقدار ($3.66*10^{-3}$ s/C^o)، واخيرا كانت نسبة دقة الجهاز (resolution) بمقدار (0.002 s).

.

INTRODUCTION

This work is focused on study the effect of the temperature on the fluidic oscillator frequency. The feedback fluidic oscillator as shown in **fig. 1** is a device with no moving parts that generate an oscillating jet of fluid. The fluidic oscillator has many implementations, it can be used as flow meter, temperature measurement device and frequency generator.

The fluidic oscillator arose from a development of the Coanda switch (Luchi, 1967).

Fluidic oscillator has also been used as a thermometer. In fact the change in the oscillation frequency can be used as a temperature indicator; Halbach, et al. (1968**)** described a fluidic temperature sensor which has been demonstrated with heated air. The sensor uses the frequency beating technique and a detector network to generate an analog pressure signal proportional to the difference in frequencies. An oscillator, used as the temperature sensitive element, generates a frequency signal from the coupling of two resonance tubes. Frequency was converted into an analog pressure signal using a pulse modulation technique. Data were presented and discussed for heated air test conditions which simulate a typical metal vapor application.

Frey, (1970) described the results of a theoretical and experimental study of the parameters affecting on the performance of fluidic feedback oscillators. A monostable wall attachment amplifier was used as the active element. Feedback elements are either constant area transmission line or a volume capacitance. An empirical model was developed for the power jet and vortex bubble dynamic and the control and output impedance. Analytical models for the feedback elements (either transmission lines or volume capacitance) were presented. The describing function was used to model the non linear components of the oscillator and the frequency predicted by non linear frequency domain stability techniques.

Yang, Chen, Tsai, Zhih Lin and Sheen (2007) designed a novel fluidic oscillator incorporating step-shaped attachment walls and acute-angle splitters and verified experimentally to stabilize the oscillation of circulation flow, to modify the flow patterns and to improve the performance. Focusing on various oscillators of plane-wall and step-wall designs. The results reveal that the novel design promotes conditions to initiate the oscillator and makes the recirculation vortices oscillate more effectively and stably. Comparison of the wave form of the spectral analysis and the ratio of signal to noise over the entire experimental range further corroborates the superior features of the novel design.

Mataoui and Schiestel (2008) developed an experimental on Self-sustained oscillatory phenomena in confined flow and proved that the oscillatory phenomena may occur when a turbulent plane jet is discharging into a rectangular cavity. The fundamental frequency of the oscillatory flow was found to be practically independent of the cavity length. Moreover, the oscillations are attenuated as the cavity width increases, until they disappear for a critical value of the cavity width. They are given for several aspect ratios of the cavity, keeping constant values for the cavity width and the jet thickness.

Khelfaui, (2009) proposed an asymmetric micro-oscillator design based on a mono stable fluidic amplifier. Experimental data with various feedback loop configurations point out that the main effect responsible for the oscillation is a capacitive and not a propagation effect. Actually, sound propagation in the feedback loop only generates a secondary oscillation which is not strong enough to provoke the jet switching; Data from a hybrid simulation using a commercial CFD code and a simple analytical model are in good agreement with the experimental data. A more compact plane design with reduced feedback loop volumes is also studied through a fully CFD simulation that confirms the previous conclusions.

THE OPERATION OF THE FLUIDIC OSCILLATOR

Oscillators are basically circuits with time delay feedback connection between their output and their input .The signal fed back causes the output pressure to be unstable, that it is oscillates between the two logic levels"o" and "1" a block diagram of the simple form of oscillator is shown in **fig. 2**.For the moment that input moment (*I*) will assumed zero, the circuit comprises a single "NOR" element with a feedback loop between the output and the input, the loop containing a restrictor and a fluidic capacitance or volume.

Oscillator's produce a square wave output known as (multivibrators), since the harmonic of

the output wave shows that it contains multiple vibrations (harmonics) of the fundamental frequencies (Charles A. Belsterling, 1971).

The frequency of oscillations of the circuit depends on both the supply pressure and the downstream loading, as well as on the resistance and capacitance of the feedback circuit .This is because the supply pressure and loading both affect the output pressure, which in turns alters the rate at which the pressure rises at the input port (K. Foster & G.A Parker, 1970).

THE OSCILLATOR FREQUENCY CALCULATION

There are two strategies to calculate the oscillator frequency theoretically; they are the lumped and distributed parameter system methods:

A. Lumped Element Method

Devices become simple if the wavelength in the fluid is much longer than the dimensions of the device .All acoustic variables are constant over the dimensions of the devices so that spatial coordinates can be ignored in the equation of motion .Acoustic devices in this long wavelength limit are defined as lumped acoustic elements . Thus, the dynamics of the lumped element systems are independent of their spatial configuration .

A signal appearing at the output of a lumped element component is assumed transmitted without delay or distortion to the next component in the system, so the distances between the components are not considered .Helmholtz resonators or segments of pipes having all dimensions sufficiently small compared to the relevant wavelengths can be considered as lumped acoustic elements, whose behavior resembles those of a simple oscillator .The lumped elements find application as convenient models for more complicated systems at low frequencies, allowing straightforward design of the noise transmission characteristics through pipes, ducts, mufflers, and so forth, without materially affecting any required steady flow of fluid through the system .

For systems in which the characteristic dimension of the device is relevantly long compared to the wavelength ($l \geq \lambda$), the spatial configuration is important .They are called distributed systems .The dynamics of the distributed system unlike the lumped element system are mathematically represented by partial differential equations .Thus, in distributed systems, there may be as many as three space variables and a time variable .There are many systems containing wave-guides (K. Foster & G.A Parker, 1970)**.** The lumped parameter system of the oscillator consists of three elements; the fluid nor gate, the fluidic capacitance and long orifice (fluid resistance) as shown in **fig. 2**

The transfer function of the system is the ratio of Laplace transforms of the output and input quantities, initial conditions being zero.The block diagram of the Bistable element oscillator shown in **fig. 3**.

This fluid capacitance (C1 and C2) associated with the properties of fixed volume of fluid. During transient flow changes within the volume the conditions of the fluid usually described by the perfect Gas Law for a gas, change relative to ambient conditions .And as used in the linearized fluid components representations for transient conditions, analogies may be drawn with equivalent electrical quantities .Thus in this case the fluid capacitance, it`s electrical equivalent is a capacitance to earth, i.e .has a value relative to ambient conditions (A.K. Jairatha, 1997).

To find the transfer function of the feedback channel, the first step is finding the feedback block diagram .The mass rate of flow is equal in the capacitance and in the restrictor

$$W_R = \frac{P1 - P2}{R} \quad (1)$$

And,

$$W_C = P1 * SC \quad (2)$$

Then;

$$P2 = P1 * (1 - R * SC) \quad (3)$$

Now, to find the transfer function of the oscillator the block diagram of the oscillator, see **fig. 3**.

$$G(S)_{feedback} = \frac{P2}{P1} = 1 - R * SC \quad (4)$$

The transfer function of the oscillator will be as the diagram;

$$G(S)_{oscillator} = \frac{P_{out}}{P_{in}} = \frac{1}{R * SC} \quad (5)$$

The transfer function shows that such circuit characterized by a first order lag with a time constant RC, see **fig. 4**. The frequency response gives a bandwidth from a steady state conditions up to the break frequency w_b where:

$$\omega_b = \frac{1}{\tau_2} = \frac{1}{RC} \quad (6)$$

$$\tau_2 = RC \quad (7)$$

So that, this circuit consider as a resistance capacitance dependent (J.R Frey & J. N. Wilson, 1970).

It's important to calculate the switching time (τ_1) of the flow from one leg to another, there are many investigations have been performed on the dynamic experimentally and theoretically. Most of them present comprehensive results on measurements of switching time of the supply jet from one side to another, [for $(Q_c/Q_s) = 0.33$ and $(\alpha = 15), \tau_1 = 19.5ms$] (Yamasaki H. et al, 1988).

Finally the oscillator frequency according to lumped modeling calculated according to equation:

$$f = \frac{1}{2(\tau_1 + \tau_2)} = \frac{1}{2(19.5 + RC)} \quad (8)$$

And the values of R and C calculated as

$$R_{31} = \frac{\Delta P_{31}}{W_{31}} = \frac{\sqrt{\Delta P_{31}}}{C_D * A_{oriffice} * \sqrt{2\rho_1 * g}} \quad (9)$$

And

$$C = \frac{\dot{m}}{\Delta P_{23}} \quad (10)$$

Where (p_1 ,p_2 ,p_3) are read directly by using the mercury liquid column.

B. Distributed Parameter Method.

The equations governing a two dimensional steady flows in the fluidic oscillator are;

The continuity equation for incompressible flow can be thought of as a constraint on the velocity field, specifically that the Velocity field is divergence-free.

$$\frac{\partial}{\partial x}(\rho u) + \frac{\partial}{\partial y}(\rho v) = 0 \quad (11)$$

The momentum equations in both X- and Y-direction with eddy viscosity (Potter, 2008) will be; X-momentum equation:

$$\frac{\partial}{\partial x}(\rho vu) + \frac{\partial}{\partial y}(\rho vv) = \frac{\partial}{\partial x}\left(\mu_{eff}\frac{\partial u}{\partial x}\right) + \frac{\partial}{\partial y}\left(\mu_{eff}\frac{\partial u}{\partial y}\right)$$
$$-\frac{\partial p}{\partial x} + \frac{\partial}{\partial x}\left(2\mu_{eff}\frac{\partial u}{\partial x}\right) + \frac{\partial}{\partial y}\left[\mu_{eff}\left(\frac{\partial u}{\partial y} + \frac{\partial v}{\partial x}\right)\right] \quad ...(12)$$

Y-momentum equation:

$$\frac{\partial}{\partial x}(\rho uv) + \frac{\partial}{\partial y}(\rho vv) = \frac{\partial}{\partial x}\left(\mu_{eff}\frac{\partial v}{\partial x}\right) + \frac{\partial}{\partial y}\left(\mu_{eff}\frac{\partial v}{\partial y}\right)$$
$$-\frac{\partial p}{\partial y} + \frac{\partial}{\partial x}\left(2\mu_{eff}\frac{\partial v}{\partial y}\right) + \frac{\partial}{\partial y}\left[\mu_{eff}\left(\frac{\partial u}{\partial y} + \frac{\partial v}{\partial x}\right)\right] \quad .....(13)$$

A computational procedure for the governing differential equation is explained by using the partial numerical differentiation.

The momentum equations in two dimensional were discussed because this work has a constant thickness fluidic oscillator, and the third dimension will not be very important.

P, u and v must be defined at the cell center on a square 2D grid with equal mesh spacing, h, in both dimensions, as shown in **fig. 5**.

In more general terms as representing a potential field likes a velocity components or the pressure corresponding at a specific point.

Now, the numerical formula will be sub in the momentum.

The boundary conditions will vary as the type of flow (Shlichting, 1979).

1- In the input channel the boundary condition is as same as that for the rectangular tube. The boundary conditions at the wall of the oscillator will be (U=0 for horizontal surface and V= 0 for

vertical) and ($\frac{\partial^2 u}{\partial y^2} = 0$ for horizontal surface and $\frac{\partial^2 v}{\partial x^2} = 0$ for vertical), and the boundary conditions at centerline of the tube is ($\frac{\partial u}{\partial y} = 0$ for horizontal surface and $\frac{\partial v}{\partial x} = 0$ for vertical).

2- The flow is developed flow since the pipe length is more than the entrance length where,

$\frac{L_E}{D} = 120$ () and D= 0.01225

$\therefore L_E = 1.47\ m$ and the pipe length is 3.7 m.

For fully developed flow; $\frac{\partial v}{\partial y} = 0$.

The distributed parameters discussed in this section executed using the Visual Basic 6.0. The model has been designed using the program AutoCAD MECHANICAL 2010 and then the Visual Basic 6.0 was used to calculate the instantaneous velocity at each node then it calculate the time of the period then the frequency calculated.

$$\tau_2 = \sum \frac{h}{V_j} \qquad \ldots (14)$$

Then the oscillator frequency can be calculated:

$$f = \frac{1}{2(\tau_1 + \tau_2)} \qquad \ldots (15)$$

THE TEST PROCEDURE

This test evaluates the effect of air temperature on the oscillator frequency as shown in **fig. 6**

The oscillator and the heater and the compressor were connected as an open loop. The air is compressed by the compressor in the storage tank to a certain stagnation pressure to obtain steady-state conditions and then the air is allowed to flow through butterfly valve, the butterfly valve allow us to maintain the flow rate Quantity **fig. 7**.

The air is allowed to flow through the gate valve, and then the air flow rate measured using the air flow meter then the static pressure and temperature measured by the gauge and thermocouple before entering the heater, then the heater rises the air temperature. The thermocouple and bourdon gauge measured the temperature and static pressure of the air before entering the fluidic oscillator then the oscilloscope evaluates the oscillator frequency **fig. 8.**

These experiment takes 10 values of temperature test (15 , 20 , 25 , 30 , 35 , 40 , 45 , 50 , 55 , 60) C^o for cases at two flow rates (80 - 100) l/m and at 1 bar stagnation pressure .

These tests take 2 attempts for each record to evaluate the average value.

RESULTS AND DISCUSSION

Figs. 9 and **10** show the relation between the temperature and the oscillator frequency for (80 and 100 l/min air flow rate) respectively. The oscillator frequency represented in these figures is calculated according the lumped parameters method for different flowrate values.

Figs. 11 and **12** show the relation between the temperature and the oscillator frequency where the frequency was calculated according to the distributed parameters for (80 and 100 l/min air flow rate).

The two methods of the calculation results show that the frequency increasing as the temperature increasing. This increasing of frequency is due to decreasing of the fluid capacitance with the temperature increasing according to the equations (19) and (20) for the constant capacitor volume and constant air flowrate, and since the "main effect responsible of the oscillation is a capacitive effect" (Khelfaoui, 2009) then the oscillator frequency will increased according to equation (21).

In the distributed parameter system results, the temperature rise decreases the air viscosity (μ) which in turns will reduces the channels

resistance and increases the air velocity at each point of the channel and the frequency will increased according to equations (16) and (17).

$$C = \frac{V}{\Re * T} \qquad (16)$$

$$w_b = \frac{1}{R * C} \qquad (17)$$

$$\tau_2 = R * C \qquad (18)$$

Figs. 13 and **14** show the effect of increasing the flow temperature on the oscillator frequency for (80 and 100 L/min respectively). The experimental results give the same conclusion about the positive relationship between the oscillator frequency and the temperature.

Figs. 15, 16 show the experimental and theoretical results (lumped and distributed). In these figures it can concluded that, the results that calculated according to lumped parameters are more realistic than that calculated according the distributed parameters.

Experimentally the hysteresis, nonlinearity and threshold were calculated. As shown in the **table. 1** and **figs. 17** and **18** explain the hysteresis analysis, the hysteresis test is done by measuring and recording the frequency while rising up the temperature from (15 to 60) ^oC step 5 ^oC . When the temperature becomes (60 ^oC) the temperature allowed to be reduced gradually and the frequency is recorded at the same points as the rise up. The results will be as shown in **table. 1** and the hysteresis calculated as:

$$hysterises = \frac{a-b}{a} * 100\% \qquad (19)$$

Where; (a) is the maximum value at the average value of the temperature range (37.5 ^oC) and (b) is the minimum value at the average value of the temperature range (37.5 ^oC) (Lapshin, 1995).

The non linearity analysis was described in **table (2)** for all temperatures and flow rate tests for the lumped and experimental results and also it describes the error analysis of the back pressure tests at (80 and 100 l/min).

CONCLUSIONS

The following conclusions have been extracted:

1- The oscillator frequency depends on many factors such as;

A- The physical dimensions of the oscillator such as the oscillator leg volume, the control orifice and the angle of deflexion.

B- The flow properties such as the temperature, viscosity and Reynolds number.

2- To measure the oscillator frequency, high response dynamic pressure transducer must be used. In the other hand, the static pressure transducer will not be suitable for such measurement.

3- The device has a low error margin and nonlinearity but has a relatively high hysteresis because of the high thermal capacity of the Neutral Detergent Fiber (NDF)

ACNOWLEDGMENT

we would like to thank very much the staff of electrical engineering department, college of engineering, university of Baghdad and special thanks to "**Dr. Fadhil Abbas mehdi Al- Qrimli** " and to "**Mr. Thamir Mosa Al-Korbasy**" for their cooperation and help.

REFERENCES

A. K. Jairath . *Solution and Problems of Control Systems* (2nd edition). New Delhi: Daria Gani,1997.

Halbach, C. R. Otsap, B. A. & Thomas, R. A. "A Pressure Insensitive Fluidic Temperature Sensor". A*SME oscillators and diaphragms devices*-session V, PP.298-312, May 1967.

Herman Shlichting. *Boundary Layer Theory* (7th edition).London: McGraw- Hill company, 1979.

J. R. Frey & J. N. Wilson. "A Study of the Parameters Affecting the Performance of Fluidic Feedback Oscillators". *Fourth Cranfield fluidic conference*, Coventry, March 1970, paper H2.

K. Foster & G.A Parker, *Fluidics Components and Circuits*, McGraw-Hill Company, (1970).

M. Epestine . Theoretical Investigations of the Switching Mechanism in Bistable Wall Attachment Fluid Amplifier. Trans *ASME*, vol. 93. Series D pp 55-62 (1971).

Merle C. Potter & David C. Wiggert. *Mechanics of fluids* (2nd edition). London: Prentice-Hall International, Inc, 1997.

P. A. Luchi. "Investigation of switching mechanism in bistable wall attachment fluid amplifier", Proc .*2nd Cranfield fluidic conference*, Cambridge , March 1967.

R. Khelfaoui, B. Dennai, B. Banyousef, A. Slimani, A. Maazouzi & A. Missoum. "Numerical Analysis of an Oscillating Micromixer". *Sensors & Transducers Journal*, Vol. 111, Issue 12, pp. 79-85, December 2009.

Steven C. Chapra. *Applied numerical methods with Matlab* (2nd edition). New York: McGraw-HILL Company, 2008.

Yamasaki, H., Takahashi, A. and Honda, S. A.," New Fluidic Oscillator for Flow Measurement", *2nd International Symposium on Fluid - Control, Measurement, Mechanics and Flow Visualization* (1988).

Yang, J., Chen, C., Tsai, K., Lin, W. and Sheen, H., "A Novel Fluidic Oscillator Incorporating Step-Shaped Attachment Walls". *Sensors and Actuators A: Physical*, vol. 135, pp. 476-483(2007).

NOTATION

Symbol	Description	Unit
$A_{1,2}$	The cross sectional area at points 1or2	m^2
C	Fluidic capacitance	m^2
C_D	Coefficient of discharge	
Q_c	Control jet volume flow rate	m^3/s
Q_s	Supply jet volume flowrate	m^3/s
$\Re$	The specific gas constant of dry air (286.9)	j/kg k
R_{12}	The fluidic resistance	s/m^2
T	The air temperature	C^o
V	The leg volume	m^3
W_{12}	The air flow rate from point 1 to point 2	Kg/s
W_c	Capacitance air flow rate	Kg/s
W_R	Resistance air flow rate	Kg/s
f	Oscillator frequency	Hz
h	Step distance of the mesh	mm
u	The x-component of the air velocity	m/s
v	The y-component of the air velocity	m/s
w_r	The control to supply port width ratio	
w_s	The supply port width	mm
w_b	Breaking frequency	Hz
w_C	The control port width	mm
α	Half angle between the legs	deg
ΔP_{12}	Pressure difference between point 1 & 2	mbar
λ	Circuit operation wave length	mm
μ_{eff}	Total dynamic viscosity	Pa.s
τ_1	Relay time	ms
τ_2	the oscillation time const	ms

Table (1) Sample thermal hysteresis analysis at (80 l/min)

Temp (^oC)	f up (Hz)	f down (Hz)	hysteresis
15	5.7471	5.8962	
20	5.8445	5.999	
25	5.9523	6.105	
30	6.031	6.205	
35	6.1312	6.325	
40	6.2383	6.410	
45	6.3653	6.514	
50	6.4808	6.644	
55	6.6313	6.7567	
60	6.8189	6.8189	
Average point (37.5 ^oC)	6.2634	6.3676	1.663

Table (2) Error analysis results for all tests

The test	St. dev	Non-lin	hyst
Temperature test at (1 bar, 80 l/min)	0.056	0.09	1.663
Temperature test at (1 bar, 100 l/min)	0.027	0.04	0.774

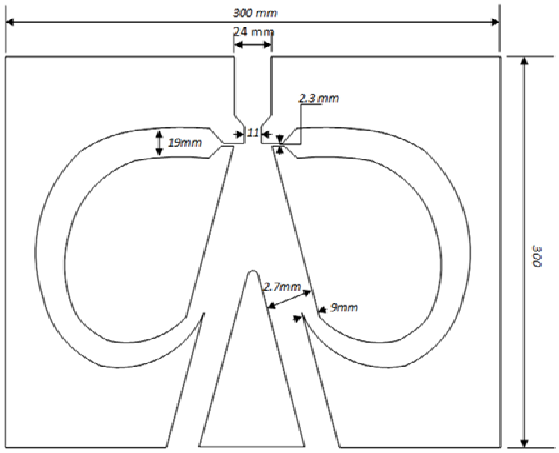

Fig (1) the fluidic oscillators diagram.

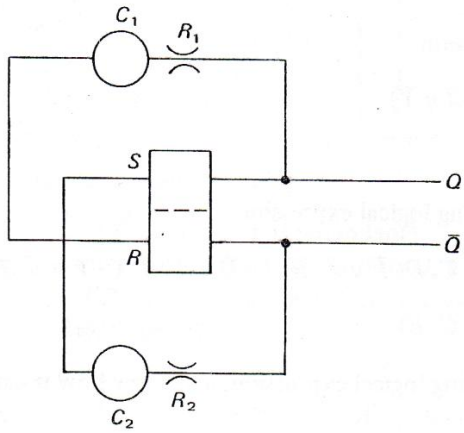

Fig (2) block diagram for Bistable feedback oscillator

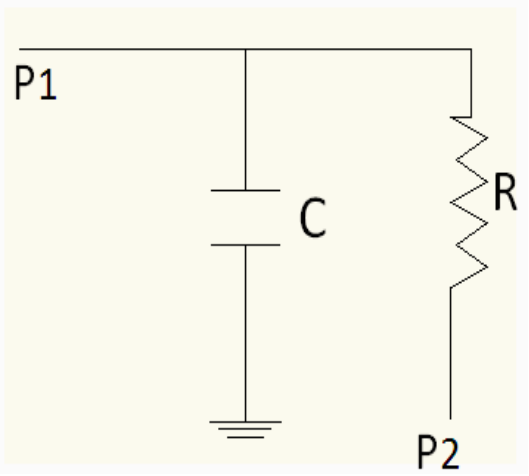

Fig (3) Block diagram of the feedback channel

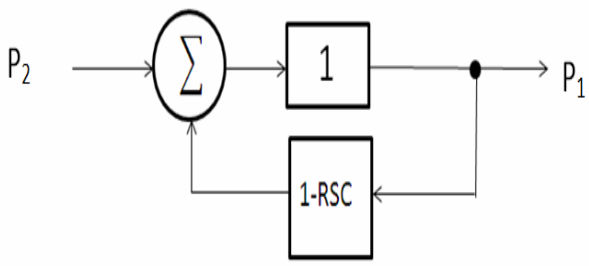

Fig (4): The transfers function of the fluidic oscillator.

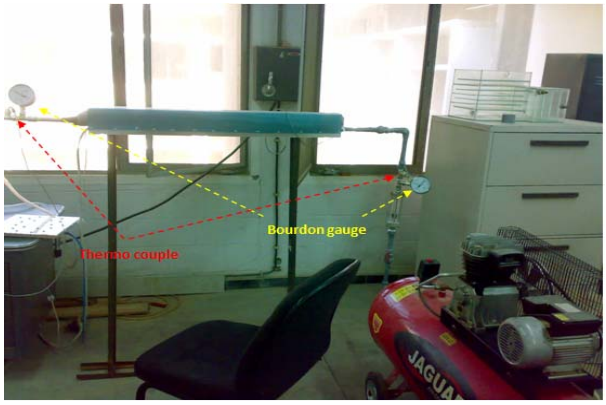

Fig (7): Air heater in the rig.

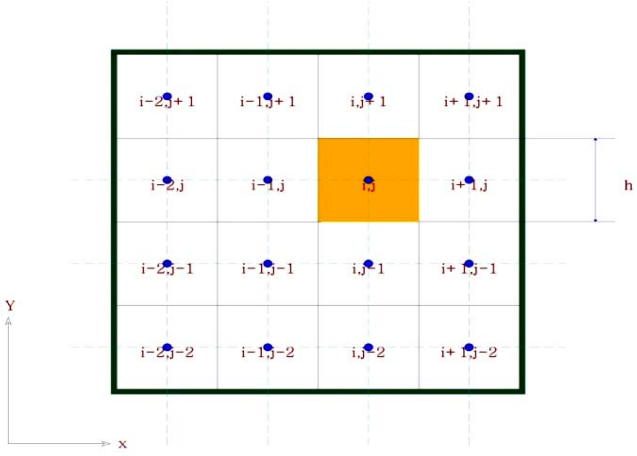

Fig (5) mesh design

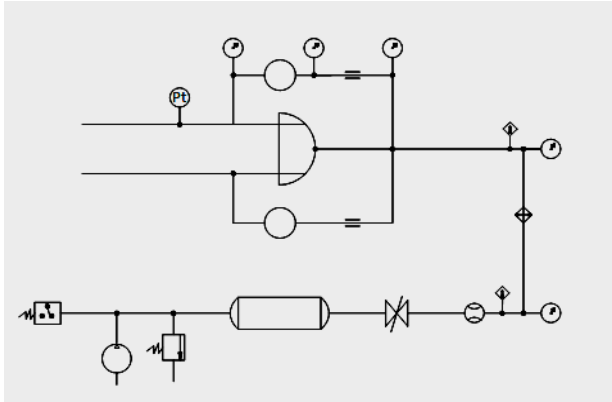

Fig (8): Temperature test rig diagram

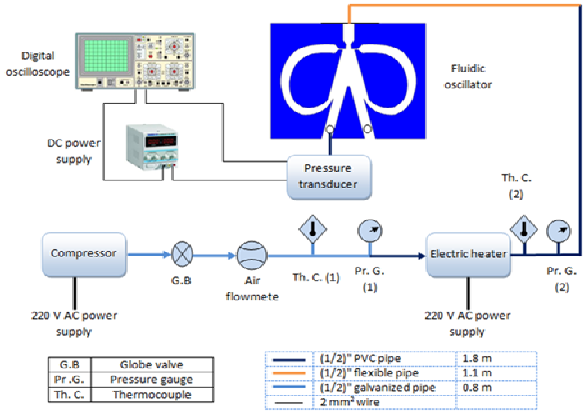

Fig (6): The Schematic Diagram of the Experimental Rig.

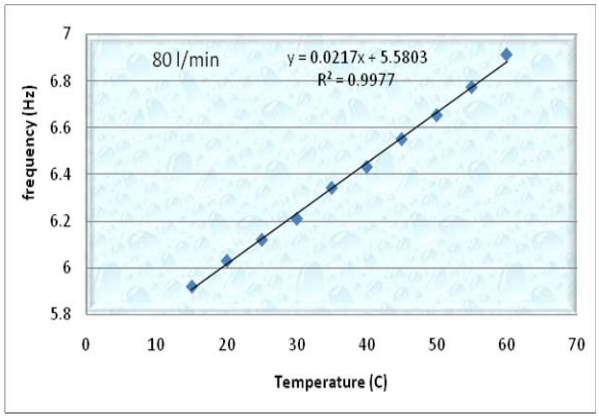

Fig (9): Theoretical Relation between Frequency and Temperature (Lumped Parameter System) (1 bar, 80 l/min)

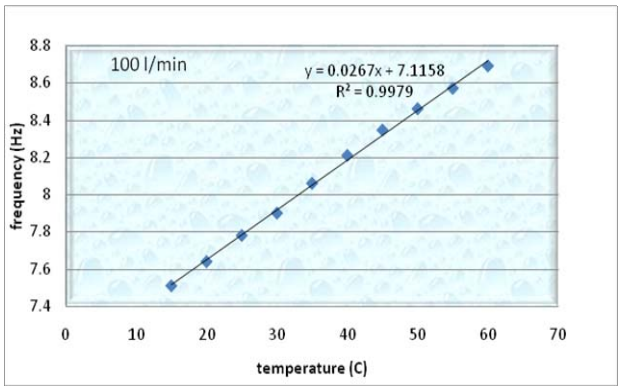

Fig (10): Theoretical Relation between Frequency and Temperature (Lumped Parameter System) (1 bar, 100 l/min)

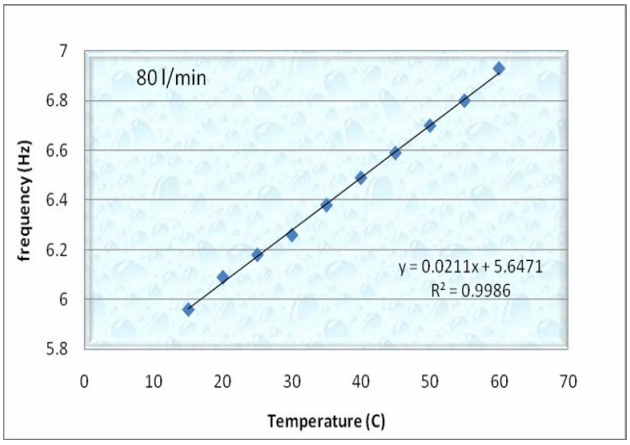

Fig (11): Theoretical Relation between Frequency and Temperature (Distributed Parameter System) (1 bar, 80 l/min)

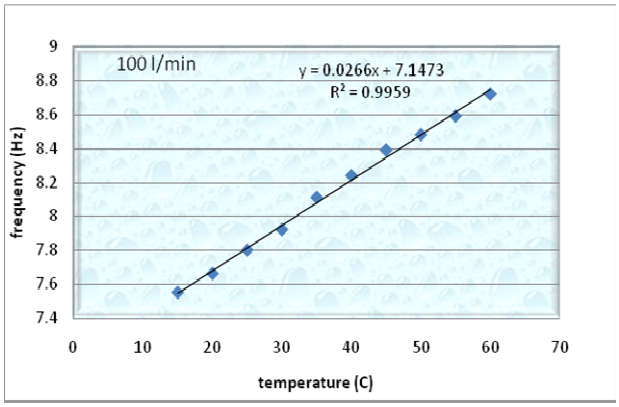

Fig (12): Theoretical Relation between Frequency and Temperature (Distributed Parameter System) (1 bar, 100 l/min)

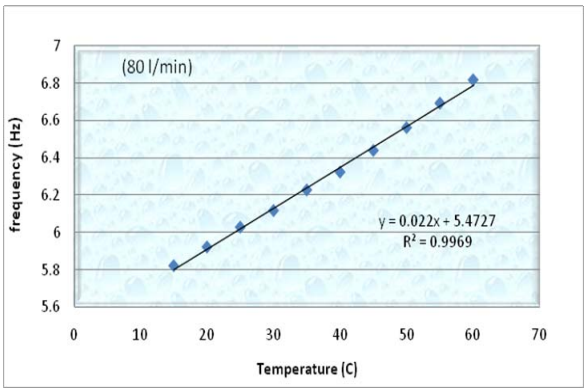

Fig (13): Experimental Relation between Frequency and Temperature (1 bar, 80 l/min).

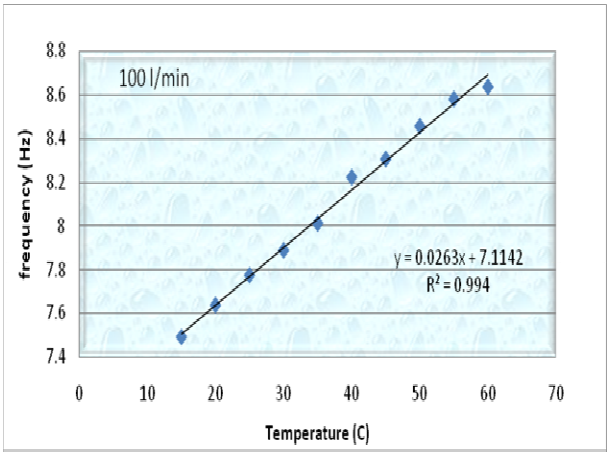

Fig (14): Experimental Relation between Frequency and Temperature (1 bar, 100 l/min).

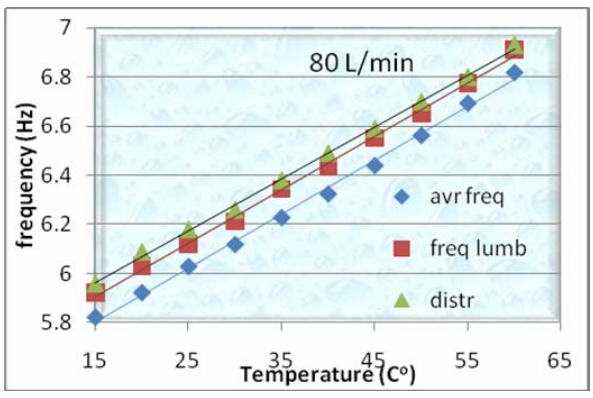

Fig (15): Comparison between the Theoretical and Experimental Results

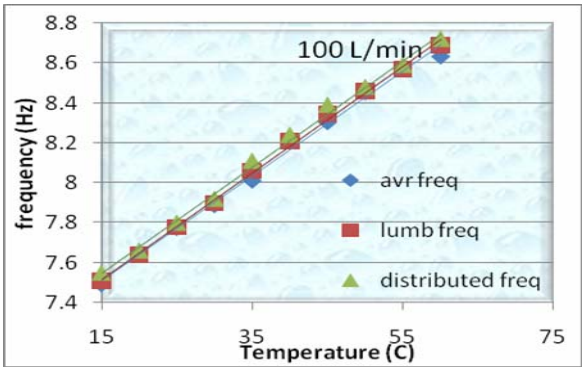

Fig (16): Comparison between the Theoretical and Experimental Results.

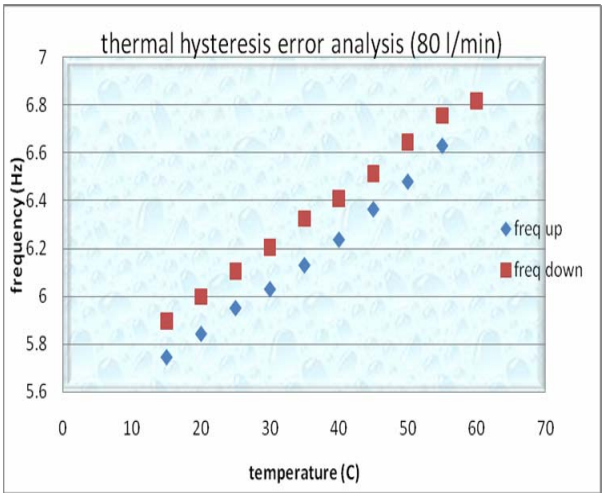

Fig (17): The Experimental Hysteresis Analysis (80 l/min).

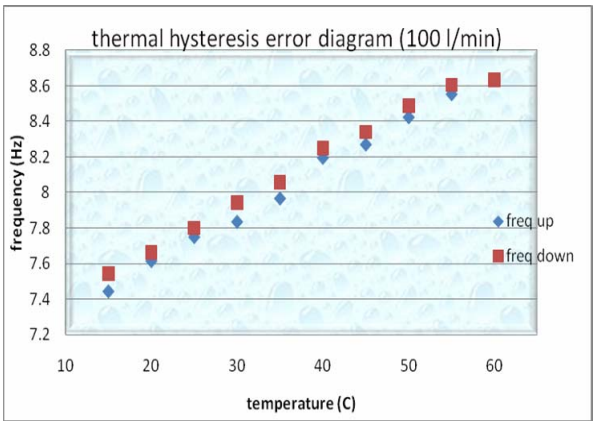

Fig (18): The Experimental Hysteresis Analysis (100 l/min).

النظـــم المنشئيـــــــة والوظيفـــة التعبيريـــــة في أبنية محطات المطارات

أ.د بهجت رشاد شاهين
جامعة بغداد / كلية الهندسة / قسم الهندسة المعمارية

أسامـــة صبـــاح محمـــد مهـاوش
جامعة بغداد / كلية الهندسة / قسم الهندسة المعمارية

المستخلص :

يختص البحث بدراسة أبنية المسافرين المعاصرة بشكل خاص والتي هي عبارة عن منشات وظيفية معقدة تلعب فيها المرونة والتقنية والنمطية دورا مهما فضلا عن القيم الإنسانية التي يجب ان توفرها هذه المنشات متمثلة بالراحة الفيزياوية والنفسية للمسافرين. وهي منشأت يلعب فيها الشكل المعماري دورا متميزا في عكس خصوصية العمارة وهويتها . وتبرز أهمية البحث في الدور الذي تلعبه ابنية المطارات في الآونة الأخيرة وضرورة دراسة مستوياتها التعبيرية والجمالية وطرق تطبيقها ودراسة مدى تكاملها مع المستوى الإنشائي ، حيث يلعب هذا التكامل دورا كبيرا في اعطاء تعبيرية رمزية وايقونية لها ، ليقود ما سبق الى طرح مشكلة البحث المتمثلة بقلة الدراسات حول الدور الذي تلعبه النظم المنشئية في تحقيق الوظيفة التعبيرية الرمزية لأبنية محطات المطارات. ووضعت الفرضية البحثية التي تنص على : النظم المنشئية أداة اللغة التعبيرية الرمزية لأبنية محطات المطارات بتكامليتها مع المنظومات الوظيفية والتشغيلية ونظم الحركة المعقدة لهذه المباني . وحدد هدف البحث الرئيسي بأستكشاف دور النظم المنشئية في ابراز الوظيفة التعبيرية لهذه الابنية كهوية مكانية وواجهة حضارية مميزة للبلد المعني تعبر عن خصوصيته المحلية بكونها اول نقطة يطأها المسافرون والسياح الوافدين للبلد .

الكلمات المرشدة : النظم المنشئية ، الوظيفة التعبيرية ، اللغة التعبيرية ، ابنية محطات المطارات ، الرمز ، الشكل المعماري ، الهوية المكانية.

The Structural systems and expressional function for Airport Terminals' buildings

ABSTRACT

The research deals with the structures of the contemporary travelers' buildings in particular, and which is a functional complex installations where flexibility, technical and stereotypes play an important role as well as the human values These facilities must represent physiological and psychological comfort for travelers. TThose are facilities where architectural form plays a distinguished role in reversing the specialty and identity of the building. Hence the importance of the subject has been in forced, as a result for the need to study these facilities and to determine the impact and affects by the surrounding environment, to the extent of the urban, environmental, urban, social, and psychological levels. The importance of the research highlights the i role, played by airports terminal buildings in recent times, and the necessity to study its expressional and, aesthetic levels and methods of application, examining its integration with construction level , where these integrations play a major role in giving expressive symbolism and iconography to these construction. The local libraries , in particular ,lack architecture studies which is related to the subject, mentioned above to settle the problem of research, represented by the shortage of studies about the role, played by structural systems in achieving the symbolic expressive function for airport buildings and terminals. Research hypothesis has been stated as following: structural systems are the tools of expressive and symbolic language for buildings of the airport stations, in integration with functional and operational system and the complex motion of these buildings. The main research objective has been determined to clarify the role of the construction system in highlighting the expressive function of these buildings as an identity for the place and

special interface characteristic of a civilized country in question which reflects its local privacy by being the first point of intercourse with travelers and tourists' arrivals and departures of the country.

1. المقدمـــــــة

تعد المطارات أحدث وسـيلة مواصـلات تعكـس تقـدم حضارة الانسان وتعكس الهوية المميزة لكـل بلـد ويعـد مبنى المسافرين المكون الاساسـي فـي مجمـع المطـار الذي بـدوره يحـوي العديـد مـن المنـشات الديناميكيـة المتطورة بشكل مستمر تبعا لازديـاد حركـة المـسافرين بالجو واسـتمرار دخـول طـائرات جديـدة ومنظومـات خدمة وتشغيلية حديثة تتجـه باسـتمرار لمحاولـة تهـسيل وتسريع السفر وإجراءاته .

1.1 المفهوم العام لمبنى المـسافرين: يعـد مبنـى المـسافرين احـد أهـم المنـشات الرئيـسية المكونـة للمطارات، وقـد صـمم عـدد منهـا كنـصب معماريـة تعكـس تقـدم ورصـانة الطيـران الـوطني والإقليمـي، فضلا عن ذلك فهي تعكس تقدم الدول مـن خـلال كونهـا أول وآخر نقطة يطأهـا القـادم والمغـادر لدولـة مـا . وتقـوم أبنيـة المـسافرين بـوظيفتين أساسـيتين تتمثـل الاولى بتغيير في وسيلة المواصـلات مـن ارضـي إلـى جوي اما الثانية فتتمثـل فـي تـأمين فـضاءات لإنجـاز المعاملات الخاصة بالسفر.وان تعقـد اغلـب المنظومـات داخل مباني المسافرين والمرونـة العاليـة التـي تتطلبهـا اغلب الفعاليات والحاجة الى التوسع ضـمن مـدة قـصيرة نسبيا كل هذه الاعتبارات تجعل مـن اسـتعمال منظومـة انـشائية ذات بحـور واسـعة احـد اهـم المتطلبـات التخطيطية والتـصميمية، وكـان عـدد مـن المطـارات الدولية قـد اتبـع هـذا الاتجـاه وكانـت اغلـب المـواد المستخدمة فـي الانـشاء الحديـد والكونكريـت باسـلوب السطوح الكونكريتية القشرية، وفـي نفـس الوقـت كـان هنالك اتجاه معماري اخر يتعامل مـع منظومـات انـشائية معقدة ومواد بنائيـة حديثـة ولكـن بـشكل يحتـرم فيـه الخصوصية المحليـة فـي خلـق التكوينـات المعماريـة ويحاول محاكاة اسـلوب العمـارة التقليديـة الـسائدة فـي المنطقة ابراز الدور التعبيـري والجمـالي لهـذه الابنيـة كهوية مكانية وواجهة حضارية مميزة للبلد المعني

تعبرعن خصوصيته المحليـة بكونهـا اول نقطـة يطأهـا المسافرون والسياح الوافدين والمغـادرين مـن البلـد. وان الوظائف التي تتم في أبنية المسافرين مـن التعقيـد بحيـث انها تجعل منها ابنية وظيفية معقـدة فـضلا عـن كونهـا ابنية يلعب فيها الشكل المعمـاري دورا مهمـا، فعليهـا ان تستوعب وتسهل انواع مختلفـة مـن الحركـة ، كحركـة المغـادرين والقـادمين والعـابرين والمـسافرين علـى الطيـران الـدولي والمحلـي، وكـذلك حركـة الحقائـب والـزوار المـودعين والمـستقبلين وأخيـرا حركـة المستخدمين والخدمة.وتلعب التقنيـة والمرونـة والنمطيـة دورا مهما في جعل مباني المـسافرين منـشأت عـصرية تستطيع ان تستوعب الكم الهائل مـن المـسافرين بـالجو وتستجيب للزيادة في أعدادهم بشكل يجعـل منهـا منـشات حيوية ذات قـدرة كبيـرة علـى الانـسجام مـع حيويـة وديناميكية النقل بالجو، ووجـد فـي اغلـب الدراسـات السابقة التي تناولت موضـوع المطـارات عـدم وضـوح دور الـنظم المنـشئية علـى مختلـف مـديات الفعاليـة التصميمية لمبـاني محطـات المطـارات خاصـة علـى مستوى الجانب التطبيقي والتعبيري فـي صـياغة انمـاط واشكال هذه المباني ، والتي أفضت الـى قـصور واضـح في أسـتيعاب العلاقـة التأثيريـة بـين الـنظم المنـشئية بأعتبارهـا الجانـب المـؤثر وبـين عمـارة محطـات المطارات كنتاج أبداعي وما ترتـب عليـه مـن ضـعف فـي القاعـدة المعرفيـة ، فـضلاً عـن غيـاب النظـرة المتعمقة لأهمية ودور ذلك التأثير فـي أغلـب الدراسـات العالمية والمحلية السابق ذكرها والتركيـز بالمقابـل علـى على الجانب التخطيطـي والتـشغيلي لمبنـى المـسافرين بغض النظر عن الجوانـب المنـشئية والتعبيريـة ضـمن الفعالية التصميمية بشكل عـام ، وعليـه تظهـر مـشكلة البحث الأتية: (**قلة الدراسات حول الـدور الـذي تلعبـه النظم المنشئية في تحقيق الوظيفـة التعبيريـة الرمزيـة لأبنية محطات المطارات**). حيث نلاحـظ قلـة الدراسـات حول مدى اهميـة ابـراز الجانـب التعبيـري والرمـزي

لأبنية محطات المطارات كهوية مكانية وواجهة حضارية مميزة للبلد المعني عن طريق استخدام أنظمة ومعالجات منشئية لها القابلية على استيعاب الوظائف المتعددة في أبنية محطات المطارات . وحدد هدف البحث الرئيسي (**بأستكشاف دور النظام المنشئية في ابراز الوظيفة التعبيرية لهذه الابنية كهوية مكانية وواجهة حضارية مميزة للبلد المعني تعبر عن خصوصيته المحلية بكونها اول نقطة يطأها المسافرون والسياح الوافدين للبلد**) . ويتطلب تحقيق ذلك منهجاً مؤلفاً من المراحل التالية :

- بناء إطار نظري لتوضيح مفهوم الوظيفة التعبيرية الرمزية لمباني محطات المطارات ، وتوضيح إمكانيات المنشأ في هذه الأبنية والتي تجاوزت ضروراته المادية ، متمثلة بإمكانياته التعبيرية والجمالية وإستخلاص المفردات الرئيسية والثانوية التي تعمل لتحقيق ذلك.
- تطبيق هذه المفردات على مجموعة من الأبنية المنتخبة التي شُخصت فيها تميزاً للنظم المنشئية .
- تسجيل النتائج وإستخلاص الإستنتاجات .

2. الأطـــــــــــار النظـــــــــري:

1.2 الجزء الأول : مفهوم النظم المنشئية لأبنية محطات المطارات:

الإنشاء وبصيغته التصميمية يعتمد شبكة إنشائية تقوم بتنسيق وأبعاد العناصر المنشئية للمبنى. حيث إن انتظام هذه الشبكة يسمح بتسهيل عملية البناء والسيطرة. هذه الشبكة يتم الاعتماد عليها وفق مفاهيم إنشائية. تتضمن هذه المفاهيم أنظمة إنشائية رئيسة وثانوية - تطورت بتطور الوظائف والمواد والتكنولوجية المتاحة و لكل نظام وفي أية مرحلة تاريخية، خصائص ومواصفات.. تعتمد جميعها على التقنية المتوفرة في تلك المرحلة وفي ذلك الموقع وعلى المواد البنائية وعلى وظيفة المبنى ودرجة تعقيدها، وكذلك على السبل والوسائل المتاحة لتنفيذ تلك الطريقة.(Foster,1975) .

لذلك نرى من البديهي، إجراء عمليات تحوليه على النظم المنشئية التقليدية وابتكار نظم أخرى تلبي المتطلبات المعمارية المعقدة لأبنية محطات المطارات - بالانجاز الدقيق لحجم وشكل وقياس الفضاءات المعمارية ومتطلبات العصر- بالكفاءة الأعلى والسرعة والدقة وأساليب متطورة- ومتطلبات تعقيد الوظيفة وذلك بابتكار طرق وأساليب تصنيعية منفردة- أي التصنيع من اجل متطلب تصميمي معين قد لا يتكرر فيما بعد في انجاز المشاريع الأخرى. والأمثلة كثيرة على حصول هذه التطورات في النظم المنشئية المبتكرة وهي تحولات في هذا المجال. وان لبعض هذه الأنظمة تفرعات حسب الطريقة التي تتكون بها إلا أنها وبشكل عام تعتمد على أشكال فعالة (form active)ومتجهات فعالة (vector active) وكتل فعالة (Bulk active) وسطوح فعالة (Surface active) وأخيرا الامتدادات العمومية مع ملاحظة حمايتها من تأثير الأحمال الجانبية. هذه الأنظمة الإنشائية، تختلف في أشكالها وعناصرها الإنشائية وفي آلياتها لنقل القوى المؤثرة، وكذلك في مقامتها وتحملها للأحمال وفي طبيعتها لتأدية الوظائف وفي كيفية التعامل مع المواد البنائية الملاءمة (Torroja,1962).

ان الغالبية العظمى من ابنية محطات المطارات تعتمد في انشائها على النظم المنشئية العملاقة وذلك لتعقد اغلب المنظومات التشغيلية والحركية داخل مباني المسافرين والمرونة العالية التي تتطلبها اغلب الفعاليات التي تتم في مبنى المسافرين والحاجة الى استيعاب اعداد كبيرة من المسافرين في وقت واحد والحاجة الى التوسع ضمن حقب زمنية قصيرة نسبيا

كل هذه الاعتبـارات وغيرهـا ، تجعـل مـن اسـتعمال منظومة منشئية عملاقـة ذات بحـور واسـعة احـد اهـم المتطلبـات التخطيطيـة والتـصميمية لابنيـة محطـات المطارات المعاصرة . يتوضح لنا بـأن الفكـر الإنـشائي لابنية محطات المطارات يتعلـق بعوامـل عديـدة، منهـا النظـام المنـشئي المـستخدم، المـواد البنائيـة، العامـل الاقتصادي حيث إن كـل هـذه العوامـل تعتمـد بـدورها على عوامل أخرى عنـد اسـتخدامها والاعتمـاد عليهـا. مثال على ذلك إن اختيار النظـام المنـشئي يعتمـد تـأثير قوى الجاذبيـة والمـؤثرة، وطبيعـة الفعاليـات الوظيفيـة والاقتصاد -الكلفة- . تتم العمليـة بإتبـاع الطـرق التـي تكفل التوصـل إلـى الهـدف المنـشود مـن وراء هـذه العملية وذلك بتقليل الجهـد والوقـت وبأسـاليب ابتكاريـه جديدة بأعلى كفاءة وبالاستغلال الأمثـل للمـوارد البنائيـة وبأسـلوب يعكـس مفـاهيم العـصر وروحـه، خدمـة للأهداف التعبيريـة المعماريـة. ذلـك لان العمـارة هـي ظاهرة إبداعية لا تقوم علـى مبـادئ مطلقـة، بـل هـي تتعامل مع معـايير إنتاجهـا علـى وفـق رؤى إبداعيـة، تتحكم بها لكي تقدم نماذج مختلفـة مـن طـرز العمـارة وأساليبها. (Torroja,1962).

1.1.2 تكاملیـــة الـــنظم المنـــشئية مـــع المنظومـات الوظيفيـة والتـشغيلية فـي أبنيـة محطات المطارات:

التكامل ما بـين الـنظم المنـشئية والوظيفيـة كمفهـوم تكنولـوجي يكمـن بـالتوازن والانـسجام بـين وظـائف المبنـى مـع عناصـر ومكونـات المنـشأ والأنظمـة الميكانيكية، ويتم ذلك من خـلال التعـاون بـين أطـراف العملية البنائية للوصـول بالنتيجـة إلـى إمكانيـة تحقيـق المعـايير التعبيريـة والجماليـة والمعـايير الوظيفيـة . فـالمبنى المتكامـل هـو ترجمـة للقـرارات المتجانـسة والمنـسقة للجهـات ذات العلاقـة بـالمبنى و يعـد هـذا الانسجام بين المنشأ والنتاج المعمـاري المفتـاح للنجـاح التعبيري للمبنى ،ونستنتج من ذلك بـأن للـنظم المنـشئية في مباني المطارات وظيفة تعبيرية جماليـة فـضلا عـن الوظيفـة العمليـة المتمثلـة بـضمان اسـتقرار المبنـى والتكامـل مـع منظوماتـه التـشغيلية ، فعنـدما تتحـول الفكرة الأنشائية الـى واقـع مـادي ملمـوس بالأنـشاء ، تنتج تعبيرية شكلية مميزة يمكـن الحـصول عليهـا مـن العلاقة التكاملية ما بـين الـنظم المنـشئية والمنظومـات التـشغيلية والخدميـة لمبـاني المـسافرين. لـذلك يـرى البحث بأن قضية مكاملة العمـارة بالمنـشأ مـن القـضايا المعقدة فمن وجهـة النظـر الإنـشائي يجـب أن تـستغل الحلول المعمارية للمنشأ بأقـصى حـد ممكـن، فمنـذ أن دخل المكون التقني كأحـد مكونـات العمـارة الأساسـية بات من الضروري أن يبـرز النظـام ألإنـشائي فـضلا عن إبراز سـلوكه والمـواد المكونـة وطريقـة الإنـشاء، ومن الناحية المثاليـة يجـب أن يوضـح المنـشأ بـشكل صريح بـصرياً وبطريقـة تـؤدي إلـى أغنـاء الـشكلَ المعماري . كما أن المنـشأ والناحيـة التعبيريـة للتـشكيل المعماري يرتبطـان أيـضا بالكفـاءة والخفـة والرشـاقة ومبادئ تقليل الـوزن والاسـتعمال الاقتـصادي للمـادة . فعندما يكون المنشأ ذا تناسب جيـد فانـه سـيبدو مميـزاً مـن الناحيـة الجماليـة، ومهمـا كانـت طبيعـة الحـل الأنشائي فانه يجب أن يكون كفوء مـن نـواحي الوظيفيـة المعمارية ويكـون متناغمـا مـع المنظومـات التـشغيلية والخدمية والخدميـة والحركيـة فـي مبـاني المـسافرين فضلا عن التقبل الجمالي، وبـالرغم مـن وجـود البـدائل الإنشائية ولكن وجود التكامـل الواضـح بـين التـصميم المعماري والمنـشائي اصـبح مـن ضـروريات عمـارة محطات المطـارات المعاصـرة ، فـان الـنظم المنـشئية تساهم في رسم الصورة لبنية النتـاج المعمـاري لمبـاني محطات المطارات. وفي كثير مـن الأحيـان فـأن بنيـة المنشأ تدمج وتصبح نفسها بنية النتـاج المعمـاري لمبنـى المسافرين ، ولكن نوعية التعامل ونمـط وخلفيـة المبنـى تحدد كيفية التعامل مع المنـشأ ومـن ثـم بنـاء الـشكل المعماري المتميز .وعليه يصبح الأنـشاء أهـم الجوانـب التي تدخل في بلورة النتاج النهائي للعمـارة لأنـه يعكـس مـدى تطـور التكنولوجيـة المتاحـة هـذا فـضلاعن أن الـضرورة التقنيـة تتطلـب نـوع معـين مـن الأنـشاء والتفاصيل والتي تضيف الكثيـر مـن الأبعـاد التعبيريـة

للمبنى والأنظمة الأنشائية وطريقة تنفيذها التي تكون لها مساهمة فعالة في رسم الصورة النهائية للنتاج المعماري ، فنستنتج بأن تكاملية القرارات المنشئية مع كامل المنظومات الهندسية والوظيفية في أبنية محطات المطارات تعد الاساس في نجاحها العمراني

2.2 الخصوصية التعبيرية لأبنية المطارات المعاصرة:

تعد المطارات من اهم الابنية المتخصصة في النصف الثاني من القرن العشرين وليس لها ماينظرها من حيث الوظيفة والمقياس والشكل على الرغم من بعض اوجه التشابه مع محطات القطارات ،الا ان المطار له حجمه الخاص وله مقياس ضخم يقزم معظم الهياكل الاخرى ،والمطارات العالمية الضخمة ،فالمطارات تبتدأ كونها مشاريع للمطارات ثم تتنهي كونها وحدات حضرية متكاملة بحد ذاتها تخدم العديد من وظائف المختلفة وتكون دائمة التوسع والتغيير في الوظائف وليس من السهولة ان يتلاءم مع نماذج المدن التقليدية لذا يعتبر البعض المطارات نوعا جديدا من انواع المدن كما هو الحال في مطار هيثرو الذي يعامل 63 مليون مسافر سنويا ، وكثالث مطار مشغول في العالم يعتبر مطار هيثرو كيان بحد ذاته في البيئة الحضرية مع ابنيته والطرق ومواقفه المشغولة التي تخدم وظائف متنوعة.

تعكس عمارة المطارات النكهة والصفة العالمية المميزة للنقل الجوي الحديث حيث هنالك شعور بالرمز التكنولوجي متوازنا مع الفخر الاقليمي لتصميم المطار. تفضل البلدان والمدن ان يكون هناك صفة عالمية مشتركة وتخصص محلي حسب معطيات المكان وخصوصا في ابنية المسافرين (Edwads,2005).

يعد المطار مزيجا للعديد من الانشطة والفعاليات التي تجري في وقت واحد مع ابنية ضخمة في مقياسها ولتصميم مثل هذا النوع من الابنية لابد من وجود تقدير للتفاعل التعبيري والثقافي للحياة المعاصرة من جهة والوظيفي من جهة اخرى لاستيعاب الامكانية الهائلة التي توفرها الحيوية المحضة لطبيعة النقل الجوي . حيث تعد المطارات كاتدرائية عصورنا الحالية والنهج المتبع في تصميم ابنية المطارات تغير وبشكل كبير خلال الجيل المنصرم.في منتصف القرن العشرين اعتبرت المطارات مرنة من السهل ادارتها وانشائها كما من الممكن بسهوله ازالتها وتغييرها ،اما اليوم فان التأكيد اكثر كون المبنى هو مبنى رمزي ودلالي (landmark) ويؤدي وظيفة تعبيرية تتلاءم مع التغييرات الداخلية السريعة على اسس وقواعد منتظمة وهذا مايعمل ضمنه المصممون بوضع نهج المرونة والادامة بالاعتبار منذ بدء التصميم.

ولغرض الوقوف على مفهوم تعبيرية أشكال محطات المطارات وبيان مستوياتها فسوف يتطرق البحث الى دراسة الاطار الفكري الخاص ضمن المسار العام لدراسة تعبيرية ابنية محطات المطارات الذي يشمل عوامل (طابع العصر،الرمزية، والقيم الجمالية، ومفاهيم التواصل).. ويبقى الشكل التعبيري حصيلة تفاعل واع لمجموعة هذه القيم المختلفة والمحددة من خلال صياغتها داخل رؤية المصمم . ودراسة المفاهيم المؤثرة على فعل التعبير وانواعه والمفردات المرتبطة والمتمثلة بالعوامل المادية (منشئية وشكلية ووظيفية) ، والفكرية (سيكولوجية إنسانية) ، وتشمل العوامل المادية تكنولوجية النظم المنشئية والمواد والإنشاء والتقنيات المتاحة، وكالأتي:

1.2.2 المستويات الفكرية للتعبير المعماري لابنية محطات المطارات :

يعد الفكر الحقيقة المثالية التي يهدف العقـل إلـى بلوغهـا لأنها كامنة. وفي الكامن يتحرك الخيـال ليـصل لا إلـى – الفكرة – ذاتها فحسب: بل إلـى التـصورات والأفكـار التي تثيرها حقيقـة هـذه الفكـرة. أي إن الحقيقـة التـي اختلفت الآراء حولها- وبغـض النظـر عـن جوهرهـا- يبحث عنهـا الإنـسان باسـتمرار. ويأخـذ الفكـر فـي العمارة مفـردات تعبيريـة أخـرى، حيـث أن جميعهـا تحمل دلالات مرجعية إلى الفكـر نفـسه. وان المـستوى الفكري خاضع لعدة عوامل و مؤثرات تـؤثر فيـه متمثلـة (بعوامـل خارجيـة كـالتغييرات الاجتماعيـة والـسياسية والاقتصادية ، ومـستوى التواصـل الثقـافي). و يمكـن تحديـد الجوانـب الأساسـية للبعـد الفكـري للتعبيـر المعماري لابنية محطات المطارات وكالأتي:

1. روح العصر والذي يؤشـر امكانيـة انتـاج عمـارة محطات مطارات تعتمد ثوابت حـسية بتعبيرهـا عـن عصرها مع احترامها لما سبق كون مـا يؤشـر لهـا دورا تاريخيـا هـو مـا سـيجعلها ترسـم لنفـسها مسارات خاصة في التاريخ ويؤكد سـمتها التاريخيـة التي تتعامل مع الوجود الثقافي لها فـي هـذه الحقبـة او تلك مع اهمية اعتبار وجود خلفيـة انـسانية عامـة في الفن او العلم يمكن العودة لها عند الحاجة.
2. فيما يخص استمرارية العمارة عبـر الـزمن لتوضـح دور الرموز في دعم المعاني التـي يحققهـا اسـتثمار الماضي في ابـداع الحاضـر ضـمن مـسار محـدد باتجاهين:- احدهما يخص رؤيـة الفـرد (المـصمم) ومقدار فهمـه للواقـع (الحاضـر) والاخـر يخـص رؤية الجماعـة ومقـدار فهمهـا للماضـي الحـاوي لجزء مـن حاجاتهـا ليـشكل ذلـك اشـكالية فكـرة الوجود بـين (فقـدان روح الماضـي وتـاخر عـن مواكبة تطلعات الحاضـر) وتطـور حركـة الـزمن باكمله.
3. ثم لتظهـر ضـرورة التوجـه لدراسـة اسـتمرارية العمارة عبـر الـزمن بمعيـة فكـرة روح العـصر كمـصدر اساسـي للاسـتلهام والاسـتثمار باعتمـاد تفاعل الفكرة القديمة مـع متطلبـات الواقـع لانتـاج الافكار الجديدة لمحطات المطارات.
4. ان للرموز دور فـي دعـم المعـاني التـي يحققهـا اسـتثمار الماضـي فـي ابـداع صـيغ الحاضـر والمستقبل ، كونهـا تعبـر عـن تجميـع واختـزال لأحداث متنوعة في مؤشـرات محـددة تمثـل هويـة لجماعة وباعادة احيائهـا واسـتعمالها تعـود الحيـاة الى الماضي القـديم ويرجـع مـع الحاضـر بـصيغ جديدة تضمن استمرار حركـة المعنـى فـي عمـارة ابنية محطـات المطـارات وبالتـالي ترسـم المـسار والتجدد المستمرين باعتماد احيـاء علاقـة الماضـي بالحاضر، فالشكل الفيزيـاوي الظـاهر يرمـز إلـى أبعاد غير فيزياوية، وهـذا المحتـوى الرمـزي هـو ذو أبعاد زمانية، وهو يمثل أيضا جـزء مـن شـبكة متداخلة مـن الرمـوز، لـذا فـإن معـاني الأشـكال المعمارية تظهر مـن خـلال دراسـتها ضـمن هـذه الشبكة
5. يطرح الـشكل الثقـافي العـام والجزئـي كمـؤثرات مهمة في فهم دلالات رموز أي نظام اشـاري معـين ،ويؤثر تغير الثقافة علـى تغييـر الـصور الرمزيـة حسب السياق العام (زمانيا ومكانيا) مما يـؤثر علـى صياغة تلك الصور الرمزية .وبالتـالي فـي تأسـيس النظام الاشاري والثقافي المعتمـد حـوار العقـل مـع منظومات الترميـز المختلفـة ،وتبـرز هنـا اهميـة مفهوم المحاكاة كاداة لتعميم مـا سـبق علـى الـنظم والأشكال الثقافية المتنوعة الاخرى.
6. ان الهويـة المكانيـة لمحطـات المطـارات تتـاثر بالمعاني والدلالات التي يمتلكها الـسياق الـذي يوجـد فيه ،وبالتالي الرمـوز التـي يحويهـا الـسياق مـن خلال ادراك المتلقي لمعـاني ذلـك الـسياق وهويتـه ،فاي جزء معين من الـسياق يـرتبط بعلاقـات مـع الاجزاء الاخرى تتحدد هويته وفقـا لتلـك العلاقـات ضمن السياق ذاته وبالتالي فهو كرمـز مـرتبط مـع بقية الرمـوز بعلاقـات معينـة تـؤثر علـى هويـة السياق باكمله.وهكـذا فالرمزيـة تـسهم فـي تلبيـة

متطلبات هوية الفـرد او المجموعـة فـي أي سـياق معين.

ما طرح أعلاه يشير الى الاطار الفكـري الخـاص ضـمن المسار العـام لدراسـة تعبيريـة العمـارة بـشكل عـام وتعبيرية ابنية محطـات المطـارات والـذي يمثـل فعـل عقلي ناتج عن مؤثر سـابق منـشأها فـي عـالم الفكـر ويرتبط قصديا بعالم المادة أو الحقيقـة المدركـة، فهـي تنتقل من ذاتية منفـردة، لتتحـول إلـى كـل موضـوعي ظاهر، تتجسد في كيان مادي، لتقوم بـدورها بعـد ذلـك باستثارة أفكـار جديـدة والمحافظـة علـى اسـتمرارية الهوية المعمارية باعادة انتـاج الـصور المخزونـة فـي الـذاكرة الجمعيـة . وسـيقوم البحـث بـالتطرق الـى المـستويات الفيزياويـة لتعبيريـة محطـات المطـارات والمتمثلة بالنظام المادي والشكلي.

2.2.2 المـستويات الفيزياويـة للتعبيـر المعماري لابنية محطات المطارات :

لكي تخرج الفكرة الى الواقع لابـد مـن الأسـتعانة بـنظم قادمة من الواقع، أي بمعنـى ان لهـا وجودهـا المعـرف وارتباطاتها النظامية المسبقة الوجـود، مـن ثـم توظيـف هذه الـنظم او عناصـرها او علاقاتهـا بطريقـة تماثـل علاقـات فـي الـصفات والقـيم الجوهريـة للمفـاهيم والإفكار، هذه النظم هـي بفئتـين متـرابطتين رئيـستين وان الفصل بينهما يأتي تحليلاً : (تعبيريـة نظـام المـادة ، تعبيرية نظام الشكل)

أولا) تعبيرية نظام المـادة لمحطـات المطـارات:

يـشمل كـل الظـواهر الفيزياويـة للمـواد الطبيعيـة والمصنعة وخواصها ومن ثم سـلوكياتها البنائيـة والهيئـة الناتجة لتلك السلوكيات، فـلا مبنـى يقـوم دون مـادة او مواد، لها نظمها الخاصة بطبيعة كل منهـا ويـشمل ذلـك نوع التقنيات الرابطة لها. هذا النظـام يبـدأ ينقـسم الـى قسمين:

الأول) تظهر فيه تلك المواد والتقنيـات المرتبطـة بمكـان معين وبيئة جغرافية محـددة والتـي بحكـم اسـتعمالاتها عبر التاريخ وخـصوصية كـل اسـتعمال خرجـت عـن نطاق كونها نظاماً مادياً مجـرداً فأصـبحت لهـا كيانـات معنوية واصبحت اشـكالها الناجحـة وسـلوكيات هيئاتهـا عناصر في مكونات طرز وتعبيرات ، وفـي هـذه الحالـة عندما يلجـأ المـصمم الـى أي منهـا، تبـدأ ارتباطاتهـا المعنوية تظهـر فـي التعبيـر الـذي يريـد المـصمم ان يحققه، سواء أكان ذلـك مقـصوداً ام لا مـن قبلـه وفـي كلتا الحالتين عليه ان يتجاهـل نـوع المعـاني المكتـسبة لتلك المواد او التقنيات عبر الزمن. ويشمل:

- التعبير عن طبيعة المادة البنائية (التكتونيك) .
- الخصائص التعبيرية للمواد المنشئية .

الثاني) يمثل كل ما هو غيـر تلـك المـواد، بمعنـى كـل المواد الجديدة والمـصنعة وتقنياتهـا أي الـنظم المنـشئية المتبعة في انشائها، وهـذه المـواد تـشترك فيهـا الحيـاة المعاصرة لمجتمعـات مختلفـة وهـي مـشتركة بمعنـى اشتراك الجميـع فـي "عـصر" حـالي تقنياتـه ووسـائل انتاجه، ولكن تجدر الإِشـارة هنـا الـى الإشـكالية التـي يفرضها البعض فـي طريقـة النظـر الـى هـذه المـواد والتقنيات، إذ ينظر لها على انها غريبـة وغربيـة، وأنهـا تمثل تحدياً للهوية والخـصوصية، وتعـد بهـذا المنظـور "معادية" وتمثـل خطـراً يجـب توخيـه، وهكـذا تظهـر الطروحات في " اثر التكنولوجيا علـى الهويـة" او علـى التصاميم العربية، حتى لتبـدو هـذه التـصاميم، موجـودة فقط عندما تكون وسائل تقليديـة. وعنـدما يـستعمل هـذه المواد فهو ايضاً لن يـتخلص مـن هـذه المعـاني التـي ارتبطت بها في ذهـن الكثيـرين ومقابـل تلـك الأفكـار تظهر طروحات " أقلمـة التكنولوجيـا او إكـسابها البعـد الخصوصي للحضارة ، وفيما يلي توضـيح لتـاثير هـذه النظم على النظام التعبيري:

- تعبيريـة الـنظم المنـشئية لأبنيـة محطـات المطارات.
- جماليات المنشأ .

ثانيـا) تعبيريـة النظـام الـشكلي لمحطـات المطـارات: ان الـشكل المعمـاري لأبنيـة محطـات المطارات يمكن انتاجه من عـدة نظـم انـشائية مختلفـة وبكفاءات انـشائية مختلفـة، وذلـك باسـتخدام وحـدات انـشائية خطيـة او وحـدات سـطح وباسـتعمال المـواد الانـشائية المختلفـة ايـضا، الا ان للتعبيـر المعمـاري المتحقق من طريقـة معالجـة هـذه الوحـدات واشـكالها التي تفرضها طبيعـة الاجهـادات التـي تقاومهـا المـادة الانشائية، فـضلا عـن ترتيـب هـذه الوحـدات، الـدور الكبير في هذه العمليـة، وان الـشعور (Feeling) يـدخل في انتاج العمارة بغض النظـر عـن الافكـار المنطقيـة المستعملة في حل مشاكلها، وهذا مايـشير الـى مـشاركة العلم والفن فـي حياتنـا المعاصـرة . وان العلاقـة بـين لشكال الهياكل الانـشائية الهندسـية والاشـكال العـضوية في تطور مـستمر منـذ الاهرامـات المـصرية القديمـة ولحد الان .

وبـذلك يمكـن اسـتخلاص علاقـات الـنظم المنـشئية بتعبيريـة أشـكال أبنيـة محطـات المطـارات كـالاتي: (اتحاد المنشأ مع الشكل ، المنـشأ وسـيلة لخلـق الـشكل المعمـاري ، المنـشأ وسـيلة لادراك مقيـاس العمـارة ، والمنشأ اداة اللغة التعبيرية للعمارة).

3.2.2 تحقيـق الوظيفـة التعبيريـة والرمزيـة لمحطات المطارات :

الجانب التعبيري أو الرمـزي لا يقتـصر علـى الأبنيـة النصبية كما شاءت سابقا، فكل نـشاط أنـساني يمكـن أن يوحي بالبيئة والأشـكال و الفـضاءات الملاءمـة لنوعيـة أو خصائص الوظيفة التشغيلية التي تمـارس داخـل ابنيـة المسافرين . وقد ينتقي المعمـاري – أن يكـون قـادرا – ويمزج بـين المـواد والأنظمـة التـشييدية التـي تخـدم المحتوى والرمز معا للنشاط الـذي يكـرس البنـاء مـن اجله. فقـد يعطـي البنـاء إحـساسا بـالغنى أو القـوة أو المعاصرة أو التـراث أو الطمـوح أو الاسـترخاء. وقـد ينتصب بمعزل عن الأرض، كشيء مـن صـنع الإنـسان يرمز إلى التقنية العلميـة الناجمـة مـن اسـتخدام العقـل البشري والصناعة القائمة في المجتمـع المعاصـر، أو قـد يبقى قريبا من الأرض، يـنهض مـن التربـة والـصخور والطبيعة ليربط الإنسان بأشكال الحيـاة الأخـرى جميعـا .

- الوظيفة الرمزية ، تعد حاجة مـن حاجـات الإنـسان، وفي نفس الوقـت تكـوّن مقومـات هويـة الفـرد.. فالرمزية إذن في هذا المفهـوم (كحاجـة) هـي تلـك المقومات التي يعيهـا الفـرد والتـي تؤلـف مركـب هويتـه، وتتمثـل هـذه المقومـات بمعـالم تتحملهـا مصنعات تشير إلى هوية الفـرد، كمـا يعلـن الفـرد عن هويته بواسطتها .
- أما الوظيفة التعبيرية ، هي ليـست وصـفا بـل هـي إن تعرض مظاهر الأبنيـة فـي الغالـب وظائفهـا.. وقد تقوم بذلك بشكل واضح كما لـو كانـت واجهـات الأبنية تصف مهماتها فـي كلمـات، حيـث إن هـذا التماسك الشكلي والوظيفي هو مـا يمكـن أن نـسميه تعبيرا .

لذلك نجد بإن كـل مـن الوظيفـة التعبيريـة والرمزيـة تتجسد بشكل مميز في مباني محطـات المطـارات والتـي طالما يتم إدراكها تصبح وسـيلة للتعبيـر وقـادرة علـى إيصال المعاني، وتنقل رسـالة معنويـة مهمـة وواضـحة تجسد الفكر الذي أنتجها. فالعمارة فـن منطقـي ، وحيـث ان اشكال مباني محطات المطارات تعتمـد علـى نظمهـا الانشائية ، فقد كان الوقوف عنـد هـذه المبـاني ونظمهـا لبحث تعبيراتهـا وعلـى مـستويات موادهـا الانـشائية ، تنظيمات وحداتها الانـشائية والتكنولوجيـة المتبعـة فـي تجميع هذه الوحدات ، ووصولاً الـى اشـكالها الانـشائية النهائية. فالهياكل المنـشئية لابنيـة محطـات المطـارات تمتاز بجمالية خاصة بها ، لكن في حالـة اسـتخدامها فـي المباني تكون مكونات الجماليات اصـعب واكثـر تعقيـداً .

وبما ان تـشكيلات الـنظم الانـشائية وتعبيراتهـا تعتمـد على العوامل الذاتية مثلما تعتمد علـى الموضـوعية منهـا ، وكـذلك علـى العوامـل الاقتـصادية ، وان الاقتـصاد العقلاني لايعني التغاضي عن الناحيـة الجماليـة ، وانمـا على المصمم اختيار الـنظم الانـشائية المناسـبة وظيفيـاً وجمالياً والمعبرة عن الفكـرة المعماريـة ضـمن اعلـى حدود للاقتـصاد ، فـالتعبير المعمـاري المتحقـق عـن طريق معالجـة الوحـدات الانـشائية واشـكالها وطرقـة تنظيمها وترتيبها يـدخل فـي انتـاج العمـارة المعبـرة ، وان الشعور (Feeling) يعتبر مساهم فعـال فـي انتاجهـا ايضاً ، وهذا ما يشير الـى مـشاركة العلـم والفـن فـي الحياة المعاصرة .

ويعتبر النجاح في التعبيـر عـن ذلـك بـالمواد وطـرق الانـشاء والتكوينـات الانـشائية ترجمـة للامكانيـات التعبيرية والجمالية للعصر والتي تـلازم طبيعتـه وتعتبـر مقياساً لتفوق المعماري.

فاسـتخدام طـرق انـشائية مختلفـة ومعالجـات شـكلية مختلفة لعناصر المبنى يؤدي الـى حلـول ذات تعبيـرات جمالية مختلفة حتى فـي حالـة اسـتخدام مـادة انـشائية واحدة ، والـذي يحقـق ذلـك هـو التقنيـة المـستخدمة لتحقيق المظهر الجمالي للمبنـى ، عـن طريـق اسـتبدال بعض الحلول التقنية الانشائية الـى حلـول تقنيـة علميـة بسبب الكلف العاليـة وبتعبيـرات جماليـة جديـدة وبـذا يكون العامـل التقنـي مـصدراً للايحـاء. ولأن الهـدف الاساسي للعمارة هو هدف اجتماعي ، فـأن تأكيـد الـدور الذي تلعبه تكوينات الهياكـل المنـشئية لابنيـة محطـات المطارات ، هو من صـميم عمليـة التـصميم المعمـاري الجمالي لها والذي يتجـه الـى زيـادة الثـروة الجماليـة للمجتمع الذي يوجد فيه . ويعتبـر النجـاح فـي التعبيـر عن ذلك بـالمواد المـستخدمة وطـرق الانـشاء الحديثـة والتكوينـات الانـشائية ترجمـة للامكانيـات الجماليـة للعصر وملازمة لطبيعته.

من خلال الطرح السابق للمفـاهيم والمـستويات الفكريـة والمادية والوظيفية للتعبيرية أبنيـة محطـات المطـارات، برز دور النظم المنـشئية المـساهمة فـي خلـق الـشكل المعماري الذي يحمل تعبيرية خاصة ناتجـة مـن خلفيـة فكرية تحمـل قيمـا ومعـاني مميـزة وذات خـصوصية محلية ومتلاءمة مع روح العصر ومـع العـادات والقـيم ومحققة استمرارية العمارة عبر الـزمن . ولكـي تخـرج الفكرة الى الواقع لابد من الأسـتعانة بـنظم قادمـة مـن الواقع، أي بمعنى ان لها وجودهـا المعـرف وارتباطاتهـا النظامية المسبقة الوجود، من ثم توظيـف هـذه الـنظم او عناصـرها او علاقاتهـا بطريقـة تماثـل علاقـات فـي الصفات والقيم الجوهرية للمفاهيم والإفكار.

وبذلك نستنتج انه بدون النظم التي لها كيانهـا فـي الواقـع لا يوجد تعبير عن افكار كلية ويبقـى القـرار والأختيـار للمصمم فـي شـقي عملـه، اولاً فيمـا يخـتص بفـصل التعبيـر وازديـاد المتغيـرات المتعلقـة بكيفيـة التعبيـر وتداخلها كمـا يتبـين فـي الطـرح الـسريع والمـوجز السابق، والأسلوب الشخصي للمـصمم فـي فهمهـا ومـن ثم بناء قراراته في توظيفها بالتعبير، وثانيـاً فـي اسـلوب فهم المصمم المعاصر لمقومات هويتـه الجوهريـة وقـوة انتمائه وثقته بها وهذا يختلف – بسبب تغييـر نمـط نظـم الأتـصالات والمعلومـات عالميـاً- ، فـالنمط الفكـري ونوع التواصل المتماسك في المجتمع التقليـدي قـد تغيـر الآن عما كـان عليـه، والمتغيـرات الآن تـشمل ثقافـة المـصمم، وثقافـة المتلقـي، ونمـط ممارسـة المهنـة، ومستوى الذوق العـام وغيرهـا، فـضلا عـن التحـديات الفكرية والسياسية الموجهة.

ونتيجة لقدرة الأنسان على ادراك العلاقـة الايحائيـة بـين الفكر و الشكل الفيزياوي تصبح للمنـشأ وظيفـة تعبيريـة جمالية فضلا عن الوظيفـة العمليـة (ضـمان اسـتقرار المبنى) التي يقوم بها . فعندما تتحـول الفكـرة الأنـشائية الى واقع مادي ملموس بالأنشاء فانها تـؤثر فينـا نتيجـة للتعبيرية التـي يمكـن الحـصول عليهـا مـن العلاقـة

الايحائية بين القوة و الشكل و التي نجـدها واضـحة فـي العديد من ابنية محطات المطـارات المعاصـرة ويقودنـا الطرح السابق لصياغة فرضية البحث التي مفادها.

(النظم المنشئية أداة اللغـة التعبيريـة الرمزيـة لأبنيـة محطات المطارات بتكامليتها مـع المنظومـات الوظيفيـة والتشغيلية ونظم الحركة المعقدة لهذه المباني) .

ويكون ذلك من خلال النجاح فـي التعبيـر عـن المـواد الإنشائية وطرق الإنشاء المتبعة فـي تـشييد هـذه المـواد والتكوينـات المنـشئية لهـا وبمـا يتـرجم الأمكانيـات الجمالية للعصر وهي بنفس الوقت تمثـل مقياسـا لتفـوق المعماري. وبما أن أشـكال وفـضاءات ابنيـة محطـات المطارات تعتمد على نظمها المنشئية فقـد كـان الوقـوف عند هذه النظم لبحث تعبيراتهـا علـى مـستويات موادهـا الإنشائية وتنظـيم هـذه المـواد فـي تـشكيلات منـشئية والتكنولوجيا المتبعة في تجميع هذه المـواد وصـولاً الـى أشكالها الإنشائية النهائية. في كـل حالـة مـن الحـالات سابقة الذكر فان الاداء الـوظيفي اغنـي بمعـاني ثقافيـة تعبر عن هوية البلـد المطـارات الحديثـة حيـث يعتمـد التصميم على استخدام المواد المحلية مـع احتـرام تقاليـد الـسكان الاصـليين للمنطقـة وخـصوصية المكـان والحضارة والمناخ بدأت توازن بـين المقـاييس العالميـة وايديولوجيات كتيبات منظمة الاياتا التـي تعمـد لتطـوير ونمو المطارات في جميع انحاء العالم .

3.2 أسـتخلاص مـستويات تحقيـق الوظيفـة التعبيرية الرمزية لأبنية محطات المطارات :

أولا) اسـتخلاص مؤشـرات الاطـار النظـري لمـستوى التكامل التصميمي لمبنى المسافرين:

1) **الـنمط التـصميمي المتبـع فـي تـصميم مبنـى المسافرين .**
2) **كفـاءة التنظـيم الفـضائي علـى مـستـوى المـخطط والمقطـع .**
3) **الكفـاءة التـصميمية للمنظومـة الوظيفيـة لمبنـى المسافرين.**

ثانيـا) اسـتخلاص مؤشـرات الاطـار النظـري لمستـوى تكاملية النظم المنـشئية مـع المنظومـات الوظيفية:

1) **نمط النظام المنشئي المستخدم .**
2) **طبيعة المادة الأنشائية المستخدمة .**
3) **خصوصية النظم المنشئية .**
4) **مـستوى تكامـل العلاقـة بـين المنـشأ والنتـاج المعماري لأبنية محطات المطارات .**

ثالثـا) اسـتخلاص مؤشـرات الاطـار النظـري للمستوى الشكلي والتعبيري:

1) **مستوى الاطـار الفكـري لتعبيريـة ابنيـة محطـات المطارات .**
2) **المستوى المادي للتعبير المعمـاري لأبنيـة محطـات المطارات .**

توزعت المفردات فـي المـستويات الثلاثـة اعـلاه وقـد تـم توضيحها بشكل منفصل في جدول رقم (1) .

3. تطبيق مؤشرات الاطار النظري :

تهدف هذه الفقـرة إلـى تحديـد الأسـس والمـستلزمات الأساسية للتطبيق للتحقق من تحقيـق الوظيفـة التعبيريـة الرمزية في ابنيـة محطـات المطـارات والناتجـة مـن النظم المنشئية المتبعة في انشائها وذلك من خـلال كـل مـن

1.3 أسـلوب القيـاس وأداتـه : إعتمـد البحـث القيـاس النـوعي Qualitative scale بنوعيـه ؛ الإسـمي Nominal ، والتسلـسلي Ordinal، وتـم تطبيقهـا علـى المـستويات الرئيـسية الثلاثـة للإطـار النظري مع مؤشراتها التي تتضمن قيمـاً ممكنـة تتـوزع بين نوعي القياس أعلاه . تـم ذلـك بمـرحلتين ؛ الأولـى بتأثير تطبيق المفردات علـى المـشاريع المنتخبـة ، ثـم إسـتخلاص هيمنـة بعـض المؤشـرات دون الأخـرى ، والثانية بتحليل العلاقة بين المفـردات الثلاثـة ، وبـشكلٍ أدق العلاقة بين المتغيرات شديدة الفاعليـة . وتـم ترميـز المتغيـرات للمفـردات الثلاثـة ، الأولـى A1,A2,... ، والثانية B1,B2,... ، والثالثة C1,C2,... .

2.3 طريقة القياس : تم تطبيق القياس بعرض مجموعة من المشاريع المنتخبة على عدد من المتلقين (إختصاص معماري) وإعطاء شروحات وافية لهم . إذ تم إنتخاب (20 مستبين) بدرجات علمية مختلفة (بكالوريوس ، ماجستير، دكتوراه) وبطريقة الملىء اليدوي قبلهم عن طريق وضع علامة (●) من قبلهم في المربع المناسب ، ملحق رقم (2).

33. أسلوب التحليل : تم أولاً إستخلاص النسب المئوية لكل متغير في الملحق رقم (3) ولجميع المستبينين لكل مشروع من المشاريع الستة الخاضعة للتطبيق ، وثانياً تحويل هذه النسب إلى ثلاثة مستويات هي : تمركز عالي يتراوح بين (99%-80%) ويرمز له بالرمز ( ) ، وتمركز وسط يتراوح بين (79%-60%) ويرمز له بالرمز ( ) ، تمركز ضعيف يتراوح بين (59%-40%) ويرمز له بالرمز ( ) . تم بعدها مقارنة طبيعة التمركزات العالية فقط للمتغيرات في (الجدول رقم - 1) للمفردة الأولى مع المفردتين الثانية والثالثة بهدف إستكشاف المتغيرات شديدة الفاعلية والتي تكون بتكرار (4-6) مرات ، متغيرات متوسطة الفاعلية بتكرار (3) مرات ، متغير ضعيف الفاعلية بتكرار من (1-2) مرات ، ومتغيرات معدومة الفاعلية الذي يكون تكراره صفراً.

4.3 العينة التطبيقية :

محددات إختيار العينة : استند اساس اختيارها الى محددات متعددة منها (شهرتها، اهميتها، عصريتها، فضلاً عن الأسلوب المنشائي المستخدم ، وتنوع معالجاتها الشكلية والوظيفية والأنشائية وغناها التعبيري).

المشاريع المنتخبة : تم إنتخاب ستة مشاريع لغرض التطبيق ، (مطار باراكاس الدولي ، مطار كانساي الدولي ، مطار بكين الدولي ، مطار جكارتا الدولي ، مطار بغداد الدولي ، مطار النجف الدولي، وكما موضح تفاصيلها في الملحق رقم (1) .

4. الاستنتاجات الخاصة بتحليل الامثلة التطبيقية:

أولا) الأستنتاجات المرتبطة بمفردات مستوى التكامل التصميمي لمبنى المسافرين:

• أظهرت نتائج تحليل الامثلة التطبيقية لمستوى التكامل التصميمي لمبنى المسافرين والمرتبطة بالمفردة الاولى (النمط التصميمي المتبع في تصميم مبنى المسافرين) تركيزا واضحا على استخدام النمط الخطي المستقيم لأبنية المسافرين حيث ظهر ذلك واضحا في كثير من الامثلة التطبيقية كما في مطار باراكاس الدولي ومطار كانساي ،وبروزه كنمط غير مباشر في العديد من الامثلة الاخرى ، حيث بينت نتائج تحليل المشاريع تمركزا عاليا لهذا المتغير وبتكرار عالي حيث يعد متغير شديد الفعالية، وبينت النتائج ايضا تمركزا متوسطا لنمط الابنية الهجينة فتعد متغير متوسط الفعالية، وتمركزات ضعيفة للمتغيرات الاخرى فتعد متغيرات ضعيفة الفعالية .

• أظهرت نتائج تحليل الامثلة التطبيقية والمرتبطة بالمفردة الثانية (كفاءة التنظيم الفضائي على مستوى المخطط والمقطع لمبنى المسافرين) تركيزا واضحا على استخدام نمط أبنية المسافرين المتعدة المستويات وظهر واضحا في العديد من الامثلة التطبيقية العالمية كمطار كانساي وباراكاس وبكين ، حيث بينت النتائج تمركزا عاليا في هذا النمط وبتكرار عالي حيث يعد متغير شديد الفعالية، وبينت النتائج ايضا تمركزات ضعيفة للمتغيرات الاخرى فتعد متغيرات ضعيفة الفعالية.

· أظهرت نتائج تحليل الامثلة التطبيقية والمرتبطة بالمفردة الثالثة (الكفاءة التصميمية للمنظومة الوظيفية لمبنى المسافرين) تمركزا عاليا في اغلب متغيراتها وبتكرارات عالية .

ثانيا) الأستنتاجات المرتبطة بمفردات مستوى تكاملية النظم المنشئية مع المنظومات الوظيفية والتشغيلية:

• أظهرت نتائج تحليل الامثلة التطبيقية لمستوى التكامل التصميمي لمبنى المسافرين والمرتبطة بالمفردة الاولى (نمط النظام المنشئي المستخدم) تركيزا واضحا على استخدام النظم ذات المتجهات الفعالة وظهر ذلك في الكثير من مباني المسافرين المدروسة وبشكل متميز خلق تعبيرا واضحا ومتميزا بابراز الهيكل المنشئي بوضوح والذي خلق صراحة انشائية اعطت تعبيرية متنوعة في جميع الامثلة التطبيقية ، وبينت نتائج تحليل المشاريع تمركزا عاليا في متغير النظم ذات المتجهات الفعالة وبتكرار عالي حيث يعد متغير شديد الفعالية، وبينت النتائج ايضا تمركزات ضعيفة للمتغيرات الاخرى فتعد متغيرات ضعيفة الفعالية حيث لم تستخدم بشكل واضح.

· أظهرت نتائج تحليل الامثلة التطبيقية لمستوى التكامل التصميمي لمبنى المسافرين والمرتبطة بالمفردة الثانية (طبيعة المادة الأنشائية المستخدمة) تركيزا واضحا على وجود كفاءة عالية لامكانات المادة الانشائية المستخدممة فضلا عن اتباع درجة عالية من التعامل الشكلي للمادة البنائية المستخدمة وظهر ذلك واضحا في الكثير من الامثلة التطبيقية وبتمركزات عالية كما في مطار براكاس حيث استخدمت مادة الخيزران في التسقيف وبكفاءة عالية في توفير الانارة الطبيعية وتسقيف مساحات كبيرة فضلا عن اعطاء جانب جمالي في السقف يعطي تعبيرية محلية متميزة ، وظهرت امكانات المادة وبشكل واضح ايضا في مطار جكارتا الدولي حيث استخدمت مادة القرميد لاعطاء تعبيرات محلية معبرة عن الهوية المكانية وبكفاءة منشئية عالية ، حيث بينت نتائج تحليل المشاريع تمركزا عاليا لجميع متغيرات مفردة طبيعة المادة المستخدمة وبتكرار عالي حيث تعد متغيرات شديدة الفعالية.

ظهرت نتائج تحليل الامثلة التطبيقية لمستوى التكامل التصميمي لمبنى المسافرين والمرتبطة بالمفردة الثالثة (خصوصية النظم المنشئية) تمركزا عاليا لمتغيرات الابتكار الجديد للنظم غير التقليدية ، وبتكرارات عالية حيث تعد متغيرات شديد الفعالية حيث بين التحليل استخداما متميزا للانظمة المنشئية غير التقليدية والمبتكرة لتعطي تعبيرات متميزة تعبر احيانا عن روح العصر التكنولوجي المعاصر تعبر عن تقدم وتطور البلد فضلا عن اعطاء تعبيرية مكانية مرتبطة بالسياق والهوية المكانية للمنطقة ، وبينت النتائج ايضا تمركزات متوسطة للمتغيرات الاخرى فتعد متغيرات متوسطة الفعالية فقد بين التحليل قلة استخدام النظم المنشئية التقليدية والبسيطة والميل نحو استخدام النظم المبتكرة والعملاقة ذات الخواص التكاملية.

· أظهرت نتائج تحليل الامثلة التطبيقية والمرتبطة بالمفردة الرابعة (خصوصية العلاقة مابين النظم المنشئية والشكل) تمركزا عاليا لمتغير بينت نتائج تحليل المشاريع تمركزا عاليا في متغير التكامل بين المنشأ والشكل وبتكرار عالي و يعد متغير شديد الفعالية

• أظهرت نتائج تحليل الامثلة التطبيقية والمرتبطة بالمفردة الخامسة (تكامل العلاقة بين النظم المنشئية والنتاج المعماري لأبنية محطات المطارات) تمركزا عاليا لمتغيرات لأغلب متغيرات هذه المفردة المتمثلة بتكاملية النظم المنشئية مع المنظومات الوظيفية والتشغيلية و تكاملية النظم المنشئية مع القشرة الخارجية لمبنى المسافرين وبتكرارات عالية حيث تعد متغيرات شديد الفعالية ، وبينت النتائج ايضا تمركزات متوسطة لمتغيرات كفاءة النظم المنشئية في تحقيق المرونه التصميمية وسهولة التوسع المستقبلي ومتغير كفاءة العزل الحراري لغلاف المبنى فتعد متغيرات متوسطة الفعالية.

ثالثا) الأستنتاجات المرتبطة بمفردات المستوى الشكلي والتعبيري:

• أظهرت نتائج تحليل الامثلة التطبيقية لمفردات المستـــوى الشكلـــي والتعبيـــري والمرتبطة بالمفردة الاولى (المستوى الفكري للتعبير المعماري لأبنية محطات المطارات) تمركزا عاليا لجميع متغيرات مفردة روح العصر وبتكرار عالي حيث تعد متغيرات شديدة الفعالية ، وبالنسبة لمفردة تحقيق الوظيفة الرمزية فقد بينت نتائج تحليل المشاريع تمركزا عاليا في متغيرات التأثير الثقافي وتحقيق الهوية المكانية وبتكرارات عالية حيث تعد متغيرات شديدة الفعالية،حيث تبرز اغلب الأمثلة التطبيقية في المجتمعات مؤسسة محتوى رمزي متنوع ومختلف خاص بالعمارة التقليدية فالشكل الفيزياوي الظاهر لأبنية محطات المطارات يرمز إلى أبعاد غير فيزياوية وعليه فالمعاني الرمزية للأشكال المعمارية لا ترتبط بتقاليد محددة تنتمي لها هذه الأشكال وإنما تتسع لتشمل شبكة من الثقافات والحضارات المتداخلة . وبينت النتائج ايضا تمركزات متوسطة لجميع متغيرات مفردة مفاهيم التواصل وبتكرار عالي حيث تعد متغيرات متوسطة الفعالية.

• أظهرت نتائج تحليل الامثلة التطبيقية لمفردات المستـــوى الشكلـــي والتعبيـــري والمرتبطة بالمفردة الثانية (المستوى المادي للتعبير المعماري لأبنية محطات المطارات) تمركزا عاليا في متغيرات تناغم الناحية الأنشائية مع الناحية الجمالية وتعبيرية الفولاذ والاعتماد على العلاقات الهندسية في التكوين الشكلي للمستوى المادي للتعبير واتجاه التفصيل المنشئي لجماليات المنشأ وبتكرار عالي حيث تعد متغيرات شديدة الفعالية، ، وبينت نتائج تحليل المشاريع تمركزا عاليا لجميع متغيرات مفردة علاقة النظم المنشئية بتعبيرية الشكل المعماري للمستوى المادي للتعبير وبتكرار عالي حيث تعد متغيرات شديدة الفعالية، حيث ظهرت الوظيفة التعبيرية والرمزية في اغلب الامثلة التطبيقية وتجسدت بشكل مميز في مطارات براكاس وكانساي وبكين وجكارتا والتي طالما يتم إدراكها تصبح وسيلة للتعبير وقادرة على إيصال المعاني، وتنقل رسالة معنوية مهمة وواضحة تجسد الفكر الذي أنتجها ويتم تحقيق الوظيفة التعبيرية الرمزية لمباني محطات المطارات من خلال النجاح في التعبير عن المواد الإنشائية وطرق الإنشاء المتبعة في تشييد هذه المواد والتكوينات المنشئية لها وبما يترجم الأمكانيات الجمالية للعصر وهي بنفس الوقت تمثل مقياسا لتفوق المعماري.

5. الاستنتاجـــــــات النهائيـــــــة للبحـــث :

1) ان للمنشأ في ابنيـة محطـات المطـارات وظيفتـان رئيـسيتان .. همـا الوظيفـة الإنـشائية والوظيفـة التعبيرية المعماري وعند تعامله مـع المنـشأ، يعتمـد علـى المعـادلات والعلاقـات الرياضـية (وظيفـة إنشائية)، فضلا عن أعتمـاده علـى حقـائق تعبيريـة وجمالية متأصلة في المنشأ (وظيفة تعبيرية) .
2) أن الفكر الإنشائي فـي أبنيـة محطـات المطـارات يتعلـق بعوامـل عديـدة، منهـا النظـام الإنـشائي المستخدم، المواد البنائية، العامـل الاقتـصادي حيـث إن كل هذه العوامل تعتمـد بـدورها علـى عوامـل أخرى عند استخدامها والاعتماد عليها.
3) تتميـز ابنيـة محطـات المطـارات علـى اخـتلاف أنواعها وأزمنتهـا فـي تحقيقهـا لمفهـوم التكامـل، سواء أكان ذلك التكامل نـاتج عـن قـصد مـسبق أو لا، بحيـث تكـون جميـع المنظومـات فاعلـة فـي المبنى.
4) ان الغالبية العظمى مـن ابنيـة محطـات المطـارات تعتمد في انـشائها علـى الـنظم المنـشئية العملاقـة وذلك لتعقد اغلب المنظومـات التـشغيلية والحركيـة داخل مبـاني المـسافرين والمرونـة العاليـة التـي تتطلبهـا اغلـب الفعاليـات التـي تـتم فـي مبنـى المسافرين والحاجة الى استيعاب اعـداد كبيـرة مـن المسافرين في وقـت واحـد والحاجـة الـى التوسـع ضـمن حقـب زمنيـة قـصيرة نـسبيا كـل هـذه

الاعتبارات وغيرها ، تجعل مـن اسـتعمال منظومـة منـشئية عملاقـة ذات بحـور واسـعة احـد اهـم المتطلبات التخطيطية والتـصميمية لابنيـة محطـات المطارات المعاصرة.

5) تميزت الانظمة الانـشائية المـستعملة فـي محطـات المطارات بكونها منظومات هيكليـة عملاقـة معقـدة ذات بحور واسعة تعكس شـكلا معماريـا ديناميكيـا يحاكي ديناميكية الطيران وفـي نفـس الوقـت يـوفر فضاءات واسعة ومرونة تـصميمية عاليـة وتكـاملا مع بقية المنظومات .

6) ان الوظيفة التعبيرية أوالرمزية تتجسد بـشكل مميـز في مبـاني محطـات المطـارات التـي طالمـا يـتم إدراكها تصبح وسيلة للتعبير وقـادرة علـى إيـصال المعاني، وتنقـل رسـالة معنويـة مهمـة وواضـحة تجسد الفكر الذي أنتجها.

7) أسـتنتج البحـث مـن خـلال الطـرح للمفـاهيم والمستويات (الفكرية والماديـة والوظيفيـة) لتعبيريـة أبنيـة محطـات المطـارات، بـروز دور الـنظم المنشئية المساهمة في خلق الـشكل المعمـاري الـذي يحمل تعبيرية خاصة ناتجة من خلفية فكريـة تحمـل قيمـا ومعـاني مميـزة وذات خـصوصية محليـة ومتلاءمة مع روح العـصر ومـع العـادات والقـيم ومحققة استمرارية العمـارة عبـر الـزمن . ولكـي تخرج الفكرة الى الواقع لابـد مـن الأسـتعانة بـنظم قادمـة مـن الواقـع، أي بمعنـى ان لهـا وجودهـا المعرف وارتباطاتها النظامية المـسبقة الوجـود، مـن ثم توظيف هـذه الـنظم او عناصـرها او علاقاتهـا بطريقـة تماثـل علاقـات فـي الـصفات والقـيم الجوهرية للمفاهيم والإفكار.

8) بدون النظم التي لهـا كيانهـا فـي الواقـع لا يوجـد تعبير عن افكـار كليـة ويبقـى القـرار والأختيـار للمصمم في شقي عمله: اولاً) فيما يخـتص بـالتعبير وازدياد المتغيرات المتعلقة بكيفيـة التعبيـر وتـداخلها ، والأسلوب الشخصي للمصمم في فهمهـا ومـن ثـم بناء قراراتـه فـي توظيفهـا بـالتعبير. ثانيـاً(فـي اسلوب فهـم المـصمم المعاصـر لمقومـات هويتـه الجوهرية وقوة انتمائه وثقتـه بهـا وهـذا يختلـف – بسبب تغييـر نمـط نظـم الأتـصالات والمعلومـات عالمياً- ، فالنمط الفكري ونوع التواصـل المتماسـك في المجتمع التقليدي قد تغير الآن عمـا كـان عليـه، والمتغيـرات الآن تـشمل ثقافـة المـصمم، وثقافـة المتلقي، ونمط ممارسـة المهنـة، ومـستوى الـذوق العـام وغيرهـا، فـضلا عـن التحـديات الفكريـة والسياسية الموجهة.

9) نتيجة لقدرة الأنسان علـى ادراك العلاقـة الايحائيـة بين الفكر و الشكل الفيزيـاوي تـصبح للمنـشأ فـي أبنية محطات المطـارات وظيفـة تعبيريـة رمزيـة فـضلا عـن الوظيفـة العمليـة (ضـمان اسـتقرار المبنى) التي يقوم بها.

10) يمكن تحقيق الوظيفة التعبيرية الرمزيـة لمبـاني محطات المطارات من خـلال النجـاح فـي التعبيـر عن المواد الإنشائية وطـرق الإنـشاء المتبعـة فـي تشييد هذه المـواد والتكوينـات المنـشئية لهـا وبمـا يترجم الأمكانيـات الجماليـة للعـصر وهـي بـنفس الوقت تمثل مقياسا لتفوق المعماري .

6. المصادر :

1) البعلبكي، منير- قـاموس المـورد (انكليـزي- عربـي)- دار العلم للملايين- الطبعـة الرابعـة عـشر- بيـروت- 1985 .

2) التميمي ، أسامة عبد المنعم، " أثـر تطـورات تكنولوجيـا المنشأ في التشكيل المعمـاري " رسـالة ماجـستير ، قـسم الهندسة المعمارية، جامعة بغداد ، بغداد ، 2006.

3) الـصابونجي، محمـد مـصطفى ، " العمـارة والـنظم الأنشائية ذات البحور الطويلة" رسـالة ماجـستير ، قـسم الهندسة المعمارية ، جامعة بغداد ، بغداد ،1993 .

4) على رأفت، "ثلاثية الإبـداع المعمـارى: الإبـداع المـادى فـى العمـارة"، مركـز أبحـاث انتركونـسلت، الجيـزة، 1996 م.عمـرو خيـر الـدين،(المعالجـات البيئيـة فـي تخطـيط المـدن الاسـلامية وتـصميم مبانيهـا)، سـجل بحوث مؤتمر انتربيلد، القاهرة ، 1997.

5) Blow, Christopher, 2005,"Transport terminals and modal interchanges,planning and design ", Architectural Press, UK.
6) Charleson, Andrew W., 2005 "Structure as architecture", Architectural Press, UK.
7) Edwards,Brian,2005," The Modern Airport Terminal: New Approaches to Airport Architecture ", Second Edition, Taylor & Francis, E & FN Spon, London.
8) Foster J & Stroud "Structure and fabric "part1, bats ford 1975.
9) Nervi, P.L., "Structures", McGraw-Hill Inc., New York, 1956 .
10) Nervi, P.L," Aesthetics& Technology in Building", Hatvard University Press Cambridge, Massachusetts, 1966 .
11) Nervi, P.L, "A Philosophy of Structure Design Architectural Engineering-New Structure", Edition by Fischer R.E, McGraw Hill Inc., New York, 1964 .
12) Torroja, Eduardo, "Philosophy of structures", University of California Press, Berkeley, 1962.
13) http://www.airporttechnology.com/projects/degaulle/ pdf

جدول رقم (1) يوضح مفردات الإطار النظري الرئيسية والثانوية وقيمها الممكنة ، المصدر : الباحث

مستوى التكامل التصميمي لمبنى المسافرين	المفردات الرئيسية		المفردات الفرعية		القيم الممكنة		الرمز
1	النمط التصميمي المتبع في تصميم مبنى المسافرين	1	استخدام نمط واحد	مبنى مسافرين مركزي مع اصابع ثانوية	بدون توابع ثانوية		A1
					ذات توابع ثانوية		A2
				مبنى مسافرين مبسط Simple terminal	ذات نمط خطي مستقيم		A3
					ذات نمط خطي منحني		A4
		2	متعدد الانماط	مباني مسافرين ذات النمط المعتمد على الناقلات			A5
				مبنى مسافرين مركزي مع توابع ثانوية			A6
				مبنى مسافرين موحد Unit terminal			A7
				ابنية المسافرين الهجينـــــة Hybrid terminals			A8
	كفاءة التنظيم الفضائي على مستـوى المـخطط والمقطــع	3	عدد المستويات ونمط توزيعها	مباني مسافرين ذات المستوى الواحد Single-level terminal			A9
				مباني مسافرين بمستويين Double-level terminal			A10
				مباني مسافرين بمستويين مع طرق وصول امامية معلقة			A11
				مباني مسافرين متعددة المستويات Multi-level terminal			A12
	الكفاءة التصميمية للمنظومة الوظيفية لمبنى المسافرين	4	كفاءة الاستجابة لأحتياجات المسافرين فيما يتعلق بالملاءمة والراحة والمتطلبات الشخصية	الهدوء والطمأنينة وحضور الطبيعة في أغلب الفضاءات العامة لازالة الضغط النفسي			A13
				استعمال الانهاءات ذات المواد الطبيعة أينما أمكن			A14
				الوضوحية الفضائية والتنظيمية			A15
				استغلال الهيكل الانشائي والضوء الذي يعبر عن نمط الاستخدام والتدرج الوظيفي			A16
		5	كفاءة التصميم للتوسع والمرونة	القابلة للتوسع جزئيا وكليا وفي اكثر من اتجاه واحد			A17
				ان تصمم بحيث يكون التغيير في الفضاءات والفعاليات الرئيسية لايؤثر على العملية التشغيلية الكلية للمبنى			A18
		6	الكفاءة التصميمية للمنظومة الحركية لمبنى المسافرين	كفاءة توقيع الفضاءات وتوزيعها بالشكل الملاءم بحيث تستوعب الحركة المتعاكسة			A19
				كفاءة تزويد الفضاءات بدرجة عالية من الوضوحية (Clarity).			A20
				سهولة التوجيه وتوفير اقصر مايمكن من مسافات السير واقل مايمكن من تغيير المستويات			A21
				كفاءة توفير توجيه حركي فعال للمسافرين ووضوح محاورالوصول والمغادرة			A22

	المفردات الرئيسية		المفردات الفرعية		القيم الممكنة			الرمز
مستـــوى تكاملية النظم المنشئية مع المنظومات الوظيفية والتشغيلية	1 نمط النظام المنشئي المستخدم	1	أستعمال نمط واحد		نظم ذات شكل فعال (Form –Active Structural System)			B1
					نظم ذات متجهات الفعالة (Vector –Active Structural System)			B2
					نظم ذات كتل الفعالة (Bulk – Active Structural System)			B3
			متعدد الانماط		نظم ذات سطح الفعال (Surface –Active Structural System)			B4
					نظم عامودية (Vertical System)			B5
	2 طبيعة المادة الأنشائية المستخدمة	3	أستخدام مادة واحدة		كفاءة امكانات المادة الأنشائية المستخدمة			B6
		4	أستخدام عدة مواد منشئية		درجة التعامل الشكلي للمادةالبنائية المستخدمة			B7
	3 خصوصية النظم المنشئية	5	نظم منشئية تقليدية		استخدام نظم منشئية ذات تكنولوجيا محلية وتقليدية			B8
		6	نظم منشئية غير تقليدية	إبتكارجديد	إستخدام مواد بنائية جديدة			B9
					طرق تصنيع جديدة للمواد التي تولف المبنى			B10
					نظام إنشائي جديد			B11
					تكنولوجيا جديدة في الإنشاء			B12
				معالجة جديدة لأفكار سابقة	علاقات إنشائية مألوفة بصيغ غير مألوفة (تحدي إنشائي)	تراكب أكثر من نمط إنشائي مع بعض		B13
						تداخل القشرة الخارجية مع النظم المنشئية بأكثر من طريقة		B14
						تحويل حالة الإستقرار إلى اللا إستقرار		B15
						نظام منشئي ديناميكي يحاكي الطيران		B16
	4 خصوصية العلاقة مابين النظم المنشئية والشكل	7	تأثيرات العلاقة التبادلية بين الشكل والمنشأ		التأثيرات المتناقضة للمنشأ والشكل			B17
					التجاوز بين المنشأ والشكل			B18
					التكامل بين المنشأ والشكل			B19
	5 تكامل العلاقة بين النظم المنشئية والنتاج المعماري لأبنية محطات المطارات	8	تكاملية النظم المنشئية مع المنظومات الوظيفية والتشغيلية في أبنية محطات المطارات		تحقيق الكفاءة الوظيفة			B20
					كفاءة تحقيق الفضاءات الخالية من العوائق			B21
					كفاءة توفير الاضاءة الطبيعية المناسبة			B22
					كفاءة النظم المنشئية في تحقيق المرونه التصميمية وسهولة التوسع المستقبلي			B23
					كفاءة العلاقة التفاعلية بين الطائرة والمسافرين ومبنى المسافرين			B24
					تحقيق متطلبات المنظومات التشغيلية والخدمية لمبنى المسافرين			B25
		9	تكاملية النظم المنشئية مع القشرة الخارجية لمبنى المسافرين		كفاءة تحقيق التوازن بين تاثيرات البيئة الخارجية ومتطلبات البيئة الداخلية للمبنى			B26
					كفاءة العزل الحراري لغلاف المبنى			B27
					خفة الوزن خصوصاً في مواد التسقيف			B28

	المفردات الرئيسية		المفردات الفرعية		القيم الممكنة		الرمز
المستـــوى الشكلي والتعبيـــري	1 المستوى الفكري للتعبير المعماري لأبنية محطات المطارات	1	تأثيرات روح العصـــر		تحقيق مثالية معمارية واضحة في التعبير		C1
					استثمار الماضي في ابداع صيغ الحاضر والمستقبل		C2
		2	تحقيق الوظيفة الرمزية	طبيعة المحتوى الرمزي	تحقيق أبعاد زمانية		C3
					تحقيق أبعاد مكانية		C4
					دور طرفي الاتصال (المرسل والمتلقي) في تأسيس روابط بين الرسالة الرمزية وسياقها		C5
					التأثير الثقافي على الصور الرمزية حسب السياق العام (زمانيا ومكانيا)		C6
					تلبية متطلبات الهوية المكانية		C7
		3	تحقيق مفاهيم		الاتصال المباشر بين المصمم والمتلقي		C8
					الاتصال غير المباشر بين المصمم والمتلقي		C9
	2 المستوى المادي	4	درجة التكتونية		تناغم الناحية الأنشائية مع الناحية الجمالية		C10

C11	تغلب أحداهما على الأخر	المنشئية		للتعبير المعماري لأبنية محطات المطارات		
C12	تعبيرية الخرسانة المسلحة	الخصائص التعبيرية للمواد البنائية	5			
C13	تعبيرية الفولاذ					
C14	تعبيرية الخشب					
C15	تعبيرية المواد الأخرى					
C16	اتجاه الحركة الملفتة	جماليات المنشأ	6			
C17	اتجاه التفصيل المنشئي					
C18	المقياس الانساني المتبع للتكوين الشكلي	الخصائص التكوينية والشكلية	7			
C19	الأعتماد على العلاقات الهندسية في التكوين الشكلي					
C20	اتحاد المنشأ مع الشكل	علاقات النظم المنشئية بتعبيرية أشكال أبنية محطات المطارات	8			
C21	المنشأ وسيلة لخلق الشكل المعماري					
C22	المنشأ وسيلة لادراك المقياس الشكلي للعمارة					
C23	المنشأ اداة اللغة التعبيرية للعمارة					

ملحق رقم (1) المشاريع المنتخبة للتطبيق

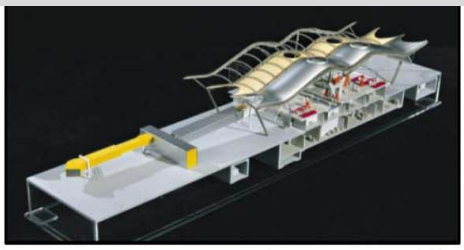



1- محطة مطار باراكاس الدولي في مدريد/اسبانيا : متكون من محطتين للمسافرين خطية بثلاث وحدات خطية مركزية متوازية تمثل كل منها وظيفة معينة السقف عبارة عن جسور مقوسة موضوعة على مراكز تبعد 9 م لتشكل هيئة تشبه جناح الطائر. والسقف مكون من 3 مقاطع حديدية منفصلة ومندفعة مع بعضها البعض

يتضمن المبنى ستة طوابق تتوزع فيها الفعاليات والوظائف المختلفة , ثلاثة طوابق فوق سطح الارض وثلاثة تحت سطح الارض تتمثل بطوابق معاملة المسافرين والامتعة , اما الطوابق السفلية فانها تمثل طوابق الصيانة وتجهيز الامتعة ومحطة النقل العام والنقل بين ابنية المسافرين. شيدت الطوابق السفلية من الخرسانة المسلحة وبتناقض مع الطوابق العليا التي تتميز بشفافية عالية وتمثل دعامات الكونكريت على شكل جذوع الاشجار تمثل نقاط ثابتة يثبت عليها النظام الهيكلي الفولاذي حيث ان اربعة ازواج من الدعامات تشكل زوجين بشكل حرف Sملتوية مزدوجة الوحدات في هذه الحالة كل زوج من العناصر مع هيكل السقف الستيل يحقق استقرار السقف وبكلا الاتجاهين . بذلك يمر خط السقف على حواف المبنى مثيرا اهتماما اكثر من الواجهة, تظليل السقف للواجهة يكون مستندا الى دعامات انيقة بشكل حرف Y. الجو المشرق والمريح داخل المبنى يعكس البيئة المحيطة .السقف الخيزراني المتموج الذي يرافق المسافرين طوال الرحلة لمبنى

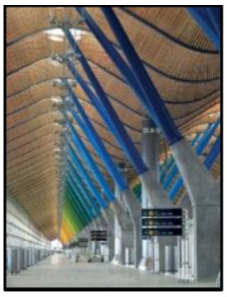
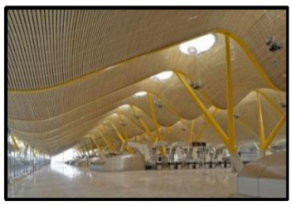

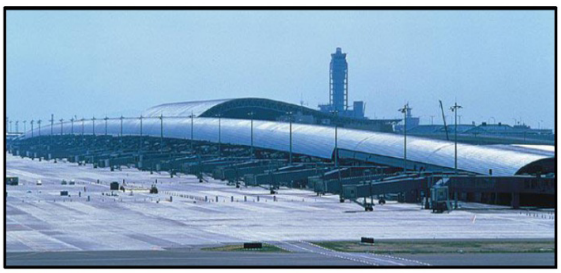


2- محطة مطار كانساى الدولي في اليابان: يقع مطار كانساي فوق جزيرة مبنية خصيصا للمشروع في ساحل مدينة أوساكا في اليابانالبناية طويلة يصل طولها إلى 1.7 كم مكونة من جزء مركزي يحتوي على نشاطات المطار الرئيسية مثل صالات القدوم والمغادرة الداخلية والخارجية وتسليم الحقائب والجوازات والجمارك وكاونترات شركات الطيران ومكاتب إدارة المطار، وجناحين طويلين ونحيفين يحتويان على 41 بوابة متصلة بجسور لركوب الطائرات والنزول منها . يتكون سقف المشروع من 18 جمالون , كل واحد من هذه الجمالونات مدعوم بأعمدة مائلة , أما السقف المزدوج فهو مدعوم بأعمدة رأسية ، الهيكل المنشئي الفضائي المميز بتعبيريته الانشائية الظاهرة , باستخدام وسائل تصميم متطورة أمكن التوصل إلى صيغة هندسية تسمح بتصغير حجم السقف باستمرار وفي نفس الوقت تمكن من استخدام صفائح من حجم وشكل واحد لتغطية كافة السقف الذي بلغة مساحته 90000 متراً مربعاً المصمم اختار هيكلاً إنشائياً خفيفاً ، فالخفة صفة شائعة في اليابان ، وأن البناية طويلة جداً بحيث يصل طولها إلى 1.7 كلم . وبالتالي كان من المهم التفكير في كيفية تخفيف الوقع البصري لهذا الطول الهائل عن طريق استخدام النسيج والملمس ، للسقف المتموج فوائد عدة بالإضافة إلى تسهيل تهوية الفراغات . إنه يعطي البناية من الخارج منظراً متميزاً ، أما من الداخل فهو يساعد المسافرين على معرفة طريقهم في هذه البناية الكبيرة إذ أن السقف يبدأ منبسطاً من ناحية الاتصالات الأرضية .

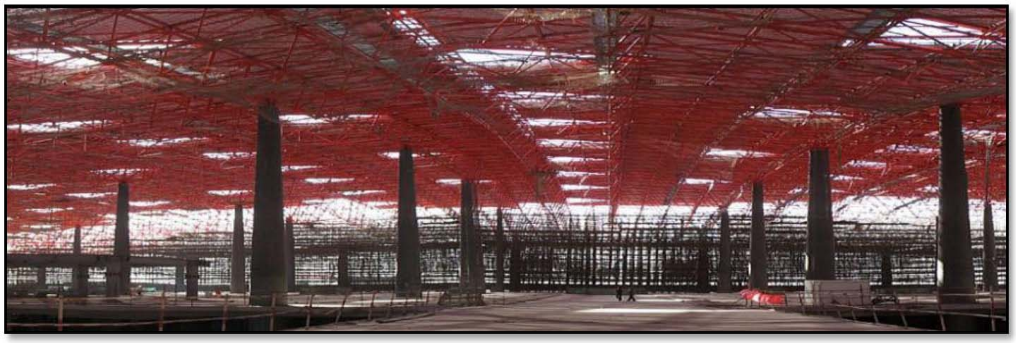

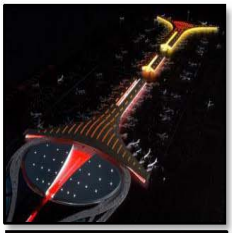

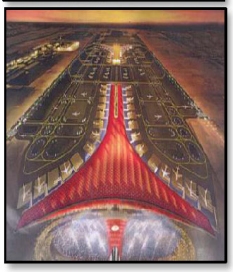

3- محطة مطار بكين الدولي : تقع بين المدرج الشرقي والمدرج المستقبلي الثالث يشكلان معا مساحة ارضية تقترب من 3.1مليون متر مربع معظمها تحت سقف واحد, ليكون هذا المبنى اول مبنى يتجاوز مساحة مليون متر مربع ,والمقاطع العمودية في بناية محطة مطار بكين الدولي توضح شكل السقف المميز وهيمنه النظام المنشئي للهياكل الفضائية على التعبيرية الكلية للمبنى يمثل المبنى بوابة ومدخلا حقيقيا للبلد يشمل محاكاة للمكان ممثلا مدخك رمزيا موجها للترحيب بكامل طاقته يعبر عنه الشكل الشبيه بالتنين ودراما السقف المرتفع التي تمثل شعلة او لهيب الالوان التقليدية الصينية, او الامبراطورية الحمراء المندمجة ضمن الاصفر الذهبي. منظر الاعمدة الحمراء الممتدة قدما على جانبي المبنى كلها تثير صورة المعبد الصيني ,والشكل الفيزياوي للمبنى يتضمن فكرة منشئية يستطيع الانسان بما يمتلكه من حدس وخبرة اكتشاف نوع النظام المنشئي, وكيفية انتقال القوة وردود الافعال في كل جزء من اجزاء الشكل ,وذلك عن طريق تقرير الاحمال ولمسارات انتقالها وتحسس المواد وقابليتها في تحمل تلك الاثقال .ان الصراحة المنشئية (اي وضوح النظام) نتجت عن تطابق الوظيفة المنشئية العملية والوظيفة الجمالية.

4- محطة مطار جاكارتا الدولي في أندنوسيا : متكون من محطتين للمسافرين شمالية وجنوبية وان كل محطة مطار محاطة بالاشجار والمناطق الخضراء وممرات للمشي بحيث يكون المسافر بتماس مباشر مع البيئة الخارجية وهي ظاهرة نادرة في المطارات الدولية الكبرى المعاصرة ,والفكرة التصميمية لمحطة المطار هي نمط مباني المسافرين الهجينة حيث يتكون من محطتين رئيسيتين شمالية وجنوبية كل محطة تتكون من نمط خطي منحني تبرز منه ثلاثة اصابع ثانوية تحوي قاعات المغادرة النهائية . النظم المنشئية المستخدمة بسيطةوتتكامل مع كافة المنظومات التشغيلية ضمن كل متكامل مع توقيع المبنى باتجاه جنوبي شرقي للاستفادة من الانارة الطبيعية في السقفية , مع استخدام التشجير ضن الفضاءات الداخلية والنظام المنشئي هو نظام الجملونات المستقيمة والذي يعطي مرونة تصميمة عالية , و يضم السقف المائل فتحات الانارة الطبيعية بشكل موجهه باتجاه جنوبي شرقييتضمن المبنى طابقين رئيسيين حيث تتم عمليات المسافرين الواصلين في الطابق الارضي بينما تتمل عمليات المسافرين المغادرين في الطابق الثاني ,وان توزيع المستويات يتأثر بالفكرة التصميمية المعتمدة على البساطة في التكوين والمقياس الانساني المندمج مع الطبيعية حيث اعتمد المصمم على اقل عدد من المستويات لضمان تطبيق تلك الفكرة المحتوى الرمزي للشكل الفيزياوي هو ذو أبعاد زمانية ومكانية مرتبطة بالبعد السياقي من خلال استخدام المصمم للمواد الانشائية المحلية تعبيرا عن الثقافة المكانية فيمثل المبنى بوابة ومدخلا حقيقيا للبلد يشمل محاكاة للمكان ممثلا مدخلا رمزيا موجها للترحيب بكامل طاقته يعبر عنه شكل محطات المطار المستوحى من البيوت التقليدية

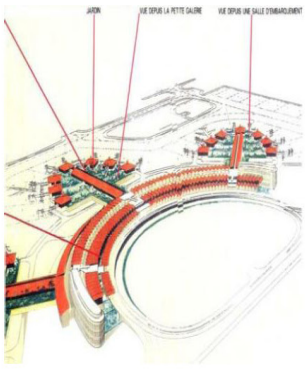

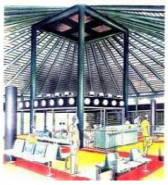

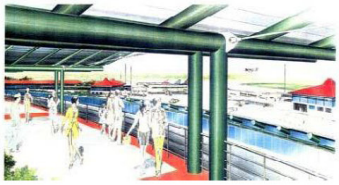


5- محطة مطار بغداد الدولي : يعتمد تصميم المطار مفهوم وحدة مبنى المسافرين termmal umt ,ويحوي المطار على ثلاث وحدات كل وحدة عبارة عن مبنى متكامل الخدمات الفكرة التصميمية للمبنى: اعتمدت الفكرة التصميمية لمبنى المسافرين على الشكل المثلث متساوي الاضلاع بطول 19 متر, وتكراره كأساس لخلق التكوينات الوظيفية والمنشئية ,وتم اختيار هذا الشكل لغرض استيعاب اكبر عدد ممكن من مواقف الطائرات حول المبنى ولتوفير سيطرة امنية جيدة في الداخل ولتقليل المسافة التي يقطعها المسافر بين موقف السيارات وبوابات الطائرات حيث لا تزيد المسافة بين أبعد نقطتين فيهما بحدود 150م تم تجميع وحدات المطار على محيط نصف دائرة يخدمها طريق مركبات بطابقين للمغادرة والقدوم وقد صممت كل من الوحدات بحيث انها تستوعب 5.2 مليون مسافر سنويا المنظومة الانشائية اعتمدت نفس الوحدة التخطيطية الاساسية وهي المثلث متساوي الاضلاع 19 متر حيث وضع عمود في كل قمة مثلث وتم مد جسور بين الاعمدة وبطول 19 متر ثم قسمت كل وحدة انشائية رئيسية الى وحدات اصغر مثلثة الشكل طول ضلع كل منها 75. 4مترالتكوين الشكي لأبنية وحدات المطار اعتمد التكوينات الهندسية الحادة , البعيدة عن الاشكال الطبيعية العضوية او الاشكال الدراماتيكية التي تعبر عن طبيعة الحدث المكاني للطيران.


6- محطة مطار النجف الأشرف الدولي : يقع المطار في شرق مدينة النجف , أنشأ على قاعدة جوية عسكرية سابقة, وفي 20 تموز 2008 ,وتم افتتاح المطار رسمياً لاستقبال رحلات الطيران القادمة لمدينة النجف الأشرف , يضم مبنى الركاب مكاتب لشركات الطيران والخدمات ومواقف للسيارات وبرج مراقبة وصالة للشحن الجوي وصالة لكبار الزوار النظام المنشئي هو نظام الجملونات المستقيمةوالذي يعطي مرونة تصميمة عالية , و والسقف مصمت بدون اي فتحات لادخال الانارة السقفية والاعتماد على الانارة الجانبية. بناية المسافرين الحالية انشأت من الهيكل الحديدي المحلي الصنع ومغلفة بالواح معزولة حراريًا من الخارج. استخدام نظم منشئية تقليدية حيث انشأت البناية من الهيكل الحديدي , المواد المغلفة للبناية من الخارج الواح الالمنيوم الملونة والمرمر والسقوف من الالواح المعزولة والتغليف من الداخل من المرمر والواح الالمنيوم الملونة مع وجود نقش اسلامي وأيات قرأنية منقوشة على الجدارن في الاجزاء الرئيسية من البناية. والسقوف الجملونية لاتحوي فتحات سقفية لادخال الانارة الطبيعية حيث يغطى الهيكل المنشئي من الداخل بسقوف ثانوية تحوي الانارة الاصطناعية ومن الجانبي توجد فتحات زجاجية واسعة لادخال الانارة الجانبية دون وجود وسيلة تضليل .

تفتقر البنية الشكلية للمطار لقيم الاثارة الحسية مثل التعبيرية والرمزية التي تعزز التجربة والهوية المكانية فجاء تشكيل الكتل باسلوب بعيد جدا عن العمارة المحلية لايحمل ابعاد زمانية ولا مكانية . واستخدام المواد لا يعكس ثقافة وهوية البلد حيث استخدم المصمم مادة حيث انشأت البناية من الهيكل الحديدي , المواد المغلفة للبناية من الخارج الواح الالمنيوم الملونة والمرمر والتي لا تعكس ابعادا سياقية وخصوصية مدينة النجف الاشرف .

ملحق رقم (2) نموذج لإستمارة الإستبيان

رموز المتغيرات		الأمثلة التطبيقية					
		1	2	3	4	5	6
مستوى التكامل التصميمي لمبنى المسافرين	A1						
	A2						
	A3						
	A4						
	A5						
	A6						
	A7						
	A8						
	A9						
	A10						
	A11						
	A12						
	A13						
	A14						
	A15						
	A16						
	A17						
	A18						
	A19						
	A20						
	A21						
	A22						
مستوى تكاملية النظم المنشئية مع المنظومات الوظيفية والتشغيلية	B1						
	B2						
	B3						
	B4						
	B5						
	B6						
	B7						
	B8						
	B9						
	B10						
	B11						
	B12						
	B13						
	B14						
	B15						
	B16						
	B17						
	B18						
	B19						
	B20						
	B21						
	B22						
	B23						
	B24						
	B25						
	B26						
	B27						
	B28						
المستوى الشكلي والتعبيري	C1						
	C2						
	C3						
	C4						
	C5						
	C6						
	C7						
	C8						
	C9						
	C10						
	C11						
	C12						
	C13						
	C14						
	C15						
	C16						
	C17						
	C18						
	C19						

						C20	
						C21	
						C22	
						C23	

ملحق رقم (3) التمركزات العالية والوسط والضعيفة للمشاريع الستة المنتخبة وفقاً لآراء المستبينين

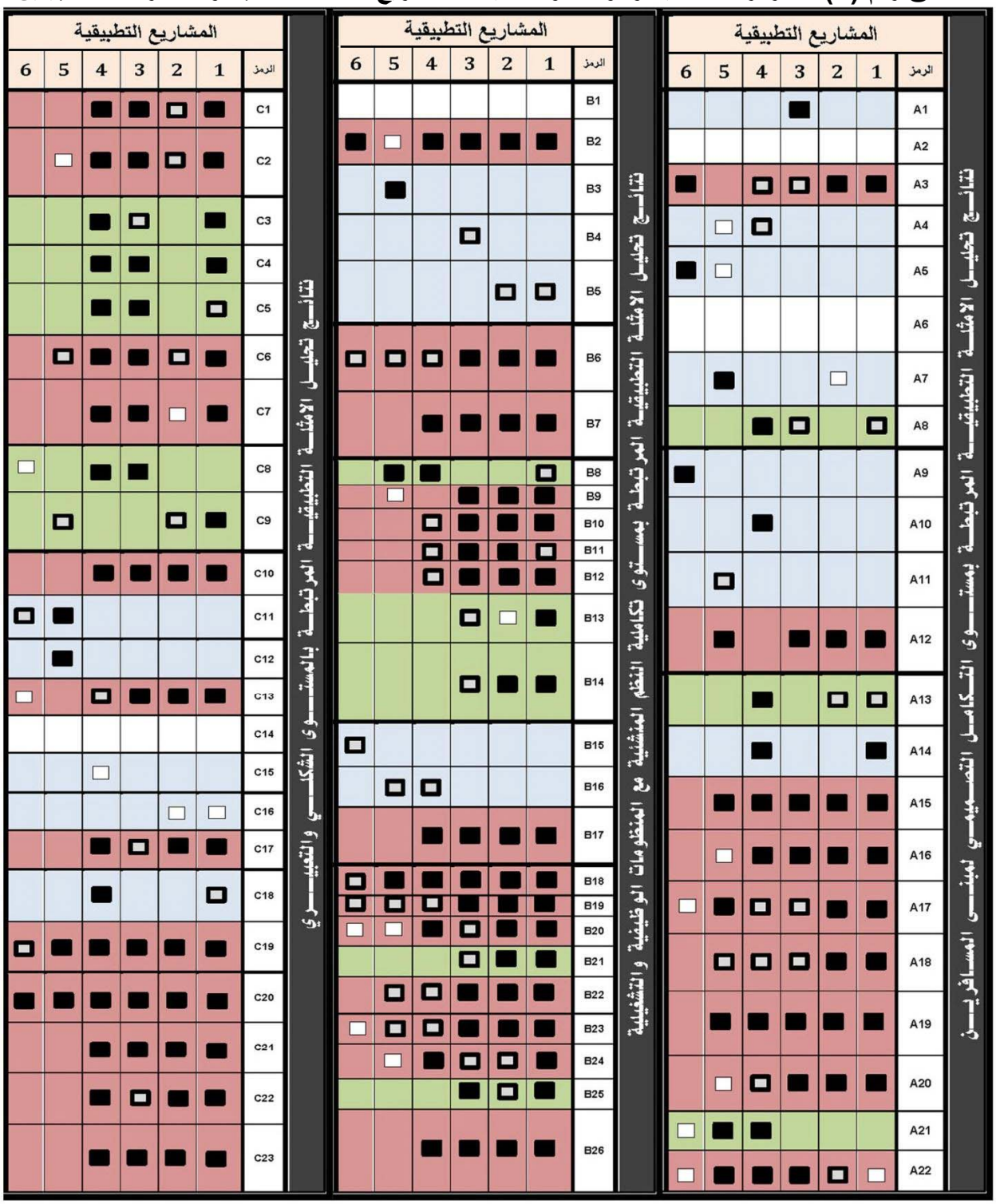

تمركز عالي يتراوح بين (80%-99%)	
تمركز وسط يتراوح بين (60%-79%)	
تمركز ضعيف يتراوح بين (40%-59%)	
تمركز ضعيف جدا اقل من (40%)	

متغير معدوم الفاعلية الذي يكون تكراره صفراً	
متغير ضعيف الفاعلية بتكرار من (1-2) مرات	
متغير متوسط الفاعلية بتكرار (3) مرات	
متغير شديد الفاعلية بتكرار (4-6) مرات	

Visual pollution and statistical determination in some of Karrada district main streets /Baghdad

Husham AbdMunaf Atta

Assistant Lecturer / Computer Center / University of Baghdad

husham@uobaghdad.edu.iq

ABSTRACT

This study objective is to identify the visual pollution in Karrada district main streets as an example of main streets in Baghdad, the public opinion about each pollutants, solutions to reduce and eliminate the pollution were suggested as well. In order to accomplish this objective different methods were used, 16 pollutants were selected, pictures of each pollutants were taken and a questioner were distributed randomly for 270 people to evaluate the public opinion with statistical methods. Garbage, their disposal and storage areas took the first two places as the highest offensive pollutants. The people showed that they find long lines of vehicles, debris and generators appearance ranked third, fourth and fifth respectively .This research showed that more than 70 percent of people are against the militarization of society and they consider any existence of heavy military machinery or personal is highly offensive issue. Other pollutants such as street sellers, beggars, and crossed wires considered as moderately offensive. Car parking in inappropriate places, badly trimmed trees, large billboards in the streets and the buildings criteria considered slightly offensive. The shops billboards and cellular phone and internet towers were considered the least offensive pollutants. Major solutions is to enhance the municipality management in both planning and operation methods relayed to pollution removal, running awareness campaigns to educate the people about the visual pollution effects and how to reduce it and reduce the military appearances in the city .

KEYWORDS :Visual pollution, garbage , militarization, billboards, Buildings frontage design and awareness campaigns.

هشام عبدمناف عطا

مدرس مساعد في مركز الحاسبة الألكترونية – جامعة بغداد

الخلاصة:إن هدف هذه الدراسة هو تحديد الملوثات البصرية في بعض الشوارع الرئيسية لناحية الكرادة، كمثال عن الشوارع الرئيسية في بغداد من وجهة نظر المواطنين ،ومحاولة ايجاد الحلول لتقليل او محو هذه الملوثات. ولتحقيق هذه الأهداف تم اختيار 16 ملوثاً رئيسيا مع التقاط صور فوتوغرافية لها ثم توزيع استبيان بصورة عشوائية على 270 شخصاً وفحصها أحصائياً لمعرفة رايهم بهذه الملوثات. بعد تحليل النتائج وجد ان مناطق تخزين وتجميع المخلفات الصلبة وطرق التخلص منها قد اخذت المرتبتين الأوائل كأكثر الملوثات كرهاً من قبل المواطنين تلتها وحسب الذكر الطوابير الطويلة من السيارات ،الأنقاض ومظهر المولدات في المراكز الثالث والرابع والخامس على التوالي .أظهرت هذه الدراسة ان اكثر من سبعين بالمائة من المواطنين هم ضد عسكرة المجتمع ، ويعتبرون ان اي تواجد للقطع العسكرية والقوى الأمنية ثقيلة التسليح هو من الأمور المزعجة بشدة .الملوثات الأخرى كبائعو الشوارع والمتسولون وتشابك الخطوط الكهربائية صنفت كملوثات متوسطة الأزعاج ؛ بينما كان ايقاف السيارات في غير المناطق المخصصة لها، الأشجار الميتة او سيئة التشذيب ، لوحات الأعلانات الكبيرة وشكل وخواص المباني أعتبرت من الملوثات القليلة التأثير . وأخيراً اعتبرت لوحات المحلات وابراج الهاتف وتجهيز الشبكة العنكبوتية عديمة او الأقل تاثيرا من الملوثات المختارة. وجدت الدراسة إن أهم المعالجات هي تحسين الأدارة البلدية من ناحية التخطيط وتنفيذ عمليات ازالة الملوثات، القيام بحملات التوعية للمواطنين بخصوص تأثير الملوثات البصرية وكيفية التخلص منها وايضاً تقليل المظاهر العسكرية في المدينة .

الكلمات الرئيسية: التلوث البصري،المخلفات الصلبة ،العسكرة ، لوحات الأعلان ، تصميم واجهات المباني ،حملات التوعية

INTRODUCTION

Visual pollution defined as any irregular formations or any negative changes that considered disturbing and leave negative impressions in the mind of people (Yilmaz & Ayse, 2011) . These Irregularity and negative changes can cause over time, a damage in the sense of beauty and the distortion of aesthetic considerations and satisfaction and acceptance of the image of the ugly (Mohamed & Abdel-Gawad, 2011), which can destruct the psychological state of citizens and damaging the Gross national product and the national economy (Kuther, 2011). Many researchers had listed the reasons below as the main reasons beyond the visual pollution;

1- **Administration and management reasons:** Neglecting, wrong decisions like exceptions for some governmental agencies and companies, lack of maintenance for buildings and Infrastructures , legal deficiencies ,lack of control, uses that are not compatible with the functions and insensitivity of local administrations (Khaled, 2009).

2- **Economic reasons:** Different architectural designs, lack of funds, which can be notice in that countries with poor national economy have worse visual pollution than those having strong economy (Al-Kurdy & Kivo, 2009).

3- **Cultural and Educational reasons:** People with lack of cultural or educational levels will have less interest in avoiding any visual pollution (Yilmaz & Ayse, 2011).

This research surpasses any other researches by adding a new reason for visual pollution, which is a Security reason. This is because of the complex situation in Iraq, people are undergoing the view of heavily armed police and army power and their battlefield equipments and vehicles such as T-72 and M1A1(Abrams) Main battle tanks ,(M1117, BTR's and BMP's) soldier carriers and (Humvee's and Dzik-3) armored vehicles. This presence will cause militarization of society. This militarization of society will lead to the creation of a culture of militarism and acceptance of weapons as a normal part of life (Louise, 1995) . (Martin-Baro, 1988) Suggests another influence for the militarization of society, which is mental militarization, in Which violence is the normal response for social problems, disrupting public rational decision-making processes and destroy perceptions of non-violent options for conflict resolution. The result is societal brutalization and the collapse of traditional value systems.

AREA OF STUDY

This study took several streets from al-Karrada district as the study area as shown in **Fig.1** , the reason beyond this choice is Al-Karrada district and its roads represent one of the most important roads in Baghdad because it connect and contain large commercial , residential, governmental and educational areas; these streets are:

1- **Al-Jamia'a (University) Street:** begins **with the** imminent of Al-Jaderia Bridge and ends with Al-Jamia'a intersection. On This Street lies the largest university in Iraq, which is University of Baghdad.

2- **Khalid Ibn Al-Walid Street:** the longest street in Al-Karrada district begins with Al-Jamia'a intersection and ends with Mohammed Al-Qasim Highway, passing through Kamal Junbalat (or Al-Hakim)square, Al-Hurria intersection , Al-Masbah intersection ,Oqba bin Nafia'a Square, Al-Tahriat Square,52 square and Al-Sina'a intersection. Both sides of this street contains mass selling and retail markets for electrical and furniture goods and could be consider as the national center to distribute these goods in Iraq.

3- **Tariq Bin Ziad Street:** Starts from Oqba bin Nafia'a square and ends with Mua'asker al-Rasheed (Rasheed Camp) highway intersection, on this street lays the mass selling and retail of Batteries, tires, vehicles and machines spare parts.

4- **Fawzi Qawoamgi Street:** starts from al-Masbah intersection and ends with Al-Fatih Square. This street is Commercial Street with mass and retail selling of electrical and menswear good.

All these streets beside their commercial importance, they have governmental buildings, cultural centers, social clubs, hotels and restaurants on their sides.

Main streets in any city , is not only some paths to drive on, it is public spaces where people can

walk, shop, meet and can do different social and recreational activities that make urban living enjoyable (Mohamed & Abdel-Gawad, 2011).
Actually, some researchers showed that people have more acceptances to green roads and the drivers showed lower levels of stress when seeing natural roadside compared with building roadside (Akbar, 2003). A research showed that car crashes had decreased in number after landscape improvement was made (Cackowski, 2003).

METHDOLOGY

Usage of photographs

The usage of photographing was essential and crucial element in this study to illustrate the visual pollutants and to work as alternative to the real pollution in the questioner as shown by many researchers , Sample pictures shown in **Fig.2**. (Herzog, 1989) used photos to investigate aspects of the public's perception of urban environments ; (Arriaza M, 2004) Used photos to evaluate the visual quality of agricultural landscapes; (Bulut Z, 2007) applied the visual quality assessment method in this study to offer some suggestions for the future planning in regarding to urban landscape visual beauties; (Jaber, 2009) the visual pollution caused by the commercial and transportation activities was displayed by site photographs; (Kuther, 2011) used the photographs to compare the visual pollution in two main road.

Usage of questioner

Questioner Method used to represent the people opinions about visual pollutants items and – from their stand of view – the major and minor visual pollutants. Interviewees answered the questioner with a condition that any pollutants in the questioners is not in physical contact with them and it is not affecting them in any way but visually; the interviewer give detailed explanation to each item required in the questioner. The 270 participants were asked to evaluate each one of the 16 pollutant scoring from 1 to 10, 10 means very offensive and 1 means low or not offensive. Photographs for each pollutant obtained in the questioner to give more details about them. Statistical methods used to determine the rank of each pollutant, the standard deviation and confidence interval for 99%, 95% and 90 % confidence degree .

In this research, we are investigating the main causes of visual pollution from the people stand of view using a questioner and statistical analysis.

Visual Pollutants

The visual pollutants evaluated in this study were;

- Garbage and boxes remnants in the walkways and curbside: this includes houses wastes, boxes, and plastic bags etc, left by the street sellers, shoppers and shops.
- Crossed over electric wires: because of the electric power lack in Iraq, people are using private generators to provide them with the electricity, they need causing the establishment of private irregular electricity network beside the national electricity network.
- Military weapons, vehicles and checkpoints: due to the security situation in Iraq, many of the main roads are having checkpoints, military police forces and other security agencies to enforce the law, these forces need some requisites like camouflage nets, concrete blocks, water and fuel tanks and other appearances that disturb the population eyes.
- Demolished buildings: this includes the buildings destroyed because of war, terrorist activity or rehabilitation.
- Excavation works & rubbles: includes private and municipality excavation works for any reason.
- Generators smoke, spilled fuel and general appearance: this includes the private sector generators distributed in the area to provide electricity. These generators have infrastructures like diesel storage tanks, circuit breakers board, and sometimes additional cooling system.
- Large advertising billboards: the size, design, materials and contain of governmental and private advertising billboards installed in the median stripes , squares and on buildings.
- Long lines of vehicles: this includes the traffic jams caused by checkpoints and/or road junctions.

- Irregular demonstration of goods: the irregular distribution and demonstration of goods in both shop windows and sidewalk seller.
- Shops and supermarkets Billboards: different sizes, color, design, materials and location of shops billboards cause lack of unity for the observer.
- The irregularity of heights, design, materials and regression of buildings: because of years of neglecting and different legislation the heights, wide verity of materials design and regression (the distance from the building to the curbside) differs widely.
- Overfilled and dirty garbage containers: few numbers of containers and long emptying and cleaning periods causing the filthiness and over fullness of the garbage containers.
- Beggars and street sellers: some beggars lay in the middle of the paved areas with dirty clothes and sometimes with different types of drugs and suspicious objects around them; while street sellers are demonstrating their goods in the walkways or even selling near the road junctions.
- Dead and badly trimmed tress: this caused by neglecting and human activities.
- Car parking in the streets and in green areas or in walk ways: This is a result of small or absence of parking lots in the area.
- Cellular phone, Internet Towers.

RESULTS AND DISCUSSION

The average offensive score for each pollutant listed in Table1.

From **table 1** and **figure 3**, the highest offensive pollutants were garbage remnant and their fallaciously disposal with 80% and 71.1% of people giving them the highest score respectively. These high ranks for garbage related pollutants are not surprising when considering the stigma and association of the word garbage. This require increasing the garbage bins and the man power working on cleaning and emptying the bins, promoting awareness campaign is needed as well to educate the population about the pollution risks in general and specially the visual pollution.

Table1 Average offensive score for visual pollutant.

Offensive rank	pollutant	Average score
1	Garbage and boxes remnants in the walkways and curbside	9.44
2	Overfilled and dirty garbage containers	9.44
3	Long lines of vehicles	8.62
4	Excavation works & rubbles	8.4
5	Generators smoke, spilled fuel and appearance	8.35
6	Military vehicles and checkpoints	8.15
7	Beggars and street sellers:	7.91
8	Crossed over electric wires	7.73
9	Demolished buildings	7.42
10	Car parking in the streets and in green areas or in walk ways	6.66
11	Dead and badly trimmed tress	6.31
12	Irregular demonstration of goods	6.26
13	Large Advertising billboards	5.35
14	The irregularity of heights, design, materials and regression of buildings	3.26
15	Shops and supermarkets irregular billboards	2.97
16	Cellular phone internet Towers	2.35

The third rank was for long lines of vehicles resulted from checkpoints and intersections in this highly populated area with many of the governmental buildings specially the University of Baghdad. This high rank is in line with other studies like (Jones, 2006) , to overcome this problem reducing the checkpoints and activation of road rules is definite. The fourth rank was for excavation works and rubbles from the renovation of buildings (both governmental and private); this pollutant might achieve higher ranks if the municipality did not enforce some regulations on the ground. Generators and their different pollutants has the fifth rank with 73.33% of people considering it highly offensive, this is a

result of the regulation absence that regulate the installation and operation of these generators.

The sixth rank is very important because it declared that despite the fact of decades of militarization and wars that the Iraqi people had suffered, 71.11% of them are considering the military existence is highly offensive appearance. The reducing of these appearances is needed by reducing and intensive the checkpoints, movement prohibition of tanks and soldier carriers during the day and even in night crowded hours, decrease the vehicles and their armament of protection forces accompany the VIP's and the use of household like infra structures in these checkpoint instead of the military like ones.

The beggars and street sellers have the seventh rank with 68.89% of people listed it as highly offensive, this high pollutant rank is due to its effect on tourism and trading. Immediate procedures should be taken to activate protection social network, capacity building for new graduated students and finding hiring positions.

Crossed wires from the private electricity network had the eighth rank; this pollutant could have higher rank if it was in the eye level. Solving the electricity problem in the long phase and the using of large cables with sub circuit boards in the short phase may reduce the effect of this pollution.

The pollutants in ranks from nine to thirteen are in controversial situation, the scoring for these pollutants highly depends on cultural and educational background of people and the location of pollutant more than other pollutants because of most of these pollutants is a result of absence of services and\or legislation.

The ranks from fourteen to sixteen had the minimum scouring because of these pollutants are not in eye level and not considered highly eye and mind stressing issue.

Table 2 shows standard deviation values and Confidence interval with confidence degree of 99%, 95% and 90% which indicate that the results were satisfactory and the data was not highly scattered and they are close to the mean with adequate confidence intervals.

CONCLUSION

This research provides the public opinion about certain visual pollutants. Garbage, their disposal and storage areas took the first two places as the highest offensive pollutants. The people showed that they find long lines of vehicles, debris and generators appearance ranked third, fourth and fifth respectively .This research showed that more than 70 percent of people are against the militarization of society and they consider any existence of heavy military machinery or personal is highly offensive issue.

Other pollutants such as street sellers, beggars, and crossed wires took middle place and considered as moderately offensive.

Car parking in inappropriate places, badly trimmed trees, large billboards in the streets and the buildings criteria considered slightly offensive.

The shops billboards and cellular phone and internet towers were considered the least offensive pollutants.

This indicates the lack of municipality activity and the need of activate legislations and rules to terminate these pollutants such as building, transportation and protection social network laws.

Reducing the military appearances and the need of promoting awareness campaigns regarding the pollution in general and specially the visible pollution is very significant issue as well.

BIBLIOGRAPHY

Akbar, K. G. (2003). Assessment of scenic beauty of the roadside vegetation in northern England. Landscape and urban planning , 63, 139-144.

Al-Kurdy, R., & Kivo, L. (2009). Architectural space analysis. Master thieses . Damascus University.

Arriaza M, Cañas-Ortega, J.F., Cañas-Madueño ,J. A., P, Ruiz-Aviles. (2004). Assessing the visual quality of rural landscapes. Landscape , 69 (1), 115-125.

Bulut Z, Y. H. (2007). Determination of landscape beauties through. Environmental Monitoring and Assessment , 141, 121-129.

Cackowski, J. a. (2003). The restorative effects of roadside vegetation: implications for automobile driver anger and frustration. Environment , 35, 736-751.

Herzog, T. (1989). A cognitive analysis of preference for urban nature. Environmental Psychology , 9 (1), 27-43.

House, M., & Herring, M. (1995). Aesthetic pollution public perception. Water Research Centre, UK. Flood Hazard.Middlesex University,.

Jaber, A. (2009). A STUDY FOR THE LANDUSES & THE TOWNSCAPE OF THE COMMERCIAL STREETS. High diploma . Higher Institute of Urban and Regional Planning University of Baghdad.

Jones, B. (2006). Visual Pollution, Systems and Technology. Australia: Marine and Estuarine Studies Section, NSW Environment Protection Authority.

Khaled, M. T. (2009). Analyzing and Evaluating Visual Pollution In Tulkarem City(Center of Tulkarem City – Case Study). master thieses . An-Najah National University.

Kuther, K. K. (2011). The visual pollution and its effect in the Iraqi townscape Case study Al-kadhimia / streets of bab – al-qibla and bab – al-murad. High Diploma thieses . Institute of Urban & Regional Planning University of Baghdad .

Louise, C. (1995, March). The social impacts of light weapons availability and proliferation. Discussion Papers . UNRISD.

Martin-Baro, I. (1988). La violencia politica y la guerra como causas del trauma psicosocial en El Salvador". Revista de psicologia de El Salvador, , 7 (28), 123-141.

Mohamed, N. M., & Abdel-Gawad, A. K. (2011). Landscape Impact on Roadside Improvement in Egypt Case Study of Salah Salem Road, Cairo, Egypt. World Applied Sciences Journal , 266-278.

Yilmaz, D., & Ayse, S. (2011). In the Context of Visual Pollution: Effects to Trabzon City Center Silhoutte. Asian Social Science , 7 (5), 98-109.

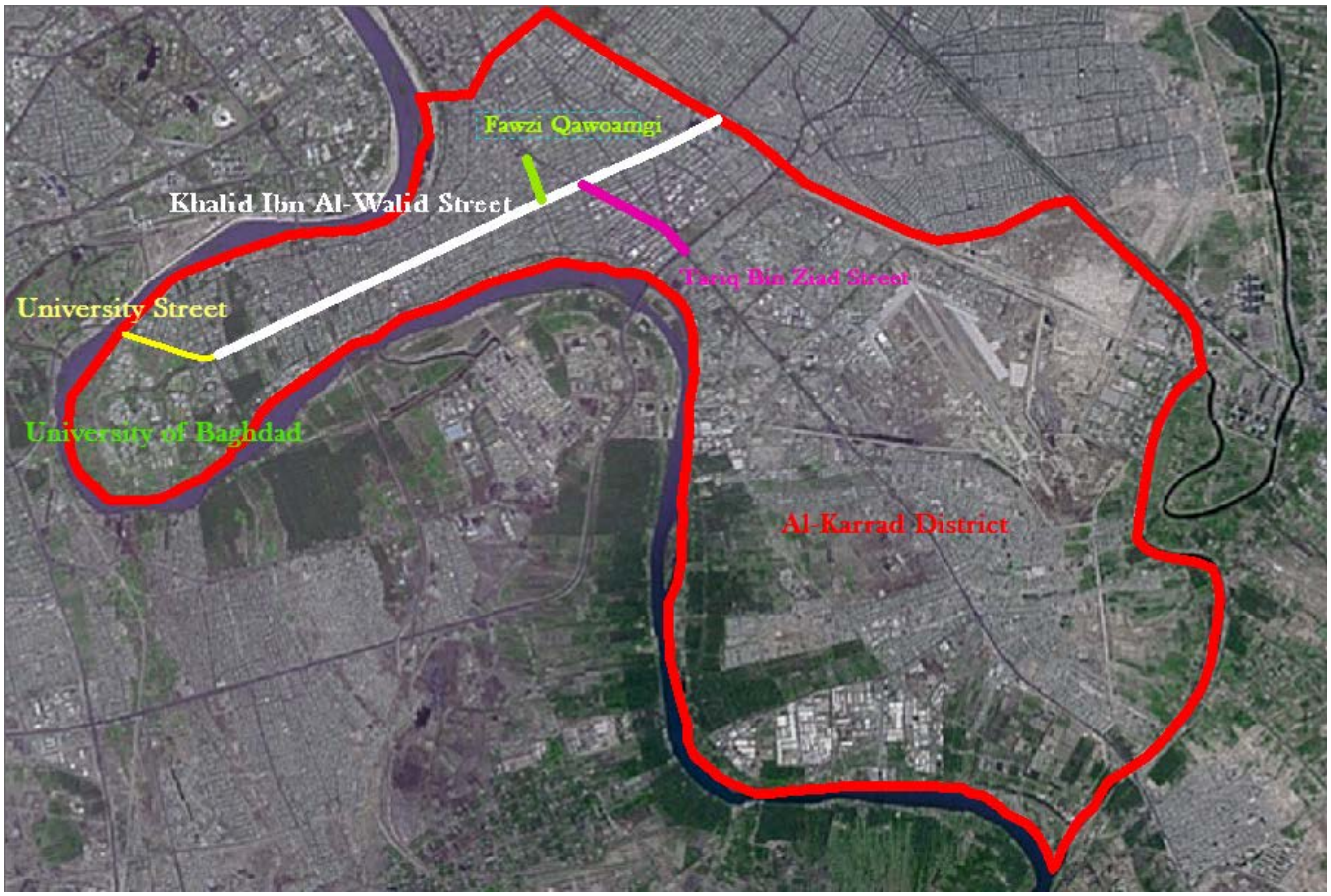

Figure 1. Satellite image of the study area Al-Karrada District with the main streets

Garbage and boxes remnants in the walkways and curbside

Overfilled and dirty garbage containers

Long lines of vehicles

Excavation works & rubbles

Generators smoke, spilled fuel and appearance

Car parking in the streets and in green areas or in walk ways

Demolished buildings

M1117 National Iraqi police Personal Carrier in Baghdad streets check point

Cell phones and internet Towers

Crossed over electric wires

Dead and badly trimmed tress

Irregular demonstration of goods and shops billboards

Large Advertising billboards

The irregularity of heights, design, materials and regression of buildings and irregular shops billboards

Figure 2. Pollutant Pictures used in the study (Taken by the Author).

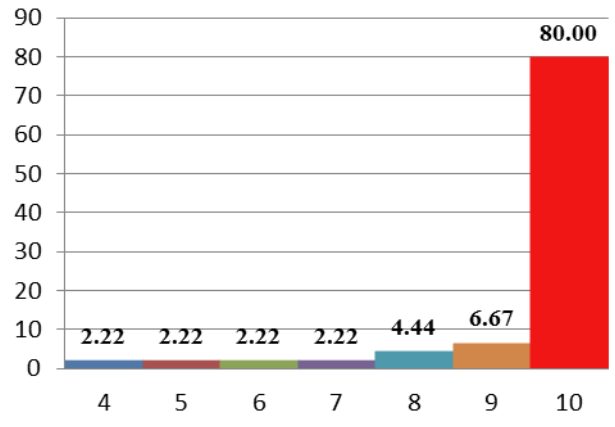

Garbage and boxes remnants in the walkways and curbside

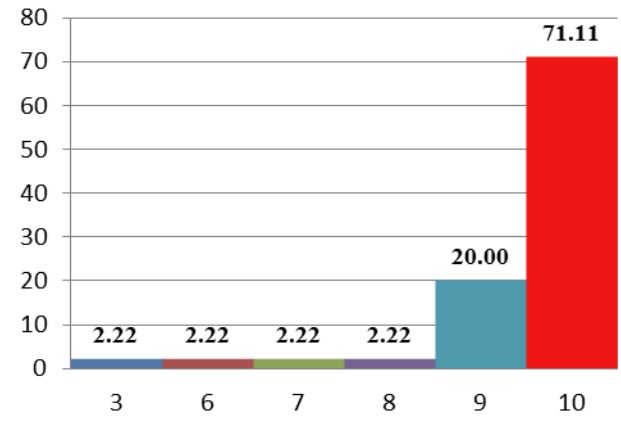

Overfilled and dirty garbage containers

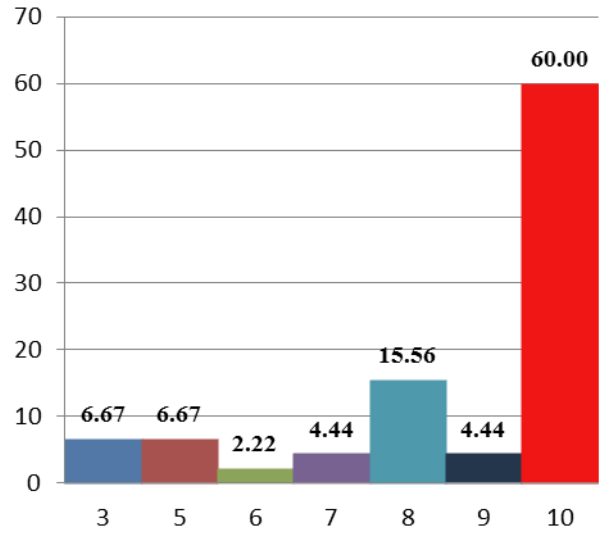

Long lines of vehicles

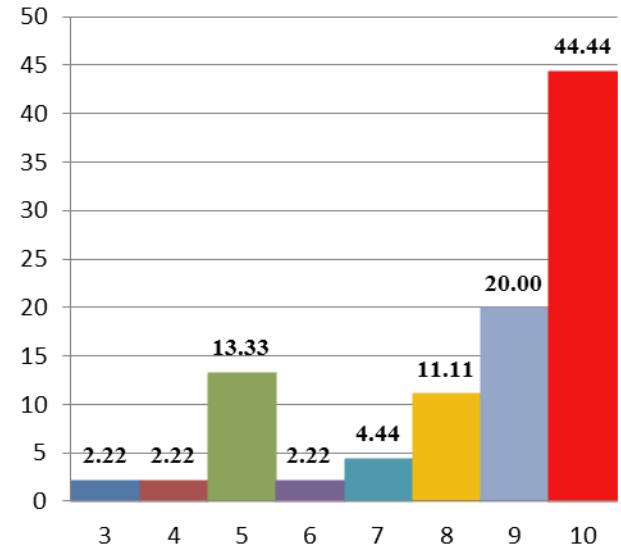

Excavation works & rubbles

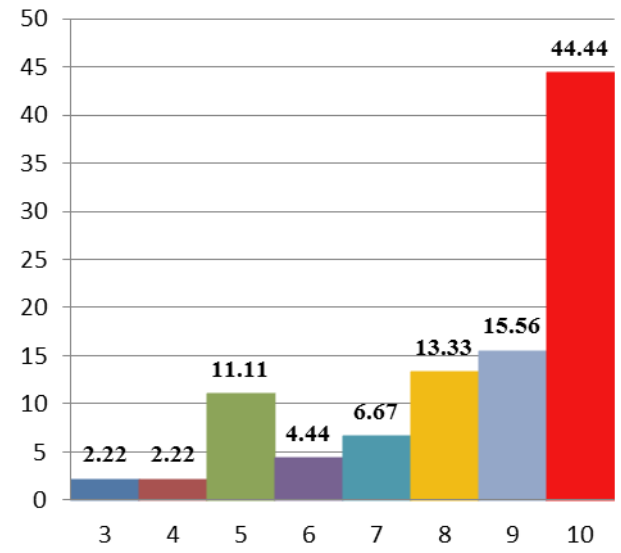

Generators smoke, spilled fuel and appearance

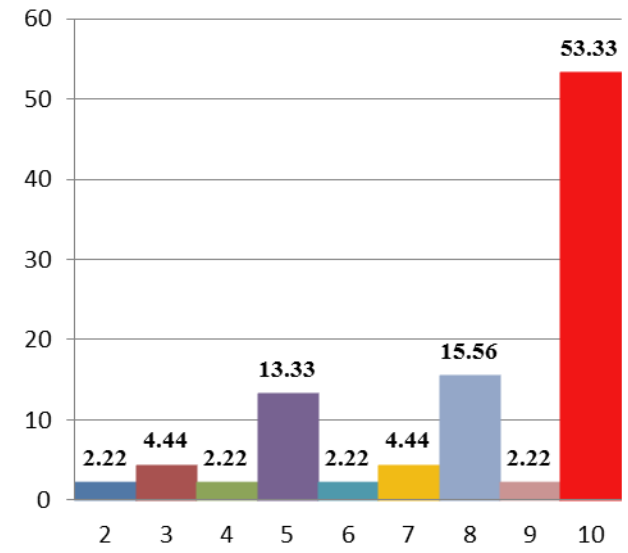

Military vehicles and checkpoints

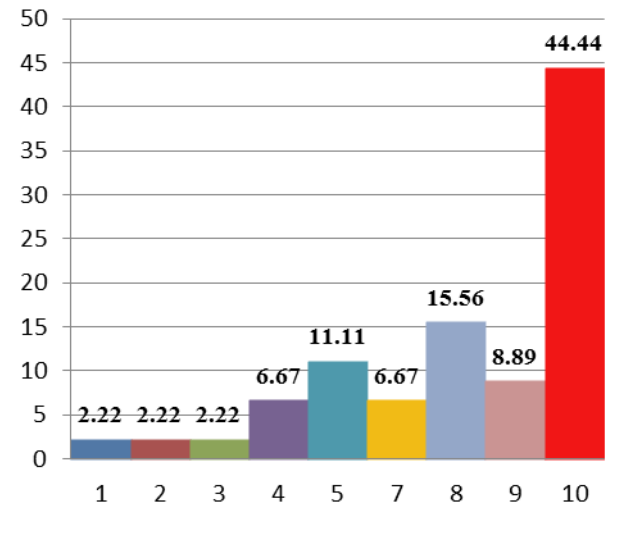

Beggars and street sellers

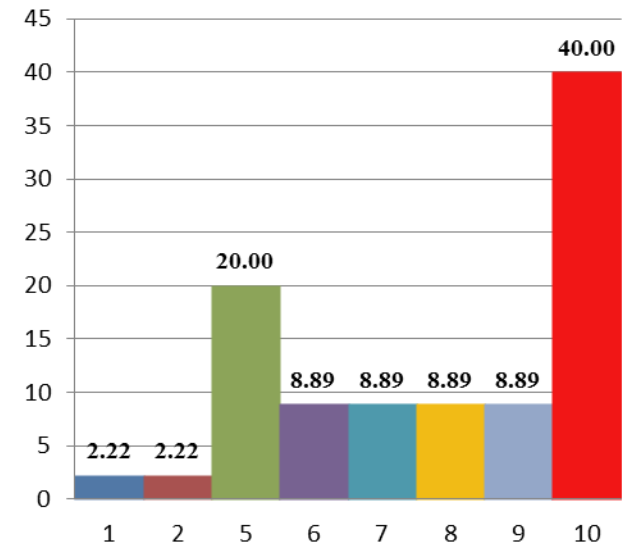

Crossed over electric wires

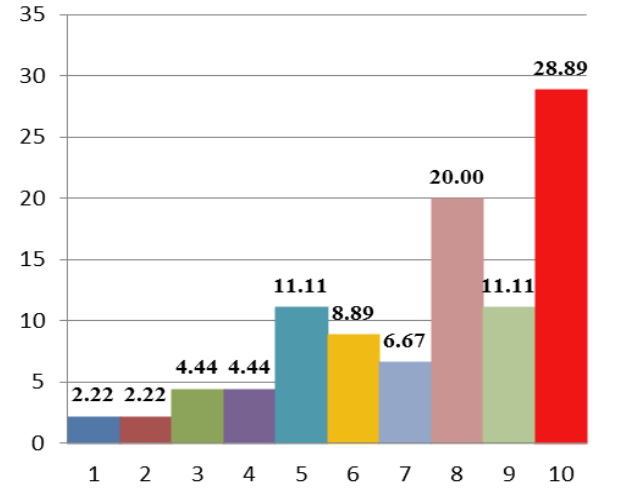

Demolished buildings

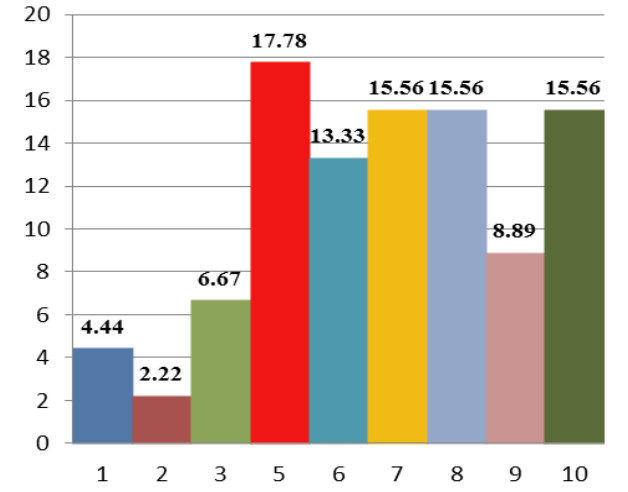

Car parking in the streets and in green areas or in walk ways

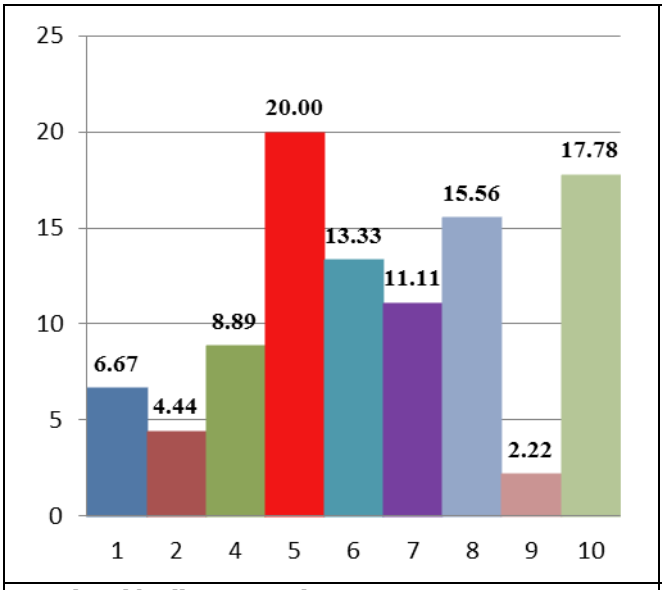

Dead and badly trimmed tress

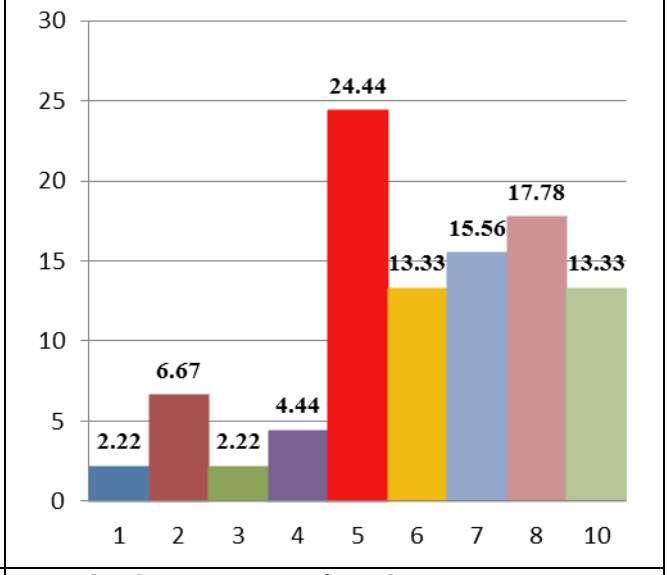

Irregular demonstration of goods

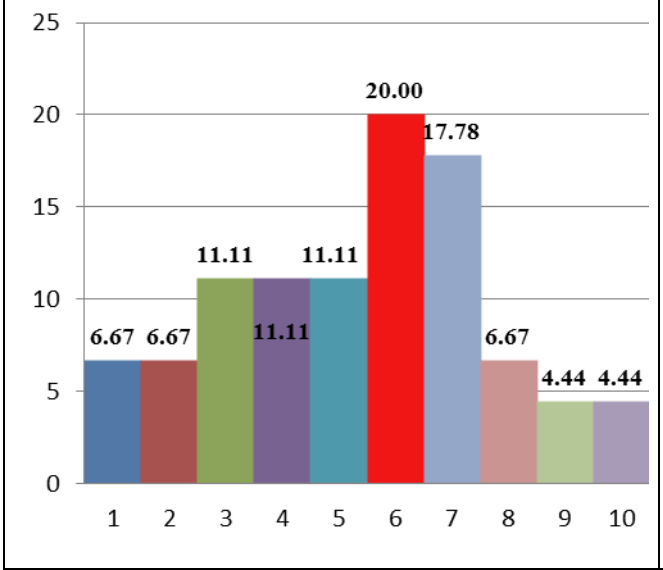

Large billboards in the median stripes

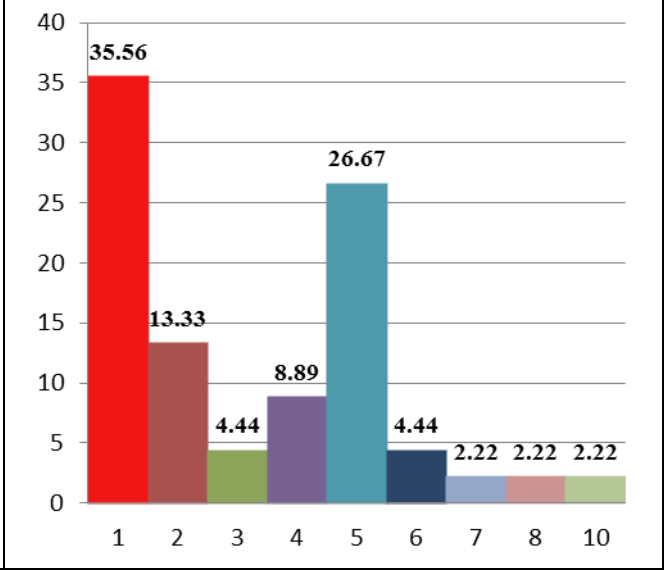

The irregularity of heights, design, materials and regression of buildings

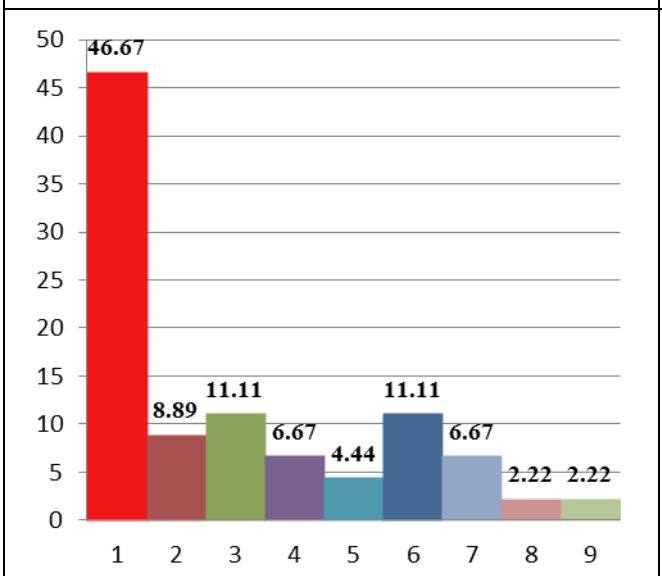

Shops and supermarkets irregular billboards

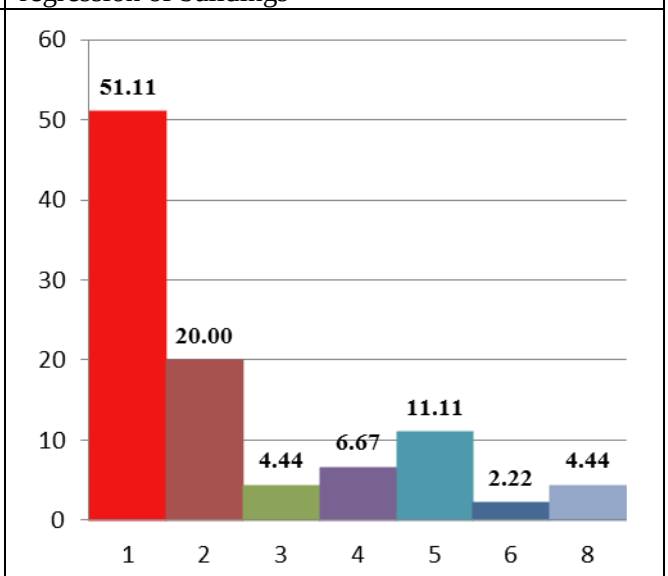

Cellular phone Towers

Figure 3. The Statistical scouring for pollutants discussed in this research.

Table 2. Standard Deviation and Confidence interval with confidence degrees of 99%, 95% and 90% for visual pollutants

Pollutant	Standard Deviation	Confidence interval with confidence degree of 99%		Confidence interval with confidence degree of 95%		Confidence interval with confidence degree of 90%	
Garbage and boxes remnants in the walkways and curbside	1.36	9.6579	9.231	9.6069	9.282	9.5807	9.3081
Overfilled and dirty garbage containers	1.28	9.6446	9.2442	9.5968	9.2921	9.5723	9.3166
Long lines of vehicles	2.12	8.9538	8.2906	8.8745	8.3699	8.834	8.4105
Excavation works & rubbles	2.02	8.7166	8.0834	8.6409	8.1591	8.6021	8.1979
Generators smoke, spilled fuel and appearance	1.99	8.6682	8.0429	8.5934	8.1177	8.5552	8.1559
Military vehicles and checkpoints	2.40	8.5316	7.7795	8.4416	7.8695	8.3957	7.9154
Beggars and street sellers:	2.54	8.3096	7.5126	8.2143	7.6079	8.1656	7.6567
Crossed over electric wires	2.40	8.11	7.3566	8.0199	7.4467	7.9739	7.4928
Demolished buildings	2.47	7.8091	7.0353	7.7166	7.1279	7.6693	7.1752
Car parking in the streets and in green areas or in walk ways	2.43	7.0471	6.2862	6.9561	6.3772	6.9096	6.4237
Dead and badly trimmed tress	2.58	6.715	5.9071	6.6185	6.0038	6.5691	6.0532
Irregular demonstration of goods	2.28	6.6239	5.9094	6.5385	5.9949	6.4948	6.0385
Large Advertising billboards	2.33	5.7215	4.9895	5.634	5.0771	5.5893	5.1219
The irregularity of heights, design, materials and regression of buildings	2.25	3.6193	2.9140	3.535	2.9984	3.4918	3.0415
Shops and supermarkets irregular billboards	2.38	3.3502	2.6053	3.2611	2.6944	3.2156	2.74
Cellular phone internet Towers	1.91	2.6557	2.0554	2.5839	2.1272	2.5472	2.1639